NRL Review

2000

This *2000 NRL Review* introduces you to the Naval Research Laboratory—the Navy's Corporate Laboratory—and focuses on research highlights from fiscal year 1999. In addition, it presents the special honors awarded to NRL employees and describes programs available to NRL and non-NRL employees. As you read the *NRL Review*, you will become even more aware that the Naval Research Laboratory comprises a dynamic team of scientists, engineers, and support personnel working together to promote programs that will continue to foster discoveries and scientific advances for the Navy of the future.

Mission

"the Navy's Corporate Laboratory"

To conduct a broadly based multidisciplinary program of scientific research and advanced technological development directed toward maritime applications of new and improved materials, techniques, equipment, systems, and ocean, atmospheric, and space sciences and related technologies.

The Naval Research Laboratory provides primary in-house research for the physical, engineering, space, and environmental sciences; broadly based exploratory and advanced development programs in response to identified and anticipated Navy needs; broad multidisciplinary support to the Naval Warfare Centers; and space and space systems technology, development, and support.

CONTENTS

View from the Top

View from the Top

CAPT Douglas H. Rau, USN, Commanding Officer

I cannot fully express how honored I am to be the Commanding Officer of the Naval Research Laboratory. This command is bathed in a proud history of success and significant impact on our military and our country. Yet we also remain an organization that is internationally renowned for the outstanding quality of our work and the legacy of the individuals who comprise the research team. As Thomas Edison had intended, we are the Navy's Corporate Laboratory, a great research laboratory to develop all the technique of military and naval progression!

In our day-to-day operations, we focus on the four Capitals of the Laboratory. I would explain it in this way: the *Business Capital* is the way we manage our financial responsibility. As a Navy Working Capital Fund with an annual budget of about $800M, we must judiciously execute our work in an efficient and productive way. Careful management is required to ensure we keep our business prospectus healthy. The *Physical Capital* is the base that we call our campus. With more than a dozen detachments, we maintain a workplace that provides state-of-the-art research centers and an atmosphere that invigorates the mind. NRL will always be a great place to go to work! *Intellectual Capital* is contained in our people, who are the heart and soul of NRL. We must do all that we can to recruit, retain, and promote the finest researchers our nation can produce. This publication showcases our employees and provides some of the recognition they greatly deserve. The *Scientific Capital* is what we have actually provided to the Navy in terms of understanding, demonstrations, and hardware. This is how we enhance the warfighting capability, improve the reliability of systems, or create a better quality of life for our Sailors. At the same time, the published papers and the patents granted continue to elevate our Corporate Laboratory as a leader in the international scientific community.

The presentations you see here in the *2000 NRL Review* are a sampling of the work done at NRL. We are proud to recognize these individuals because they exemplify what we are most proud of ... the passion for discovery! We are not sure where this research will end, but we know that we are on an amazing journey to uncover what has not yet been seen, imagined, or understood.

In closing, I must recognize the great work of one of my predecessors and the present Chief of Naval Research. Rear Admiral Paul Gaffney II was the Commanding Officer of NRL in 1991-1994. By the time this *Review* has been published, he will have been relieved as CNR and moved on to bigger and better things. I wish to thank him for his continued support of NRL and his tremendous leadership of the Navy's Research Community. He is a great mentor, shipmate, and friend.

Dr. Timothy Coffey, Director of Research

As NRL moves into the next millennium, we find ourselves confronted with a remarkable mix of challenges and opportunities. As you will see from the pages of this year's *NRL Review*, the Laboratory continues its outstanding scientific and technical contributions to the Naval forces and the Nation. One must recognize, however, that the "Sputnik generation" which has been the predominant force at NRL for the past two decades is approaching retirement age. This single development will tax the Laboratory while, at the same time, it will provide marvelous opportunities to chart entirely new directions. The Laboratory must maintain continuity on the one hand, while on the other hand it must ensure that appropriate redirections of the technical program occur. The last opportunity for renewal on this scale occurred in the late 1960s. The track record of NRL over the subsequent 30 years provides solid testimony that the Laboratory took proper advantage of that opportunity. Hopefully, we will do as well this round. While we have challenges in this regard, we also have new tools, such as a new personnel system that provides considerably more flexibility than the one that operated in the late 1960s. We are also nearing completion of a major renovation program of the Laboratory's facilities. This positions us well for moving out into new directions. We have also made a number of key hires over the past decade who will play important roles in moving the Laboratory forward. There is no doubt that NRL can step proudly into the next millennium with full confidence that we will continue our outstanding contributions to the Naval forces and to the Nation.

Timothy Coffey

The Naval Research Laboratory

NRL—Our Heritage

Today, when government and science seem inextricably linked, when virtually no one questions the dependence of national defense on the excellence of national technical capabilities, it is noteworthy that in-house defense research is relatively new in our Nation's history. The Naval Research Laboratory (NRL), the first modern research institution created within the United States Navy, began operations in 1923.

Thomas Edison's Vision: The first step came in May 1915, a time when Americans were deeply worried about the great European war. Thomas Edison, when asked by a *New York Times* correspondent to comment on the conflict, argued that the Nation should look to science. "The Government," he proposed in a published interview, "should maintain a great research laboratory....In this could be developed...all the technique of military and naval progression without any vast expense." Secretary of the Navy Josephus Daniels seized the opportunity created by Edison's public comments to enlist Edison's support. He agreed to serve as the head of a new body of civilian experts—the Naval Consulting Board—to advise the Navy on science and technology. The Board's most ambitious plan was the creation of a modern research facility for the Navy. Congress allocated $1.5 million for the institution in 1916, but wartime delays and disagreements within the Naval Consulting Board postponed construction until 1920.

The Laboratory's two original divisions—Radio and Sound—pioneered in the fields of high-frequency radio and underwater sound propagation. They produced communications equipment, direction-finding devices, sonar sets, and perhaps most significant of all, the first practical radar equipment built in this country. They also performed basic research, participating, for example, in the discovery and early exploration of the ionosphere. Moreover, the Laboratory was able to work gradually toward its goal of becoming a broadly based research facility. By the beginning of World War II, five new divisions had been added: Physical Optics, Chemistry, Metallurgy, Mechanics and Electricity, and Internal Communications.

The War Years and Growth: Total employment at the Laboratory jumped from 396 in 1941 to 4400 in 1946, expenditures from $1.7 million to $13.7 million, the number of buildings from 23 to 67, and the number of projects from 200 to about 900. During WWII, scientific activities necessarily were concentrated almost entirely on applied research. New electronics equipment—radio, radar, sonar—was developed. Countermeasures were devised. New lubricants were produced, as were antifouling paints, luminous identification tapes, and a sea marker to help save survivors of disasters at sea. A thermal diffusion process was conceived and used to supply some of the ^{235}U isotope needed for one of the first atomic bombs. Also, many new devices that developed from booming wartime industry were type tested and then certified as reliable for the Fleet.

NRL Reorganizes for Peace: Because of the major scientific accomplishments of the war years, the United States emerged into the postwar era determined to consolidate its wartime gains in science and technology and to preserve the working relationship between its armed forces and the scientific community. While the Navy was establishing its Office of Naval Research (ONR) as a liaison with and supporter of basic and applied scientific research, it was also encouraging NRL to broaden its scope and become, in effect, its corporate research laboratory. There was a transfer of NRL to the administrative oversight of ONR and a parallel shift of the Laboratory's research emphasis to one of long-range basic and applied investigation in a broad range of the physical sciences.

However, rapid expansion during the war had left NRL improperly structured to address long-term Navy requirements. One major task—neither easily nor rapidly accomplished—was that of reshaping and coordinating research. This was achieved by transforming a group of largely autonomous scientific divisions into a unified institution with a clear mission and a fully coordinated research program. The first attempt at reorganization vested power in an executive committee composed of all the division superintendents. This committee was impracticably large, so in 1949, a civilian director of research was

named and given full authority over the program. Positions for associate directors were added in 1954.

The Breadth of NRL: During the years since the war, the areas of study at the Laboratory have included basic research concerning the Navy's environments of Earth, sea, sky, and space. Investigations have ranged widely—from monitoring the Sun's behavior to analyzing marine atmospheric conditions to measuring parameters of the deep oceans. Detection and communication capabilities have benefitted by research that has exploited new portions of the electromagnetic spectrum, extended ranges to outer space, and provided a means of transferring information reliably and securely, even through massive jamming. Submarine habitability, lubricants, shipbuilding materials, fire fighting, and the study of sound in the sea have remained steadfast concerns, to which have been added recent explorations within the fields of virtual reality, superconductivity, and biomolecular science and engineering.

The Laboratory has pioneered naval research into space from atmospheric probes with captured V-2 rockets through direction of the *Vanguard* project—America's first satellite program—to inventing and developing the first satellite prototypes of the Global Positioning System. Today NRL is the Navy's lead laboratory in space systems research, fire research, tactical electronic warfare, microelectronic devices, and artificial intelligence.

The consolidation in 1992 of NRL and the Naval Oceanographic and Atmospheric Research Laboratory, with centers at Bay St. Louis, Mississippi, and Monterey, California, added critical new strengths to the Laboratory. NRL now is additionally the lead Navy center for research in ocean and atmospheric sciences, with special strengths in physical oceanography, marine geosciences, ocean acoustics, marine meteorology, and remote oceanic and atmospheric sensing. The expanded Laboratory is focusing its research efforts on new Navy strategic interests and needs in the post-Cold War world. Although not abandoning its interests in blue-water operations and research, the Navy is also focusing on defending American interests in the world's littoral regions. NRL scientists and engineers are working to give the Navy the special knowledge and capabilities it needs to operate in these waters.

1999 in Review

In this last year of the century, NRL researchers continued to carry out innovative research across a broad swath of the physical sciences. In a further indication of the international state of post-Cold War science, researchers from the Laboratory's Marine Geosciences Division and the Materials Science and Technology Division participated in a research cruise to the Greenland-Norwegian Sea, with scientists from Russia, Germany, and Norway. The Russian oceanographic vessel *Akademik Mstislav Keldysh* served as home to the multinational team. The Americans investigated sites on the ocean floor where methane gas, hydrogen sulfide gas, and porewater are squeezed into the water column. Additionally, they looked for the presence of methane hydrates, whose presence in the sub-seafloor can affect acoustic propagation and which are also a future fuel source. The Greenland-Norwegian Sea has been a continuing site of research interest for NRL scientists.

In another area of historic research interest to NRL scientists, that of the ionosphere and near space, Laboratory researchers have developed a suite of ultraviolet and X-ray sensing instruments for use onboard the Air Force Space Test Program's Advanced Research and Global Observation Satellite (ARGOS). Observational data from the instruments, along with radio measurements of total electron content, will study the changing effects of solar radiation on the upper atmosphere and ionosphere. Scientists will thereby be able to create dynamic maps of the ionosphere, showing changes in chemistry, density, and temperature. ARGOS carries nine primary experiments with 31 different sensors and subexperiments. Five of the primary experiments were developed by NRL researchers and another two were developed with NRL collaboration. Laboratory scientists have been involved in scientific study of the ionosphere since the path-breaking research of E.O. Hulburt and A.H. Taylor on radio propagation in the upper atmosphere in the mid-1920s.

One of ARGOS's primary sensors was developed by NRL's Naval Center for Space Technology. This, the High Temperature Superconductivity Space Experiment (HTSSE), has as its mission demonstrating the feasibility of incorporating high-temperature superconductivity components into space-based sensors. Operating at about −200 °C, these components hold the promise of offering greatly increased capa-

After the Reading of Orders, CAPTs Rau and Buckley perform the Passing of Command.

bilities for microwave components and improved communications and signal processing onboard satellites. NRL initiated the HTSSE program in 1998.

In yet another satellite-based experiment, NRL's Polar Ozone and Aerosol Measurement (POAM) III detector successfully monitored the evolving high-altitude plume from the eruption of the Shishaldin volcano in the Aleutian Islands. POAM measures vertical profiles of the atmosphere, and during the spring of 1999 it detected enhanced amounts of aerosols or particles in narrow layers. On April 23, POAM showed volcanic aerosols as high as 17 km, and from these observations NRL scientists have inferred that the plume was lofted as high as 19 km. The altitude and evolution of volcanic ash plumes are important because of the hazard they present to aviation. The POAM program has provided valuable insights into a variety of polar atmospheric processes, including the possible destruction of Arctic ozone and the development of ozone holes.

Scientists within NRL's Chemistry and Optical Sciences Divisions have developed composite aerogels for use as high-surface-area electrodes, catalysts, battery structures, and advanced thermoelectric materials, and as architectures around which to design chemical, physical, and optical sensors. Aerogels provide high surface areas and highly open spaces. This makes them well-suited to catalytic and sensing applications where rapid transport of reactants and large accessible surface areas are critical. The NRL researchers have developed design flexibility and expanded the range of aerogel properties by using colloidal silica sol, the gel's building block, as a nanoglue to trap suspended particles or colloids into the network of the wet gel. This technique has been

successful in producing composite aerogels of silica with a range of physically and chemically diverse particulates. When the second phase of the composite is present above a certain threshold, its transport characteristics are imparted to the composite aerogel, even though it retains the low density and openness characteristic of pure silica aerogels.

Within the Laboratory's Optical Sciences Division, researchers have demonstrated a new diamond-pressure bonding (DPB) technique for heat-sinking semiconductor lasers, resulting in record-breaking performances. The new DPB technique greatly enhances the maximum continuous-wave operating temperature for optically pumped semiconductor lasers. It permits devices with their epitaxial sides adjacent to the heat sink to be illuminated from the top, and DPB is more convenient than conventional epitaxial-side-down heat-sinking procedures. When the technique is applied to the optical-pumping of mid-infrared type-II quantum well lasers emitting wavelengths between 3.0 and 7.0 microns, the method yields maximum continuous wave operating temperatures that significantly exceed any reported for semiconductor lasers in the same wavelength range.

Finally, in continuing efforts at NRL to produce environmentally safe materials, the Laboratory has negotiated a Project Arrangement between the U.S. and Canadian departments of defense. The objective of the project is to qualify high-velocity, oxygen-fuel (HVOF) thermal spray coatings as a viable replacement for hard chrome plating on military aircraft components. It is expected that by the conclusion of the project, HVOF thermal spray coatings will be in production within both the U.S. and Canada, resulting in both a cleaner environment and the savings of millions of dollars in maintenance costs. Chrome plating uses hexavalent chromium, which is a highly toxic carcinogen. Increasingly stringent environmental and worker-safety regulations are making chrome plating more expensive for manufacturers and the Department of Defense. HVOF thermal spraying is capable of depositing metal alloy, ceramic/metal composite, and polymer coatings rapidly and to thicknesses comparable to those of chrome plating without the environmental drawbacks. The HVOF development work was carried out within NRL's Chemistry Division.

Technology Transfer: During 1999, NRL's Technology Transfer Office continued to facilitate the implementation of NRL technology for commercial use and to benefit the civilian community. The two principal mechanisms for transfer of NRL technology and expertise are Cooperative Research and Development Agreements (CRADAS) and licenses to

Under license from NRL, Lockheed Martin markets the LaserNet Fines system for automated online analysis of wear particle debris in engine lubricants. The small size of the system makes it ideal for deployment on ships, at field sites, and on factory floors where it can be used to assess machine condition and assist in the implementation of a proactive machine maintenance program to prevent operational failures.

NRL's James Yesinowski and colleagues Robert Kleinberg from Schlumberger-Doll Research and Peter Brewer and George Malby from the Monterey Bay Aquarium Research Institute prepare a low field proton nuclear magnetic resonance instrument for future deployment on a remotely operated submersible vehicle to study the formation of solid gas hydrates in the deep ocean.

NRL patents. NRL signed CRADAs in 1999 on topics ranging from fundamental investigations with long-term prospects for commercialization to projects that involved the implementation of mature technology developed for defense use into commercial systems. NRL also used the CRADA mechanism to formalize its participation in a project aimed at educating schoolchildren about space science.

Under the scope of a CRADA with Utah State University, NRL worked with the NASA Space Grant Consortium on Project Starshine. NRL assisted in fabricating the Starshine satellite, which was covered with 878 reflective aluminum mirrors polished by schoolchildren around the world. After its launch by NASA in May 1999 on the Space Shuttle, students worldwide were able to make measurements, which were exchanged via the Internet, to calculate the satellite's orbit and various atmospheric parameters.

In a more commercial application of NRL technology, NRL is working with several companies to transition its Matrix Assisted Pulsed Laser Evaporation (MAPLE) and MAPLE Direct Write technologies for the deposition of thin film materials. For example, YSI, Inc., has entered into a CRADA to develop and evaluate chemical sensors using NRL's deposition technology and polymer chemistry expertise. NRL has also entered into a CRADA with Potomac Photonics to develop a commercial tool for fabricating electronic devices by MAPLE Direct Write. Both companies have expressed an interest in licensing NRL's patents on the technology.

An excellent example of commercial interest in NRL technology, originally developed for military purposes, is the application of software to the auto-mated assembly of automobiles. This particular software determines the location and orientation of an object from range data. A CRADA has been signed by NRL and members of a joint venture that includes the Ford Motor Company, Perceptron, Inc., and Microdexterity Systems, Inc., with funds provided in part by an Advanced Technology Program funded by the National Institute of Standards and Technology. Under the agreement, NRL will assist in developing software for a vision system that will be part of a robotic tool for assembling automobiles.

Among NRL's CRADAs directed at fundamental research is an agreement whereby NRL, Schlumberger Technology Corporation, and the Monterey Bay Aquarium Research Institute (MBARI) will perform in situ experiments on the seafloor to study gas hydrate formation. The results will help understand these widespread, but hard to reach, materials and possibly lead to new energy sources for the future.

Lockheed Martin signed a license with the Navy in 1999 for NRL's LaserNet Fines Oil Debris Monitor, which was originally developed for Navy condition-based maintenance programs. The LaserNet Fines system uses laser imaging technology and wear particle analysis software to perform online measurements of wear debris in engine lubricants.

Also in 1999, NRL licensed its portfolio of patents on tip-based probes for measuring the nanomechanics of surfaces and single molecules to Graviton, Inc. Graviton will commercialize high-resolution chip devices for rapid identification of compounds of importance to the environmental, diagnostic, and drug discovery industries.

NRL Today

ORGANIZATION AND ADMINISTRATION

The Naval Research Laboratory is a field command under the Chief of Naval Research, who reports to the Secretary of the Navy via the Assistant Secretary of the Navy for Research, Development and Acquisition.

Heading the Laboratory with joint responsibilities are CAPT Douglas H. Rau, USN, Commanding Officer, and Dr. Timothy Coffey, Director of Research. Line authority passes from the Commanding Officer and the Director of Research to three Associate Directors of Research, a Director of the Naval Center for Space Technology, and an Associate Director for Business Operations. Research divisions are organized under the following functional directorates:

- Systems
- Materials Science and Component Technology
- Ocean and Atmospheric Science and Technology
- Naval Center for Space Technology.

NRL operates as a Navy Working Capital Fund (NWCF). All costs, including overhead, are charged to various research projects. Funding in FY 99 came from the Chief of Naval Research, the Naval Systems Commands, and other Navy sources; government agencies, such as the U.S. Air Force, the Defense Advanced Research Projects Agency, the Department of Energy, and the National Aeronautics and Space Administration; and several nongovernment activities.

PERSONNEL DEVELOPMENT

At the end of FY 99, NRL employed 3003 persons—50 officers, 127 enlisted, and 2826 civilians. In the research staff, there are 840 employees with doctorate degrees, 396 with masters degrees, and 570 with bachelors degrees. The support staff assists the research staff by providing administrative, computer-aided design, machining, fabrication, electronic construction, publication, personnel development, information retrieval, large mainframe computer support, and contracting and supply management services.

Opportunities for higher education and other professional training for NRL employees are available through several programs offered by the Employee Development Branch. These programs provide for graduate work leading to advanced degrees, advanced training, college course work, short courses, continuing education, and career counseling. Graduate students, in certain cases, may use their NRL research for thesis material.

NRL main site, located off Interstate 295 in S.W. Washington, D.C., as viewed from the Potomac River.

For non-NRL employees, several postdoctoral research programs exist. There are also agreements with several universities for student opportunities under the Student Career Experience Program (formerly known as Cooperative Education), as well as summer and part-time employment programs. Summer and interchange programs for college faculty members, professional consultants, and employees of other government agencies are also available.

NRL has active chapters of Women in Science and Engineering, Sigma Xi, Toastmasters International, Federally Employed Women, and the Federal Executive and Professional Association. Three computer clubs meet regularly—NRL Microcomputer User's Group, NeXT, and Sun NRL Users Group. An amateur radio club, a drama group (the Showboaters), and several sports clubs are also active. NRL has a Recreation Club that provides basketball and softball leagues and swim, sauna, whirlpool bath, gymnasium, and weight-room facilities. The Recreation Club also offers classes in martial arts, aerobics, swimming, and water walking.

The Community Outreach Program traditionally has used its extensive resources to foster programs that provide benefits to students and other community citizens. Volunteer employees assist with and judge science fairs, give lectures, and serve as tutors, mentors, coaches, and classroom resource teachers. The program also sponsors African American History Month art and essay contests for local schools, student tours of NRL, a student Toastmasters Youth Leadership Program, an annual holiday party for neighborhood children in December, a computer transfer program that provides surplus computers and peripherals to partnership schools, and a book donation program for both students and teachers. Through the Community Outreach Program, NRL has active partnerships with four District of Columbia, three Aberdeen, Maryland, and three Calvert County, Maryland, public schools.

NRL has an active, growing Credit Union. Since its creation in 1946, NRL Federal Credit Union (NRL FCU) has grown to over $200 million in assets and serves about 23,000 NRL employees, contractors, and their families. NRL FCU is a leader in providing innovative financial services such as a dynamic home page and Online Access (Internet home banking) with bill payer. Focusing on the credit union philosophy of *People Helping People*, NRL FCU offers a wide array of no-fee services plus financial education and assistance. NRL FCU is a full service financial institution providing various mortgage programs and creative lending services. For information about membership or any financial service, call (301) 839-8400 or click www.nrlfcu.org.

Public transportation to NRL is provided by Metrobus. Metrorail service is three miles away.

For more information, see the *NRL Review* chapter, "Programs for Professional Development."

SCIENTIFIC FACILITIES

In addition to its Washington, D.C., campus of about 130 acres and 102 main buildings, NRL maintains 14 other research sites, including a vessel for fire research and a Flight Support Detachment. The many diverse scientific and technological research and support facilities are described in the following paragraphs.
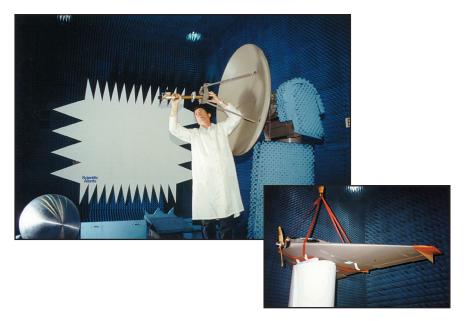
RESEARCH FACILITIES

Radar

NRL has gained worldwide renown as the "birthplace of radar" and, for a half-century, has maintained its reputation as a leading center for radar-related research and development. A number of facilities managed by NRL's Radar Division continue to contribute to this reputation.

A widely used major facility is the Compact Antenna Range (operated jointly with the Space Systems Development Department) for antenna design and development, as well as radar cross section measurements. The range is capable of simulating farfield conditions from 1 to 110 GHz with a quiet zone of approximately 7 ft in diameter and 8 ft in length. Instrumentation covers from 1 to 95 GHz. Another strong division capability is in the Computational Electromagnetics (CEM) Facility, which has capabilities for complex electromagnetic modeling, including radar target and antenna structures. The Radar Signature Calculation Facility within this group produces detailed computations of radar cross sections of various targets, primarily ships. The CEM facility includes multiple-cpu supercomputers that are also used to design phased array radar antennas. There is tremendous synergism between the CEM group and the Compact Range Facility. This provides the ability to design in the CEM environment, test in the compact, and have immediate feedback between the theoretical and experimental aspects to shorten the development cycle for new designs.

In connection with airborne radar, the division operates a supercomputer-based Radar Imaging Facility, and an inverse synthetic aperture radar (ISAR) deployed either in the air, on the ground, or aboard ship for radar-imaging data collection. A P-3 aircraft equipped with the AN/APS-145 radar and cooperative engagement capability is also available for mounting experiments.

A view of the interior of the compact range, with the primary reflector in the background. In the foreground, an antenna assembly is being readied for testing on the range positioner, while the inset photo shows a small unmanned aerial vehicle as it undergoes radar cross section measurements.

In connection with ship-based radar, the division operates a Radar Test Bed Facility at the Chesapeake Bay Detachment (CBD), Randle Cliffs, Maryland. Represented are radars for long-range air search, point defense, and surface search functions. The point defense radar, with its large (4 ft × 8 ft) X-band phased array antenna, and the ANSPQ-9B ADM systems are designed to be mobile so that testing is not limited to this specific environment.

Other installations operated by the division include an Electromagnetic Compatibility (EMC) Facility supported by a mode-stirred chamber, and a Computer-aided Engineering (CAE) Facility. The microwave microscope, a high-resolution (2-cm) capability for investigating backscatter from both surface and volumetric clutter is now operational, and a millimeter-wave radar system operating in the 94 GHz region is currently being developed. The division provides direct technical support and has direct access to data from the AN/TPS-71, the Navy's relocatable over-the-horizon radar. Concepts and engineering developments in connection with target identification are explored by using an experimental Cooperative Aircraft Identification system.

Information Technology

The Information Technology Division (ITD) is at the forefront of DoD research and development in artificial intelligence, telecommunications, computer networking, human-computer interaction, information security, parallel computation, and computer science.

The division maintains local area computer networks to support its research and hosts testbeds for advanced high-performance fiber-optic network research. These networks make available hundreds of high-performance computers to local and remote users. The ITD research networks connect to NRL's internal network via high-speed links ranging from DS-3 (45 Mbps) links on NASA Science Internet (NSI); to OC-03c on DREN/S-DREN; to OC-48c (2.4 Gbps) on ATDnet. The ATDnet is a metropolitan ATM network that supports advanced network research at OC-48c speeds and higher; other major partners include the National Aeronautics and Space Administration, the National Security Agency, the Defense Intelligence Agency, the Defense Advanced Research Projects Agency, and the Defense Intelligence Security Agency. Research on ATDnet includes introduction and testing of new networking protocols; wave division multiplexing to greatly increase network capacity; and the evolution to all-optical networks, with switching at the optical layer. Research on the high-end computational assets and networks result in close association with applications that demand these leading-edge capabilities and have allowed ITD to achieve significant results in a number of areas. These include current efforts in pushing the state of the art in motion imagery with progressive scan in high-definition TV (HDTV) where 1.5 Gbps data streams are needed to handle the raw output. The Defense Re-

The 128-processor Silicon Graphics Origin2000 system, currently with 128 Mbytes of RAM. The NRL Center for Computational Science, as a Distributed Center of the DoD High Performance Computing Modernization Program, provides such systems (at no cost) for anyone approved by the Program Office. The NRL CCS routinely upgrades high-end computing resources such as this.

search and Engineering Network (DREN) is a high-speed continental United States network that connects the four Major Shared Resource Centers (MSRCs) and fifteen Distributed Centers (DCs) of DDR&E's High Performance Computing Modernization Program (HPCMP) as well as a number of user organizations that use the HPCMP resources.

As a Distributed Center in the HPCMP, ITD's Center for Computational Science supports a range of shared resources including massively parallel computer systems and high-performance networks. Current systems include an SGI Origin2000 with 128 processors and 128 Gbytes of memory; an HP Exemplar SPP-2000 with 80 processors and 20 Gbytes of memory; and a Sun HPC Ultra with 148 distributed processors and 30 Gbytes of memory. The CCS also has more than 2.5 Tbytes of on-line shared rotating disk and robotic storage systems for fileserving and archiving that hold 300 Tbytes of multimedia data but are scalable to over a Petabyte. The Scientific Visualization Laboratory in CCS provides general support across NRL to assist scientists and engineers in producing visual renderings of their work. The Center manages the NRL local area network, NICEnet, which is transitioning from the older FDDI and shared Ethernet local area networks to a fully switched environment based on ATM backbones and both Fast Ethernet and ATM to the users's desktops. The evolutionary goal is to provide digital transparency of resources with security across the information infrastructure—from globally available archives, to the computational engines, to the networks that bring it all together at 10 Gbps directly to the desktops of the most demanding users in 2001. NICEnet provides external connections to other networks and to the Internet.

The division facilities also include an Information Security Engineering Laboratory, a Robotics Laboratory, a high-data-rate multimedia satellite transmission facility, and an experimental facility with special displays, eye and gesture trackers, and speech I/O devices for research in human/computer interaction. Laboratories for the development and testing of communication and network protocols both for Internet Protocols (IP) and ATM research are also included. These network testbeds are routinely interfaced to the DoD wide-area research networks for collaboration with other government laboratories. A wireless networking testbed is being used to develop Mobile Ad Hoc Networking (MANET) standards that can meet a wide range of military and commercial needs.

The Virtual Reality (VR) Laboratory provides the facilities and expertise to allow NRL scientists to use virtual reality in a variety of scientific investigations. Research areas include shipboard firefighting, simulation-based design, command, and control, and scientific visualization. A number of high-speed graphics workstations, including Onyx Reality Engine 2 and Infinite Reality computers, and a variety of VR peripherals comprise the VR Lab computer equipment inventory.

Current VR technologies available include desktop VR systems, head-mounted displays (HMDs), the Responsive Workbench, and the surround-screen Immersive Room. The Responsive Workbench is an interactive 3-D tabletop environment that displays computer-generated, stereographic images on the workbench surface for use in battlespace situation awareness, simulation-based design, and other applications. The surround-screen Immersive Room is a multiuser, high-resolution 3-D visual and audio en-

vironment that projects computer-generated images onto three walls and the floor to create an immersive, large-scale, shared virtual environment. It uses an SGI Onyx RE2 so scientists can interact and control their supercomputing calculations in real time.

The NEWAVE facility has been developed as a multiscreen distributed simulation laboratory and viewport. Powered by SGI and Pentium workstations and linked to the NRL parallel computing facilities with ATM/SONET networking, the facility is capable of handling high-performance computing, graphics, and distributed simulation.

Optical Sciences

The Optical Sciences Division has a broad program of basic and applied research in optics and electro-optics. Areas of concentration include fiber optics, integrated optical devices, signal processing, optical information processing, fiber-optic and infrared sensors, laser development, surveillance, and reconnaissance.

The division occupies some of the most modern optical facilities in the country. This includes an Ultralow-loss, Fiber-Optic Waveguide Facility using high-temperature infrared glass technology. There is also a Focal-Plane Evaluation Facility to measure the optical and electrical characteristics of infrared focal-plane arrays being developed for advanced Navy sensors. The IR Missile-Seeker Evaluation Facility performs open-loop measurements of the susceptibilities of IR tracking sensors to optical countermeasures. The Large-Optic, High-Precision Tracker system is used for atmospheric transmission and target signature measurements.

There are several fiber-optic sensor facilities with fiber splicers, an acoustic test cell, a three-axis magnetic sensor test cell, equipment for evaluating optical fiber coatings, and various computers for concept analysis. The Digital Processing Facility is used to collect, process, analyze, and manipulate infrared data and imagery from several sources. The Emittance Measurements Facility performs measurements of directional hemispherical reflectance. An extensive set of laboratories exist to develop and test new laser and nonlinear frequency conversion concepts and to evaluate nondestructive test and evaluation techniques.

The newest facility is the Infrared Test Chamber, or IR Range, which is an ultradry test chamber used to measure the IR signatures of new surface treatments, scale models, and components used for observables control on ships, aircraft, and missiles.

Electronic Warfare

The scope of the Tactical Electronic Warfare (TEW) Division's program for electronic warfare (EW) research and development covers the entire electromagnetic spectrum. The program includes basic technology research and advanced developments and their applicability to producing EW products. The range of ongoing activities includes components, techniques, and subsystems development as well as system conceptualization, design, and effectiveness evaluation. The focus of the research activities extends across the entire breadth of the battlespace. These activities emphasize providing the methods and means to counter enemy hostile actions—from the beginning, when enemy forces are being mobilized for an attack, through to the final stages of the engagement. In conducting this program, the TEW Division has an extensive array of special research and development laboratories, anechoic chambers, and modern computer systems for modeling and simulation work. Dedicated field sites and an NP-3D EW flying laboratory allow for the conduct of field experiments and operational trials. This assembly of scientists, engineers, and specialized facilities also supports the innovative use of all fleet defensive and offensive EW resources now available to operational forces through the Naval Science Assistance Program.

Laboratory for Structure of Matter

This laboratory investigates the atomic arrangements in materials to improve them or facilitate the development of new substances. Various diffraction methodologies are used to make these investigations. Subjects of interest include the structural and functional aspects of energy conversion, ion transport, device materials, and physiologically active substances such as drugs, antibiotics, and antiviral agents. Theoretical chemistry calculations are used to complement the structural research. A real-time graphics system aids in modeling and molecular dynamics studies.

Chemistry

NRL has been a major center for chemical research in support of naval operational requirements since the late 1920s. The Chemistry Division continues this tradition with a broad spectrum of basic and applied research programs focusing on controlled energy release (fuels, fire, combustion, countermeasure decoys, explosives), surface chemistry (corrosion,

Color-enhanced scanning tunneling microscopy image of a cross-section showing the atomic-scale structure at the interfaces between GaSb and InAs superlattice layers. This work, incorporating sample preparation by scientists in the Electronics Sciences and Technology Division, STM measurement and interpretation by Chemistry Division staff, and modeling by theorists in the Materials Science and Technology Division, illustrates the multidisciplinary character of NRL research.

adhesion, tribology, adsorbents, film growth/etch), advanced materials (high-strength/low-weight structures, drag reduction, damping, polymers, thin films), and advanced detection techniques (environment, chemical/biological, surveillance). Facilities for research include:

Chemical analysis facilities, including a wide range of modern photon/electronic, magnetic- and ion-based spectroscopic/microscope techniques for bulk and surface analysis;

X-ray facility, with laboratory X-ray sources, monochromator, detectors, and related equipment for 0.7 to 25 KeV and dose rates up to 10^5 rads/s;

Synchrotron Radiation Facility, with intense, monochromatic X-ray photon beams tunable from 10 eV to 12 KeV available from two beam lines developed by NRL at the National Synchrotron Light Source at the Brookhaven National Laboratory. Environmental target chambers span a pressure range from 10^{-12} to 10^5 atm and temperatures from 10 to 1500 K;

Nanometer measurement facility, which includes fabrication and characterization capability based on scanning tunneling microscopy/spectroscopy, atomic force microscopy, and related techniques; materials synthesis/property measurement facilities with special emphasis on polymers and surface/film processing; and

Fire research facilities, ranging from laboratory combustion chemistry, to a 10^4 ft^3 fire-research chamber (Fire I) and the 475-ft ex-USS *Shadwell* (LSD-15) advanced fire research ship.

The new Environmental Quality Sciences Section has a mission that includes characterization of chemically polluted environments, remediation technologies and evaluations, pollution-prevention strategies for Fleet and shore-side operations, environ-mental security, and disposal of chemical-warfare agents. Facilities in support of this research are laboratories for molecular biology, microbiology, biodegradation assessment, environmental biosensors, and geochemistry. In addition, a mesocosm facility has been established to bridge between laboratory and field work, with controlled scale-up of environmental systems.

Materials Science and Technology

NRL has capabilities for X-ray and electron-diffraction analyses and for electron and Auger spectroscopy. Scanning, transmission, and combined scanning-transmission electron microscopes are used to study surface and/or internal microstructures. The division has a secondary ion mass spectrometer for surface analysis that significantly extends the diagnostic capability of the technique. A high-resolution, reverse-geometry mass spectrometer is used to probe reactions between ions and molecules. The Laboratory has a fully equipped fatigue and fracture laboratory, a modern vacuum arc-melting furnace for reactive metals, an ultrasonic gas-atomization system for making metal powders, and hot isostatic press facilities. The Laboratory's cryogenic facilities include dilution refrigerators and superconducting magnetic sensors for measuring ultrasmall magnetic fields. Also available are two molecular beam epitaxy devices for growing thin films. In addition, division facilities include:

High-Power Microwave (HPM) Facility: The large anechoic chamber (4.9 m × 4.9 m × 9.8 m) can be used at frequencies ranging from 0.5 to 94 GHz. Effects, susceptibility, and survivability of systems are the major research areas of interest.

Trace Element Accelerator Mass Spectrometry (TEAMS) – 3 MV Tandem Pelletron Accelerator Facility: Used for standard materials analysis such as Rutherford backscattering, for MeV-energy ion implantation, and for accelerator mass spectrometry (AMS). AMS measures trace elements in parallel with 3-D imaging at 10-µm lateral resolution (0.01 µm in depth) to 10-ppt sensitivity, and isotopes for sample dating and forensics.

Laser Facilities: Pulses of up to several joules are available from one system, while time resolutions down to 30 femtoseconds are produced by another. Synchronized Q-switched oscillators are configured for pump-probe experiments.

Thin-Film Preparation Facilities: The division has several major capabilities for preparation of thin films of advanced materials, such as high-temperature superconductors and active dielectrics. These include ion-assisted evaporation (which produces dense, adherent films), various dc plasma sources (which can etch as well as deposit films), and pulsed laser deposition (for production of chemically complex films).

Ion Implantation Facility: The facility consists of a 200-keV ion implanter with specialized ultra-high vacuum chambers and associated in situ specimen analysis instrumentation.

Laboratory for Computational Physics and Fluid Dynamics

The Laboratory for Computational Physics and Fluid Dynamics is in round-the-clock production for computational studies in the fields of compressible and incompressible fluid dynamics, reactive flows, fluid-structure interaction (including submarine, ship, and aerospace applications), atmospheric and solar magnetoplasma dynamics, application of parallel processing to large-scale problems such as unstructured grid generation for complex flows, target tracking and correlations for battle management, and other disciplines of continuum and quantum computational physics. The facility is used to develop and maintain state-of-the-art analytical and computational capabilities in fluid dynamics and related fields of physics, to establish in-house expertise in parallel processing and on-line graphical rendering for large-scale scientific computing, to perform analyses and computational experiments on specific relevant problems, and to transfer this technology to new and ongoing projects through cooperative programs.

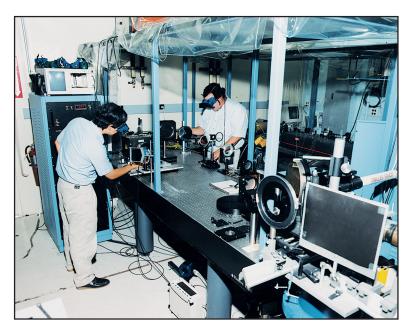The Parallel High Performance Computer/ Graphics Facility is a heterogeneous high-performance computer system composed of a number of autonomous computers with a composite peak speed equivalent to about 15 Cray 90 processors. The system is coupled directly to the advanced video recording center described below. The main computational engine comprises three Intel iPSC/860 Touchstone Gamma parallel supercomputers supported by the hardware and software environment necessary to develop, debug, and benchmark parallel simulations. With multi-Mflop processors as building blocks, the Intel iPSC/860 is a MIMD-distributed memory machine configured as a hypercube. These three machines comprise a block of 224 parallel nodes with a peak computational speed of 18 Gflops with a cross-connected disk farm file system and network connections.

The facility's disk farm also supports three IBM RS/6000 and three DEC AXP high-capacity compute-server computers, providing the facility with medium-to-large-scale memory and computational power enabling heterogeneous simulations with a significant scalar component, algorithm development, and diagnostic and postprocessing for large simulations. Special software allows simultaneous use of these computers on a single problem. Access to various other HPC capabilities around the United States is accomplished through this system by using the new DoD high-bandwidth communication networks. A six-processor, 5-Gbyte SGI Onyx provides the division with state-of-the-art high-performance visualization.

A high-quality video studio has been created around a Sony D2 digital recording system, with a coupled Lyon-Lamb animation controller and a large memory Silicon Graphics ONYX workstation. Through the network, other graphics stations, including the extensive resources of NRL's Visualization Laboratory, can create and record high-quality graphical images of simulation data for analysis and presentation by using digital recording techniques.

Plasma Physics

The Plasma Physics Division is the major center for in-house Navy and DoD plasma physics research. The division conducts a broad experimental and theoretical program in basic and applied research in plasma physics, which includes laboratory and space plasmas, pulsed-power sources, plasma discharges, intense electron and ion beams and photon sources, atomic physics, laser physics, advanced spectral diagnostics, plasma processing, nonlinear dynamics and chaos, and numerical simulations. The facilities in-

The NRL Table-Top-Terrawatt (T^3) Laser Facility. The T^3 laser currently operates at 0.4 ps, 2.5 TW, and 5×10^{18} W/cm^2 and provides a facility to conduct research in intense laser-plasma interactions, intense laser-electron beam interactions, and intense laser-matter interactions.

clude an extremely high-power laser—Pharos III—for the laboratory simulation of space plasmas and nuclear weapons effects studies and a short pulse, high-intensity Table-Top Terawatt (T^3) laser to study intense laser-plasma, laser-electron beam, and laser-matter interactions. The division also has an 11 m^3 space chamber capable of reproducing the near-Earth space plasma environment and a Large Area Plasma Processing System (LAPPS) facility to study material modification such as surface polymerization or ion implantation. The division has developed a variety of pulsed-power sources to generate intense electron and ion beams, powerful discharges, and various types of radiation. The largest of these pulsers—GAMBLE II—is used to study the production of megampere electron and ion beams and to produce very hot, high-density plasmas. Other generators are used to produce particle beams that are injected into magnetic fields and/or cavities to generate intense microwave pulses. A large array of high-frequency microwave sources (35 to 120 GHz) are available to conduct research on microwave processing of advanced ceramic materials. In particular, the division added a 15-kW, continuous wave, 83 GHz gyrotron to its facility for research on high-frequency microwave processing of materials. The Russian-made gyrotron produces a focused, high-intensity millimeter-wave beam (10^3-10^5 W/cm^2) that has unique capabilities for rapid, selective heating of a wide range of nonmetallic materials. The new gyrotron-based system will be used to investigate the application of such beams to important areas of material processing, including coating of materials, soldering and brazing, and treatment of ceramics, semiconductors, and polymers.
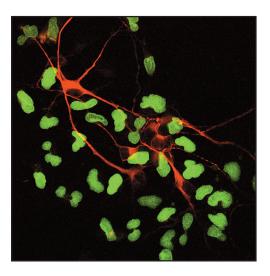
A major 3 kJ KrF laser facility (Nike) opened in June 1995. This facility is made up of 56 laser beams and is single pulsed (4 nanosecond pulse). This facility provides intense radiation for studying inertial confinement fusion (ICF) target heating at short wavelengths (0.25 microns) and high-pressure physics.

Electronics Science and Technology

In addition to specific equipment and facilities to support individual science and technology programs, NRL operates the Nanoelectronics Processing Facility (NPF), the Penthouse Processing Facility (PPF), the Laboratory for Advanced Material Synthesis (LAMS), the EPICENTER, the Laser Facilities (LF), and the Space Solar Cell Characterization Facility (SSCCF). The NPF's mission is to provide service to both NRL and external organizations requiring micro- and nanofabrication processing support. Lithography is a particular strength of the NPF, with definition of feature sizes down to 150 angstroms possible with an e-beam nanowriter. The NPF can supply items ranging from individual discrete structures and devices to circuits with very-large-scale integration complexity. The PPF is dedicated to processing III-V semiconductor devices and circuits in addition to serving

the hands-on fabrication needs of individual NRL scientists. The PPF uses a single-pass air-ventilation system to minimize human risk from potentially hazardous III-V semiconductor processes and associated chemicals, thereby further meeting existing safety standards. The LAMS uses organometallic vapor phase epitaxy to synthesize a wide range of thin films such as InSb, InGaP, InP, and GaN. The EPICENTER (a joint activity of the Electronics Science and Technology, Materials Science and Technology, Optical Science, and Chemistry Divisions) is dedicated to the production of multilayer microstructures using in situ surface analytical techniques in one of several ultrahigh vacuum, molecular-beam-epitaxy growth and processing chambers—one for growth of conventional III-V semiconductors, one for vacuum processing, one for growth of III-V semiconductor ferromagnetic materials, one for growth of 6.1 angstrom II-V semiconductors and another for growth of magnetic materials and II-VI semiconductors. The Laser Facilities consist of an Ultrafast Laser Laboratory (ULL) that is optimized for the characterization of photophysical and photochemical processes in materials on a timescale of tens of femtoseconds and a Laser Single-Event Effects Facility (LSEF) that uses a synchronously pumped dye laser system for simulating the effects of charge deposited in semiconductors characteristic of space radiation. The SSCCF studies the effect of particle irradiation on new and emerging solar cell technologies for space applications.

Bio/Molecular Science and Engineering

The Center for Bio/Molecular Science and Engineering conducts research and development using biotechnological approaches to solve problems for the Navy, DoD, and the nation at large. Problems currently being addressed include advanced material development (for electronic, biomedical, and structural applications), environmental quality (including pollution cleanup and control), and biological warfare defense. The approach to these problems involves long-term research focused on the study of complex materials systems, coupled with integrated exploratory and advanced development programs. The staff of the center is an interdisciplinary team that performs basic and applied research and development in areas that require expertise in bio- and surface chemistry, biophysics, genetic engineering, cell biology, advanced organic synthesis, solid-state and theoretical physics, and electronics and materials engineering. In addition, the center has many collaborations throughout the Laboratory, at universi-

Fluorescence photomicrograph of neural stem cells and stem cell-derived neurons. These cells supply cell elements for a cell-based sensor that can be used to detect toxins.

ties, and in industry to ensure that a broad base of the required expertise and critical evaluations are part of the research and development programs. Highlights of the program include the manipulation of biologically derived structures on the nanometer scale, the development of ferroelectric liquid crystal systems with microsecond response times, discovery of an advanced resist system for high-speed, high-density integrated circuits, the patterning of neuronal cells to form neural networks, and the development of biosensors for environmental monitoring.

The center occupies recently renovated laboratories and offices in Building 30. These modern facilities, designed to be used well into this century, include general laboratories for research in chemistry, biochemistry, molecular biology, and physics. Specialized areas include a 600-ft^2 Class 1000 clean room; an advanced Electron Microscope facility; and a Scanning Probe Microscope laboratory. Instrument rooms provide access to a variety of spectrophotometers (IR, GC-MS, NMR, and UV-Vis) and other equipment used in biochemical or physical analyses of biomaterials. Additional laboratories accommodate an X-ray diffraction instrument, a liquid crystal fabrication facility, and equipment for advanced electronics and biosensor programs.

Acoustics

The Acoustics Division has three integrated acoustic pool facilities, including one with a sandy bottom, that support research in submarine target characteristics for antisubmarine warfare, submarine acoustic design and quieting, sensors for hull-mounted sonars,

NRL's Satellite-Linked Vertical Line Array (SVLA) buoy during a recent ocean deployment. Data from an array of hydrophones are collected and stored within the buoy and simultaneously transmitted to both ships in the vicinity and distant shore stations using RF and satellite communications.

and structural acoustics for mine countermeasures and torpedo quieting. Scaled submarine targets, real mine structures, sensors mounted on hull simulators, underwater buried objects, and actual torpedoes can all be examined with advanced nearfield holographic and scanning 3-D laser vibrometer systems to measure and visualize the sound fields near a structure, the vibrations of the structure itself, the resulting farfield sound fields, and the physics of the sound-structure-fluid interactions.

The division operates several sound sources and receiving arrays for the generation and reception of sound in at-sea experiments. Sound sources include three XF-4 units that can be operated while being towed by a ship and two battery-operated organ-pipe sources that can project single tones from offboard moorings. In addition, the division has a battery-operated rubidium-clock-controlled, programmable sound source mooring that can transmit sounds having arbitrary waveforms. Receive systems include a moored 32-channel array that RF telemeters data to a recording site at a rate up to 50 kHz/channel, and a 64-channel seismic oil-filled array. The division also has unique, self-recording digital acquisition buoy systems (DABS) that are used to obtain multichannel (up to 128) acoustic data in the 10 Hz to 5 kHz regime. These systems provide up to 250 Gbytes of data on a single 15-inch reel of 1-inch tape. A Satellite Vertical Line Array (SVLA) Buoy System is de-

signed for the collection of acoustic and oceanographic data unattended for up to one month; is capable of handling arrays of up to 64 hydrophones; and is capable of implementing signal processing algorithms onboard the buoy prior to transmission. The system supports two-way satellite communication—providing a high data-rate link (up to 1.5-Mbit/s) for data transfers from the buoy to shore, and a low-data-rate link in the opposite direction, permitting scientists to control buoy functions. A high-data-rate line-of-sight telemetry capability based on GPS-linked directional antennas is currently being installed.

The division conducts underwater acoustic communications research using digital, acoustic modems capable of receiving and processing signals from 8 channels at various carrier frequencies and with various bit rates. An Acoustic Communication Laboratory provides environment simulation, pre-experiment testing and preparation, and post-experiment data analysis.

The division operates high-frequency (up to 600 kHz) acoustic measurement systems to obtain scattering, target strength, and propagation data using bottom-moored instrumentation towers and a high-speed, remotely operated vehicle. These data are used to simulate the performance of weapons and mine countermeasure sonars.

The Tactical Oceanography Simulation Laboratory (TOSL) is a modeling and simulation architecture consisting of a set of tools for processing climatology and real-time environmental data and applying energy propagation models to those data. TOSL features a high-performance computational capability to provide real or near-real-time calculations in support of training, war games, operations rehearsal, and other distributed simulation functions. TOSL is coupled via Ethernet and SIPRNET with the Tactical Oceanography Wide Area Network (TOWAN) repository of environmental data, which allows full participation in a distributed simulation environment.

Remote Sensing

The Remote Sensing Division conducts a program of basic research, science, and applications to develop new concepts for sensors and imaging systems for objects and targets on Earth, in the near-Earth environment, and in deep space. The research, both theoretical and experimental, leads to discovering and understanding of the basic physical principles and mechanisms that give rise to background environmental emissions and targets of interest and to absorption and emission mechanisms of the inter-

vening medium. Accomplishing this research requires the development of sensor systems' technology. The developmental effort includes active and passive sensor systems used for study and analysis of the physical characteristics of phenomena that evolve from naturally occurring background radiation, such as that caused by the Earth's atmosphere and oceans and man-made or induced phenomena, such as ship/submarine hydrodynamic effects. The research includes theory, laboratory, and field experiments leading to ground-based, airborne, or space systems for use in remote sensing, astrometry, astrophysics, surveillance, nonacoustic ASW, meteorological/oceanographic support systems for the operational Navy, and the environmental/global climate change initiatives. Special emphasis is given to developing space-based platforms and exploiting existing space systems.

The Remote Sensing Division conducts airborne hyperspectral data collections for characterization of the environment. Hyperspectral data are series of pictures, taken simultaneously, of a scene at many different wavelengths (colors). The sensors are built and calibrated in-house, although they rely heavily on commercial off-the-shelf elements. The most recent sensor was specifically designed for use over ocean areas. It covers the 400 to 1000 nanometer wavelength range with 128 different wavelengths (channels). The sensor consists of a standard video camera lens, a grating spectrograph, and a 1024×1024 pixel charge-coupled device (CCD). The spectrograph and CCD are specially designed to achieve high sensitivity in the blue end of the spectrum to optimize water-penetrating measurements. This makes possible measurements such as the determination of the ocean bottom type (coral, sea grass, sand, rock, etc.) to water depths of as much as 20 meters (in clear water), and the identification of material in the water column (phytoplankton, sediments, colored dissolved organic matter, etc.). The sensor is very compact and can be flown at heights of 8000 to 10,000 feet, simply "looking" out of a hole in the bottom of the airplane. At ground speeds of 90 knots, the data can still be collected digitally and stored on computer. It is then processed in a ground system operating on a standard personal computer.

Proper interpretation of the hyperspectral data requires calibration of the sensor. This means both radiometric calibration and spectral calibration. The latter plays a critical role in the successful correction of the data for atmospheric effects. The Remote Sensing Division operates an Optical Calibration Facility to perform these calibrations. NIST radiometric standards are transferred to a large integrating sphere.

The integrating sphere has 10 precisely controlled quartz-halogen lamps to enable linearity measurements. A set of gas emission standards provides wavelength calibration. As a result, the complete process of data collection through data analysis can be handled in-house.

The Navy Prototype Optical Interferometer (NPOI), a major facility of the Remote Sensing Division, is actually two collocated instruments for making high-angular-resolution optical measurements of stars. Light from widely separated individual siderostats is combined simultaneously to synthesize the angular resolution of a telescope tens to hundreds of meters in diameter. Four siderostats are placed in an array with extremely accurate metrology to enable very-high-precision measurements of stellar positions (wide-angle astrometry). These measurements are used by the U.S. Naval Observatory to refine the celestial reference frame, determine Earth rotation parameters, and thus satisfy Navy requirements for precise time and navigation data. They also provide determinations of basic astrophysical parameters, such as stellar masses and diameters. Additional relocatable siderostats can be placed out to distances of 250 m from the array center and used to construct very-high-resolution images of stars. These images provide fundamental astrophysical information on stellar structure and activity. When complete, the NPOI will be the most advanced high-resolution imaging optical interferometer in the world.

To validate numerical and theoretical efforts ongoing within the Remote Sensing Division, extensive hierarchical-coupled experiments are carried out in the Free-Surface Hydrodynamics Laboratory. This laboratory is used to study free-surface turbulence interactions, wave-generation phenomena, jet-flow phenomena, vorticity dynamics, and free-surface/surfactant interactions. Emphasis is placed on those processes that determine the fluxes of heat, mass, and momentum across the air-sea interface. State-of-the-art diagnostic tools are available, such as Langmuir film balance to measure the properties of surface films, hot-wire and laser-Doppler anemometry, and the new quantitative flow techniques of laser speckle, particle tracking, and particle image velocimetry. The laboratory is also equipped with an IR camera with a 20×10^{-3} K resolution. These experimental diagnostic techniques use high-powered lasers, high-tolerance optical lenses, and extensive ultra-high-resolution video-imaging hardware and PC-based computerized systems. Further computational assets consist of powerful graphical computer work stations, the NRL Connection Machine, and other off-site Cray supercomputer systems.

Oceanography

The Oceanography Division is the major center for in-house Navy research and development in oceanography. It is known nationally and internationally for its unique combination of theoretical, numerical, experimental, and remote sensing approaches to oceanographic problems. The division numerically models the ocean and coastal areas of the world. This modeling is conducted on the Navy's and DoD's most powerful vector and parallel-processing machines. To study the results of this intense modeling effort, the division operates a number of highly sophisticated graphic systems to visualize ocean and coastal dynamic processes. The seagoing experimental programs of the division range worldwide. Unique measurement systems include towed sensor and advanced microstructure profiler systems for studying micro- and fine-scale ocean structures; a wave measurement system to acquire in situ spatial properties of water waves; a salinity mapper that acquires images of spatial and temporal sea surface salinity variabilities in littoral regions; an integrated absorption cavity, optical profiler system, and towed optical hyperspectral array for studying ocean optical characteristics; and self-contained bottom-mounted upward-looking acoustic Doppler current profilers for measuring ocean variability. In the laboratory, the division operates an environmental scanning electron microscope for detailed studies of biocorrosion in naval materials. The division's remote sensing capabilities include the ability to analyze and process multi/hyper-spectral, IR, SAR, and other satellite data sources. The division is a national leader in the development and analysis of Sea WiFS data for oceanographic processes and naval applications in littoral areas.

Marine Geosciences

The Marine Geosciences Division is the major Navy in-house center for research and development in marine geology, geophysics, geodesy, geoacoustics, geotechnology, and geospatial information and systems. The division has unique suites of instrumentation and facilities to support laboratory and field experimental programs.

The instrumentation used in the field experiments is deployable from ships, remotely operated and unmanned vehicles, and airborne platforms and by divers. Seafloor and subseafloor measurements use the Deep-Towed Acoustic Geophysical System (DTAGS—250 to 650 Hz); high-resolution sidescan sonars (100 and 500 kHz); the Acoustic Seafloor Classification System (ASCS-15, 30, and 50 kHz); ocean bottom seismometers and magnetometer; the In Situ Sediment Acoustic Measurement System (ISSAMS); underwater stereo photography; and nearshore video imaging systems. ISSAMS has specialized probes that measure acoustic compressional and shearwave velocities and attenuation, pore water pressure, and electrical conductivity in surficial marine sediments. Three unmanned, diesel-powered, radio-controlled, 8-m semisubmersibles are used to develop improved hydrographic survey techniques, sensor systems, and navigation capabilities. Two vehicles are modified 1985 Sea Lions called ORCAs, and one is a new vehicle called Remote Mine Hunting System Oceanographic (RMSO).

Laboratory facilities include sediment physical, geotechnical, and geoacoustic properties and sediment core laboratories. The Electron Microscopy Facility is the focal point for research in microscale biological, chemical, and geological processes. The key instrumentation includes 100 and 300 kVa transmission electron microscopes with environmental cells. The environmental cells allow hydrated and gaseous experiments. The Moving Map Composer Facility is used to design and write mission-specific map coverages for F/A-18 and AV-8B tactical aircraft onto militarized optical disks. The National Imagery and Mapping Agency also uses this state-of-the-art computer facility to update the compressed aeronautical chart library on CD for distribution. The Geospatial Information Data Base (GIDB) capability provides Internet access to the Digital Nautical Chart data, mapping data, imagery, and other data types such as video and pictures. This development tool can be used for planning, training, and operations. The division also operates the NRL Magnetic Observatory at Stennis Space Center, Mississippi. This magnetically clean area consists of an array of magnetometers that measure Earth's ambient magnetic field. The observatory is part of a worldwide observing system.

Marine Meteorology

The Marine Meteorology Division is located in Monterey, California. NRL-Monterey (NRL-MRY) is the only Navy facility with a mission to serve the Navy's needs for basic research in atmospheric sciences and its need for the development of meteorological analysis and prediction products to support global and tactical operations. The division is dedicated to advancing fundamental scientific understand-

ing of the atmosphere, to applying scientific discoveries in the development of innovative objective weather prediction systems, and to developing ways to provide atmospheric data input to the tactical decision maker.

NRL-MRY is collocated with Fleet Numerical Meteorology and Oceanography Center (FNMOC), the Navy's operational center of expertise in numerical weather prediction. This provides NRL-MRY efficient access to a variety of classified and unclassified computer resources, databases, and numerical prediction systems. Large supercomputer mainframes and databases at FNMOC are used along with DoD High Performance Computing Modernization Program resources and local NRL-MRY resources to develop and transition operational analysis and prediction systems, and to provide on-site and remote access to the model output data for continued research purposes. In addition, interfaces to the Defense Research and Engineering Network have also been established.

Locally, to support research and development needs, NRL-MRY has established the Bergen Data Center. This Center includes a 24TB capacity data center with a hierarchical storage management capability to provide archival and easy retrieval of research data sets. The John B. Hovermale Visualization Laboratory provides state-of-the-art capability for data visualization, which aids the interpretation of both observational and modeled data and the development of weather briefing tools. High-performance graphics workstations, network file-servers, and tactical applications systems are used to conduct numerical weather prediction experiments, process and analyze satellite data, perform simulation studies, and provide demonstrations of tactical weather products. State-of-the-art satellite receiving and processing systems allow local collection of real-time geostationary

data globally, from four different satellites, for applications research in support of the Navy and Joint Typhoon Warning Center operations. This capability has allowed NRL-MRY to take the lead in developing meteorological applications of satellite data for the NSDS-E (Navy Satellite Display System-Enhanced), which is currently being installed at the Navy's regional meteorological/oceanographic (METOC) centers.

Space Science

The Space Science Division conducts and supports a number of space experiments in the areas of upper atmospheric, solar, and astronomical research aboard NASA, DoD, and other government-agency space platforms. Division scientists are involved in major research thrusts that include remote sensing of the upper and middle atmospheres, studies of the solar atmosphere, and astronomical radiation ranging from the ultraviolet through cosmic rays. In support of this work, the division maintains facilities to design, construct, assemble, and calibrate space experiments. A network of computers, workstations, image-processing hardware, and special processors is used to analyze and interpret space data. The division's space science data acquisition and analysis efforts include: mission operations and data analyses of the Oriented Scintillation Spectrometer Experiment (OSSE) for NASA's Compton Observatory; observation of the Sun's interaction with the Earth's upper atmosphere through the Solar Ultraviolet Spectral Irradiance Monitor (SUSIM) experiment in support of NASA's Upper Atmosphere Research Satellite (UARS); observation and analysis of solar flares using the Bragg Crystal Spectrometer (BCS) on the Japanese Yohkoh space mission; and observation and

In May, a group of 23 students involved in the Arizona State University satellite program visited NRL to learn more about the Navy's history and experience in the development and demonstration of space systems.

analysis of the evolution and structure of the solar corona from the disk to 0.14 AU. This latter effort involves acquiring and analyzing data from the Large-Angle Spectrometric Coronagraph (LASCO) and Extreme Ultraviolet Imaging Telescope (EIT) on the Solar Heliospheric Observatory satellite. In each of these missions, NRL maintains a complete database of spacecraft observations and control over acquisition of data from new observations. These data are available to qualified investigators at DoD and civilian agencies. In addition, the division has a sounding rocket program that affords the possibility of obtaining specific data of high interest and of testing new instrument concepts. These include the general area of high-resolution solar and stellar spectroscopy, extreme ultraviolet imagery of the Sun, and high-resolution, ultraviolet spectral-imaging of the Sun.

In addition, selected celestial and atmospheric targets in the ultraviolet and X-ray bands are observed by three Advanced Research and Global Observation Satellite (ARGOS) experiments—Global Imaging of the Ionosphere (GIMI), High-Resolution Airglow and Auroral Spectroscopy (HIRAAS), and Unconventional Stellar Aspect (USA). ARGOS was successfully launched on February 23, 1999. As part of this program, NRL is establishing collaborative programs to make use of ARGOS data to validate various upper atmosphere models and to study time phenomena in X-ray sources.

Optical calibration facilities, including clean rooms, are maintained to support these activities. These calibration facilities are routinely used by outside groups to support their own calibration requirements.

Space Technology

In its role as a center of excellence for space systems research, the Naval Center for Space Technology (NCST) designs, builds, analyzes, tests, and operates spacecraft as well as identifies and conducts promising research to improve spacecraft and their support systems. NCST facilities that support this work include large and small anechoic radio frequency chambers, clean rooms, shock and vibration facilities, an acoustic reverberation chamber, large and small thermal/vacuum test chambers, a control system interaction laboratory, satellite command and control ground stations, a fuels test facility, and modal analysis test facilities. Also, the Center maintains and operates a number of electrical and electronic development laboratories and fabrication facilities for radio frequency equipment, spacecraft power systems, telemetry, and command and control systems, and includes an electromagnetic interference-electromagnetic compatibility test chamber. NCST has a facility for long-term testing of satellite clock time/frequency standards under thermal/vacuum conditions linked to the Naval Observatory; a 5-m optical bench laser laboratory; and an electro-optical communication research laboratory to conduct research in support of the development of space systems.

RESEARCH SUPPORT FACILITIES

Technical Information Services

The Ruth H. Hooker Research Library carries out a comprehensive program of scientific information services to support the research of NRL-DC employees, on-site contractors, and ONR Headquarters staff. The Library maintains a 50,000-volume research collection of technical books and scholarly monographs; a scientific journal collection containing approximately 1,000 current subscriptions, with extensive back files maintained as bound volumes or on microfilm; and a research reports collection of more than one million items stored in paper, microform, and digital format. Services include the circulation of library materials, interlibrary loan, literature searches, and a full range of reference and information services covering both open-literature and classified information sources.

The Library is in the forefront in implementing digital services to enable researchers to meet their information needs 24 hours a day, 7 days a week, from work, at home, or while on travel. Through the InfoWeb Information System and Gateway [http://infoweb.nrl.navy.mil], NRL users in Washington, DC, Bay St. Louis, Mississippi, Monterey, California, and at ONR Headquarters in Arlington, Virginia, have a single point of entry to hundreds of locally stored and distributed databases and publications. Some important examples of InfoWeb resources are: the STILAS Web-based catalog with hyperlinks to thousands of reports the Library has digitized; OCLC First Search for searching 50 databases; the ISI "Web of Science" Science Citation Index Expanded, covering the years 1973 to present; the subscription module for the Contents-to-Go journal alerting service; and TORPEDO Ultra, for browsing and searching some 250 locally archived journals, thousands of research reports, and NRL publications including press releases, journal articles, and conference papers. InfoWeb also links users to another 300 journals available from publisher Web sites under license agreements implemented by the Library.

The Library has entered into a collaborative relationship with publishers and with other libraries to increase the range of digital resources it can make available. For example, it is currently assisting the American Institute of Physics in expanding the digital contents of its Web-based Online Journal Service under a Cooperative Research and Development Agreement (CRADA). In 1997, the Library formed the National Research Library Alliance with the libraries of the National Institute of Standards and Technology, NASA Goddard Space Flight Center, and the National Science Foundation. In 1998, it became an associate member of the New Mexico Library Alliance, strengthening its relationships with both Los Alamos National Laboratory and the Air Force (Phillips) Research Laboratory. In 1998, it also became part of the collaborative Digital Library Initiative at the University of Illinois at Urbana-Champaign. The NRL Library joins with other Navy libraries to license databases and electronic publications through the Consortium of Navy Libraries.

The new Technical Information Services Branch combines publications, graphics, and photographic services into an integrated organization.

Publication services include writing, editing, composition, publications consultation and production, and printing management. Quick turnaround black and white as well as color copying services are provided. The primary focus is on using computer-assisted publishing technology to produce scientific and technical information containing complex artwork, equations, and tabular material.

Graphic and photographic support includes technical and scientific illustrations, computer graphics, design services, photographic composites, display panels, sign making, and framing. Photographic services include still-camera coverage for data documentation both at NRL and in the field. Photographic images can also be captured with state-of-the-art digital cameras. Photofinishing services provide custom processing and printing of black and white and color films. Quick-service color prints are also available. Video services include producing video reports of scientific and technical programs. A video studio and editing facility with high-quality Beta Cam and digital video editing equipment are available to support video production. The NRL Exhibits Program develops and produces displays, audiovisual material, and multimedia programs for presentation at technical meetings, conferences, and symposia. The Multimedia Center has the capability of authoring/producing multimedia programs. The Center uses two complete multimedia systems with Macromedia Director and Adobe Photoshop and a digital video editing system, the AVID Media Composer 1000. The Imaging Center offers high-quality output from computer-generated files in EPS, Postscript, PICT, TIFF, Photoshop, and PowerPoint. Photographic-quality color prints and viewgraphs are available from Kodak dye-sublimation printers. High-resolution scanning to a Macintosh or PC disk is available. The NovaJet Pro 600c printer offers exceptional color print quality up to 600 dpi. It produces large-format posters and signs up to 60 inches wide.

The Administrative Services Branch is responsible for collecting and preserving the documents that comprise NRL's corporate memory. Archival documents include personal papers and correspondence, laboratory notebooks, and work project files—documents that are appraised for their historical or informational value and considered to be permanently valuable. The branch provides records management services, training, and support for the maintenance of active records, including electronic records and

The Visual Imaging Services Section of the Technical Information Division has a color, wide-format Novajet Pro 600E printer and laminator that produces prints up to 60 inches wide, unlimited length, and at resolutions up to 600 dpi.

21

e-mail, as an important information resource. The Administrative Services Branch is also responsible for NRL's postal mail services, NRL's Forms and Reports management programs (including electronic forms), coordination of NRL's parking facilities, and scheduling of NRL auditoriums. The Administrative Services Branch also compiles and publishes the NRL Code Directory and Organizational Index and provides NRL Locator service.

Center for Computational Science

The Center for Computational Science (CCS) conducts research and development to further the advancement of computing and communications systems to solve Navy problems. Promising technologies are transitioned to production systems. The CCS develops and maintains a leading-edge information infrastructure that provides support for NRL, Navy, and DoD research. The CCS participates as a Distributed Center in the DoD High Performance Computing Modernization Program with three massively parallel High Performance Computing (HPC) systems: a 128-processor SGI/Cray Origin2000 with 128 Gbyte of memory, an 80-processor HP/Convex Exemplar SPP-2000 with 20 Gbytes of memory, and a 148-processor Sun HPC Ultra with 30 Gbytes of memory. File services and archival storage are provided by robotic storage systems running the Multiresident Andrew File System (MRAFS) for both NRL and HPC applications.

The CCS pioneered and maintains the Washington area ATDnet experimental ATM network and is a partner in the MONET research effort. MONET is a leading-edge, all-optical, transparent network being deployed within ATDnet as a part of the DARPA/HPCC Next Generation Internet initiative.

The CCS collaborates with industry and DoD in the development of leading-edge progressive motion imagery for broadcast and network dissemination of all-digital HDTV signals at 720-p and 1080-p.

Additional CCS computational facilities are provided for general NRL use. These include the Scientific Visualization Laboratory (Viz Lab), which functions as an information center, a video production unit, and a training center for the latest tools in scientific visualization and visual supercomputing. Researchers have direct or networked access to computational and high-end graphics workstations. The Viz Lab staff also assists researchers in porting their scientific applications to the Virtual Reality Lab's GROTTO for 3-D, interactive, stereo viewing. In addition, the Viz Lab has recently installed a completely digital, broadcast-video editing suite. Alone

or assisted, a researcher can quickly produce a professional-quality video, including titles and special effects, from a montage of computer-generated video, stills, graphs, overheads, or even raw data.

The CCS manages the NRL local area network, NICEnet, which provides access to NRL campus-wide and remote assets, including DoD unclassified and classified networks and the Internet. NICEnet has FDDI backbones and Ethernet, Fast Ethernet, ATM, and FDDI to the desktops. NICEnet provides dial-in services, including SLIP/PPP and ISDN, and has a laboratory-wide cable television network.

The CCS provides site license and support contracts for most workstations and desktop computers and manages acquisition contracts, on-line software distribution, consulting and e-mail support, and training services. The CCS staffs a help desk and facilitates software demonstrations to assist NRL researchers.

FIELD STATIONS

NRL has acquired or made arrangements over the years to use a number of major sites and facilities for research. The largest facility is located at the Stennis Space Center (NRL-SSC), in Bay St. Louis, Mississippi. Others include a facility at the Naval Postgraduate School in Monterey, California (NRL-MRY), and the Chesapeake Bay Detachment (CBD) in Maryland. Additional sites are located in Maryland, Virginia, Alabama, and Florida.

Flight Support Detachment (NRL FSD)

Located at the Naval Air Station Patuxent River, Lexington Park, Maryland, the Flight Support Detachment (NRL FSD) is manned by approximately 9 officers, 80 enlisted, four civilians, and 20 contract maintenance technicians. NRL FSD is currently responsible for the maintenance and security of six, uniquely configured, P-3 Orion turboprop research aircraft. The FSD conducts numerous single-aircraft deployments around the world in support of a wide range of scientific research projects.

In FY-99, NRL FSD provided flight support for diverse research programs including: Advanced Radar Periscope Detection and Discrimination (ARPDD), an advanced variant of the APS-137 ISAR radar used for detecting submarine periscopes; Cooperative Engagement Capability (CEC), an airborne suite to test USN Aegis Cruiser systems; Remote Ultra-low Light Imager (RULLI); Airborne Geographical Sensor Suite (AGSS), involving data and gravimeter testing to detect variations in the ocean floor; Real Ap-

NRL's Flight Support Detachment with one of the P-3 aircraft.

erture Radar (RAR); Integrated Electronic Warfare System (IEWS), a system that simulates radar of various surface and airborne platforms; Navy Tactical Aircraft Directional Infrared Countermeasures/Advance Technology Demonstration (TADIRCM), in-flight detection, threat determination and tracking technology testing; and NAVOCEANO Oceanographic Surveillance (OS).

The Flight Support Detachment continues to improve both capabilities and diversity among its aircraft platforms. Researcher 442 has completed its scheduled rework to install an E-2C "Hawkeye" rotodome antenna and is currently supporting the Navy's Theater Air Defense programs. The FSD also completed its 37th year of mishap-free flying, accumulating more than 57,000 flight hours.

Chesapeake Bay Detachment (CBD)

CBD occupies a 168-acre site near Chesapeake Beach, Maryland, and provides facilities and support services for research in radar, electronic warfare, optical devices, materials, communications, and fire research. A ship-motion simulator (SMS) is used to test and evaluate radar, satellite communications, and line-of-sight RF communications systems under dynamic conditions (various sea states). The SMS can handle up to 12,000 pounds of electronic systems. A roll motion of up to 30 degrees (15 degrees to port and 15 degrees to starboard) can be applied to this axis. The pitch axis has a fixed motion of 10 degrees (5 degrees to stern and 5 degrees to bow). Periods along both axes, pitch and roll, are variable—from a slow 32-s to a brisk 4-s rate. Variable azimuth motion can also be added to the pitch and roll action. Synchronized positioning information (×1 and ×36) is available for each of the three axes of the SMS.

Because of its location high above the western shore of the Chesapeake Bay, unique experiments can be performed in conjunction with the Tilghman Island site, 16 km across the bay from CBD. Some of these experiments include low clutter and generally low-background radar measurements. By using CBD's support vessels, experiments are performed that involve dispensing chaff over water and radar target characterizations of aircraft and ships. Basic research is also conducted in radar antenna properties, testing of radar remote-sensing concepts, use of radar to sense ocean waves, and laser propagation. CBD also hosts facilities of the Navy Technology Center for Safety and Survivability, which conducts fire research on simulated carrier, surface, and submarine platforms.

The ship-motion simulator, located on the shoreline of the Chesapeake Bay at NRL's Chesapeake Bay Detachment, allows radar, satellite communications, and line-of-sight RF communications systems to be tested before shipboard installation or in lieu of actual at-sea testing.

Marine Corrosion Test Facility

Located on Fleming Key at Key West, Florida, this facility offers an ocean-air environment and clear, unpolluted, flowing seawater for studies of environmental effects on materials. Equipment is available for experiments involving weathering, general corrosion, fouling, and electrochemical phenomena as well as coatings, cathodic protection devices, and other means to combat environmental degradation.

Stennis Space Center (NRL-SSC)

NRL-SSC, a tenant activity at NASA's John C. Stennis Space Center, is located in the southwest corner of Mississippi, about 50 miles northeast of New Orleans, Louisiana, and 20 miles from the Mississippi Gulf Coast. Other Navy tenants at SSC include the Commander, Naval Meteorology and Oceanography Command and the Naval Oceanographic Office, who are major operational users of the oceanographic and atmospheric research and development performed by NRL. The Naval Oceanographic Office provides access for NRL researchers to one of the Navy's largest supercomputers. This unique concentration of operational and research oceanographers makes SSC the center of naval oceanography and the largest such grouping in the Western world. Additional Navy tenants at SSC include Special Boat Unit 22, and the Human Resources Service Center, South East.

NRL-SSC provides administrative and business operations for entities of the Acoustics, Marine Geosciences, and Oceanography Divisions. NRL-SSC occupies more than 175,000 square feet of research, computation, laboratory, administrative, and warehouse space. Facilities include the new microscopy center, a visualization laboratory, numerous large antennas to receive available oceanographic and meteorological satellite data, the Magnetic Observatory—part of a worldwide observing system, the Pattern Analysis Laboratory, a Map Data Formatting Facility, and numerous laboratories for acoustic and oceanographic computation, instrumentation, analysis, and testing. Special areas are available for constructing, staging, refurbishing, and storing sea-going equipment.

Marine Meteorology Division (NRL-MRY)

NRL's Marine Meteorology Division (NRL-MRY) is located in Monterey, California, on the grounds of the Naval Postgraduate School (NPS) Annex, which

Hands-on experience puts summer students in the middle of research and data collection at NRL-SSC.

is about a mile from the NPS main campus. As a tenant activity of the Naval Support Activity, Monterey Bay, the NRL facility is collocated with the Navy's operational Fleet Numerical Meteorology and Oceanography Center (FNMOC) and with a NOAA National Weather Service Forecast Office (NWSFO). The NPS Annex campus, which covers approximately five acres, comprises four primary buildings—one occupied exclusively by NOAA, one that houses the FNMOC supercomputer/operational facility, and two large buildings containing office space, computer laboratories, and conference facilities that are shared by FNMOC and NRL-MRY personnel. The site also provides warehouse space and recreational facilities. NRL-MRY occupies approximately 30,000 square feet in shared buildings. This includes not only office space, but also a small library, the John B. Hovermale Visualization Laboratory, the Bergen Data Center, the Geostationary Satellite Processing Facility, and space for the hardware supporting the Tactical Environmental Support System (TESS), the Tactical Atmospheric Modeling System/Real-Time (TAMS/RT), and the Master Environmental Laboratory.

NRL-MRY is dedicated to advancing fundamental scientific understanding of the atmosphere, including the air-sea interface, and to applying those scientific discoveries in the development of innovative objective weather prediction systems. FNMOC is the Navy's central site facility for the production and distribution of numerical weather prediction products in

THE NAVAL RESEARCH LABORATORY

support of Navy operations around the globe, as well as to other defense-related activities. Fleet Numerical, and the Navy's regional METOC Centers, are the primary customer for the numerical weather prediction systems that are developed by NRL-MRY. This collocation of the scientific developer with the operational customer offers advantages for the successful implementation of new systems and system upgrades, and for the rapid infusion of new research results from the community at large. NRL-MRY has efficient access to FNMOC's large classified vector supercomputer and other systems. This allows advanced development to take place using the real-time on-site global atmospheric and oceanographic databases. Collocation also offers the opportunity for FNMOC scientists to team with NRL-MRY scientists during the transition and implementation process, and NRL-MRY scientists remain readily available for consultation on any future problems that arise.

NRL-MRY benefits from the opportunities provided by NPS for continuing education and for performing collaborative research with the Department of Meteorology and others. The NWSFO has also proven to be a valuable partner for both NRL-MRY and FNMOC. Data and products are exchanged, and valuable feedback is provided about the performance and utility of the numerical models and satellite-based products developed at NRL-MRY.

Midway Research Center

The Midway Research Center (MRC) is located on a 158-acre site in Stafford County, Virginia. Lo-

cated adjacent to the Quantico Marine Corps' Combat Development Command, the MRC has 10,000 square feet of operations and administration area and three precision 18.5-m-diameter parabolic antennas housed in 100-ft radomes. The MRC, under the auspices of the Naval Center for Space Technology, provides NRL with state-of-the-art facilities dedicated solely to space-related applications in naval communications, navigation, and basic research.

Other Sites

Some field sites have been chosen primarily because they provide favorable conditions to operate specific antennas and electronic subsystems and are close to NRL's main site. Pomonkey, Maryland, a field site south of NRL, has a free-space antenna range to develop and test a variety of antennas. The antenna model measurement range in Brandywine, Maryland, has a 4.6-m diameter turntable in the center of a 305-m-diameter ground plane for conducting measurements on scale-model shipboard and other antenna designs. A site on the cliffs overlooking the Chesapeake Bay provides an over-the-water range of approximately 10 miles to Tilghman Island.

Research Platforms

Mobile research platforms contribute greatly to NRL's research. These include six P-3 Orion turboprop aircraft and one ship, the ex-USS *Shadwell* (LSD-15), berthed in Mobile Bay, Alabama. The ex-*Shadwell* is used for research on fire-suppression techniques on-board ship.

Looking Ahead

To provide preeminent research for tomorrow's Navy, NRL must maintain and upgrade its scientific and technological equipment to keep it at the forefront of modern research facilities. The physical plant to house this equipment must also be state of the art. NRL has embarked on a Corporate Facilities Plan to accomplish these goals. This plan and future facility plans are described below.

THE CORPORATE FACILITIES INVESTMENT PLAN (CFIP)

The CFIP is a financial spending plan to provide modern research facilities at NRL for the future. The plan calls for both Congressional and Laboratory investment and is updated and altered as changes occur in scientific emphasis and Congressional policy. During the past five years, Congressionally approved military construction (MILCON) funds were used to construct the new Electro-Optics Laboratory and a high-bay facility for the Naval Center for Space Technology. MILCON funds were approved in the FY 97 Congressional budget for the construction of an Ocean Acoustics Research Laboratory building at NRL-SSC. Future MILCON funds have also been requested for the construction of a Nano Science Research building at NRL-DC.

To complement these efforts, overhead funds have been used to renovate and upgrade laboratory and support areas in several existing buildings. Modern laboratory facilities have recently been provided for the Center for Bio/Molecular Science and Engineering, the Materials Science and Technology Division, the Remote Sensing Division, and the Acoustics Division. Work that is currently in progress will provide new facilities for the Information Technology Division and the Radar Division.

In parallel with efforts to upgrade laboratory buildings to the most modern standards, those buildings that were built during World War II and do not lend themselves to renovation are being demolished. This will provide space for the construction of future MILCON buildings, and it will also reduce the Laboratory's overhead costs.

Information Technology

The Information Technology Division's Center for Computational Science (CCS) operates three scalable, massively parallel Global Shared Memory (GSM) computer systems. A 128-processor SGI/Cray Origin2000 and 80-processor HP Exemplar SPP-2000 have cache-coherent Non-Uniform Memory Access (ccNUMA) architectures. A 148-processor Sun HPC Ultra distributed system has 96 processors that operate symmetrically in a Cache-Only Memory Access (COMA) architecture. These systems comprise the Distributed Center (DC) at NRL whose hardware is funded by the DoD High Performance Computing Modernization Program (HPCMP). The systems are used in the innovative exploration and evaluation of MPP technology for the solution of significant militarily relevant problems relating to computational and information science. The systems allow for leading-edge research in support of heterogeneous parallel processing applications by the Navy and DoD science and technology communities.

Chemistry

Nanostructured materials promise both challenges to current models of materials performance and opportunities for new technological solutions to Navy problems. A new laboratory building is planned to provide the carefully controlled environment (temperature, vibration, magnetic, electrical, humidity) necessary to work with atomic scale precision (0.1 nm).

Plasma Physics

The Plasma Physics Division has set up a Large Area Plasma Processing System (LAPPS) facility to investigate a new technique to produce plasmas for plasma processing. Applications include production of large-area flat-screen displays or elements for phased arrays or materials modification such as surface polymerization or ion implantation. The system is based on low-energy electron beam ionization of a background gas to produce the desired plasma. The system may have advantages over existing techniques for production of large-area (square meter) plasmas, efficiency of plasma production, and control of reactive species.

Electronics Science and Technology

Important division emphasis is focussed on the continual upgrading of the Nanoprocessing Facility (NPF) and the Penthouse Processing Facility (PPF) and expanding activities in the nanoelectronics, heterostructures, and vacuum electronics science and

technology programs. The PPF has upgraded its capabilities in scanning electron microscopy. The NPF is replacing its Cambridge e-beam nanowriter with a second JEOL nanowriter to give this facility superior capability in defining nanoscale patterns and lines. The Laboratory for Advanced Material Synthesis facility will continue to upgrade its organometallic vapor-phase epitaxy equipment for thin-film semiconductors and provide safer and more environmentally benign processing and waste-disposal techniques. The EPICENTER (a joint activity of the Electronics Science and Technology, Materials Science and Technology, Optical Science, and Chemistry Divisions) will continue to expand into new materials areas to provide new insight into epitaxial semiconductor growth processes that will form the basis for use in the electronic devices of tomorrow. These facilities are enhanced by the new Joint Laboratory for Proximal Probe Nanofabrication that serves as a resource for characterization patterning and process definition necessary for advanced nanodevice fabrication.

Ocean Research Laboratory

NRL's Ocean Research Laboratory (MILCON Project P-006) is a 52,000 square-foot building that houses the Oceanography Division of the Ocean and Atmospheric Science and Technology Directorate. The building contains office space, oceanographic laboratories, staging areas, a small machine shop, electronic and secure laboratories, and computing facilities for research and development in ocean science and remote sensing.

Acoustics

NRL's Salt Water Tank Facility is designed to provide a controlled environment for studying complex bubble-related processes found in the ocean. It is an experimental pool facility for studies of underwater acoustics, fluid dynamics, and air-sea interface environmental topics under saline conditions. This facility is used to study the acoustics of bubbly media, including bubble entrainment and ambient noise generation, scattering from bubbly structures, and propagation through bubbly media. Related studies include the interaction of bubbles with turbulent flows, bubble coalescence and dissolution, effects of surfactants and contaminants, and bubble-related gas exchange across the air-sea interface.

For acoustic experiments at sea, the division is acquiring a new 128-channel, rubidium-precision-timed, internal recording system with vertical and horizontal arrays that can record up to 780 Gbytes (expandable to 1.8 Tbytes) of data on a schedule that can be either programmed prior to deployment or altered via acoustic modem after deployment.

Remote Sensing

The Remote Sensing Division has developed and installed 74 MHz receivers on the National Radio Astronomy Observatory's Very Large Array (VLA), thereby producing the world's highest angular resolution and most sensitive astronomical interferometric array operating below 150 MHz. In contrast to the VLA's maximum baseline of 35 km, all previous astronomical interferometers operating below 150 MHz had baselines less than 5 km because ionospheric structure had been thought to impose phase variations that would corrupt the interferometric imaging. Work in the Remote Sensing Division has shown that radio astronomical techniques can now remove the ionospheric phase variations and extend interferometer baselines to arbitrary lengths. In its first year of operation, the NRL/NRAO 74 MHz system has been used for a variety of innovative observations with encouraging initial results in solar system, Galactic, and extragalactic astrophysics. The success of the NRL/NRAO 74 MHz system indicates

NRL's Ocean Research Laboratory (MILCON Project P-006) at Stennis Space Center houses the Ocean and Atmospheric Science and Technology Directorate.

that it is possible to open a new high-resolution, high-sensitivity astronomical window by going to an even larger, more sensitive system. The Remote Sensing Division, in collaboration with the Netherlands Foundation for Research in Astronomy, is currently designing a follow-on instrument, the Low Frequency Array (LOFAR). LOFAR will be a fully electronic, broadband array operating in the 15 to 150 MHz range, with a collecting area of 1 square km at 15 MHz and a maximum baseline of 500 km resolution and sensitivity over the state of the art.

The Remote Sensing Division is also developing other new facilities-class sensors including the Navy Ultrawideband Synthetic Aperture Radar (NUSAR). NUSAR is a fully capable high-resolution (less than 1 meter impulse response) synthetic aperture radar system made to be operated from light aircraft. It is fully polarimetric and can operate as an along-track interferometer. Its frequency range will be expandable, and ultimately it will operate from VHF to X-band.

Marine Geosciences

The Marine Geosciences Division has greatly enhanced the capabilities and quality of seafloor sediment fabric analyses through completion of installation and staff training for its 300-kV transmission electron microscope (TEM) and accompanying environmental cell (EC). The TEM-EC is housed in a specially built facility imparting a null effect on the functioning of the TEM-EC electronics. The new facility will improve transition of developed capabilities and sediment fabric understanding to applied issues of acoustic and shock-wave propagation, mine burial, and mine countermeasures.

Vacuum Ultraviolet Space Instrument Test Facility

The Space Science Division facilities include an ultraclean solar instrument test facility in Building A-13 on the main NRL campus. The new facility is designed to satisfy the rigorous contamination requirements of state-of-the-art solar spaceflight instruments. The facility has a 400-ft^2 Class 10 clean room and a large Solar Coronagraph Optical Test Chamber (SCOTCH). This completely dry-pumped, 550-ft^3 vacuum chamber is maintained at synchrotron levels of cleanliness. Solar instrumentation up to 1 m in diameter and 5 m in length can be physically accommodated in the chamber. The instrument's optical performance is probed and calibrated with a variety of visible and XUV sources mounted on the chamber's 11-m beamline. The optical testing and char-

acterization of the Large-Angle Spectrometric Coronagraph (LASCO) instrument for the European Space Agency's Solar Heliospheric Observatory satellite were conducted in this chamber. Coronagraph stray-light characterization was carried out by mounting a set of baffles in the main beamline, illuminating the instrument with a simulated solar beam, and measuring the residual radiation. A stray light background measurement of 10^{-12} was successfully measured in the LASCO C3 channel. Coronagraph calibration was carried out by installing back-illuminated calibrated opals in front of the instrument entrance aperture. Instrument polarization properties were analyzed by using a variety of polarizers installed in a wheel located between the opal and the instrument. The wheel was remotely controlled from outside the chamber. Instrument Mueller matrices were verified with a 12-in. diameter, two-plate partial polarizer. Calibration and focus of XUV solar instrumentation are accomplished by exposing the instrument to an XUV windowless collimator at the end of the tank. The facility also has a small thermal bake/vacuum test chamber used for vacuum conditioning and thermal testing of spaceflight components and subassemblies. Both the SCOTCH and the small test chamber are instrumented with temperature-controlled quartz-crystal monitors and residual gas analyzers for real-time, quantitative measurements of volatile contamination.

REHABILITATION OF SCIENTIFIC FACILITIES

Specialized facilities are being installed or upgraded in several of the research and support divisions.

Flight Support Detachment

NRL's Flight Support Detachment (FSD) has continued to improve both capabilities and diversity among its aircraft platforms. Aircraft 153442 continues to undergo extensive modifications with Lockheed Martin to install a "rotodome" antenna and full AEW radar system. These modifications will support the Navy's Theater Air Defense programs, while providing a testbed for advanced EW radar research. Additionally, all aircraft have completed extensive bomb-bay design improvements that will allow the aircraft to carry more diverse scientific payloads. Aircraft 158227's communications capabilities were significantly upgraded with a state-of-the-art satellite telephone; aircraft 154589 is next in line to receive this INMARSAT system. These upgrades

and modifications will ensure that NRL will have the finest airborne research capabilities well into this century.

Information Technology

The Information Technology Division continues to transition stable technology from high-performance network testbed activities into the NRL local area network. This effort includes deployment of ATM technology at stream rates of 622 Mbps (OC12c) and 2.5 Gbps (OC48) across the enterprise. The current computing architectures, the SGI Origin2000, the HP Exemplar SPP-2000, and the Sun Ultra, are continuously undergoing upgrade and evaluation of both hardware and software. The NRL CCS works closely with the DoD HPC community and the HPC vendors to provide insight, balance, and value-added capabilities within the MPP testbed infrastructure.

Materials Science and Technology

Renovation is in progress for Building 3, which is composed of two of the original five buildings at NRL, to contain modern laboratories for studies of thin-film deposition and characterization, superconducting materials, magnetic materials, and other materials science projects. The new space will feature the most modern molecular beam epitaxy and other materials synthesis and processing equipment, an up-to-date fatigue and fracture laboratory, and state-of-the-art diagnostic equipment, including electron microscopes, spectrometers, and electron and X-ray diffraction equipment. The renovated building will also contain office and laboratory space for approximately 70 technical personnel.

Plasma Physics

A state-of-the-art short-pulse (0.4 ps), high-intensity Table-Top Terawatt (T^3) laser currently operates at 2.5 TW and 5×10^{18} W/cm^2 for a variety of physics studies. The T^3 laser will be upgraded to boost its power to 25 TW and intensities to $>10^{19}$ W/cm^2. This will provide a facility to do fundamental physics experiments in intense laser-plasma interactions, intense laser-electron beam interactions, and intense laser-matter interactions.

The division is building a repetitively pulsed (5 pps) krypton fluoride (KrF) laser called Electra. Electra will develop the technologies needed for inertial fusion energy (IFE). A laser for a power plant would have to fire five times per second, run for several years, and meet stringent cost and efficiency requirements. Electra will develop the technologies that can meet these requirements. It will have a laser output of around 400 to 700 Joules. The size of Electra was chosen to be large enough to be scalable to a power plant size, but small enough to be flexible.

Electronics Science and Technology

The Electronics Science and Technology Division continues to upgrade and expand its capability in nanofabrication science. Facilities will be enhanced with the addition of two new laboratories and an expanded EPICENTER that includes a new vacuum processing chamber and two new epitaxial growth chambers. The additional epitaxial growth chambers will allow new classes of ferromagnetic II-VI semiconductors to be grown. These semiconductors allow the realization of new device structures based on spin-polarized transport and the creation of lasers, detectors, and high-speed electronics important to DoD. The new laboratories are the Laboratory for Proximal Probe Nanofabrication (LPPN), which will explore the limits of nanolithography with proximal probes, and the Laboratory for Advanced Materials Processing (LAMP), which will explore the chemistry and physics of processes used routinely in the formation of modern devices and extend these processes into the nanoscale fabrication range.

The preceding pages dramatically illustrate the range of research capabilities that have been and are being developed to provide the Naval Research Laboratory with the world-class facilities for which we are known. However, these inanimate objects, however expensive and complex, are of no value without the highly motivated people who work here. It is these people who make the Laboratory the great institution that it is, who provide the ideas and sustained efforts to make these great research capabilities "come to life." In this section, we highlight some of these special people.

Our People Are Making a Difference

Mr. Don DeYoung is the Executive Assistant to the Director of Research. He was selected for the position in July 1997 to investigate general management issues, conduct special studies, and develop responses to Navy, DoD, and congressional policy. He came to NRL in 1980 after receiving a master's degree in Public Administration from Syracuse University. Since that time he has performed developmental assignments within the Office of the Secretary of Defense and the Office of Naval Research, earned a master's degree in National Security Studies from Georgetown University, and served as a Navy analyst on two DoD base closure projects. His efforts during BRAC-95 were recognized with a Special Act award presented by the Secretary of the Navy and with a Navy Meritorious Civilian Service award presented by NRL's Commanding Officer.

"I'm a strong believer in the role of the Government laboratory, in its value to our country, and in its continued relevance for the 21st century. I'm a believer largely because of NRL's extraordinary impact on science and national security. I consider NRL one of the Navy Department's crown jewels—along with the Carriers, the Marine Corps, and the "Silent Service." This elite group gives the U.S. Fleet its ability to project decisive combat power around the globe. Even though NRL isn't an operational force like the other three "jewels," it nonetheless gives the Fleet that kind of power. There was radar in World War II, lubricants for new gas turbine warplanes in Korea and for M-16s in Vietnam, the intelligence satellite in the Cold War, NAVSTAR GPS in the Gulf War, and electronic warfare decoys in The Balkans. These and many other NRL innovations have helped make the American Fleet the most formidable naval fighting force in the world. I'm proud of that."

Dr. Dylan Schmorrow is a Lieutenant Commander serving as an Aerospace Experimental Psychologist in the U.S. Navy's Medical Service Corps. He works in the Information Technology Division as the military scientist for modeling, virtual environment, and simulation science and technology. In this role, he coordinates the development and implementation of research and development programs that are focused on the rapid transition of NRL, ONR, and DARPA science and technology to the Fleet. "The need to capture knowledge from a sea of data and the demands of rapid decision making can only be dealt with through the advancement of modeling, virtual environments, and simulation science and technology. NRL provides the critical foundations for tomorrow's Navy through world-class, multidisciplinary research programs. I have learned first hand that this mission is, and will continue to be, accomplished through the focused team work I witness daily in the Information Technology Division and throughout NRL. It is an honor for me to have the opportunity to serve with the internationally renowned scientists and engineers at NRL and this, more than anything, continues to contribute to my development as a naval officer and scientist."

Ms. Jonna Atkinson is a Visual Information Specialist in the Publications Services Section of the Technical Information Division. She has worked in TID since she came to NRL in 1985. She designs and coordinates NRL's annual publication, the *NRL Review*. The numerous publications she has designed and produced have contributed immeasurably to the preservation of the "award-winning" reputation of the section. Ms. Atkinson is also responsible for maintaining the computers, hardware, and software for the entire section. Her continuity and efficiency in streamlining the work processes benefit the production of publications immensely. "I have enjoyed working at NRL from day one. I have learned an enormous amount about computer technology and the publishing process just by doing my job. I am grateful for the opportunities my supervisors have given me to expand my knowledge and creativity. I enjoy all aspects of my job. The *NRL Review* is such an enjoyable project for me and I look forward to its production each year. I truthfully believe I could not find a better place to work or a nicer group of people to work with. And for that I am grateful."

Dr. Jill Dahlburg is a research physicist in the field of plasma physics. She has been a member of the NRL Nike KrF Laser Program since its inception. She is head of the Theory Section in the Laser Plasma Branch of the Plasma Physics Division. She has developed and applied advanced numerical techniques in the fields of laser matter interactions, fundamental hydrodynamics, magnetohydrodynamics, and turbulence physics. "I think that NRL provides a paradigm for technical research for several reasons. One is that NRL has had a tremendously stable base of basic research funding. Another is the idea of the stable pyramid, which supports research that ranges from basic to highly applied and researchers who can interact on a daily basis over this range. Scientists here feel free to take risks because there is a safety net of reliable funding and intelligent oversight. This has created a lively, innovative, and daring research community that makes good use of the research investment. Finally, and probably the most important, reason why NRL is an ideal research environment is because of the people who work here. Together we have accomplished some amazing and wonderful things."

Dr. Curtiss Davis is head of the Optical Sensing Section of the Remote Sensing Division. The Section is pioneering the use of hyperspectral imaging for characterizing the coastal environment. Spectral information is used to estimate water depth, bottom type, and the properties of the water column. The section is unique in having the ability to build, calibrate, and characterize the sensors, and to make all of the necessary sea-truth measurements to develop and validate algorithms and products for the Navy. "In the five years that I have been at NRL, we have put together the team of scientists and the equipment and facilities needed to assume a world leadership role in this promising new area of research. I greatly appreciate the foresight and flexibility of NRL management that has made this rapid development possible. I am also the Project Scientist for the Naval EarthMap Observer (NEMO) spacecraft. The Optical Sensing Section is responsible for the algorithms that are used in that program. When NEMO is launched in 2001, it will provide a demonstration of the utility of hyperspectral imaging to meet Naval needs around the globe."

33

Featured Research

Advanced Multifunction RF Systems (AMRFS)

P.K. Hughes II, J.Y. Choe, J.B. Evins, and J.J. Alter
Radar Division

J.P. Lawrence III, D.C. Wu, G.P. Hrin, and W. Habicht II
Tactical Electronic Warfare Division

P.J. Matthews
Optical Sciences Division

In 1996, the Office of Naval Research initiated the Advanced Multifunction RF System (AMRFS) program. The program addresses the serious technological challenges posed by the U.S. Navy for increasing the number of shipboard topside radio frequency (RF) functions while significantly reducing ship signature. The AMRFS program is focused on a proof-of-principle demonstration of the concept of broadband RF apertures that are capable of simultaneously performing a large number of radar, electronic warfare, and communications functions from common, low signature apertures. Thus the goals of the program are reducing dramatically the number of topside RF system apertures while increasing effective functionality and bandwidth. This will reduce the aggregate radar cross section (RCS) contribution of the topside RF system apertures. This multifunction RF system concept puts the functionality into the software. In addition to the proof-of-principle demonstration, the AMRFS program is developing new component technologies that allow more efficient cost-effective design architectures.

TECHNICAL CONCEPT

The AMRFS concept integrates multiple RF functions by incorporating them within a set of versatile and intelligent apertures. Implementation of this concept faces formidable challenges because of the great diversity of RF functions. The diversity includes: types of functions (radar, communications, and electronic warfare), operational frequency (from 1 MHz to more than 44 GHz); instantaneous bandwidth (from a few kHz to more than 2 GHz); beam profiles (omnidirectional, fan, pencil, and numerous sidelobe tapering/blanking); waveforms (pulsed and continuous), transmit RF power (milliwatt to megawatt); timeline utilization; and polarization (vertical, horizontal, and circular). This diversity imposes configuration constraints and requires new and innovative capabilities from RF system electronics.

For a tactical system, the frequency spectrum will need to be partitioned after a careful cost-performance trade-off study. The use of very large per-centage bandwidths minimizes the number of apertures required for a given frequency coverage but puts unrealistic burdens on components. On the other hand, an optimal choice of spectral band partitioning could reduce the size of specific arrays. For the AMRFS demonstration program, a 5 to 1 bandwidth has been chosen as being within the available or near-term state of the art in components.

After examining functional requirements, separate transmit and receive apertures were found to be necessary. Operational requirements dictate that the electronically steered array radars function in surveillance modes a large percentage of the time, utilizing low (10%) duty cycle waveforms. Conversely, communications and electronic warfare (EW) sometimes require very high duty or even continuous wave (CW) transmission. The transmit-to-receive isolation required to support radar signal reception and EW and communications signal transmission at the same time is extremely difficult (if not impossible) to obtain using a single transmit/receive (T/R) aperture. Sepa-

rate transmit and receive apertures enhance the ability to achieve the needed isolation, and they also allow optimal utilization of the entire timeline for the transmitter and the receiver, thereby supporting greater compression of the number of required apertures.

The common aperture must be highly capable since it has to meet all the stressing requirements of all functions. This means that the components should support simultaneous RF functions, multiple simultaneous beams for transmit and receive, wide operating and instantaneous bandwidth, and multiple high-purity polarization. Several state-of-the-art RF components/techniques are used in this program. Examples include active antenna systems; wideband solid-state microwave monolithic integrated circuit (MMIC) amplifiers; miniature broadband RF components (radiating elements, filters, isolators); wideband digital and photonic beam formers; and multiple simultaneous RF function control (management of frequency, array apertures, beam-space, and time-line) in real time.

Simultaneous beams will be achieved by grouping several antenna element modules together as an independently controllable subarray unit, and then allocating these subarrays for different transmit and receive functions. Because of the diversity in functions and timelines, allocation of the subarrays needs to be dynamically reconfigurable. Moreover, for the receive function, each subarray should be able to form multiple, simultaneous receive beams. In other words, to have as much flexibility as possible, both spatial (dynamically reconfigurable) and spectral multiplexing (temporally simultaneous) schemes are used within the arrays. Figure 1 illustrates these essential AMRFS concepts. As shown, the transmit array enables multiple beams via spatially allocating different subarrays (shown with four beams in four different colors), while each receive subarray supports forming multiple (four shown) simultaneous receive beams. The separation of transmit and receive apertures is also shown in the figure.

Many technical challenges are being addressed by the AMRFS program. They include: antenna issues associated with dynamically reallocable subarrays; distribution of signals and reference local oscillator (LO) signals to the subarrays; photonic wideband beam steering; generating multiple receive beams via digital beamforming algorithms; and the issue of intelligently controlling the system resources in real-time. These issues are being addressed as part of the development of the AMRFS experimental testbed that will be used to demonstrate the concept.

ANTENNA SYSTEM

The ability to design a functional wideband aperture depends on several array parameters as well as the dimensional constraints imposed by the components located behind the radiating elements. The bandwidth over which a phased array can operate depends on the radiating elements used, the geometry of the element distribution, the element spacing, and the maximum scan angle of the array. It is well known that the instantaneous bandwidth of a phased array is severely limited when phase shifters are used at each element in the array to steer the beams. For very large instantaneous bandwidth sig-

TRANSMIT ARRAY   RECEIVE ARRAY
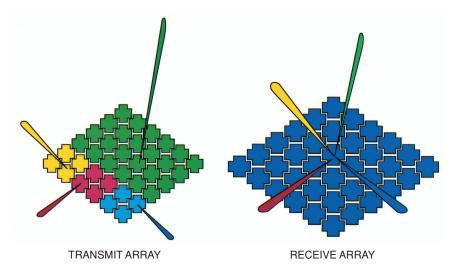
FIGURE 1
AMRFS technical concept: separate transmit and receive arrays with dynamic allocation of subarrays for multiple simultaneous beams.

nals, it is necessary to use time-delay beam steering rather than phase steering. It can be costly to provide a time-delay network at each element. A more affordable technique for increasing the instantaneous signal bandwidth of a phased array is to use time-delay at the subarray level. Using phase shifters at the radiating elements within the subarrays and time-delays at the subarray level is an attractive approach for some applications. For such an arrangement, the instantaneous bandwidth will decrease as the size of the subarray increases. At present, both transmit and receive arrays designs in the AMRFS proof-of-principle test-bed use this subarray configuration.

The Planar Array Calculation program, developed by Dr. Hung Ly of NRL, was used to analyze array performance and degradation effects for subarray configurations. Figure 2 shows the sidelobe distributions for a 64 (8 × 8)-element subarray antenna configuration. The calculation has been made at a center frequency of 3.4 GHz, using a 30 dB sidelobe Taylor distribution.

The plots (red and blue) are for two extreme frequencies, 3.4 ± 0.25 GHz. The associated average sidelobe level over the 500 MHz frequency bandwidth is shown in green. Note that the average sidelobe level is lower but still significantly higher than the designed sidelobe level. To eliminate high sidelobes for a wide instantaneous frequency signal, RF time-delay must be used instead of phase shifters for the subarray. Such a RF time-delay device is currently under investigation for a 4 × 4 subarray. Digital and photonic real time delay implementations are discussed below.

The polarization of a signal radiated by an antenna depends on the orientation of the antenna and the angular position of the field point. For example, a horizontally polarized dipole introduces different linear polarized fields at different locations away from the principal planes, as shown in Fig. 3.

For an electronically steered phased array, the physical orientation of the antenna elements remains fixed while the main beam is being steered to various angles. Thus, the polarization on the main beam can be quite different from the desired polarization on broadside. In other words, polarization purity of a phased array is not maintained with electronic steering. Hence, for applications that require polarization purity, significant correction must be applied to the array terminals to compensate for the undesired polarization effect.

In theory, correction for any polarization (horizontal, vertical, circular, arbitrarily linear) at the main beam of a phased array with dual polarized elements may be performed with proper adjustment of the amplitudes and phases at the element pairs. The Planar Array Calculation program provides the necessary amplitude and phase corrections for the dual polarized elements at a specified scanned angle. The penalty, in general, is a loss of signal power because the compensation essentially involves signal subtraction. Depending on scan angles and desired polarization, this loss can be only a few dB, or worst case as much as 6 dB.

WAVEFORM AND SIGNAL GENERATION

An innovative signal generation and distribution design concept was developed to meet the requirements of the AMRFS functions and support the system requirement of dynamic real-time reallocation of antenna subarrays to those functions. A trade analysis was performed to compare the attributes of many
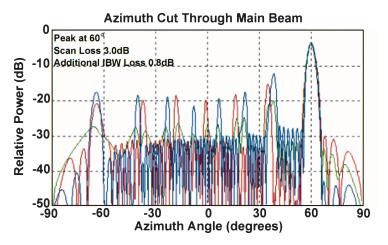
FIGURE 2
Wideband response (green trace is average of frequencies).
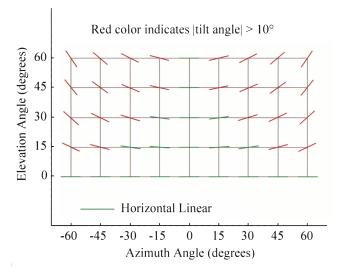
FIGURE 3
Polarization states for horizontally polarized dipole element.

design concepts including distributed vs centralized architectures for both waveform and local oscillator generation and distribution. Six narrowband-signal and eight wideband-signal design options were evaluated for criteria of performance, risk, cost, calibration and stability, capability to remote, and growth potential. The results show that a distributed waveform generation approach with digital signal distribution coupled with centralized local oscillator generation with analog fiber optic distribution is the best choice for the AMRFS test-bed demonstration.

Many features of the selected signal generation and distribution design, shown in Fig. 4, combine to make it an advanced concept with good growth potential. The signal distribution design supports transmit beam allocation on a subarray basis, which was selected as the preferred method of producing simultaneous radar, electronic warfare, and communications functions with real-time operating dynamics (microsecond transmit beam switching). The generator design uses digital signal generation techniques to produce high-fidelity signals. Digital signal generation enables digital signal distribution using a digital cross-point switch for full flexibility of switching high-data-rate signals with no fidelity loss or noise accumulation. Digital fiber-optic transducers and cables carry the signal data to the remote subarrays. This transmission medium features low electromagnetic interference (EMI) susceptibility, low noise contribution, and immunity to cross-talk.

The design features distributed waveform generation at the subarrays, with both narrow and wide bandwidth channels. The narrowband channel (10 MHz) has very high fidelity and low noise for use

with functions, such as radar, that require those signal attributes. The wideband channel (400 MHz) is for moderate fidelity signals where wider bandwidth is critical. At each subarray, a waveform generator (shown in Fig. 5) converts the high-data-rate digital signal to an analog first intermediate frequency (IF) signal. This process is a digital-to-analog conversion, and it first resynchronizes the digital data stream with a precision clock that is distributed to the subarrays through a companion local oscillator (LO) distribution network. This establishes the signal coherency between the subarrays needed for the array antenna transmission. The propagation delay differences in the distribution paths for the digital signal data are overcome through the use of first-in first-out (FIFO) registers to resynchronize the data to the clean system clock prior to analog conversion. This process enables true-time delay digital beam steering, required in the wideband channel, by adjusting the timing of the resynchronization clock from subarray to subarray. Distributed waveform generation also enables more accurate subarray calibration and high growth potential for the future. The design features selectable L- and S-Band outputs, as required by the transmit array configuration, which has separate modules for each band. The narrow or wideband channel can connect to either the L- or S-Band outputs, including simultaneous dual band outputs. For example, narrowband to L-Band and wideband to S-Band.

A centralized LO design approach was selected for good performance at affordable cost. The pool of LOs can be tailored to the stability requirements of the functions, reducing the number of high-cost, high-stability tunable LOs in a distributed design. The
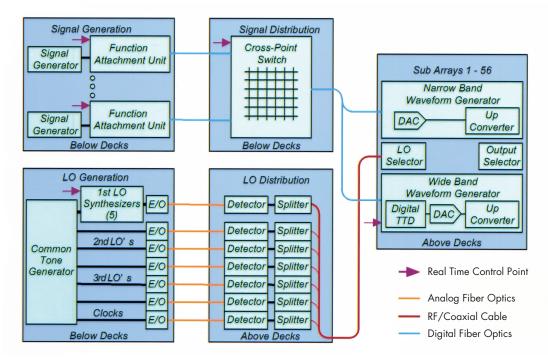
FIGURE 4
Transmit Signal and Local Oscillator Distribution.
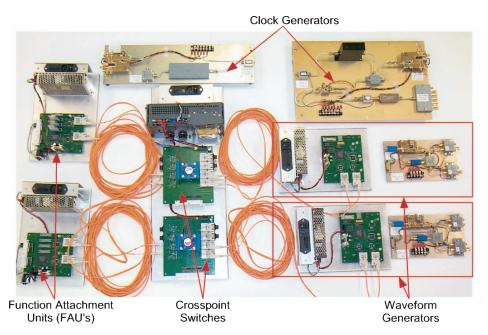
FIGURE 5
Distributed waveform generator breadboard hardware.

centralized LO design does require a more complicated distribution network that features analog fiber optic transmission for low EMI susceptibility, low cross-talk, and good high-frequency performance, but poorer phase noise performance than RF distribution methods.

RECEIVE SIGNAL DISTRIBUTION/ PHOTONIC BEAMFORMING

The incorporation of functions requiring large instantaneous bandwidths into electronically steered array antennas such as those used in the AMRFS concept poses a unique challenge. As stated previously, a traditional array antenna is steered by adjusting the *phase* of each element in the array. In such a system, phase shifter adjustments made in each element path to steer the antenna in a given direction are valid for only one frequency f_0. Thus, short pulse or special signals (e.g., chirped pulse) that contain a large spectrum of frequencies (i.e., wide bandwidth) will have components of the desired signal that are not steered in the proper direction. As a result, an observer or target in the desired beam steering direction will see an attenuation of frequencies not close to f_0. The degree to which frequencies are steered improperly is a function of the array size, the deviation of the frequency from f_0, and the steering angle

of the array. Solving this problem involves steering the beam using a phase that varies linearly with frequency, i.e., a time delay.

Over the years, the Optical Sciences Division of NRL has developed a practical, fiber-optic technique for implementing time-steered arrays. The technique, the dispersive prism technique, is based on a dispersive photonic delay line combined with a simplified beamforming architecture. This method solves many of the problems associated with previous attempts at optical true time-delay (TTD). The use of a fiber-optic beamforming technique has other advantages, including a natural resistance to EMI, low weight, small size, and the ability to easily remote components.

Figure 6 is a schematic of the receive beamformer architecture. The microwave outputs of the subarrays are amplitude-modulated onto a common, wavelength-tunable, optical carrier using an integrated optical Mach-Zehnder modulator. The modulated optical carrier from each subarray traverses an optical fiber link, which has an amount of optical dispersion that is proportional to the relative position of the subarray. This results in a dispersion gradient across the fibers that produces a time-delay gradient that adjusts as the laser wavelength is tuned. One such dispersive element, to be used in the AMRFS test-bed high-band receive beamformer, is a chirped fiber-optic Bragg grating.
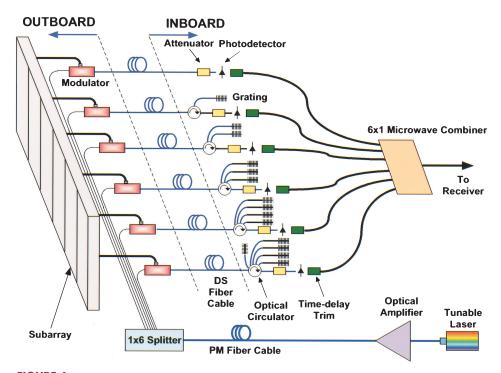
FIGURE 6
Schematic of the fiber-optic, dispersive prism, time-steered receive beamformer architecture for the AMRFS high-band receive array

The power of the fiber-optic dispersive prism technique lies in the simplified architecture, which allows the tuning of a single laser wavelength to set the time-delays for all subarrays in one dimension. The technique uses commercially available components that have been successfully developed by the telecommunications industry. It makes efficient use of optical power and minimizes the required number of expensive components (i.e., lasers and photo detectors). This approach is capable of producing time delays with a resolution better than 1 picosecond. Additionally, the use of chirped gratings as the dispersive element results in a beamformer that is virtually immune to ambient temperature variations, with a very low signal latency through the subsystem. Extremely rapid beam steering ($<<$ 1 µs) is enabled through the use of a unique mixed analog/digital laser driver circuit developed at NRL.

The receive beamforming system concept was demonstrated on an eight-element, one-dimensional dispersive prism beamformer feeding a pseudorandom sparsely populated array of spiral antennas. The system was tested in the NRL Radar Division's anechoic chamber. Figure 7 shows a measured time-steered, far-field antenna pattern as a function of frequency, with the laser tuned so that the system forms a beam at 60° off broadside. The measured beam is properly steered for all frequencies from 6 to 18 GHz, demonstrating the ability of this novel photonic approach to steer wide instantaneous-bandwidth signals. In contrast, a traditional phase-steered system is only able to steer ~0.2 GHz in the proper direction at any given phase shifter setting.
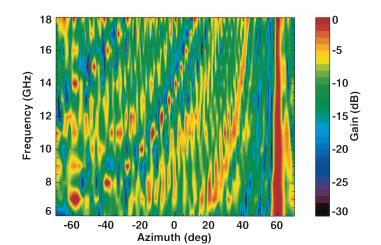
RECEIVE DIGITAL BEAMFORMING

The AMRFS concept requires the formation of multiple simultaneous receive beams in space to support different RF functions. At the same time, any one of those functions may require multiple beams. For example, a radar function may need to form six beams. One main beam is centered at the desired pointing angle in space. Two pairs of horizontally and vertically squinted beams surround the main beam for a more accurate "monopulse-like" angle estimation of a target's position. Finally, a broad, low-gain beam helps determine if a particular detection is due to an echo in the main antenna beam or one of its sidelobes. Communication functions may also require a cluster of beams to track a particular satellite. In AMRFS, these multiple simultaneous beams are produced by digital beamforming.

As described earlier, the AMRFS receive array is composed of a number of directional subarrays. Since a subarray is composed of a small number of elements, the beam it forms has low gain and is relatively broad. The outputs of multiple subarrays may be combined to provide narrower beams with higher gain. To accomplish this, the subarrays assigned to forming a composite beam must first be directed to point their beams in the desired direction. The outputs of all of these subarrays are then added coherently to form the main beam. Applying different phase shifts to each of the subarray outputs before they are summed can produce multiple beams in the same general direction.

The RF output of each subarray is passed through an analog receiver that downconverts the received signal to an intermediate frequency (IF). This IF signal is sampled and digitized by an analog-to-digital (A/D) converter. The digitized IF signal is sent to a digital receiver, which further downconverts the signal to baseband, producing digital in-phase and quadrature (I & Q) samples at a 10 MHz rate. At this point, the complex samples are adjusted in phase and amplitude to compensate for any subarray-to-

FIGURE 7
Measured antenna patterns of a one-dimensional, 8-element receiver array steered to 60° using a photonic time-delay beamformer.

43

subarray mismatch, and then they are sent on to the digital beamformer. For each beam to be formed, the digital beamformer applies a different phase shift to the output of each subarray and adds them all together.

The AMRFS digital beamformer uses field-programmable gate array (FPGA) technology. FPGAs are integrated circuits that incorporate a large number of logic gates that a circuit designer can arbitrarily connect to implement specific functions. The circuit is designed in a high-level hardware description language that is interpreted by software tools that map the design onto the FPGA. Today, FPGAs with one million logic gates are in production, and devices with two million gates are being released. These devices can be clocked at rates in excess of 100 MHz.

FPGAs allow the development of a very efficient pipelined implementation of the digital beamformer for AMRFS. Figure 8 is a block diagram of a 32-channel beamformer. As seen in the diagram on the left, the digitized I & Q data from 32 digital receivers are fed into four FPGA beamformer modules, each of which has eight channels and is implemented in a one-million-gate FPGA. As can be seen in the expanded view of the FPGA beamformer module, each module applies the appropriate phase shifts to each channel and forms a partial sum of its eight inputs. While the channel data are input at a 10 MHz sample rate, the phase shifts are computed at a 60 MHz

rate, which allows six beams to be formed for each input sample. Data from subarrays not used to form a particular beam are zeroed in the computation of that beam. The partial sums are passed to the succeeding FPGA beamformer modules, each of which adds the partial sum from the previous stage to its own partial sum and passes the result on to the next stage. This ultimately results in six 10 MHz beams flowing out the bottom of the architecture. The entire beamformer can be implemented in a few circuit cards, compared to several racks of general-purpose computer equipment that would be required to perform the same task.

REAL-TIME ARRAY CONTROL

The AMRFS test-bed will consist of a large number of diverse hardware resources that must be controlled in real time. These resources include transmit and receive subarrays, receivers, signal generators, LO generators, digital beamformers, and signal distribution systems. To compound the problem, these resources must also be dynamically reallocated to different RF functions without stopping the system for reconfiguration. In one real-time control concept being implemented for the AMRFS test-bed, the allocation and control of these resources is directed by the system's Resource Allocation Manager (RAM). The RAM is a software process resident within the system's centralized processor. It is responsible for
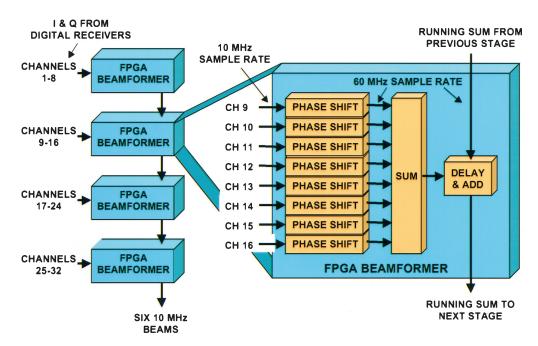
FIGURE 8
32-Channel digital beamformer implementation using FPGA technology.

analyzing the current requirements of the active functions, prioritizing these requirements, and resolving resource conflicts. The actual resource allocation and setup is done on behalf of the RAM by a distributed network of embedded real-time computers throughout the system.

Like and related system resources are grouped into logical subsystems, each with a local embedded real-time control processor. Each resource interfaces to its subsystem controller through one or more digital control points. Literally thousands of digital control points are distributed throughout the system. The subsystem controllers isolate the RAM from the intricate and sometimes computationally intensive task of providing this low-level digital control.

The RAM initiates the allocation and setup of resources by broadcasting allocation messages to all subsystem controllers over a low-latency real-time network. Each allocation message provides a high-level description of a temporary "virtual system" and a set of high-level parameters, such as beam position and frequency, to satisfy the immediate requirements of a single function. Each subsystem controller then uses this information to configure its resources for this "virtual system." Multiple "virtual systems" may exist simultaneously, as long as they do not have resource conflicts.

The resource allocation and setup process is synchronized to a global 1 kHz time base (Fig. 9). The RAM, the subsystem controllers, and the resources operate pipeline fashion in lockstep with this time base. During the first clock interval of the allocation setup process, the RAM initiates this process by broadcasting a set of allocation messages. Over a predetermined number of subsequent clock intervals, the subsystem controllers interpret these high-level allocation messages and determine proper low-level settings for each digital control point, through either calculation or lookup tables. During the following clock interval, these settings are loaded into the setup registers of each resource's digital control point(s). At the leading edge of the final clock interval, these settings are strobed into the working registers of all affected resources throughout the system.

This distributed infrastructure provides two benefits: it isolates the RAM from the low-level details of allocation and setup of a large number of resources, and it synchronizes the setup of these diverse resources throughout the system.

SUMMATION

The AMRFS program consists of two equal but distinct parts. This program description has provided details of design for equipment that would provide a proof-of-concept demonstration to be carried out by building an experimental test-bed and showing in real-time that the integration of RF functions, such as radar, electronic warfare, and communications, into a single system is technically feasible. This part of the program deals with all the system issues of establishing requirements, designing, building, testing, and
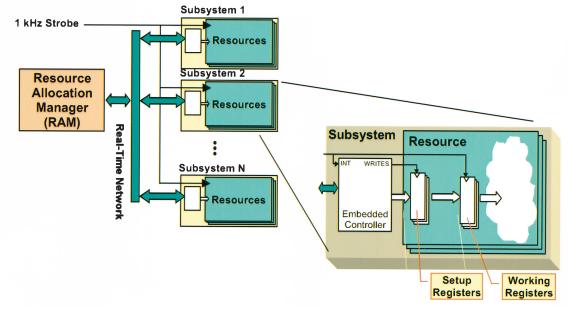
FIGURE 9
Distributed real-time control synchronization strategy.

demonstrating an integrated RF system. One purpose of this part of the program is to provide risk reduction at the system level within a science and technology program. This is deemed important because of the large risk involved in building a first-of-a-kind multifunctional integrated RF system. The other part of the program is concerned with advanced new components and subsystems technologies that would enable a more practical, cost-effective, tactical system to be developed and deployed by the Navy. This second part of the program is being executed within ONR. The ultimate objective of both parts of the program is the transition of the integrated RF

system technology to operational platforms within the Navy.

ACKNOWLEDGMENTS

THE AUTHORS

PAUL K. HUGHES II received his B.S. degree in electrical engineering from West Virginia Institute of Technology in May 1971, his M.S. degree in electrical engineering from Virginia Polytechnic Institute and State University in June 1974, and the Degree of Engineer in electrical engineering from George Washington University in May 1981. He also did extensive graduate studies at Ohio State University. Since June 1981, he has worked for the Radar Division of the Naval Research Laboratory, Washington, DC. In 1987 he became head of the Radar Analysis Section. In May 1995, he became head of the Radar Analysis Branch. In October 1997, he became the Technical Program Manager for the Advance Multifunction RF System (AMRFS) Program and was assigned to the Senior Consultant Staff of the Radar Division. Mr. Hughes is a Senior Member of the IEEE and Tau Beta Pi.

JOON Y. CHOE is currently a Deputy Program Manager for the Advance Multifunction RF System (AMRFS) Program in the Radar Division of NRL. He received a B.S. degree from Seoul National University in 1966, and a Ph.D. degree from the University of Kansas in 1972, both in physics. He has worked at various research institutes and universities including New York University, University of Maryland, Naval Surface Warfare Center, and the Naval Research Laboratory. He has worked as a research physicist in plasma fusion, microwave tubes, solid state amplifiers, broadband antennas, high-power microwaves, atmospheric plasma production, and RF photonics. He is the author of more than 70 refereed papers and patents. Dr. Choe also managed DARPA high-power microwave programs and ONR Navy RF photonics programs.
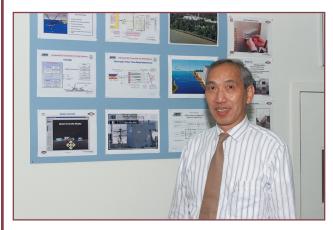
JAMES B. EVINS is a graduate of the George Washington University, where he received a B.S. degree in electrical engineering in 1985. Mr. Evins joined NRL as a cooperative education employee in the Radar Target Characteristics Branch in 1981. During his career at NRL, Mr. Evins's specialties have been digital signal processing and radar system control. He has been involved in the development of real-time digital signal processors for a variety of experimental radar systems. He has also developed hardware and software for several phased array antennas. He is currently head of the Software Systems Section of the Advanced Radar Systems Branch of the Radar Division. His current area of interest is real-time computing related to radar control and signal processing. He is a member of the IEEE and Tau Beta Pi.

JAMES J. ALTER received his B.S. and M.S. degrees in electrical engineering from the University of Maryland at College Park in 1973 and 1980, respectively. He has worked in the Radar Division of the Naval Research Laboratory for the last 26 years in the development of real-time radar signal processors. He is currently head of the Signal Processing Section of the Advanced Radar Systems Branch. His current area of interest is in the application of field-programmable gate array (FPGA) technology to radar signal processing. Current FPGA-based development projects include a digital pulse compressor, a wideband beamformer, and the narrowband beamformer described in this article. Mr. Alter is a member of the IEEE, Eta Kappa Nu, and Tau Beta Pi.

JOSEPH P. LAWRENCE III received a B.S. degree in 1968 from the University of Maryland, College Park, an M.S.E. degree from Princeton University in 1970, and a Ph.D. degree in 1974 from the University of Maryland, College Park, all in electrical engineering. Since 1966 he has been a member of the technical staff at the Naval Research Laboratory in Washington D.C. From 1966 to 1973 he was with the Search Radar Branch working on a variety of radar and multisensor integration projects. From 1973 to 1991 he was with the Advanced Techniques Branch. Since 1991 he has been the head of the Surface EW Systems Branch, which is responsible for research and development of systems and techniques spanning the full timeline of shipboard and other surface EW engagements.

47
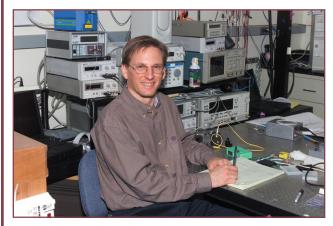
DAVID C. WU received his B.S., M.S., and Ph.D. degrees in electrical engineering from the Ohio State University in 1966, 1967, and 1971, respectively. Dr. Wu joined the Naval Research Laboratory's Tactical Electronic Warfare Division in 1974. His research areas include antenna/radome analysis, design of the large anechoic chamber and the seeker hardware-in-the loop simulation facility, and electronic countermeasures and electronic counter countermeasures techniques and system analysis. He was instrumental in the design and development of the hardware-in-the-loop simulation facility and the central target simulator. Dr. Wu is currently head of the RF Systems Engineering Section, Surface EW Branch and serves as IPT leaders on the High Band Multifunction Transmit System and Low Band Multifunction Transmit System programs.

GREGORY P. HRIN earned a B.S.E.E. degree in 1973 and an M.S.E.E. degree in 1975 from Carnegie-Mellon University. He is the head of the Counter-targeting Electronic Attack (EA) Techniques Section in the Surface EW Systems Branch of the Tactical EW Division of NRL. Before being appointed section head in 1998, Mr. Hrin was the lead RF and Systems design engineer in the Counter-targeting Electronic Attack (EA) Techniques Section. By using digital RF memories, he developed EA techniques for use against targeting and acquisition radars with advanced features. He is currently chairman of the AMRFS Signal Generation Integrated Product Team, EA consultant to AN/SLY-2 and AN/SLQ-32 Navy EW systems, and principal investigator on Network-Centric Battleforce EA Architecture and Digital Target Imaging research projects.

WILLIAM HABICHT II is the head of the Systems Development Section in the Surface Electronic Warfare (EW) Systems Branch of the Tactical Electronic Warfare Division of NRL. He earned a B.S.E.E. degree from the University of Delaware in 1966 and an M.S. degree in electrical engineering from the University of Illinois in 1968. From 1968 to 1973 he worked at NRL in the Communications Sciences Division. From 1973 to 1976 he was employed by the Eastman Kodak Company in Rochester, New York, and from 1976 to 1978 he worked at the Naval Electronic Systems Security Engineering Center in Washington, DC. In 1978, Mr. Habicht rejoined NRL where he has been working on EW systems. He currently is co-chairman of the AMRFS High Band Multifunction Receive System (HBMRS) Advanced Technology Demonstration (ATD) Integrated Product Team.

PAUL J. MATTHEWS received a B.S. degree in physics from Loyola University in 1986, and M.S. and Ph.D. degrees in electrical engineering from the University of Colorado, Boulder, in 1988 and 1991, respectively. From January 1992 to October 1992 he was employed by CAI/Recon Optical. In October 1992 he joined the staff of the Advanced Photon Source at Argonne National Laboratory were he was engaged in efforts to design, model, and fabricate a millimeter-wave linear accelerator using deep-etch X-ray lithography techniques. In September 1995, Dr. Matthews joined the Optical Sciences Division of NRL. He is currently the head of the Microwave Photonics Technology Section. His interests include optical control schemes for phased array antenna applications, photonic analog-to-digital conversion, high-performance fiber optic links, and photonics signal processing.

Octanitrocubane—A New Energetic Material

R.D. Gilardi
Laboratory for the Structure of Matter

Octanitrocubane was synthesized and identified in April 1999, in a joint collaboration between the University of Chicago and NRL. Most energetic materials have three or four nitro groups; octanitrocubane has *eight* nitro groups and eight carbons, and nothing else. It has taken more than 15 years to develop the chemistry needed for this synthesis. An article by the author about nitrocubanes in the 1995 *NRL Review* predicted that octanitrocubane would soon be made, and that it would be stable. It took three years, but it is stable—all the way up to 275 °C!

INTRODUCTION

In 1999, octanitrocubane was finally synthesized at the University of Chicago by Dr. Mao-Xi Zhang and Professor Philip Eaton. The success was corroborated when the structure of the molecule was identified at NRL by the author using single-crystal X-ray diffraction analysis on a crystal from a 2 to 3 mg sample. The synthesis was reported in mid-1999 to *Angewandte Chemie*, and reviewers called it a "Very Important Paper." In January 2000, it was published, and the journal featured the molecule on the cover.[1] This brings to fruition a long and difficult project.

As early as 1979, researchers in Army and Navy propellant programs realized that cubane could provide the fuels, propellants, and explosives of the future, but little was known then of its chemistry. Cubane was first made in 1964, with two substituents on opposite corners of the cube, but no way was known to add more groups to this cubane. Stepwise substitution methodology for cubanes had to be developed first. The chemistry for making highly nitro-substituted cubane derivatives has advanced tremendously in recent years. These advances have been stimulated by basic research funding from Army and Navy energetic materials programs and, for a while, from the Strategic Defense Initiative (SDI). "Energetic material" is a generic name for molecules that might be useful as fuels, propellants, or explosives. For military purposes, most interest is focused on high-density organic compounds that contain all of the elements needed for complete combustion to gaseous products in the absence of air. Nitrocubanes were identified early in Army, and later, Office of Naval Research (ONR) and SDI synthesis programs to be highly desirable energetic materials because of the dual predictions of high density and high energy of combustion. All nitrocubanes with more than five nitro groups also contain enough oxygen to oxidize all carbon and hydrogen atoms in the compound to gaseous CO, CO_2, or H_2O. It is the expansion caused by conversion from a dense solid to hot gas that produces the desired effect in a propellant or in an explosive. In the case of the higher (5-8) nitrocubanes, each molecule in the solid gives rise to 12 gaseous molecules in combustion.

In addition, octanitrocubane (ONC, Fig. 1) contains no hydrogen atoms, and thus produces no water when burned. Oxygen-balanced zero-hydrogen propellants leave little or no visible smoke (or steam) behind the rocket. The absence of hydrogen products also greatly reduces the near-infrared absorption and emission spectra; thus, these materials are called low-signature propellants. A dense rocket plume serves no useful purpose. Enemies can more easily track such a rocket, and the smoke may obscure sensors of friendly forces attempting to monitor a battle scene.

ENERGETIC MATERIALS AND DENSITY

The heat released by the decomposition reaction, the number of moles of gas, and the molecular weight of the gases are all critical factors contributing to the effectiveness of a propellant or explosive. But density is also crucial, and so it is mentioned often in

FIGURE 1
The molecular structure of octanitrocubane as it occurs in the crystal. The ellipsoids represent the magnitude of atomic displacements that are primarily due to harmonic vibrations.

describing new energetic materials. Of course, the more moles of "active ingredient" that can be packed into the limited volume of a shell or rocket the better, and that depends directly on the density. But less obviously, the density affects the detonation velocity of an explosive, which is a specialized "linear" rate of reaction that ranges from 5 to 10 km/s in explosives. This reaction rate in turn directly affects the maximum pressure that can be attained. In a given material, the detonation velocity is proportional to the *square* of the density, so great effort is made to formulate materials in their most dense form. It is less clear how to compare the effect of density in different chemical entities, especially when the basic framework of the molecule changes. However, there is certainly an historic correlation between highest densities and best performers, so high density is always a goal in energetic materials synthesis. Algorithms have been developed that statistically relate the density of all known energetic compounds to their structural formula and predict the densities of known compounds to within 3%. They can be used to predict densities for target molecules that have not yet been made. Computational chemistry, using techniques known as ab initio quantum chemistry and molecular mechanics, can be used to actually predict detailed crystal structures for unknown molecules. This can also be used to predict density, but there are

pitfalls. Because a large number of molecules are essential to model the forces governing crystal formation, the mathematical problem contains vast numbers of variables; approximations are still necessary. Both statistical and computational types of algorithms predicted densities of 2.1 to 2.2 for ONC.

PROPERTIES OF THE HIGHER NITROCUBANES

Two properties, density and thermal stability, are unusually high in all of the nitrocubanes, but they are especially striking in those containing more than five nitro groups. We were concerned that putting that many energetic groups in close proximity might lead to compounds that easily decomposed when heated. But the nitrocubanes, even ONC, can be heated beyond 250 °C before rapid decomposition sets in. High densities were expected and certainly do occur. The penta-, hexa-, hepta-, and octa-nitrocubanes have densities of 1.959, 1.947, 2.028, and 1.979 g/cm^3, respectively, from X-ray analyses of crystals at NRL (Fig. 2). Such values are almost never seen for organic compounds; no more than 10 other compounds made from C, H, N, and O have densities beyond 1.95, and less than five are known with $D > 2.0$.

Penta- and Hexanitrocubane

These compounds were the first to contain adjacent nitro groups, and thus their very existence provided an essential proof-of-principle milestone in this project. Hexanitrocubane is anomalously low in its density; its value actually dips slightly lower than that observed for pentanitrocubane. This has not been explained or explored very much to date; perhaps a denser crystal form, grown under different conditions, will be found in the future. The density of pentanitrocubane is of much more interest. This seems to be the only case of a nitrocubane having an anomalously high density, and this must be due to its molecular packing. Before discussing it further, a few words about molecular contacts in solids are needed.

Each atom has a characteristic radius, called the van der Waals (vdW) radius, that is the radius for the best hard-sphere model for that atom. In other words, if one were building model crystals with molecular models made from rigid spheres, using vdW radii for the spheres (tabulated in reference books and articles) would give the best geometric correspondence with actual crystal structures. Actually atoms are not perfectly hard. They approach one another at various distances when they are "touching" in the solid state. The vdW radius is a threshold; the repulsive energy
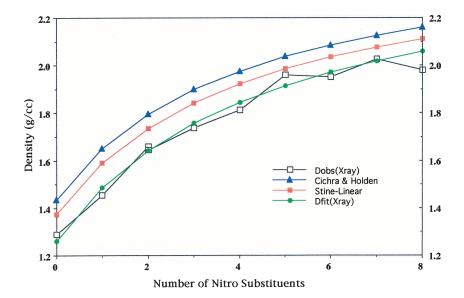
FIGURE 2

Nitrocubane densities. Dobs (squares) are the observed X-ray densities derived from the measured volumes of the crystal unit cells. Dfit (solid circles) mark a hyperbolic smooth curve that is fit to the X-ray observations. The other curves show predictions from two "statistical" algorithms (see text) used to estimate densities.

rises sharply when two atoms approach to a distance shorter than the sum of their vdW radii unless an unusual intermolecular attraction exists between the molecules. In the nitrocubanes, because of the difference in the electron affinity of different atoms, the nitro oxygen atoms withdraw electrons from the electron density distributions of nearby carbon and nitrogen atoms. Thus all oxygen atoms are expected to be negatively charged (to the extent of a fraction of an electron), and all carbon, hydrogen, and nitrogen atoms positively charged. This gives rise to electrostatic interactions that can affect intermolecular contact distances and cause deviations from the vdW rigid-sphere model.

Figure 3 shows a layer of pentanitrocubane molecules as they are packed in the crystal. Distances less than the sum of vdW radii are shown by dashed lines, and O...C and O...H distances of electrostatically attractive (opposite charges) types are seen. A few distances less than vdW are noted in most crystal structures, but 29 are around the perimeter of the pentanitrocubane molecule. In fact, some of these distances are very short. Eight pairs of O...C contacts in the 2.80 to 3.06Å range are considerably below the accepted O...C vdW contact distance of 3.22Å. In this crystal, there is obviously such an opportune fit that the negative oxygen atoms of the nitro groups can approach closely to the electron-deficient faces of neighboring molecules, even though these cube-faces bear up to three nitro groups themselves. Seeing this, we had hopes that when ONC was made, its density might equal or even better the predictions. Modeling calculations say that this is still possible, but it has so far not occurred.

Heptanitrocubane

Heptanitrocubane might have been a stumbling-block on the way to ONC. There was theoretical reason to believe that the final hydrogen might be reactive and the compound only transiently stable. However, it is stable and easily soluble in polar solvents, e.g., acetone, tetrahydrofuran (THF), and CH_2Cl_2, without reaction. Beautiful, colorless, solvent-free crystals form when its solution in fuming nitric acid is diluted with sulfuric acid. X-ray analysis of a single crystal determined the crystal structure and provided an accurate density at 21 °C of 2.028 g/cm^3. As might be expected from its extremely high density, the crystal structure shows many very close intermolecular contacts about each molecule. There are many atom-atom contacts shorter than the sum of their vdW radii—21 between nitro oxygen atoms and 12 between a nitro oxygen and a C, N, or H atom. The latter contacts are electrostatically favorable and help increase the density. In addition, the lone hydrogen atom participates in a weak hydrogen bond [CH...ON distance: 2.53Å, C-H...O angle: 165.5°] that links molecules in a chain along the b axis. This is shown in Fig. 4. A hydrogen bond is a

53
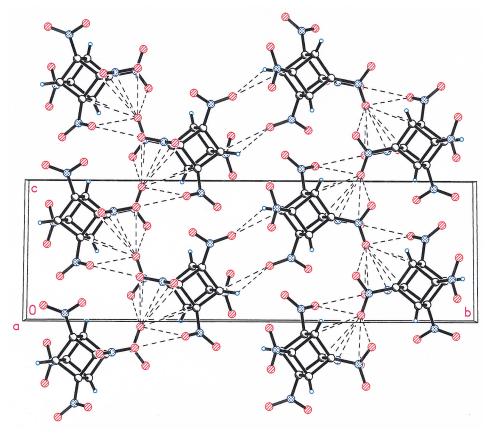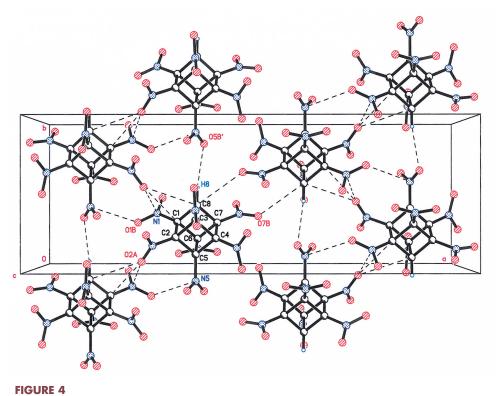
FIGURE 3
Packing in pentanitrocubane. Dashed lines illustrate unusually close contacts.

FIGURE 4
Packing in heptanitrocubane. Dashed lines are unusually close contacts. A hydrogen-oxygen contact connects molecules vertically in this view (see text).

special type of attractive interaction between molecules that has a strong electrostatic component. They are not often found in energetic materials but are famous for their crucial role in allowing peptides and nucleic acids to bind and recognize one another in biochemical processes.

Octanitrocubane

ONC itself is a stable white solid, somewhat soluble in hexane, and readily soluble in most common organic solvents. Solvent-free crystals for X-ray analysis were obtained from trifluoroacetic acid or from fuming nitric acid/sulfuric acid. Unless they were scrupulously dried, crystals of a hydrate were formed from benzene, chloroform, and numerous other solvents. X-ray analyses have been performed at NRL on single crystals from most batches grown to date, and only one crystal form of the neat compound has thus far been seen. In it, the average CC cubane-edge distance is 1.562Å, which is within the observed range of stable C-C single bonds. The molecule displays a close approach to a fourfold axis of symmetry, although this is not required by the crystal symmetry. This is probably the highest symmetry attainable by ONC. The twofold symmetry of the nitro groups is not compatible with the threefold symmetry seen at the corners of a truly "cubic" cube. Although ONC's density is high, it is lower than that of heptanitrocubane and well below predictions (Fig. 2). The latest and most sophisticated calculations from computational chemistry still predict a density of about 2.1 g/cm^3 for ONC, so we are of course searching for a denser form. There is a precedent for the possible existence of other forms: Current state-of-the-art explosives HMX and CL20 each display several

different crystal packing arrangements, called polymorphs, that differ in density. The four known polymorphs of CL20 (Fig. 5) have densities (also measured at NRL) ranging from 1.91 to 2.044 g/cm^3.

The packing of octanitrocubane is fairly ordinary from a crystallographic standpoint. Although the cubane framework has essentially cubic symmetry, and the eight nitro groups are oriented so that the overall molecule has fourfold symmetry, the molecule crystallizes in a common monoclinic crystal system, with only twofold symmetry in its packing environment. The density is high, but lower than expected, as can be seen from the graph of nitrocubane densities (Fig. 2). Even the simple extrapolation of the observed X-ray densities of the other nitrocubanes shown would lead to an expected value of 2.06 g/cm^3. A look at the packing in this crystal form helps to explain this anomaly. Figure 6 shows that all close contacts are between oxygen atoms. Since all close contacts are of the O...O type, and all O's are negative due to electron withdrawal, the primary electrostatic effect is repulsive. Of course, many more, slightly longer contacts are attractive, and other types of interaction can make this a high-melting cohesive crystal overall. But the strong nitro-nitro interactions in this crystal form probably explain the anomalous lowering of density.

Is it inevitable that an ONC molecule is shielded by its own nitro groups? Perhaps another molecule bearing a nitro group can never approach without encountering a primarily repulsive set of intermolecular contacts. Luckily, the answer to this is no, leaving the door open to the possibility of a denser form. Figure 7 shows a small portion of the packing in an ONC-nitrobenzene solvate. In this crystal, the overall density is lower, 1.758 g/cm^3, because of the ad-

FIGURE 5
A view of the molecular structure of CL20, a powerful hexanitro energetic material synthesized in 1987 at the Naval Air Warfare Center, China Lake, California. Its backbone is a cage made from an equal number of N and C atoms, arranged in 5-, 6-, and 7-membered rings.

55
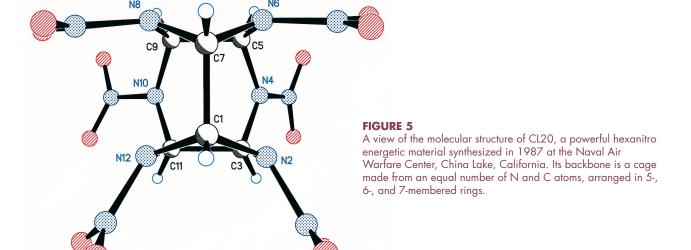
FIGURE 6

A view of a single layer of the molecules of ONC as they occur in the crystal. This layer is the most closely packed of several views that could be chosen from the 3D crystal structure. The dashed lines, which occur only between oxygen atoms, mark unusually close approaches.
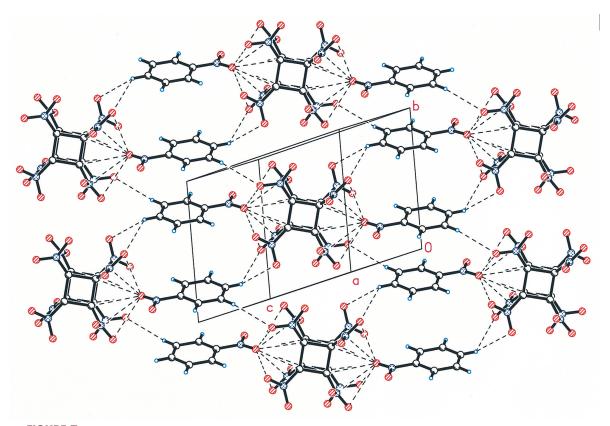
FIGURE 7

The packing in the crystal of a nitrobenzene:octanitrocubane solvate. The dashed lines are unusually close contact distances. This view shows that a nitro oxygen atom can insert itself between the nitro groups on ONC and interact with the carbon atoms of the cube.

dition of two molecules of low-density solvent for each ONC. The nitro group of the solvent, however, penetrates a quartet of nitro groups on one cube-face to form four very close electrostatically attractive O…C contacts. This type of close solvent-ONC interaction has been seen in two other cases. Water forms a monohydrate with ONC, and, in fact, the two molecules seem to have a positive affinity since ONC picks up water from almost-dry solvents. In addition, another 2:1 solvent complex, very similar to the nitrobenzene solvate, is formed by ONC and dimethylsulfoxide (DMSO), with very close approaches between the sulfonyl (S = O) moiety and an ONC cube face. The density of the monohydrate is 1.925 g/cm^3 and that of the DMSO solvate is 1.735 g/cm^3.

BONDING AND STABILITY OF THE CUBANE BACKBONE

Atoms attach, or bond, to other atoms at specific angles that are characteristic of each molecule. Cubane is a hydrocarbon that has eight atoms of carbon forming the corners of a regular cube. Thus, all angles between the C-C bonds in cubane are exactly 90°. This is far from normal for a carbon-containing molecule. The normal, unstrained angle between C-C single bonds (e.g., in diamond or a fuel such as propane) is 109.5°. Angles observed between multiple bonds are even larger and farther from 90°. For example, in benzene and in buckminsterfullerane (both molecules whose frameworks are constructed from single and double C-C bonds), the angles are close to or equal 120°. Compounds containing 3- and 4-membered carbon atom rings do occur, with unusual bond angles of 60 to 90°, but they are highly energetic (i.e., they release energy when they dissociate), and some will spontaneously decompose.

The large bond angle deformations in cubane, away from the typical 109.5 to 120° range, make it a powerhouse of stored energy. Each bent bond can be thought of as a storage site for potential energy—just like the spring in a set mousetrap—and the molecule as a whole is literally set to burst. The total strain energy has been measured[2] to be 181 kcal mol^{-1}, making it the most highly energetic hydrocarbon compound known. For comparison, the energy needed to dissociate ethane, C_2H_6, into two CH_3 fragments is estimated to be 85 kcal mol^{-1}.[3] Surprisingly, cubane is quite stable. It can be heated beyond 200 °C before decomposition; it can be sublimed easily at 100 °C, and it has a shelf life measured in years.

How can cubane be stable when its stored energy is so much greater than the energy needed to break a single bond? One reason is that the strain energy is balanced so well by the symmetry of the molecule—12 bonds share the strain equally. Another reason is that breaking a single bond does not really relax the molecule very much. The cage would open slightly, but it would still retain most of the angle strain, and would tend to reconnect itself. It really takes concerted dissociation of two bonds to begin unraveling the cube. The high activation energy of this step slows the rate of the overall process. This is called kinetic stability, and it might be likened to the amazing stability of diamond. Diamond is metastable; it is thermodynamically unstable with respect to a transition to graphite, but the bonding rearrangement needed is so drastic that it just does not occur under normal ambient conditions.

THE SYNTHESIS OF ONC: PART I. GETTING TO TETRANITROCUBANE

A molecule containing the cubane framework was first reported in 1964 by Eaton and Cole.[4] (Unless otherwise mentioned, all syntheses mentioned took place at the University of Chicago.) The original synthesis produced a cubane with two carboxymethyl (-COOCH$_3$) substituents at diagonally opposite corners of the cube. This product is still the most common cubane, and it is available commercially at a price of about $90/gram ($40K/pound). For about 20 years, few derivatives of cubane were known because no good way was known to add more substituents to the cubane once it was made. The primary route to new cubanes was through manipulation of the two carboxyl substituents on the original cubane product. When interest in cubane as an energetic material was first stimulated in the 1980s, a substituent-transforming route led to the first nitrocubane, 1,4-dinitrocubane, reported in 1984. At about that same time, basic research on the reactivity of cubane to various reagents led to the discovery that sites adjacent to an amide substituent were activated with regard to substitution by active metals such as lithium. Lithium atoms could, in turn, be replaced by less reactive metals, and those eventually by organic groups such as carboxyl groups. This process, called ortho metalation, is not an easy route to general substitution by more common groups. It involves difficult reagents and usually many steps of successive replacement to get to a specific polysubstituted cubane. However, in this way, in 1989/1990, the target energetic molecules 1,3,5-trinitro- and 1,3,5,7-tetranitrocubane were made. Analyses at NRL reported[5] quite high densities (1.74 and 1.81 g/cc for

tri- and tetra-nitrocubane, respectively) and indicated no structural instabilities in the molecules, such as extra-long C-C or C-N bonds (signs of incipient weakness).

Similar stepwise metalation and substitution led to tetra- and penta-carboxyl substituted cubanes, and even several new octa-substituted cubanes. However, direct attempts to add more than four nitro groups to the cube failed, and there was speculation that the placement of nitro groups on two adjacent carbons might inevitably destroy the cube. It now is accepted that placing a nitro group, known to be an electron-withdrawing group, next to an amino substituent, known to be electron-donating, leads to immediate cubane instability. Unfortunately, the most common transformation route used to convert a carboxylate substituent to a nitro group involves going through some type of amine substituent along the way. A new type of reaction had to be discovered.

Familiarity with the properties of tetranitrocubane helped, eventually, show the best way to proceed. Research on tetranitrocubane was aided by the discovery, at the Army Research Development & Engineering Center (ARDEC), of a more direct synthesis of tetranitrocubane and other polysubstituted cubanes. Bashir-Hashemi at ARDEC reported that a photochemical reaction of the commercially available 1,4-cubanedicarboxylate with oxalyl chloride can lead directly to tetra- and penta-carboxyl-substituted cubanes in high yields. The structures of several of these new cubanes were also identified by X-ray analysis at NRL.

THE SYNTHESIS OF ONC: PART II. BEYOND TETRANITROCUBANE

Most hydrogen atoms connected to carbon in organic molecules are chemically neutral and relatively unreactive. Tetranitrocubane was found to have somewhat acidic hydrogen atoms in NMR proton-exchange studies at Chicago, and it was found that with care, a hydrogen ion (a proton) could be stripped off by a strong base [NaN(SiMe$_3$)$_2$] to form a cubyl anion in a THF solution at −75 °C, but that higher temperatures led to decomposition. Reaction of this ionic cubane form with nitration reagents N$_2$O$_4$ or NO$_2$Cl was possible at very low temperatures (from −75 to −196 °C). This leads to pentanitrocubane, and then, by further nitration of purified pentanitrocubane under similar conditions, to hexanitrocubane. These compounds[6] were the first cubanes to contain adjacent nitro groups, and they were found to be stable, with no obvious shock sensitivity. In a rapid heating test known as differential

scanning calorimetry, decomposition was seen only above 250 °C. The next step, the synthesis of heptanitrocubane, was accomplished in basically the same way, through the anion, but only by discovery of substantially different reaction conditions. The amount of base used was increased by three- or fourfold, and the solvent, THF, was diluted in midreaction with isopentane, allowing the attainment of a lower temperature without freezing. Under these reaction conditions, a step-wise reaction from tetranitrocubane to heptanitrocubane was achieved in one continuous sequence with an isolated yield of 74% crystalline (heptanitrocubane) product.

However, none of the variations tried with these nitrating reagents led to any octanitrocubane. The heptanitrocubane could react with non-nitrating reactants, going through its anion stage to form other products such as iodoheptanitrocubane and methylheptanitrocubane, but it would not react with any common nitrating reagents. The successful route was a two-step indirect process, although both were performed in the same vessel. Heptanitrocubane was added to nitrosyl chloride (NOCl) in base at −78 °C (anion-forming conditions), probably producing *nitroso*heptanitrocubane in solution. This compound was not isolated, it was found to be unstable. But treating this solution with ozone (O$_3$) oxidized the nitroso group to a nitro group and gave the long-awaited octanitrocubane in 45-55% yield.[1]

THE ROLE OF X-RAY DIFFRACTION IN SYNTHESIS RESEARCH

At NRL, in the Laboratory for the Structure of Matter (LSM, Code 6030), 60 new cubanes have been analyzed since 1987 by single-crystal X-ray diffraction analysis. Many have come from the nitrocubane project described here, but others have come from other projects and other laboratories that are developing other aspects of cubane chemistry. These compounds are made in milligram quantities, and are often not easy to identify through infrared or nuclear magnetic resonance spectra. X rays scattered by a single crystal, grown by slow evaporation of a solution containing just a milligram (or less) of pure material, reveal the molecular structure of the compound, its density, and how its molecules pack in the solid state. If the cubic backbone of the molecule has rearranged, the spectra may be almost unaffected, but it is immediately apparent through X-ray analysis, and research along that pathway can be halted or modified.

The NRL X-ray diffraction group (LSM) has optimized its techniques and response capability for rapid

crystal data analysis. This has been accomplished through acquisition of advanced X-ray diffraction hardware and software and continual refinement of laboratory procedures. LSM also provides access to a database of crystal analyses of more than 650 energetic-materials crystals amassed at NRL; most (>95%) were analyzed here at NRL. These data are used to model energetic material properties such as sensitivity and thermal stability. Coordinates from crystal structures are provided many times each year to ONR researchers in universities, industry, and other government laboratories. NRL/LSM also provides a number of facilities that are not available in a routine X-ray analysis laboratory. Three diffraction scientists are certified for explosives handling and are aware of the special techniques needed to deal with the stability problems often seen in energetic materials samples. The NRL X-ray instrument inventory is well-suited for samples that are unstable or difficult to crystallize. The laboratory has a 1024×1024 CCD (charge-coupled device) area detector (with an upgrade scheduled for a still larger version) mounted on a 5 KW Rigaku rotating anode source, with a phosphor optimized for $CuK\alpha$ radiation and a high-intensity focusing-mirror monochromator. This is a state-of-the-art diffractometer for rapid examination and data collection from weakly scattering (e.g., very tiny) crystals, especially organic crystals. The laboratory also owns three low-temperature controllers that can cool a crystal in the X-ray beam by bathing it in a stream of gas from a liquid N_2 source. This is sufficient to stabilize a crystal that is thermally unstable, is low melting, or contains labile solvent. X-ray diffraction analyses of materials are usually provided to the chemist within a week. Recrystallization is provided here at NRL/LSM also. This can be a challenge with very small samples, but we have often succeeded with samples of less than 10 mg. The X-ray analysis proceeds with no requirement for a structural formula so unexpected unknowns can be identified.

OUTLOOK

The synthesis of four state-of-the-art and beyond energetic materials was accomplished through the research described here. Although octanitrocubane catches the imagination with its symmetry, heptanitrocubane currently is significantly easier to make than ONC, is denser, and is probably more powerful than any molecule now in use. But in all honesty, it is likely to be a long time before it will be seriously looked at by the military. The problem is cost. This was alluded to briefly above when I mentioned the cost of the only commercially available cubane precursor—$40K/pound. That is not a lot for a pharmaceutical or a laboratory research chemical, but it is impractical for a propellant or explosive, and that number is just the cost of the starting material. Obviously, now that the goal is known to be feasible, research must be focused on the problem of an *economic* synthesis of cubane and/or octanitrocubane. This may look to be impossible now, but need not be. Four molecules of acetylene are a stoichiometric (atom-by-atom) equivalent of one molecule of cubane, and acetylene is an energetic molecule that we have learned to make cheaply and handle safely. Acetylene forms products other than cubane when it reacts, but that could be a matter of conditions or of finding the right catalyst. Recent years have seen revolutionary advances (right here at NRL) in the synthesis of large diamond crystals, also once thought to be impractical. Thus, several alternative routes to cubanes are being explored at the University of Chicago, and the X-ray identification of intermediates has already begun at NRL.

ACKNOWLEDGMENTS

REFERENCES
[1] M-X. Zhang, P.E. Eaton, and R. Gilardi, "Hepta- and Octanitrocubanes," *Angew. Chem. Int. Ed.* **39**, 401-404 (2000).
[2] D.R. Kirklin, K.L. Churney, and E.S. Domalski, "Enthalpy of Combustion of 1,4-Dimethylcubane dicarboxylate," *J. Chem. Thermodyn.* **21**, 1105-1113 (1989).
[3] S. Benson, "Bond Energies," *J. Chem. Ed.* **42**, 502-515 (1965).
[4] P.E. Eaton and T.W. Cole, Jr., "The Cubane System," *J. Am. Chem. Soc.* **86**, 962-964 (1964).
[5] P.E. Eaton, Y. Xiong, and R. Gilardi, "Systematic Substitution on the Cubane Nucleus: Synthesis and Properties of 1,3,5-Trinitrocubane and 1,3,5,7-Tetranitrocubane," *J. Am. Chem. Soc.* **115**, 10195-10202 (1993).
[6] K. Lukin, J. Li, P.E. Eaton, N. Kanomata, J. Hain, E. Punzalan, and R. Gilardi, "Synthesis and Chemistry of 1,3,5,7-Tetranitrocubane … and the First Preparations of Pentanitrocubane and Hexanitrocubane," *J. Amer. Chem. Soc.* **119**, 9591-9602 (1997).

THE AUTHOR

RICHARD D. GILARDI graduated from the Massachusetts Institute of Technology in 1961 with a B.S. degree in chemistry. He received a Ph.D. degree in physical chemistry from the University of Maryland in 1966; his thesis concerned the analysis of the vibrational behavior and far-infrared spectra of clusters of polar gas molecules. Dr. Gilardi joined NRL in 1966 as a National Research Council postdoctoral associate in the Optics Division Diffraction Group (Code 6030, now the Laboratory for the Structure of Matter). He came to NRL to learn the techniques of single-crystal X-ray diffraction analysis and stayed to participate in the further development of new diffraction analysis algorithms and their application to crystals of organic molecules. He is an author or co-author of 200 articles in structural chemistry, and has received eight NRL Research Publication Awards. In 1986, Dr. Gilardi received the U.S. Navy Meritorious Civilian Service Award.

Dr. Gilardi's structural research at NRL has involved a variety of materials, such as antimalarial drugs from the Walter Reed Army Institute of Research, insect pheromones from the U. S. Department of Agriculture, and a number of bioactive compounds (drugs, toxins) from the National Institutes of Health. Since the early 1980s, Dr. Gilardi's research has been focused on energetic materials (explosives, propellants, and extremely strained organic molecules). He collaborates regularly with more than a dozen laboratories across the United States that are participating in DoD energetic materials synthesis development, and he has aided this research community by identifying or corroborating of the crystal structures of more than 600 energetic precursors, intermediates, and final target molecules.

Growth of High-Quality Organic and Polymer Thin Films by the Matrix Assisted Pulsed Laser Evaporation (MAPLE) Technique

A. Piqué, R.A. McGill, J. Fitz-Gerald, E.J. Houser, and D.B. Chrisey
Materials Science and Technology Division

Thin organic and polymer films will play a pivotal role in the development of next-generation electronic devices, passivation coatings, and chemical or biological sensors. Novel methods are needed to deposit high-quality thin films over large wafer and small component areas with precise thickness control for improved device and system performance. The Naval Research Laboratory has developed a novel laser-processing technique for organic materials, polymers, and biomaterials called MAPLE (matrix assisted pulsed laser evaporation). MAPLE is a laser-based physical vapor deposition technique capable of producing ultra-thin and uniform coatings of many classes of organic and polymeric materials. Careful control of the processing conditions allows complex organic and polymeric molecules to be transferred intact to a substrate. Thin uniform films (10 to 1000 nm) of materials such as chemoselective polymers, biodegradable polymers, carbon nanotubes, carbohydrates, biomaterials, and composites have been deposited onto a variety of substrates. Using MAPLE, large or small regions within a substrate can be discretely coated with monolayer thickness control. Coatings prepared by the MAPLE technique have been used to fabricate chemical sensors with improved device performance when compared to the same devices coated by traditional techniques.

INTRODUCTION

Next-generation applications for functional materials will require tighter tolerances on the structural, morphological, and chemical composition of the thin films used in their fabrication. This is especially true for the deposition of high-quality thin films of organic or polymeric materials. Depending on the particular application, it may be desirable to deposit films containing single or multilayer structures of different organic or polymeric materials, homogeneous composite materials, or materials with graded compositions. In many situations, it will be necessary to discretely deposit the films, achieve conformal coverage, and provide high-quality films, especially in regard to surface coverage uniformity and thickness control. For electronic and optical device applications, the materials of choice cover a wide range—from polymeric materials for fabrication and passivation of electronic components to organic dye molecules for nonlinear and optical limiting applications. Thin films of poly-

meric, inorganic, and organic materials also play an important role in batteries, high-performance dielectrics, optical data storage, optical communications, and displays based on organic electroluminescent materials. Polymer and organic coatings are essential for the fabrication of chemical and biochemical sensors and in biomedical applications. These applications range from passivation films for prosthetic devices to coatings for targeted drug delivery systems. Figure 1 shows some examples of these applications. In most cases, state-of-the-art examples of these applications have pushed conventional deposition techniques to their limits. In the search for a universal approach to producing thin films of organic and polymeric materials, a new technique called MAPLE (matrix assisted pulsed laser evaporation) has been developed at the Naval Research Laboratory (NRL).[1] This article describes the MAPLE technique and how it has been successfully used for depositing high-quality thin films of organic and organometallic polymers, low and high molecular weight carbohydrates,
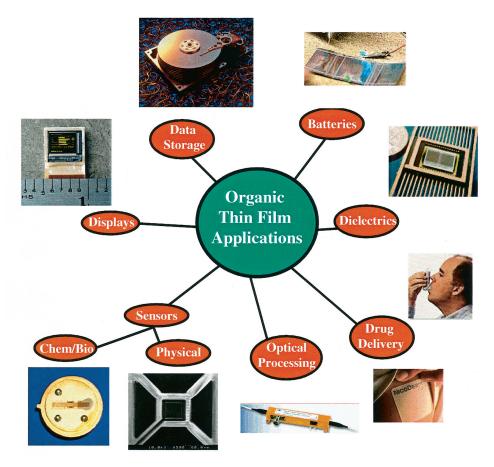
FIGURE 1
Applications where organic and polymer thin films play a significant role.

biodegradable polymers, and carbon nanotube/polymer composites.

Currently, thin films of organic and polymeric materials can be deposited by many techniques that range in complexity and applicability. The choice of which deposition technique to use depends on the physicochemical properties of the material, the tolerance requirements for film quality, the substrate that is being coated, and the costs involved. The simplest methods for applying a thin organic film are solution casting, aerosol, dip, or spin coating in which a solution of organic material in a volatile solvent is dispersed on a substrate surface. When the solvent evaporates, it leaves behind a coating of the polymer. Other techniques include in situ polymerization using plasma, electrochemical, catalytic, or photoactivated processes to polymerize monomer material in situ on the substrate surface. In addition, processes such as vacuum sublimation, plasma deposition, and pulsed laser deposition (PLD) have been applied with limited success to a few types of

polymeric materials. For certain classes of materials, thin films can be prepared by Langmuir-Blodgett, self-assembly, and other molecular-aggregation processes. Within this wide range of techniques, advantages and disadvantages restrict the utility of the process to certain types or classes of materials and the quality of the resulting films (Table 1 provides an overview of the capabilities for these thin film deposition techniques). By using MAPLE, a wide range of organic and inorganic polymers and lower molecular weight organics can be deposited as thin, high-quality, uniform, adherent coatings over an extended substrate surface area (10×10 cm^2), or in localized areas (10×10 µm^2) with high quality and without compromising the physicochemical properties of the deposited materials. Fundamentally, MAPLE appears similar to conventional PLD.[1] However, when comparing the two techniques, MAPLE provides a more gentle process for fabricating thin films of a wide variety of materials. To date, MAPLE has been successfully used for processing thin films of organic materials ranging

Table 1 — Comparison of Different Techniques Used
for Growing Organic and Polymeric Thin Films

Coating Technique	Aerosol Coating	Spin Coating	In Situ Polymerization	Vacuum Sublimation	Molecular-aggregation Processes	Ink Jet	MAPLE
Compatible with broad range of organic and polymer materials.	●	●				●	●
Monolayer thickness control			●	●	●		●
Uniform films over 6 in. dia. wafers		●	●	●	●		●
Film distribution not affected by solvent			●	●	●		●
Enhanced film-substrate adhesion					●		●
Not susceptible to contamination							●
Compatible with contact masking techniques			●	●	●	NA	●
Compatible with noncontact masking techniques						NA	●
Room temperature process	●	●	●		●	●	●
Atmospheric pressure process	●	●	●		●	●	
Works with small amounts of material					●	●	●
Can be automated	●	●	●	●	●	●	●
Compatible with active thickness feedback control	●		●	●		●	●
Multilayer capability				●	●		●
Used for depositing composite thin films	●	●				●	●

from macromolecules as large as 600,000 atomic mass units (a.m.u.) (hydrogels) to small molecular species with < 200 a.m.u (C_6-sugars).

MATRIX ASSISTED PULSED LASER EVAPORATION (MAPLE)

The key to the MAPLE process is the use of a frozen solid matrix as the laser target. This matrix consists of a dilute solution of a polymer or other solute material in a volatile organic solvent. Only solvents that are sufficiently volatile and do not form a film when evaporated by a laser are used. The solvent and solution concentration are selected so that the solute material of interest dissolves to form a di-lute, particulate-free solution, and so that most of the laser energy is initially absorbed by the solvent molecules, not by the solute molecules. At the molecular level, MAPLE is a photothermal process. Simply stated, the photons absorbed by the bulk solvent molecules are converted to kinetic energy, which is then transferred to the solute through collective collisions, resulting in the desorption of large molecular weight species. By careful optimization of the MAPLE deposition conditions, this process can occur without any apparent material decomposition. The MAPLE process proceeds layer by layer, depleting the target of solvent and polymer or organic material. Similar to PLD, the evaporated material is highly forward-directed from the region illuminated by the
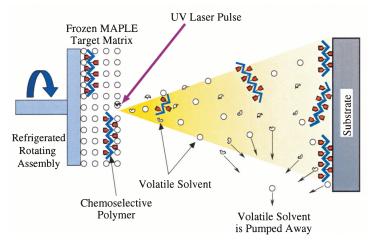
laser pulse along a direction normal to the target surface. When a substrate is positioned directly in the path of the evaporant plume, it is uniformly coated with the solute molecules while the volatile solvent molecules are removed by dynamic vacuum. Figure 2 is a schematic of the MAPLE process and a photograph of the interior of the MAPLE chamber. The mechanistic basis of the MAPLE technique is similar to the analytical technique called matrix assisted laser desorption/ionization-mass spectrometry (MALDI-MS). MALDI-MS is a soft ionization technique that allows desorption and ionization of large molecular species (approximately 10^4 to 10^6 a.m.u.). This process has been developed for studying macromolecules to determine their molecular weight distributions. A significant difference between the MAPLE and MALDI techniques lies in the treatment of the evaporated material. In the MAPLE process the material of interest is not deliberately ionized or decomposed, but is collected on a substrate to form a coating rather than directed into a mass spectrometer for analysis.
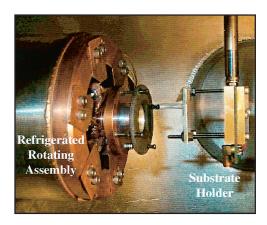
The MAPLE deposition system consists of a conventional pulsed laser deposition chamber with a modified substrate holder fixture that houses a surface acoustic wave (SAW) device and associated electronics. The SAW resonator is used to monitor the deposition rate in real time. For a target-to-substrate distance of 5 cm, a region of about 6 cm^2 is uniformly coated. The substrates are typically at room temperature during the deposition process, but they can be heated to anneal the growing film. A UV pulsed laser firing at rates between 1 to 20 Hz is used. The laser fluence at the target is typically varied between 0.01 and 0.5 J/cm^2, depending on the solute material and solvent used. A matrix solution is prepared by dissolving the material to be deposited in a solvent at a concentration between 0.005 to 0.050 g/g.[2] Depending on the organic or polymeric material to be deposited, various solvents have been used, including t-butyl alcohol, chloroform, toluene, and water. After dissolution, the matrix is frozen in a target die and then mounted on a cryogenically cooled rotating target assembly with the open die end facing the laser (see Fig. 2). Once the chamber is evacuated, the target can be cooled to −150 °C for as long as necessary. After each deposition process the target can be recovered for later use. Using these conditions, the deposition rate for the polymer/organic materials is about 1Å every 10 laser pulses. Post deposition analysis can include a variety of techniques, such as thickness profilometry, Fourier transform infrared (FTIR) analysis, electrospray mass spectroscopy (EMS), and size exclusion chromatography (SEC). Any significant decomposition or denaturation that occurs during the MAPLE process can be readily detected by FTIR and mass spectroscopy. SEC is used to determine the molecular weight distribution of a polymer film before and after MAPLE deposition.

One of the unique advantages of MAPLE is that it can be easily combined with noncontact shadow masks to limit the deposition to the required area on the substrate. This is important for fragile substrates and is much less expensive and less time-consuming than subsequent removal by patterning and etching. Furthermore, for those polymers that are dissolved

(a) Basic elements of the MAPLE process. The UV laser interacts with the volatile solvent in the frozen matrix releasing the polymer molecules, which form a film over the substrate. The solvent is pumped in the process.

(b) Interior of the MAPLE chamber. The refrigerated target holder is on the left, the brass block on the right holds the SAW resonator and the substrates.

FIGURE 2
Matrix Assisted Pulsed Laser Evaporation (MAPLE).

by the same solvents used to wash off the resists, depositing the polymer through a mask might be the only way to deposit many discrete thin film structures. The MAPLE process has been used successfully to deposit polymers through masks with features in the micron size range (Fig. 3). This capability is very important for the manufacture of sensor arrays and electronic components. At the wafer level in production applications, a larger number of identical devices could be manufactured with a single deposition step with the use of masks.
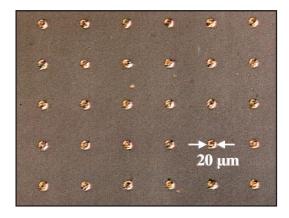
FIGURE 3
Optical micrograph showing the pattern generated after MAPLE depositing an additive polymer through a shadow mask.

THIN FILMS OF CHEMOSELECTIVE POLYMERS

For chemical sensor applications, the physicochemical properties of the chemoselective coating are critical for the sensor performance.[3] NRL has taken a leading role in the design and development of chemoselective polymers for toxic gas sensor applications. One NRL chemoselective polymer that has a variety of desirable properties is a hydrogen bond acid functionalized polysiloxane known as SXFA (Fig. 4). To provide improved sensor signal kinetics, the deposition of very thin (10 to 50 nm) and highly uniform films of SXFA or any other chemoselective polymer is highly desirable.

Initial laser processing studies with SXFA films grown by PLD proved to be fruitless because of excessive decomposition of the polymer. The FTIR spectra of the material collected after PLD of SXFA (Fig. 4(c)) demonstrates that the PLD processing resulted in massive decomposition. Similar decomposition problems have been observed using PLD to deposit other polymers as well. Our early studies clearly showed that most polymeric materials would require a more gentle process than conventional PLD for the coating deposition to proceed without significantly modifying the physicochemical properties of the native material. This goal was achieved with the MAPLE technique; in later experiments, high-quality thin films of SXFA were deposited by MAPLE on a variety of substrates. The FTIR spectra of the native SXFA (Fig. 4(a)) and MAPLE-coated SXFA (Fig. 4(b)) are essentially identical, with very similar absorbance ratios for the key absorption bands.

One of the key technical advantages of the MAPLE process is that the polymer is deposited on a substrate free of bulk solvent. In contrast, deposition techniques such as aerosol, spin, ink jet, or dip coating require a solution of a polymer in a solvent to physically wet the surface of the substrate to be coated. The uneven and unpredictable wetting, distribution, and evaporation of the solvent molecules result in nonuniform polymer coatings. Regardless of the surface quality of the substrate, the MAPLE process allows a coating to be deposited in a reproducible fashion. This is not the case for deposition techniques where bulk solvent is allowed to wet the surface. The wetting of the solvent to the substrate is critical in determining the spreading of the solution, and this is highly dependent on the substrate material and the surface free energy.
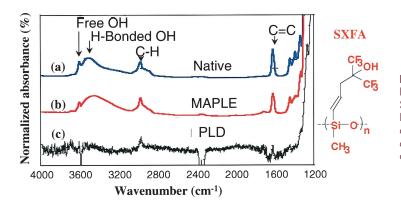
FIGURE 4
FTIR spectra belonging to various samples of SXFA, a chemoselective polymer developed at NRL. (a) native SXFA, (b) SXFA from a film deposited by MAPLE, and (c) SXFA from a film deposited by PLD. Notice that only the MAPLE-deposited SXFA film matches the native spectra.
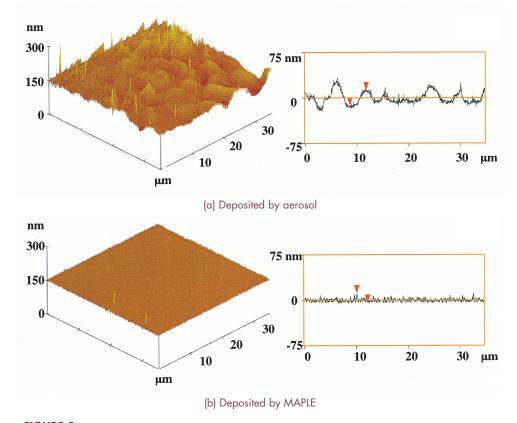
Optical microscopy, SEM, and AFM analysis of SXFA films deposited by both aerosol and MAPLE on various substrates revealed significant differences between the surface morphology and uniformity of the films deposited by each technique. Figure 5 shows the AFM images (35 μm × 35 μm) for SXFA films deposited by aerosol and MAPLE techniques on silicon substrates. The root-mean-square surface roughness of the SXFA film coated by aerosol was 11.3 nm, compared to a value of 2.6 nm for the SXFA film deposited by MAPLE. The AFM images confirm that the MAPLE-deposited films have a surface quality superior to those deposited by the aerosol technique.

THIN FILMS OF BIOCOMPATIBLE MATERIALS

There is considerable interest in thin film processing of technologically important organic and biocompatible materials. This would allow further developments in areas such as screening of biomaterials, drug delivery systems, biomolecular devices, integrated neuronal-electronic devices, biocomposites, and biosensors. One example of a biocompatible ma-

terial is dextran. Dextran is a carbohydrate polymer with average molecular weights ranging from 10,000 to 2,000,000 a.m.u. When hydrated, dextran can be used to prepare hydrogels as thin films for biosensor applications. In these applications, a highly hydrated surface- or water-retaining surface is required to support higher order macromolecular structures or allow diffusion of molecules such as analytes or nutrients for detection and metabolism, respectively. Using the MAPLE technique, thin and uniform films of dextran and one of its building blocks, glucose, have been prepared. Figure 6 shows the FTIR spectra corresponding to the fingerprint region for a native carbohydrate sample and for a thin film produced by MAPLE of dextran. Based on the FTIR spectrum, the material collected in the films appears to be essentially identical to the native carbohydrate. Figure 7 shows the EMS spectra for the glucose film, which is essentially identical to that of the native material.

The deposition of thin biocompatible polymer films for drug delivery systems is one potential application area for MAPLE. In this application, thin polymer films are used to either form a diffusive layer to allow a constant dosage of a drug through a patch applied to the skin or encapsulate a drug in a biode-

(a) Deposited by aerosol

(b) Deposited by MAPLE

FIGURE 5
AFM images of SXFA films on silicon substrates. The surface nonuniformities on the aerosol deposited film are due to evaporation of the solvent. MAPLE allows for the deposition of solvent-free polymers with superior surface morphology.
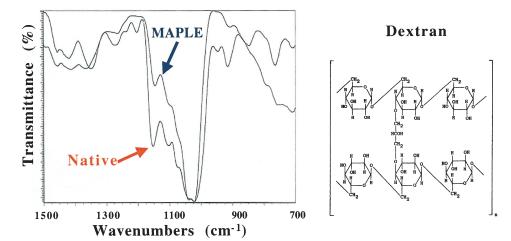
FIGURE 6
FTIR spectra showing the carbohydrate fingerprint region from native and MAPLE samples of dextran.
The full transmittance spectra showed the presence of the expected major and minor absorption bands.
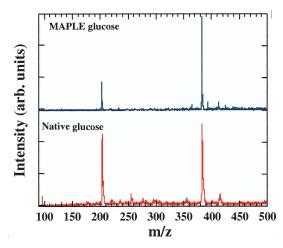
FIGURE 7
Electrospray mass spectra of native and MAPLE sample of glucose; the agreement between spectra of the native and MAPLE deposited glucose is excellent.

gradable coating. Varying the thin polymer coating in either instance allows control of the dosage rate of the drug. For example, biodegradable thin polymer coatings can be used to tailor the release of drugs that once had to be administered from hours to several days. This would improve the local vs systemic effects profile and thereby target a specific time or even possibly a specific organ. By depositing nanometer-thick coatings using the MAPLE technique, a sterile, dry coating with less than 1% by weight coating material can obtained with a chemical composition identical to the native material. Initial studies using the biodegradable polymer poly(lactic-co-glycolic) acid (PLGA 50:50) with molecular weights of 40,000 a.m.u. have produced promising results. Figure 8

shows FTIR profiles of original native PLGA and a thin film of PLGA grown by MAPLE. The similar spectra clearly shows that the basic structure of the PLGA material is not altered after MAPLE processing. Further characterization by SEC indicates that the molecular weight of the PLGA has remained constant after processing by MAPLE.

THIN FILMS OF CARBON NANOTUBE COMPOSITES

Carbon nanotubes were discovered in 1991 as a new form of carbon. They exist as closed tubular structures that consist of nested cylindrical graphitic layers capped by fullerene-like ends with hollow internal cavities. These structures can be metallic or semiconducting, depending on the tube geometry. They show promise for a variety of applications, in particular those that can take advantage of their excellent electron field emitter characteristics. Carbon nanotubes also can be used in various composite forms as both mechanical load-bearing structures and as active electronic conductors in chemical sensor arrays. For polymer nanotube composites (PNTC), major obstacles exist in thin film preparation because of carbon nanotube agglomeration, polymer viscosity, and control over film thickness. By using the MAPLE technique, PNTC thin films can be grown at controlled thicknesses ranging from 1 nm to 1 micron, with a high volume fraction of carbon nanotube constituents. Currently, studies using MAPLE to deposit thin films of carbon nanotubes with and without a polymer matrix are being conducted. Figure 9(a) is a scanning electron micrograph of a PNTC array structure using poly-(ethyleneglycol) (PEG) as a
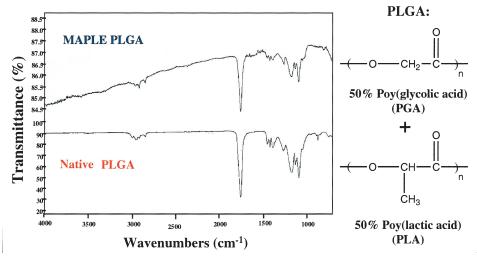
FIGURE 8

FTIR spectra from native PLGA and a MAPLE-deposited PLGA 50-50 film. Both spectra are essentially identical. PLGA is a biodegradable polymer obtained by the mixture of poly(glycolic acid) and poly(lactic acid).
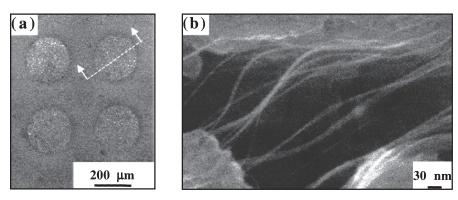
FIGURE 9

SEM micrographs of MAPLE-deposited composites made with a polymer matrix of poly-(ethyleneglycol) and carbon nanotubes. (a) Image belonging to an array of the composite deposited by MAPLE through a shadow mask. (b) Detail showing the carbon nanotubes present in the composite film after fracture along the line indicated in (a).

polymer matrix material. Figure 9(b) is a scanning electron micrograph of the fractured PNTC array element depicted schematically in Fig. 9(a). Although the alignment of the carbon nanotubes is in the direction of the applied force during fracture, it is clear that carbon nanotubes are distributed throughout the bulk thin film.

THE FUTURE OF MAPLE

To date, MAPLE has been successfully used to deposit high-quality films of materials spanning a broad range of molecular weights. These include carbohydrates, biodegradable polymers, carbon nanotube composites, and a wide variety of inorganic and organic polymeric materials. The MAPLE deposition of several biomaterials is being studied, and this may lead to new applications to explore. It is clear that the MAPLE technique would have a great impact with polymers used in bio-applications, and early results with drug delivery/release applications appear promising. Other possible future applications of MAPLE include polymer/organic multilayers, light-emitting organics, and novel microelectronics based on organic thin films.

The ability to fabricate these types of coatings could revolutionize areas such as electronics, display technologies, MEMS, chem-biosensing, genomics, and tissue-based engineering. In addition, novel biomaterial structures could be fabricated for which there

are no naturally occurring analogs, *e.g.*, heterogeneously patterned biomaterials with micron-size lateral dimensions and even finer resolutions for multilayer biomaterial structures. These novel biomaterial structures will require conventional electronic interfaces for signal transduction and control, pushing the current state of the art to an unexplored regime. MAPLE has opened the door to this new world, and the Naval Research Laboratory is poised to play a leading role in its exploration and development.

ACKNOWLEDGMENTS

REFERENCES

[1] R.A. McGill and D.B. Chrisey, "Method of Producing a Film Coating by Matrix Assisted Pulsed Laser Deposition," U.S. Patent 6,025,036, issued February 15, 2000.

[2] A. Piqué, R.A. McGill, D.B. Chrisey, D. Leonhardt, T.E. Mlsna, B.J. Spargo, J.H. Callahan, R.W. Vachet, R. Chung, and M.A. Bucaro, "Growth of Organic Thin Films by the Matrix Assisted Pulsed Laser Evaporation (MAPLE) Technique," *Thin Sol. Fi.* **355-356**, 536-541 (2000).

[3] R.A. McGill, M.H. Abraham, and J. Grate, "Choosing Polymer Coatings for Chemical Sensors," *CHEMTECH* **24**(9), 27-37 (1994).

THE AUTHORS
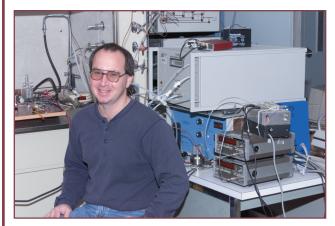
ALBERTO PIQUÉ received a B.S. (Honors) degree in physics and an M.S. degree in nuclear physics from Rutgers University in 1987 and 1990, respectively, and a Ph.D. degree in materials science and engineering from the University of Maryland at College Park in 1996. Dr. Piqué joined Neocera, Inc., in 1990 and became manager of the Thin Films and Coatings group. In 1997, Dr. Piqué joined the Naval Research Laboratory as a research physicist. He has more than 10 years of thin film growth experience. His research has focused in laser-materials processing and in the design and fabrication of multilayer structures and large area coatings by pulsed laser deposition for applications in electronics, sensors and protective coatings. He has authored more than 50 scientific articles and proceedings, holds three U.S. patents, and has four pending.
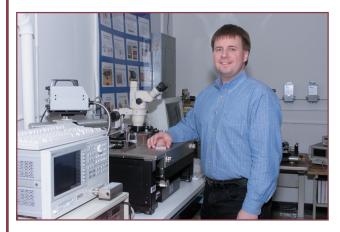
R. ANDREW McGILL received B.Sc. (Honors) and Ph.D. degrees in chemistry from the University of Surrey, England, in 1984 and 1988, respectively. He was a postdoctoral research fellow at the University of Alabama from 1988-1990, after which he moved to Washington, D.C., where he has worked at the Naval Research Laboratory since 1991. Dr. McGill is currently the head of the Functional Materials and Devices section and leads a chemical sensor research and development team. His research interests span basic and applied areas, including molecular interactions, design and synthesis of chemoselective coatings and polymers, and chemical sensors.

JAMES FITZ-GERALD is currently a postdoctoral research fellow NRL. He is performing research in the areas of thin film devices, flat panel display materials, pulmonary drug delivery, laser direct-write processing, and bio-electronic materials. He received a B.S.M.E. degree from the University of Lowell in 1993 and M.S. and Ph.D. degrees from the University of Florida in 1995 and 1998, respectively. His interests cover the adhesion of diamond thin films, formation of large area surface structures by pulsed laser processing for electronic materials, and nano functional material synthesis via pulsed laser processing of novel biomedical and electronic materials. He has recently accepted a faculty position in the Department of Materials Science and Engineering at the University of Virginia, starting in May 2000.

ERIC J. HOUSER received a B.A. degree in chemistry from Rockford College in 1987 and a Ph.D. degree in inorganic chemistry from the University of Illinois, Urbana-Champaign, in 1992. He spent two years as a postdoctoral fellow at the University of Virginia studying metallacarboranes. In 1995, he came to NRL as a postdoctoral fellow and became a staff member in 1998. His interests include chemical synthesis, high-temperature polymeric materials, and chemical sensing.

DOUGLAS B. CHRISEY received a B.S. degree in physics from the State University of New York at Binghamton in 1983, and a Ph.D. degree in engineering physics from the University of Virginia in 1987. He joined NRL as an Office of Naval Technology postdoctoral fellow in 1987, investigating radiation effects in thin films of high-temperature superconductors. Dr. Chrisey became a staff member in 1988 and currently heads the Plasma Processing Section of the Surface Modification Branch. His research at NRL has focused on the deposition of thin films of ceramics and organic materials by pulsed laser processing and the application of these films. He has authored more than 200 scientific papers and proceedings, holds six U.S. patents (with four pending), and has edited a handbook on the pulsed laser deposition of thin films.

Mountain Waves in the Stratosphere

S.D. Eckermann
Space Science Division

D. Broutman
Computational Physics, Inc.

K.A. Tan
University of New South Wales

P. Preusse
University of Wuppertal

J.T. Bacmeister
Universities Space Research Association

This article describes recent progress in our efforts to model, forecast, and observe mountain waves in the stratosphere. We have developed a numerical model that globally forecasts stratospheric mountain wave effects. Recent improvements to that model are outlined briefly. We illustrate the potential usefulness of these model forecasts by successfully "hindcasting" some cases where unexpected severe turbulence was encountered by aircraft at stratospheric cruise altitudes. We also show the model's usefulness in forecasting mountain-wave-induced polar stratospheric clouds, which play a crucial role in stratospheric ozone depletion. Finally, we describe some recent satellite observations that have provided us with global data on stratospheric mountain wave distributions, allowing us to benchmark our global mountain wave predictions against data for the first time.

INTRODUCTION

Fluids radiate waves when disturbed by an obstacle. A familiar example is the V-shaped pattern of surface waves produced by a moving ship at sea or by a stationary rock in a stream. A related phenomenon occurs when winds blow over a mountain. The resulting oscillations in the wind and temperature profiles are known as mountain waves, and they can radiate energy over very large distances, both vertically and horizontally. Mountain waves can sometimes be identified by rows of lenticular clouds that form in the ascent (cooling) phases of the waves.

Mountain waves are important in many contexts. They can trigger intense downslope windstorms and severe clear-air turbulence, both of which pose safety hazards to aviation. Mountain waves also cause im-

portant changes to the winds, on a global as well as local scale. Yet the mountain waves themselves are too small in scale (typically 10 to 100 km horizontal wavelengths) to be resolved adequately in global numerical weather prediction (NWP) models. Hence their effects must be parameterized, and much research has been directed at improving such parameterization schemes. In models such as the Navy Operational Global Atmospheric Prediction System (NOGAPS), the inclusion of parameterized mountain-wave effects has led to more accurate forecasts.

Mountain waves can often propagate into the stratosphere (heights of ~10 to 50 km) and beyond, although far less is known about the waves at these higher altitudes. Here we summarize some recent research and forecasting work that has shed new light on high-altitude mountain waves and their influence on stratospheric processes.

THE MOUNTAIN WAVE FORECAST MODEL

Our main modeling tool is the Mountain Wave Forecast Model (MWFM). MWFM blows atmospheric winds (from NWP forecasts, for example) over digital representations of the Earth's major topographical features and calculates a spectrum of forced mountain waves. The model simulates subsequent propagation of these waves, keeping track of their amplitudes along the way. The MWFM code has been developed over the past 7 years at NRL into an operational forecasting model (MWFM 1.0)[1] that is run daily over the continental United States and on a campaign basis over other regions of the globe.

The basic MWFM 1.0 algorithm incorporates a number of simplifying assumptions. For instance, it deals exclusively with the long quasi-two-dimensional ridges that characterize many mountainous regions. These ridges tend to force plane wave patterns that are easier to model. However, many hills and mountains are more three-dimensional (3D) in nature, and tend to radiate nonplanar wave fields that sometimes resemble ship wave patterns. For example, Fig. 1(a) shows ship wave-like mountain wave patterns over Jan Mayen, a small island approximately 550 km northeast of Iceland. The wave patterns here are made visible by banded wave clouds in the troposphere associated with the ascent (cooling) and descent (warming) phases of waves. These waves originated from Mount Beerenberg , a large quasi-circular volcanic mountain that dominates the topography of Jan Mayen and above which mountain wave clouds are often observed.

We have investigated ways in which mountain wave patterns like these can be accurately yet efficiently parameterized in a global forecast model like MWFM. To study them in more depth, we have developed and used a nonlinear 3D model of atmospheric flow over topography. Results for flow over a circular bell-shaped hill are shown in Fig. 1(b). In this experiment, the wind vector rotates counterclockwise with altitude (so-called "turning flow"). We see that a skewed V-shaped mountain wave pattern is generated.

We have developed numerical ray-tracing algorithms that can accurately reproduce these 3D mountain wave fields. Figure 1(c) shows output from a formal ray-tracing algorithm that we have developed for 3D mountain wave problems,[2] applied here to an idealized turning-flow problem over a circular bell-shaped mountain. The result here agrees very well with formal numerical solutions. Peak wave amplitudes only are plotted in Fig. 1(c). Figure 1(d) shows results from a simpler ray-based algorithm, except here the synthesis incorporates both amplitude and phase. Again, the salient features of the radiated mountain wave field are captured.

Ray-based algorithms and other improvements are being built into the next-generation model, a test version of which now exists (MWFM 2.0-β). Next we discuss applications of the MWFM models to stratospheric forecasting and research problems.
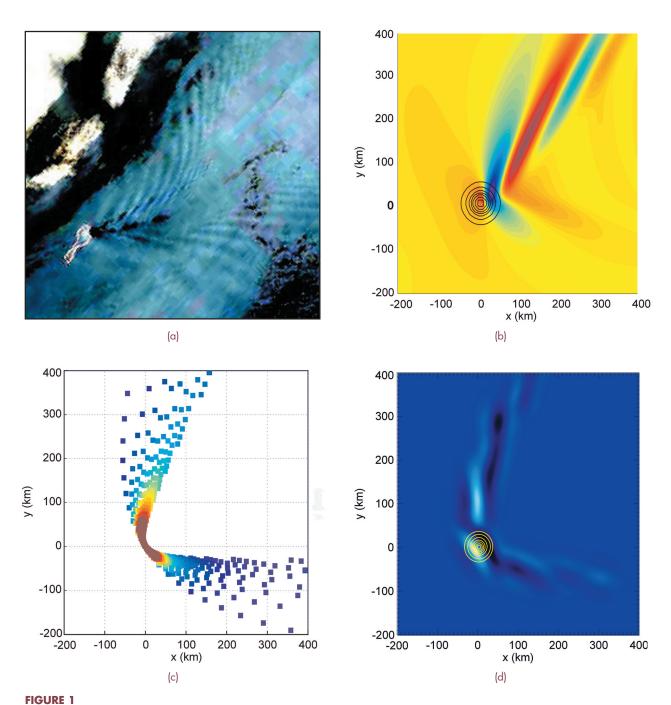
TURBULENCE FORECASTS FOR STRATOSPHERIC AIRCRAFT

The NASA ER-2
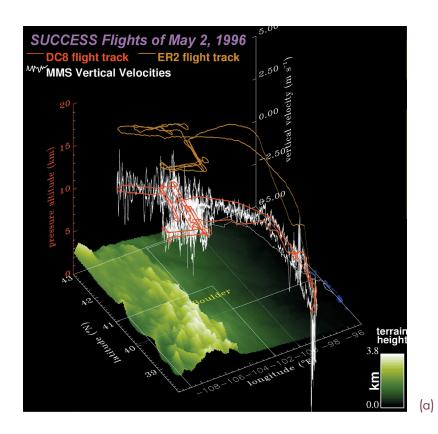
NASA uses a Lockheed ER-2 aircraft in its research program. The ER-2 is similar to a U-2 military aircraft, but it is approximately 30% bigger, with a 20-ft longer wingspan to accommodate large scientific payloads (up to ~1 ton). Like the U-2, it is a long-range aircraft (~4000 km) that flies in the stratosphere at cruise altitudes of ~20 to 22 km, or ~70,000 ft, which is twice as high as commercial airliners.

While generally stable and safe, weight constraints mean that the ER-2 does not have a wing spur, which makes it structurally vulnerable to turbulence. The stratosphere, being drier and more naturally stable than the troposphere, does not produce much of the weather-related turbulence found lower down. However, severe turbulence can occur in the stratosphere. Accumulated experience from MWFM forecasts, pilot notes, and in-flight ER-2 data have revealed that breaking mountain waves are a primary source of turbulence at ER-2 cruise altitudes. Accordingly, ER-2 flight planners have used our MWFM turbulence forecasts for some years now.[1]

Figure 2 shows an example of an ER-2 turbulence encounter. Figure 2(a) shows flight paths taken on May 2, 1996 by the NASA DC-8 (flight path shown in red) and ER-2 (flight path in brown) during the Subsonic Aircraft Cloud and Contrail Effects Special Study (SUCCESS). Both flights took off from Salina, Kansas, and headed northwest toward the Rocky Mountains looking for mountain wave clouds. Note the similar flight patterns: this occurred because the ER-2 carried nadir-viewing instruments to study the wave clouds intercepted by the DC-8, as well as any effects of DC-8 exhaust on the clouds. The irregularity of the flight patterns was due to the hunt for suitable wave clouds.

(a)

(b)

(c)

(d)

FIGURE 1

(a) Digitally enhanced false-color image of banded tropospheric clouds produced by mountain waves radiated from Jan Mayen (71.0°N, 8.5°W) on 25th January 2000 at 16:27 UT (these NOAA/AVHRR images were provided by Andreas Dörnbrack and Robert Meisner of DLR, Oberpfaffenhofen, Germany). The yellow-white bands at the top left are probably polar stratospheric cloud decks; (b) vertical displacement oscillations due to mountain waves forced by turning flow over a circular Gaussian-shaped mountain (shown with black contours, centered at $x = y = 0$), simulated with a three-dimensional atmospheric model; (c) ray-based synthesis of mountain wave vertical displacement amplitudes from turning flow over a circular mountain, with red depicting largest amplitudes and dark blue showing smallest amplitudes; (d) a simpler ray-based synthesis of the same mountain wave problem as in (c), but here incorporating both amplitude and phase.
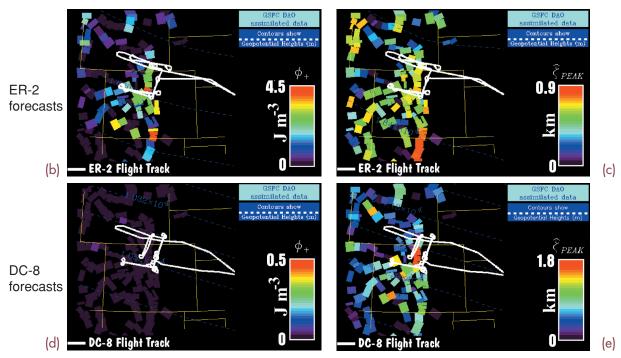
FIGURE 2
(a) Three-dimensional plot of flight paths taken on May 2, 1996 by NASA's DC-8 (red curve) and ER-2 (brown curve) research aircraft. Underlying topographic elevations are plotted in green (see color bar). Vertical velocities measured on the DC-8 are plotted along the flight track in white. (b) MWFM 1.0 turbulence forecast at 70 to 100 hPa (heights ~16-18 km, the approximate ER-2 cruise altitude here) using assimilated data for May 2, 1996 at 06:00 UT from NASA's DAO. (c) MWFM 1.0 forecast of peak vertical displacement amplitudes due to mountain waves at 70 hPa. (d) MWFM 1.0 turbulence forecast at 200 to 250 hPa (heights ~10-12 km); (e) MWFM 1.0 forecast of peak vertical displacement amplitudes at 200 hPa. In panels (b)-(e), the relevant flight track is plotted in white, the squares correspond in each case to the "ridge element" that forced this particular mountain wave, and yellow lines show state borders.

The white curve superimposed on the DC-8 flight path in Fig. 2(a) shows atmospheric vertical velocities measured onboard the DC-8. Large-amplitude oscillations are evident over the Rockies, which were later analyzed and shown to be mountain waves.[3] Despite the large wave activity, the DC-8 pilot reported no unusual in-flight turbulence. On the ER-2, no vertical velocity measurements were made, although wave oscillations were evident in the routine navigational wind data. The ER-2 pilot reported "heavy turbulence" at cruise altitudes and classified the flight afterwards as "highly turbulent". Interestingly, MWFM turbulence forecasts were made available during SUCCESS, but they do not appear to have been utilized, apparently because tropospheric clouds and contrails were the primary focus of the mission. Thus, it is interesting to reanalyze the May 2, 1996 situation using MWFM.

Since the NWP forecast data are no longer available, we use analyzed winds and temperatures for that day from NASA's Data Assimilation Office (DAO). The resulting MWFM 1.0 "hindcasts" are shown in the remaining panels of Fig. 2. At DC-8 cruise altitudes (atmospheric pressures ~190 to 240 hPa for this flight, altitudes ~10 to 11 km), MWFM predicts large mountain wave amplitudes along the flight track (Fig. 2(e)) but essentially no wave-induced turbulence (Fig. 2(d)). This is consistent with the in-flight data. Conversely, MWFM hindcasts at ER-2 altitudes (pressures ~60 to 80 hPa on this flight) show moderate wave activity (Fig. 2(c)) and fairly intense wave-induced turbulence (Fig. 2(b)). Experience with MWFM forecasts has shown that a useful working threshold for "uncomfortable" stratospheric turbulence is a value ~1 J m^{-3}. Many values in Fig. 2(b) along the ER-2 flight track are well in excess of this, with a peak value of 6.4 J m^{-3} forecast 6 hours earlier (not shown). Again, these features are entirely consistent with the navigational data and pilot notes from this flight.

Figure 3 shows the turbulence hindcast from the MWFM 2.0-β model, which has interesting similarities and differences to the MWFM 1.0 forecast (Fig. 2(b)). While the activity here is more limited, both in absolute magnitude and geographical coverage, intense turbulence occurs here also at the lower corner of the U-shaped ER-2 flight pattern. A significant portion of this ER-2 flight occurred in this region, with four separate flight segments passing through the hindcasted turbulent region. Again, this hindcast is consistent with the available data from this flight.

Alaska Airlines Flight 67

Forecasts like these may also have applications for existing commercial fleets. Though they fly considerably lower than the ER-2, these aircraft can also encounter severe unforecast turbulence in the lowermost regions of the stratosphere, often with serious consequences for passengers and crew.
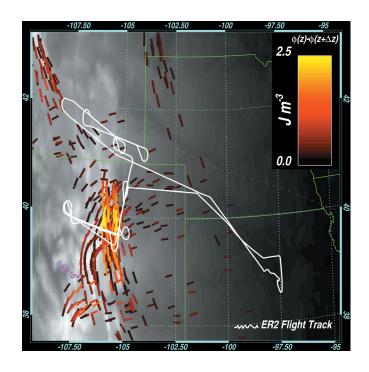
FIGURE 3
MWFM 2.0-β forecast of mountain-wave-induced turbulence at 70 to 100 hPa on May 2, 1996 at 12:00 UT, using DAO assimilated data of 2.5° × 2° grid resolution (see dotted blue grid). The ER-2 flight track on this day is plotted in white, state borders are plotted in green. The line color corresponds to the intensity of wave-induced turbulence, while its alignment corresponds to the orientation of wave phase fronts (see Fig. 1), as provided by the newly implemented ray-tracing algorithms. The underlying gray scale shows topographic elevations.

We illustrate this by using MWFM 2.0-β to investigate an unexplained encounter with severe turbulence by an Alaska Airlines Boeing 737 aircraft. The National Transportation Safety Board (NTSB) report of this incident makes compelling reading: only the salient details are summarized below. The flight took off from Juneau, Alaska, at 6:10 p.m. on December 22, 1996, and headed for Anchorage at a cruise altitude of 35,000 ft. In-flight turbulence was light until it flew over Mount Fairweather, whereupon turbulence immediately became moderate. Severe clear-air turbulence occurred roughly 30 miles east of Yakutat, Alaska, a region marked with the green diamond in Fig. 4. All three flight attendants were injured, two seriously (one attendant suffered a fractured pelvis and elbow, the other a fractured vertebrae in her back). The seriously injured attendants were at the back of the plane, preparing the drinks cart, when they were thrown violently into the ceiling and then onto the cabin floor by "two massive jolts."

SIGMET (significant meteorological information) advisories indicated no turbulence in this region; however, these advisories did not account for mountain waves. Figure 4 shows results of an MWFM 2.0-β hindcast for the region using National Center for Environmental Prediction (NCEP) reanalysis data for December 23, 1996 at 00:00 UT. We see a zone of mountain-wave-induced turbulence predicted between Mount Fairweather and the estimated location of the incident. Given our criterion for "uncomfortable" turbulence of ~1 J m^{-3}, the values of ~2 to 4.5 J m^{-3} in this region are consistent with the moderate-to-severe turbulence encountered along this flight segment. Interestingly, turbulence was almost entirely absent in the MWFM postcast at the next level down (250 to 300 hPa: ~28,000 to 33,000 ft). Thus, if these forecasts had been available at the time, a simple reroute to a slightly lower flight altitude may have avoided this incident.

At present, we provide daily MWFM forecasts of mountain wave amplitudes in the lower atmosphere over the continental United States <http://uap-www.nrl.navy.mil/dynamics/html/mwfmforecasts.html>, mainly in response to repeated requests from the gliding community. The above examples indicate that our upper-level turbulence forecasts have important potential applications not just for the ER-2 and other high-altitude aircraft, but also for commercial and military aviation. Other operational stratospheric aircraft include the M-55 Geophysica, the Grob 520T Egrett, the SR-71 Blackbird, and many jet fighter aircraft, like the Navy F-15 jet fighters and the Russian MiG-25. Furthermore, NASA and the aerospace industry are developing technologies for next-generation high-altitude research aircraft, through the APEX and ERAST programs, and for a supersonic passenger aircraft that would fly at or just below typical ER-2 altitudes (i.e., well into the stratosphere). Global forecasts of mountain-wave-induced stratospheric turbulence would clearly be desirable to ensure
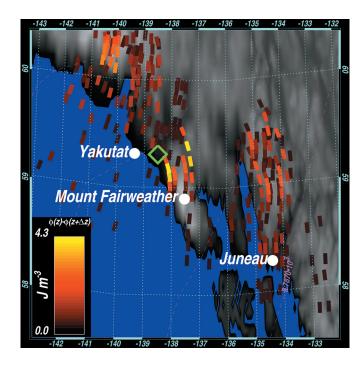
FIGURE 4
MWFM 2.0-β hindcast of mountain-wave-induced turbulence at 200 to 250 hPa (~33,000-38,000 ft) on December 23, 1996 at 00:00 UT, using NCEP reanalysis data of 1° × 1° grid resolution (see dotted blue grid). The green diamond shows the approximate estimated location of a severe turbulence encounter by Alaska Airlines Flight 67 at ~35,000 ft at 7:12 pm local time on December 22.

smooth, safe flight routes for such aircraft. How these forecasts could be rapidly and accurately communicated for in-flight applications remains to be explored.

POLAR STRATOSPHERIC CLOUDS AND OZONE DEPLETION

Polar ozone is destroyed when stratospheric temperatures become very cold and polar stratospheric clouds (PSCs) form. PSC-related chemistry denitrifies the stratosphere and activates chlorine into efficient ozone-destroying forms. PSCs made of nitric acid trihydrate (NAT) form at stratospheric temperatures below T_{NAT} ~195 K (–109 °F), while ice PSCs form below the frost point temperature T_{ICE} ~188 K (–121 °F). Thus, forecasting ozone depletion requires accurate forecasts of the temperature drops that lead to PSC formation.

On November 30, 1999, stratospheric ozone levels over the United Kingdom, Belgium, the Netherlands, and Scandinavia plummeted to Antarctic-like lows, prompting a press release from the European Space Agency. That same day, NASA's DC-8 flew to Kiruna, Sweden, to commence Phase 1 of the SAGE III Ozone Loss and Validation Experiment (SOLVE). As it circled to land, PSCs were observed visually from the aircraft well to the south of Kiruna (Fig. 5(b)). The following day, spectacular banded PSCs were visible from the ground in Oslo, Norway (Fig. 5(c)). On November 30, the POAM science team in Code 7227 reported PSC detections over Scandinavia (see Fig. 5(a)) using NRL's POAM instrument, which routinely detects Arctic PSCs from space.[4]

In recent years, we have used MWFM to predict and research mountain-wave-induced PSCs over Scandinavia in support of airborne PSC measurements made during winter by European research teams.[5-7] During SOLVE, as well as mountain-wave turbulence forecasting, we provided daily MWFM forecasts to help direct NASA's DC-8 and ER-2 aircraft toward possible encounters with nonturbulent mountain-wave-induced PSCs.

November 30, 1999 was one of the first days when MWFM forecasts were supplied operationally for SOLVE. MWFM 2.0-β predictions based on 18-hour NOGAPS forecasts for this day are shown in Fig. 5(a). Color-coded lines show peak mountain-wave temperature amplitudes at 30 hPa (an altitude of ~24 km). These plots are similar to the wave amplitude plots in Fig. 1(c): here, too, we see V-shaped wave patterns forecast west of Oslo. The NOGAPS forecast data are made available to us year-round by Dr. Timothy Hogan of Code 7500 at NRL, Monterey.

Mean stratospheric temperatures are plotted with blue dashed contours in Fig. 5(a). A broad region with temperatures below 192 K was forecast by NOGAPS over northern Britain, southern Scandinavia, and regions of northern Europe. Thus, NAT PSCs can form here and deplete ozone, possibly accounting for the reduced ozone levels reported over this region (although a regional ascending circulation may also be implicated[8,9]). Forecasts a few days later gave significantly warmer temperatures, consistent with the return of more normal observed ozone levels a day or so later.

NAT PSCs, however, are generally hazy and hard to see from the ground. Conversely, the PSCs photographed in Figs. 5(b) and 5(c) are quite opaque. They are clearly visible from a long way away, and so are more likely to have been ice PSCs. However, ice formation at these altitudes requires temperatures below 188 K, which were not forecast by NOGAPS or other NWP models.

The MWFM forecasts appear to explain the ice PSCs over southern Scandinavia. In Fig. 5(a), stratospheric mountain waves are forecast west of Oslo, with peak amplitudes in the ~4 to 8 K range. This provides additional cooling that drops temperatures below the frost point in the cooling (ascent) phase of the wave, thereby triggering ice formation. Indeed, like the low-level clouds in Fig. 1(a), the PSCs in Fig. 5(c) show the "banding" that is characteristic of clouds formed in the various cooling (ascent) phases of a mountain wave. Other observations and MWFM results have revealed that mountain-wave-induced PSCs commonly form over northern Scandinavia and other mountainous Arctic regions during winter.[5,6] The combined effects of wave-induced PSC formation over the entire Arctic may result in an overall reduction in stratospheric ozone levels.[7]

The reduced ozone and spectacular PSC displays over Europe on November 30 were unusual and somewhat troubling; these processes are usually confined to less-inhabited polar regions. Nonetheless, the basic features of this event appear to have been forecast in Fig. 5(a), indicating that model forecasts of this kind might be useful for low ozone alerts over populated mountainous regions. At the time of writing, these and other MWFM forecasts are being generated daily at NRL and made available to in-field science teams during SOLVE throughout the Arctic winter of 1999-2000.

(a)

(b)

(c)
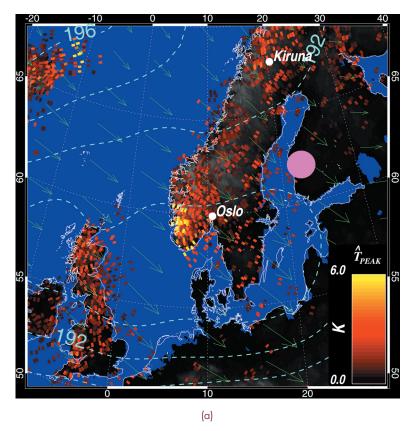
FIGURE 5

(a) 18-h MWFM 2.0-β forecasts of stratospheric mountain waves at 30 hPa on November 30, 1999, using NOGAPS forecast output. Dashed blue contours show mean temperatures, red-yellow bars show ray-based forecasts of peak mountain wave temperature amplitudes. The pink spot shows the ground-level location of the POAM III PSC detection on this day. Blue arrows indicate wind direction. (b) Photograph from the DC-8 by Dr. Mark Schoeberl, NASA Goddard Space Flight Center, on November 30, 1999. Cirrus-like PSCs are visible in the distance above the DC-8 wingtip. (c) Photograph by Geir Braathen, Norwegian Institute for Air Research, of iridescent red PSCs over southern Norway at dusk on December 1, 1999.

GLOBAL MOUNTAIN WAVE MEASUREMENTS FROM SPACE

Previous sections have shown how regional stratospheric data help in assessing and refining MWFM stratospheric forecasts. MWFM can also provide global forecasts, which are useful for studies of global PSC formation[5,6] and associated ozone depletion,[7] as well as global circulation patterns produced by mountain wave drag. Unfortunately, no global measurements have been made of stratospheric mountain waves to allow similar observational assessments of these global forecasts. This is because, like global NWP and climate models, the global data provided by satellite instruments have been too coarse spatially to resolve mountain waves.

On November 3, 1994, the Space Shuttle Atlantis took off from Cape Canaveral with CRISTA-SPAS (a Shuttle pallet satellite) in the payload. This recoverable satellite experiment carried two atmospheric measuring instruments: the University of Wuppertal's Cryogenic Infrared Spectrometers and Telescopes for the Atmosphere (CRISTA) and Code 7640's Middle Atmosphere High Resolution Spectrograph Investigation (MAHRSI). The CRISTA instrument was cryogenically cooled to liquid helium temperatures and acquired data using three telescopes and four infrared spectrometers. This allowed CRISTA to acquire some of the highest spatial resolution stratospheric data to date from a space-based platform. Still, until recently, it was unclear whether even these measurements had adequate resolution to detect mountain waves. Many years of careful modeling and data analysis have finally answered this question definitively: CRISTA did measure stratospheric mountain waves.[10]
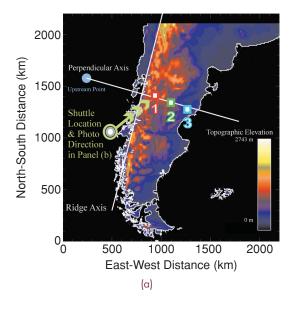
As summarized in Fig. 6, one of the clearest mountain wave detections by CRISTA occurred over the southern tip of South America. During deployment of CRISTA-SPAS from the shuttle on November 4, the astronauts took a series of photographs: one of them is shown in Fig. 6(b). As shown in Fig. 6(a), the Shuttle was orbiting northwestward over the east coast of South America at the time, and the photo in Fig. 6(b) looks northwestward across the southern Andes. It shows a broad linear cloud band running north-south along the Andes, and banded wave clouds downstream of this region. This suggests that mountain waves were being generated in the lower atmosphere by flow across the Andes at the time CRISTA-SPAS was deployed.
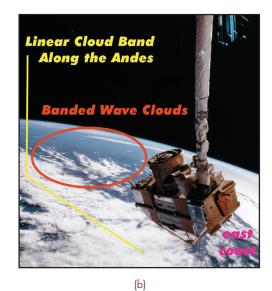
Two days later, CRISTA-SPAS was in free orbit (~20 to 100 km behind the Shuttle) and CRISTA was acquiring stratospheric data. At ~06:24 UT on No-

vember 6, CRISTA took three successive stratospheric temperature measurements over South America, at the locations labeled 1, 2, and 3 in Fig. 6(a). Vertical profiles of temperature fluctuations extracted from those measurements are plotted in Fig. 6(c). All three show similar wavelike temperature oscillations in the stratosphere from 15 to 30 km, with a vertical wavelength λ_z ~ 6 to 7 km and peak temperature amplitudes $\hat{T}$ of ~ 3 to 7 K.
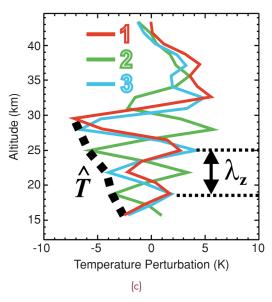
MWFM hindcasts predicted intense stratospheric mountain wave activity at this particular time and location.[10] The remaining panels in Fig. 6 show results of a model simulation of atmospheric flow across the Andes, using a two-dimensional version of the nonlinear regional model used in Fig. 1(b).[11] This model experiment used actual background winds and temperatures at the time of these particular CRISTA measurements, as well as realistic Andean topography (Fig. 6(d)). Figure 6(e) shows the resulting stratospheric temperature response, with mountain waves penetrating into the uppermost regions of the stratosphere and temperature amplitudes of ~4 to 8 K. The potential temperature surfaces in Fig. 6(e), which remain flat in the absence of waves, begin to fold and overturn near 30 km, indicating that these mountain waves are breaking and generating intense turbulence. Figure 6(f) compares a model vertical profile at $x = 650$ km with the CRISTA data from measurement location 1. The amplitude, phase, and vertical wavelength of the two oscillations are quite similar. These and other tests[10,11] prove beyond doubt that the fluctuations in the CRISTA data in Fig. 6(c) are stratospheric mountain waves that emanated from the southern Andes.

CRISTA took measurements like these over the entire globe during the week-long mission. The results in Fig. 6 suggest that these CRISTA data can provide global information on stratospheric mountain waves. Figure 7(a) shows peak amplitudes of temperature perturbations ($\hat{T}$, see Fig. 6(b)) estimated from all CRISTA stratospheric temperature measurements in the Northern Hemisphere on November 9, 1994, at a height of 25 km. Most noticeable is a region of enhanced oscillation amplitudes over a mountainous region of central Eurasia, which takes in the Sayan Ranges, Altay Mountains, and Tian Shan (Fig. 7(b)). An MWFM 2.0-β hindcast for November 9 at $z = 25$ km is shown in Fig. 7(c). The hindcast reproduces this region of enhanced stratospheric mountain wave activity. Interestingly, the hindcast shows little or no mountain wave activity over other mountainous regions, such as western North America, in agreement with the observations.
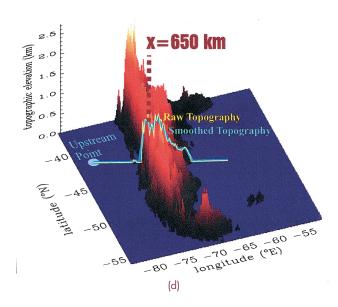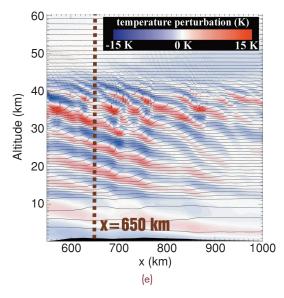
FIGURE 6

(a) Topographic elevations for southern South America (linear color scale). (b) Astronaut photograph over southern South America showing deployment of CRISTA-SPAS from Atlantis, November 4, 1994, 12:18 UT. The nadir point and orbital motion of the Shuttle at this time are shown with a circle and arrow, respectively, in panel (a). The cylindrical assembly on the satellite houses CRISTA. The east coast of Argentina and Atlantic Ocean are visible to the right, banded mountain wave clouds downstream of the Andes are visible to left of CRISTA-SPAS. (c) Vertical profiles of temperature perturbations from three successive CRISTA scans on November 6, 1994 at ~06:24 UT, acquired from locations 1, 2, and 3 shown in panel (a). (d) Three-dimensional topographic elevations, including a section perpendicular to the Andean ridge axis used for two-dimensional model simulations, results of which are shown in panel (e).

(e)

(f)
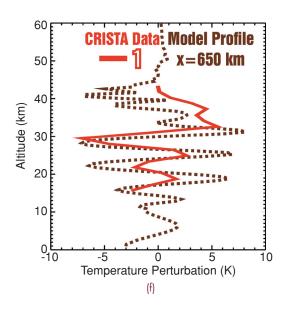
FIGURE 6 (continued)
(e) Model-generated temperature variability in the troposphere and stratosphere on November 6, 1994 due to flow over the smoothed topography in panel (d). Contours show potential temperature surfaces (essentially, material surfaces), with constant logarithmic separation between adjacent contours. Colors show temperature perturbations (color-scale given top-right); (f) Dotted brown curve shows a vertical profile of simulated temperature perturbations at x = 650 km, 10 hours into the model simulation. Red curve shows CRISTA data from location 1, shown also in panel (c).

(a)

(b)

(c)
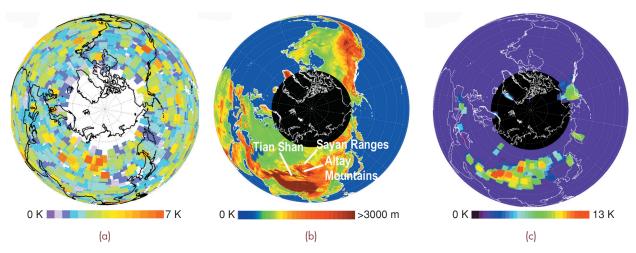
FIGURE 7
(a) Polar orthographic maps of amplitudes $\hat{T}$ from CRISTA temperature profiles taken over the Northern Hemisphere on November 9, 1994 at z = 25 km; (b) topographic elevations in the Northern Hemisphere; (c) MWFM 2.0-β hindcasts of amplitudes $\hat{T}$ at 25 km, using DAO assimilated winds and temperatures at 12:00 UT on this date. Modeled waves with λ_z < 5 km were not plotted since CRISTA is not sensitive to them. Pixels in (a) and (c) are plotted in order of ascending amplitude and are sized to maximize coverage while minimizing pixel overlap. These plots are adapted from Ref. 10.

These results show that advances in remote sounding satellite technology can now provide global data on mountain waves in the stratosphere. Such data offer the prospect of improved observational assessments of global MWFM forecasts.

SUMMARY

We have summarized ongoing work in the Upper Atmospheric Physics Branch (Code 7640) related to stratospheric mountain waves. Theoretical and algorithmic developments are being used to improve the NRL Mountain Wave Forecast Model (MWFM). Regional data from aircraft campaigns have proved particularly valuable in assessing the performance of both older and newer versions of the model. Data from the latest satellite instruments can now be used to extract information on stratospheric mountain waves, permitting observational assessments of MWFM's global forecasting capabilities. Other areas where improvements can be made in the model have been identified and targeted for future research.

We have used MWFM to investigate some of the important effects that mountain waves exert on the dynamics, chemistry, and cloud physics of the stratosphere. We have shown how mountain waves produce severe stratospheric turbulence, which poses a safety hazard to stratospheric aircraft, as well as polar stratospheric clouds, which deplete ozone. MWFM now forecasts these phenomena. This recent modeling and forecasting work has interfaced synergistically with several other NRL research projects, such as satellite measurements made by the Space Science Division (Code 7600) and the Remote Sensing Division (7200) and global forecasts issued by the Marine Meteorology Division (Code 7500).

When compared with the extensive literature on mountain waves in the lower atmosphere, we have probably only scratched the surface in uncovering and understanding mountain wave effects in the stratosphere. Parallel improvements in models and observations offer exciting prospects for future discoveries and improved knowledge and modeling capability.

[Sponsored by ONR and NASA]

REFERENCES

[1] J.T. Bacmeister, P.A. Newman, B.L. Gary, and K.R. Chan, "An Algorithm for Forecasting Mountain Wave-Related Turbulence in the Stratosphere," *Weather Forecast.* **9**, 241-253 (1994).

[2] D. Broutman, J.W. Rottman, and S.D. Eckermann, "A Hybrid Method for Wave Propagation from a Localized Source, with Application to Mountain Waves," *Q.J.R. Meteorol. Soc.*, submitted (2000).

[3] J. Dean-Day, K.R. Chan, S.W. Bowen, T.P. Bui, B.L. Gary, and M.J. Mahoney, "Dynamics of Rocky Mountain Lee Waves Observed During SUCCESS," *Geophys. Res. Lett.* **25**, 1351-1354 (1998).

[4] M.D. Fromm, R.M. Bevilacqua, J. Hornstein, E. Shettle, K. Hoppel, and J.D. Lumpe, "An Analysis of Polar Ozone and Aerosol Measurement (POAM) II Arctic Polar Stratospheric Cloud Observations, 1993-1996," *J. Geophys. Res.* **104**, 24,341-24,357 (1999).

[5] K.S. Carslaw, M. Wirth, A. Tsias, B.P. Luo, A. Dörnbrack, M. Leutbecher, H. Volkert, W. Renger, J.T. Bacmeister, and T. Peter, "Particle Microphysics and Chemistry in Remotely Observed Mountain Polar Stratospheric Clouds," *J. Geophys. Res.* **103**, 5785-5796 (1998).

[6] K.S. Carslaw, T. Peter, J.T. Bacmeister, and S.D. Eckermann, "Widespread Solid Particle Formation by Mountain Waves in the Arctic Stratosphere," *J. Geophys. Res.* **104**, 1827-1836 (1999).

[7] K.S. Carslaw, M. Wirth, A. Tsias, B.P. Luo, A. Dörnbrack, M. Leutbecher, H. Volkert, W. Renger, J.T. Bacmeister, E. Reimer, and T. Peter, "Increased Stratospheric Ozone Depletion Due to Mountain-induced Atmospheric Waves," *Nature* **391**, 675-678 (1998).

[8] K.B. Petzoldt, B. Naujokat, and K. Neugebohren, "Correlation Between Stratospheric Temperature, Total Ozone and Tropospheric Weather Systems," *Geophys. Res. Lett.* **21**, 1203-1206 (1994).

[9] Å. Rabbe and S.H.H. Larsen, "On the Low Ozone Values Over Scandinavia During the Winter of 1991-1992," *J. Atmos. Terr. Phys.* **57**, 367-373 (1995).

[10] S.D. Eckermann and P. Preusse, "Global Measurements of Stratospheric Mountain Waves from Space," *Science* **286**, 1534-1537 (1999).

[11] K.A. Tan and S.D. Eckermann, "Numerical Model Simulations of Mountain Waves in the Middle Atmosphere over the Southern Andes," in *Atmospheric Science Across the Stratopause*, AGU Monograph Series, D.E. Siskind, M.E. Summers, and S.D. Eckermann, editors, in press (2000).
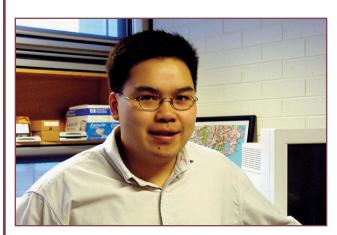
THE AUTHORS
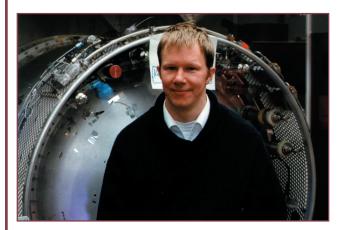
STEPHEN D. ECKERMANN grew up in Adelaide, Australia, and studied at the University of Adelaide, receiving an Honours degree in physics in 1986 and a Ph. D. degree in physics in 1990. As a postdoctoral research scientist, he worked at the Clarendon Laboratories at Oxford University, England, from 1990-1992, and at the Department of Physics and Mathematical Physics at the University of Adelaide from 1992-1994. In 1994 he joined Computational Physics, Inc., in Fairfax, Virginia, and began working on atmospheric research problems in collaboration with NRL scientists in the Upper Atmospheric Physics Branch. He joined NRL as a full-time employee in 1998. Dr. Eckermann's primary research interests are the modeling and forecasting of atmospheric dynamics, particularly atmospheric gravity waves.

DAVE BROUTMAN is a graduate of the University of California Los Angeles (B.A. degree in meteorology) and of Scripps Institution of Oceanography (Ph.D.). He completed postdoctoral fellowships at Cambridge University, England, and at the University of Melbourne, Australia, before joining the faculty of the University of New South Wales (applied mathematics) in Sydney, Australia. In 1998, Dave joined Computational Physics, Inc., as a research scientist and has been working closely with members of the Upper Atmospheric Physics Branch at NRL in research problems in atmospheric dynamics. His research interests include stratified fluids, gravity waves, and ocean waves.

KWOK AUN TAN received a B.S. degree in applied mathematics in 1995 from the University of New South Wales, Sydney, Australia. His primary interests are numerical techniques for high-performance computing and geophysical fluid dynamics. He was a long-term visitor to NRL DC in 1999, and worked closely with scientists in the Upper Atmospheric Physics Branch on mountain wave research problems. He is currently completing his Ph.D. dissertation at the University of New South Wales.

PETER PREUSSE joined the Physics Department at the University of Wuppertal in 1993 and works in the CRISTA science team under the leadership of Professors Dirk Offermann and Klaus Grossmann. He worked extensively on calibration hardware for the CRISTA instrument, and published his diploma thesis in 1995 on radiance calibration from CRISTA. Since 1995, his graduate work has focused on improving the retrieval software for CRISTA, and he is now in charge of the temperature and ozone retrieval work. Since 1997 he has also worked on extracting and studying gravity wave signatures in temperature and ozone data from CRISTA.

JULIO T. BACMEISTER worked in the Upper Atmospheric Research Branch at NRL from 1992 to 1998. His research interest in mountain waves began in graduate school, where he worked on simulations of downslope windstorms (also known as foehns or chinooks) as part of his Ph.D thesis. He became interested in forecasting turbulence for aircraft as a result of involvement with several NASA Polar Ozone research campaigns that used the ER-2 airplane to probe the stratosphere. Since 1998, he has worked at NASA's Seasonal-to-Interannual Prediction Project at the Goddard Space Flight Center in Greenbelt, Maryland. His current research involves climate simulation with coupled atmospheric and oceanic general circulation models.

Acoustics

89   In-Flight Acoustical Holography
          E.G. Williams and B.H. Houston

In-Flight Acoustical Holography

E.G. Williams and B.H. Houston
Acoustics Division

Introduction: Noise control in enclosed spaces, such as near the ship service turbine generator inside a submarine, is critical to the quieting of a submarine hull. Before control can be achieved, diagnostic techniques must be developed to uncover the physics behind the structure/air/fluid interactions. Inverse methods to probe sound fields and structure vibrations have been developed based on nearfield acoustical holography (NAH) mated with boundary element methods (BEM). This paper describes the first such effort. It has been applied to the interior of an aircraft in flight and successfully reconstructs interior pressure fields and fuselage vibration, identifying dominant structureborne and airborne paths from the propeller noise source to the fuselage.

Experiment: The experimental exercise involved a highly spatially sampled pressure measurement on the interior of a Beech 1900D aircraft (Fig. 1). The experiment was conducted at a speed of 218 knots and at an altitude of 16,000 feet. This is a standard operating condition of the aircraft, and the

FIGURE 1
The Beech 1900D experimental aircraft.

flight occurred on a clear day with relatively smooth conditions.

A scanning boom with 55 microphones mounted in the vertical plane traversed the interior space of the Beech 1900D passenger cabin to acquire the pressure data that constitutes the hologram. Figure 2 shows this array mounted in the aircraft interior, looking aft, and the caption describes some of the details of the experiment. Seats and trim panels have been removed. The aircraft's insulation material is intact, and the internal structural complexity (frames, stringers, windows, and flooring) of the plane are left unmodified.
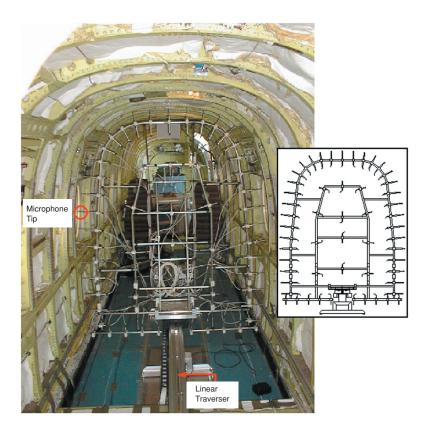
FIGURE 2
Microphone boom consisting of 43 microphones on the outer ring and 12 spaced evenly in the internal region, all located in the same vertical plane. The boom was moved on a linear traverser to 32 different axial locations during the experiment (5.12 m total scan length). Time domain data were sampled at 5 kHz and were processed at the BPF and its harmonics. The total acquisition time for the data scan was 66 minutes.
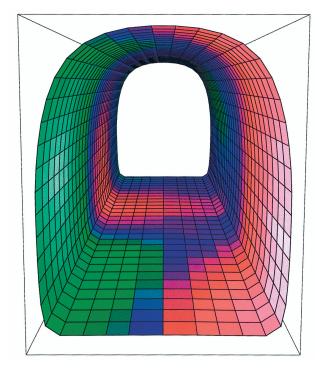
FIGURE 3
The hologram pressure, looking aft, measured at 103.7 Hz using the outer 43 microphones of the array, acquired during the in-flight experiment. The real part of the field is plotted; the pressure is 180 degrees out of phase on either side of the aircraft. The quality of the data is outstanding.
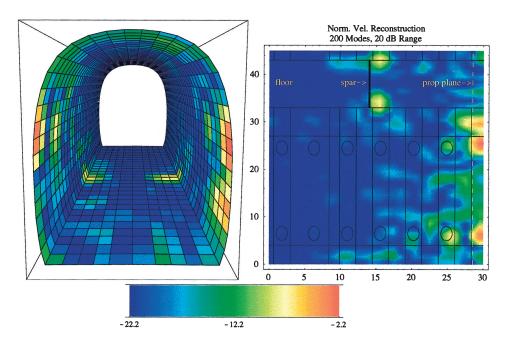
FIGURE 4
Magnitude (in decibels) of the normal velocity reconstruction for the first overtone of the BPF, at 207 Hz. The top 20 dB of data is displayed. The highest vibration levels are just in front of the propeller plane (latter indicated by vertical dashed line). The floor just in front of the spar also appears to be vibrating at a high level.

The pressure hologram was generated from a Fourier transform of the time domain data acquired during the experiment, choosing the frequency bins corresponding to the blade passage frequency (BPF) signal and its harmonics. The BPF and its harmonics represent the dominant noise source in the interior of the fuselage. Figure 3 shows the resulting pressure hologram for the first frequency (103.7 Hz).

Inversion: BEM provides a transfer function H_f between the measured pressure hologram p and the desired fuselage normal velocity v, that is, $p = H_f v$. This transfer function is developed rigorously from the Helmholtz integral equation. To solve for v, the transfer function matrix must be inverted. Because of the existence of evanescent waves/modes, which decay exponentially from the fuselage surface to the hologram surface, much care must be exercised in this inversion. Inversion is made possible by the use of the singular value decomposition (SVD), which reveals the evanescent modes and allows for truncation (elimination) of the modes with the severest decays. It is this truncation that regularizes the inversion.

Figure 4 shows the reconstruction (using the SVD) of the normal velocity at the first overtone (207.5 Hz) of the BPF. Two hundred modes were used in this reconstruction. Modes beyond this were too highly evanescent and dropped below the noise levels in the hologram. In the reconstruction, the vibration levels are confined to the front of the aircraft, with the highest levels in front of the propeller plane, as indicated. The floor in front of the spar (wing support) can be seen vibrating, revealing a structureborne path from the engines mounted on the wings.

Conclusions: The in-flight hologram and reconstruction were very successful. The correlation of reconstructed high-velocity regions to actual structural details of the fuselage provides a great deal of credibility to the success of the NAH-BEM effort. Clearly, the marriage of BEM and NAH provides a powerful tool for the study of interior noise in propeller-driven aircraft, as well as in more general structures—locating sources of excess vibration and providing a means to evaluate the effectiveness of noise control procedures. Furthermore, with the reconstructed velocity, the Helmholtz integral equation can be used to compute the pressure, velocity, energy densities, and acoustic intensity throughout the interior of the fuselage.

✦

Atmospheric Science and Technology

SAMI2: A New Model of the Ionosphere

J. Huba and G. Joyce
Plasma Physics Division

J. Fedder
LET Inc.

Introduction: Military systems are relying increasingly on space-based assets for communication and navigation systems. A critical aspect of the operation of these systems is the nature of the ionosphere. The ionosphere, a partially ionized gas surrounding the Earth in the 90- to 1000-km altitude range, can strongly affect the propagation of electromagnetic waves. Under certain circumstances, the ionosphere can severely degrade electromagnetic signals and, for example, interrupt communication links. Thus, it is critical that the ionospheric environment be known, and even forecasted, for reliable military operations.
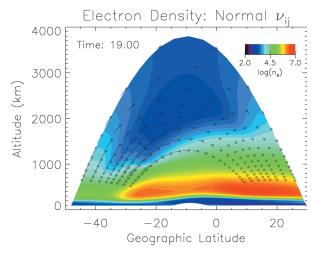
The Naval Research Laboratory is funding an Accelerated Research Initiative, "Ionospheric Specification and Forecasting," to meet the Navy's needs in defining the ionospheric environment. The program comprises experimental and modeling efforts. The experimental program focuses on specifying the ionosphere using space-based extreme ultraviolet remote sensors and radio wave tomography. NRL currently has several experiments on the ARGOS satellite that are providing ionospheric data. The modeling program involves developing first-principles models of the near-Earth space environment: the ionosphere, the plasmasphere, and the magnetosphere, and eventually coupling these models self-consistently. We report here on the development of a new ionospheric model, SAMI2 (SAMI2—Another Model of the Ionosphere), and we present exciting new results from this model.

SAMI2: SAMI2 is a low- to midlatitude model of the ionosphere recently developed at the Naval Research Laboratory. It is an outgrowth of a midlatitude ionospheric model developed at NRL in the mid 1970s.[1] SAMI2 models the dynamic plasma and chemical evolution of seven ionospheric ion species (H^+, He^+, N^+, O^+, N_2^+, NO^+, and O_2^+). The neutral species are specified using existing empirical codes (MSIS86 and HWM93). Major enhancements to our modeling capability include extending the ionosphere plasma along the Earth's dipole field from hemisphere to hemisphere, incorporating the electric field drift of a flux tube (both in altitude and in longitude), and

accounting for ion inertia in the ion momentum equation for plasma motion along the dipole field line. Existing ionospheric models assume the ions are collisional at all altitudes. To our knowledge, SAMI2 is the first comprehensive ionospheric model that includes ion inertia, which becomes important at high altitudes (above 1500 km).

Simulation Results: The simulation results presented here use the following geophysical parameters: day 173 (summer solstice); longitude 293.4°E (Arecibo, Puerto Rico); Ap 2; F10.7 180; and F10.7A 180. Figure 1 is a color contour plot of the logarithm of the electron density as a function of geographic latitude vs altitude at 1900 local time (LT). Also shown are the O^+ velocity vectors, which are denoted by wind flags. The large dots lie on grid points and indicate the tail of the velocity vector. The maximum velocity shown is approximately 400 m/s.

Typical diurnal behavior of the ionosphere is observed during the 24-hour simulation run. In the daytime, the ionosphere rises and the peak electron density reaches a few $\times 10^6$ cm^{-3} in the 250 to 400 km altitude range. At night, the ionosphere falls and the peak density drops to a few $\times 10^5$ cm^{-3}, with a strong reduction in the electron density below 200 km. During the late afternoon and early evening (1600 to 2100 LT), the peak electron density occurs

FIGURE 1
Electron density as a function of geographic latitude and altitude at time t = 1900 LT. Also shown are the O^+ velocity vectors (wind flags). The large dots lie on grid points and indicate the beginning of the velocity vector; the wind flags are plotted every fourth grid point above approximately 600 km. The parameters used in this simulation are given in the text. Note the "electron hole," closed dark blue contours, centered at approximately 2100 km and $\theta_g \sim 15°S$.

at the 25°S and 7°N latitudes in the 300- to 400-km altitude range. This latitudinal extent is roughly ±15 degrees from the magnetic equator and agrees with observations of the Appleton anomaly. A surprising new result of this simulation is the formation of an electron hole (or depletion) in the topside electron density.[2] The hole shows up as a closed, dark blue contour at ~2000 km and θ_g ~15°S. It forms in the early afternoon and decays during the early morning hours.

The physical mechanism for the topside electron hole is described as follows. The high-altitude hole forms because transhemispheric O^+ flows collisionally drag H^+ and transport it to lower altitudes. The resultant reduction of H^+ at high altitudes over the geomagnetic equator is responsible for the electron depletion. For the hole to develop, relatively strong, persistent transhemispheric O^+ flows are necessary. These flows develop because of an asymmetric oxygen pressure profile along a magnetic flux tube. This asymmetric profile is more likely to form at the solstices because the summer to winter neutral wind transports O^+ to higher altitudes on one side of the magnetic equator, and to lower altitudes on the other side. In addition to transhemispheric O^+ flows, the O^+ density must be comparable to the H^+ density for efficient collisional coupling. We find that the ion densities are comparable at the altitude and latitude that the hole forms in the early afternoon.

Future Investigations: We are not aware of experimental observations of a topside equatorial electron hole. The region in which the hole occurs—high altitude at equatorial latitudes—is difficult to diagnose; it is not accessible with ground-based radar and there are few in situ satellite measurements. Data that could possibly provide evidence of an electron hole are Alouette/ISIS topside sounder ionograms.[3] We are currently investigating the availability of suitable topside sounder data to search for the high altitude electron holes.

More information on SAMI2 can be found at <http://wwwppd.nrl.navy.mil> under the hyperlink to "What's New." Animations of the electron hole formation and evolution are provided.

[Sponsored by ONR]

References
[1] E.S. Oran, T.R. Young, D.V. Anderson, T.P. Coffey, P.C. Kepple, A.W. Ali, and D.F. Strobel, "A Numerical Model of the Mid-Latitude Ionosphere," NRL Memorandum Report 2839, July 1974.
[2] J.D. Huba, G. Joyce, and J.A. Fedder, "The Formation of an Electron Hole in the Topside Equatorial Ionosphere," to be published in *Geophys. Res. Lett.*, 1999.

[3] R.F. Benson, "Ionospheric Investigations Using Digital Alouette/ISIS Topside Sounder Ionograms," in *Proceedings of the 1996 Ionospheric Effects Symposium*, J.M. Goodman, ed., 1996, sponsored by the Office of Naval Research and the Naval Research Laboratory, p. 202.   ◆

Tropical Cyclone Concentric Eyewalls via Passive Microwave Imagery

J.D. Hawkins, F.J. Turk, T.F. Lee, and K.A. Richardson
Marine Meteorology Division

M. Helveston
Analysis & Technology, Inc.

Monitoring Tropical Cyclones: Near real-time analysis of tropical cyclones (TCs) with regard to their location, eye shape, and rainband structure is crucial for issuing accurate warnings. However, user dependence on visible (vis) and infrared (IR) imagery is inherently flawed, since the user can see only the uppermost layer of any satellite-viewed cloud. These upper-layer clouds often obscure important mid- and low-level cloud structure needed for precise storm location and intensity estimates. These cloud limitations must be mitigated to improve TC warnings that both the Navy and the general public depend on to take appropriate actions (e.g., ship routing, property protection, and evacuation of dangerous areas).

Passive microwave data from the Special Sensor Microwave/Imager (SSM/I) can significantly assist in depicting TC structure since its frequencies do not suffer from many of the vis/IR limitations.[1] The SSM/I is a four-frequency (19, 22, 37, and 85 GHz), seven-channel instrument that images the Earth over a 1400-km swath. SSM/I imagery represents the combined effects of microwave energy emitted and scattered by the Earth and the atmosphere, with each channel and polarization behaving differently. The variation in sensitivity to the atmosphere and its constituents (e.g., water vapor, cloud liquid water, rain droplets, or hydrometeors and ice crystals) as well as the ability to sense the land/ocean surface is paramount to applying this data to the TC monitoring task.

Passive microwave data from the SSM/I's 85 GHz channel is strongly influenced by ice particles aloft that scatter microwave energy and effectively lower the observed brightness temperatures. Thus, high con-

centrations of ice particles that make up spiral rainbands and the eyewall in heavy convective thunderstorms can be readily depicted in SSM/I data. The smaller ice crystals in high cirrus clouds have a much smaller impact, thus enabling the SSM/I to essentially "see" through these high clouds and map out the more important heavy rain regions.
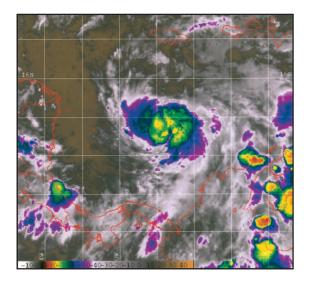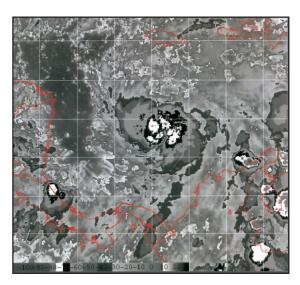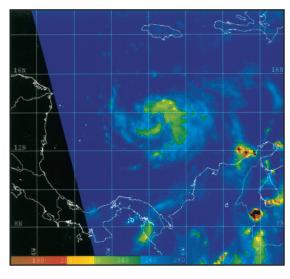
Tropical Cyclone Examples: Figure 2 is a four-panel image that depicts how passive microwave data can assist in monitoring tropical cyclone structure. The upper panels are two geostationary IR images

that use color (left-hand panel) and gray-scale enhancement (right-hand panel) to enable viewers to see the cloud features for hurricane Mitch on 24 October 1998 at 0115 GMT. The ~1500 × 1500-km domain reveals the spiral cloud structure and the most-intense convection associated with the very cold cloud tops near the approximate storm center. However, neither image allows the viewer to pinpoint the storm center with certainty.

The center position and storm structure is much clearer when viewing the passive microwave data (lower panels). The left-hand panel represents a
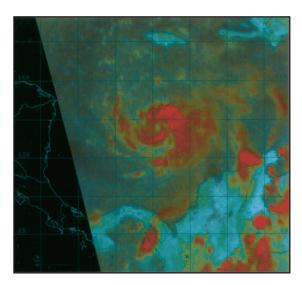
FIGURE 2

Multi-panel image representing four distinct views of Hurricane Mitch as it gathers strength in the Caribbean Sea on 24 October 1998 (0118 GMT). Top left panel is a false-color IR image designed to reveal colder (higher) cloud. Top right panel is an IR-BD enhancement image used by analysts. Lower left panel is the polarization correction temperature (PCT) image that combines 85 GHz H and V polarization (pol) channels to highlight areas of heavy rain due to scattering/emission. The lower right panel is a false-color composite that uses three inputs; PCT, 85 GHz H-pol, and 85 GHz V-pol.

combination of 85 GHz frequencies created to enhance strong convection. The right-hand panel is another multichannel product that not only maps the storm's center, eyewall, and heavy rain, but also enables the viewer to see banding features away from the storm center as well as low-level clouds. Increasing the accuracy of center positions is crucial for the warnings issued by the Navy from centers at the Joint Typhoon Warning Center, Pearl Harbor, Hawaii, and Norfolk, Virginia, as well as from the Tropical Prediction Center in Miami, Florida. These operational centers routinely use passive microwave data because of the inherent advantages these frequencies provide.

Figure 3 is a time series of SSM/I 85 GHz images for super typhoon Oliwa. This western Pacific tropical cyclone reached an intensity with sustained winds near 150 kt ($\sim$75 ms^{-1}) while being observed 15 times between 7-12 September 1997. The brightness temperature displays in Fig. 3 represent snapshots of the storm's structure covering a 512×512-km domain. The red, green, and blue brightness temperatures represent progressively more scattering by ice particles and are a good proxy for heavy convection and precipitation. The best estimate of

Oliwa's intensity is shown in the upper left-hand corner of each subimage and is expressed in knots.

The time sequence shows the development of the spiral bands beginning on the eastern side, the formation of an eyewall, and contraction of the eye to a small diameter on 9 September. A secondary eyewall begins to form on the 9th, and this feature becomes a dominant circulation by the 10th, cutting off inflow to the inner eyewall. The inner eye is denied the moisture flux required to maintain its circulation and heavy convection and thus weakens considerably by the end of the 10th. Oliwa then begins the eyewall replacement cycle again as noted by the double eyewall structure on the 11th and 12th.

An eyewall replacement cycle is a very important TC structural change and is directly related to intensity fluctuations. Knowledge of eyewall cycles is crucial to understanding the current intensity trend (up, down, neutral) for forecast centers worldwide. These cycles are rarely observed in vis/IR imagery since cirrus clouds almost always hide the cloud details needed to extract these ring-like features, but they have been noted in aircraft radar data.[2] Users can monitor storms for eyewall cycles by viewing near
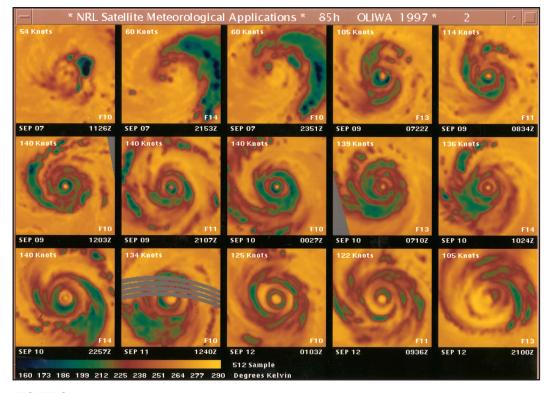
FIGURE 3

Time series display of multiple SSM/I 85 GHz H polarization images for Super Typhoon Gay in 1992. Each image is approximately storm centered and covers a 512-km square box.

real-time data on the NRL-Monterey tropical cyclone web page <http://www.nrlmry.navy.mil/sat-bin/tchome.html>.

[Sponsored by ONR]

References
[1] M.B. Black and H.E. Willoughby, 1992, "Concentric Eyewall Cycle of Hurricane Gilbert," *Mon. Wea. Rev.* **120**, 947-957 (1992).
[2] J.D. Hawkins, D.A. May, J. Sandidge, R. Holyer, and M.J. Helveston, "Satellite Tools for Monitoring Tropical Cyclone Intensity Change," *AMS Symposium on Tropical Cyclone Intensity Change* (American Meteorological Society, Boston, MA, 1998) pp. 51-55.   ◆

NRL's Forward-Deployed Atmospheric Data Assimilation System

J. Cook, P.T. Tsai, L.D. Phegley, J. Schmidt, and R. Lande
Marine Meteorology Division

Introduction: Since the Continental Congress authorized a small fleet in October 1775, the U.S. Navy has had a rich history of deploying as far forward as possible the responsibility and decision-making authority for military operations. Weather conditions impact all military missions, and the ability to accurately assess and predict the current and future state of the atmosphere is fundamental to conducting safe and effective operations. As an aid to fleet weather forecasters, NRL has developed the Tactical Atmospheric Modeling System-Real Time (TAMS-RT), an end-to-end, portable, workstation-based atmospheric mesoscale analysis, forecast, and data assimilation system. A prototype system was tested at sea onboard the USS *Nimitz* during a transit down the West Coast of the U.S. during June 1997. TAMS-RT has been demonstrated operationally in Bahrain since November 1998 under sponsorship from the ONR "Blue Book" program, and in San Diego since May 1998 under SPAWAR sponsorship. TAMS-RT helps meet needs specified by the Oceanographer of the Navy's (N096) Rapid Environment Assessment initiative[1] and partially fulfills several operational requirements for on-scene meteorological data processing.

Configuration: The core of TAMS-RT is the atmospheric component of the NRL Coupled Ocean/Atmosphere Mesoscale Prediction System (COAMPS). COAMPS is a multiscale, nested, mesoscale forecast and data assimilation software system that uses a nonhydrostatic atmospheric model that explicitly predicts three-dimensional wind, temperature, pressure, humidity, cloud, ice, rain, snow, and turbulence.[2] COAMPS includes worldwide databases of static surface parameters, such as 400-m horizontal resolution coastlines and 1-km resolution terrain height and land use characteristics. COAMPS is very well suited to perform in littoral regions where there is significant mesoscale forcing from the surface. Surface irregularities such as topography and coastlines can force mesoscale circulation features in COAMPS, even though they may not be well represented in the initial data. Figure 4 shows a TAMS-RT result from a triple-nest COAMPS forecast for the West Coast. In this figure, the 10-m wind field from each nest is overlaid, showing the increasingly finer scales of motion resolved by the COAMPS coarse, medium, and fine nests that are important for tactical planning.

In addition to COAMPS, TAMS-RT consists of the Tactical Environmental Data Server (TEDS) for storing and handling the background fields, output, and observations. Time-dependent lateral boundary conditions for COAMPS are provided by Fleet Numerical Meteorology and Oceanography Center from the Navy Operational Global Atmospheric Prediction System (NOGAPS). TAMS-RT also includes a user-friendly graphical user interface (GUI) for controlling the COAMPS set-up and data processing sequence, as well as a World Wide Web-based data dissemination, product visualization, and remote monitoring suite of software. TAMS-RT is hosted on three UNIX workstations—a COAMPS server, a TEDS server, and a dedicated graphics workstation for fast three-dimensional interactive graphics. User-designed graphical products are automatically produced by TAMS-RT using GrADS software (developed at the Center for Ocean-Land-Atmosphere Studies, Maryland) and maintained concurrently on a Web server. Vis5D software (developed at the University of Wisconsin) is used for interactive graphics and animation.

On the current generation of multiprocessing UNIX workstations (Silicon Graphics Inc.'s four-processor Origin 2000), COAMPS takes approximately 2.25 hour to complete a 36-hour forecast for a triple nest, $43 \times 43 - 81$ km, $61 \times 61 - 27$ km, $52 \times 52 - 9$-km resolution grid, with 30 vertical levels. Execution time depends on the configuration of COAMPS including resolution, number of grid nests, and size of the grids.
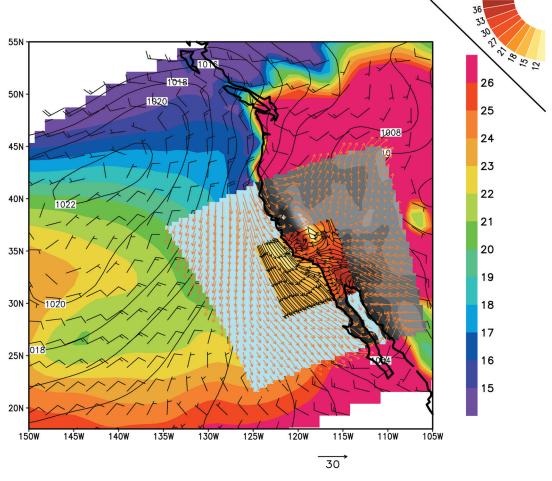
FIGURE 4
COAMPS multiscale 24-hour forecast from TAMS-RT. Coarse nest (108-km resolution) shows contoured sea level pressure, 10-m wind barbs, and shaded skin temperature (color bar – °C); medium nest (36-km resolution) shows shaded topography and 10-m wind vectors; fine nest (12-km resolution) shows shaded 10-m air temperature (color slice – °C) and wind streamlines.

Applicability: With TAMS-RT, a Fleet Meteorology and Oceanography (METOC) unit can expand traditional weather support to analyze perishable local data and obtain tailored, tactical weather forecast guidance out to 48 hours. Atmospheric data from traditional sources are used in TAMS-RT with support for satellite-derived winds and shipboard weather radar data planned for the future. The METOC user can easily select the desired geographical area and model resolution, and tailor the output data products to meet rapidly changing tactical requirements and to maintain situational awareness of the battlespace environment. By using TAMS-RT as a "front end" to decision-aid applications, this system has the potential to address operational issues beyond weather forecasting, such as ship self defense, electromagnetic and electro-optical sensor prediction, and chemical and biological transport and dispersion modeling. In particular, we have adapted the Vapor Liquid Solid Tracking model (VLSTRACK), a chemical/biological dispersion aid developed at the Naval Surface Warfare Center, Dahlgren Division, to use the COAMPS wind, temperature, and humidity forecasts as inputs. Additionally, we have developed the methodology to transmit the resulting VLSTRACK forecast graphic as an overlay to the Joint Maritime Command Information System (JMCIS) for use in operational decision making (Fig. 5).

Future Plans: In the process of transition to operations, TAMS-RT software has been set up in a version management system, and software installation bundles have been created using a commercial installation package. These software management

FIGURE 5
Graphical overlay example from the VLSTRACK model displayed on the JMCIS operational display. VLSTRACK was run using COAMPS forecast data as input for a fictional chemical release north of Charleston, South Carolina. The colored plume shows the predicted location and strength of the fallout in arbitrary units.

techniques will facilitate future upgrades and maintenance of version control for our customers. The TAMS-RT User and System Administrator documentation has also been improved, and training materials have been developed, including on-line contextual help. To maximize portability and customer base, we are porting the software to Sun (Solaris) and Windows NT platforms, and the GUI is being rewritten in JAVA. Upgrades in progress include new visualizations for automatic verification and analysis results, use of either NOGAPS or COAMPS fields for time-dependent lateral boundary conditions, and implementation of improved atmospheric and ocean analysis programs.

Summary: TAMS-RT installed at a Navy regional site provides the ability to organically perform customized high-resolution atmospheric analyses and forecasts in support of decision aids and tactical models that require high-fidelity, high-resolution data not available from current operational sources. TAMS-RT is designed to exploit perishable local data sources, including on-scene observations and satellite data available from the TEDS database. The GUI built for operator control of COAMPS allows numerical weather analyses and forecasts to be easily tailored for areas of tactical interest and customized output data sets to be set up. TAMS-RT has shown the ability to significantly enhance the atmospheric support currently provided to tactical decision makers, particularly with high temporal resolution information about changing weather conditions that affect chemical and biological agent dispersion. Based on several successful demonstrations, the Commander, Naval Meteorology and Oceanography Command, has accepted TAMS-RT for operational transition to six remaining regional METOC sites.

[Sponsored by ONR (322 MM) and the Oceanographer of the Navy through SPAWAR (PMW 185)]

References
[1] R.M. Hodur, "The Naval Research Laboratory's Coupled Ocean/Atmosphere Mesoscale Prediction System (COAMPS)," *Mon. Wea. Rev.* **125**, 1414-1430 (1997).
[2] E.C. Whitman, "EM/EO Performance Prediction in the Navy's METOC CONOPS," *Proceedings of Electromagnetic/Electro-Optics Prediction Requirements and Products Symposium*, Monterey, CA, 1997.

Chemical/Biochemical Research

High-Velocity Oxygen-Fuel Thermal Spray Coatings Replace Hard Chrome

B.D. Sartwell
Chemistry Division

One of the key issues associated with developing new technologies is their ultimate transfer to those entities that can best make use of them. Within the Department of the Navy, this is usually referred to as transferring technology "to the Fleet." In addition to performing the research and development work that can establish new technologies that would have an impact on Naval operations, NRL also can play a role in the actual transfer of new technology by working with Fleet activities to demonstrate, validate, or qualify a new technology that has achieved a certain level of maturity. The program described in this article is just such a case wherein NRL is exercising a leadership role in putting a new technology into the Navy's maintenance activities.

Hard Chrome Plating: This technique has been in commercial production for more than 50 years and is a critical process in manufacturing and maintenance operations on aircraft, ground vehicles, and ships. Within the Department of Defense (DoD), the total value of hard chrome plating operations in overhaul and repair facilities exceeds $100 million annually. Looking at only the aircraft sector, the types of components onto which hard chrome is applied include landing gear, hydraulic actuators, propeller hubs, helicopter transmissions and rotor heads, and gas turbine engines. With this technique, chromium deposits with thicknesses ranging from 2.5 to 500 μm are obtained from a solution of chromic acid and a catalyst. It is used to provide resistance to wear, abrasion, heat, and corrosion; to provide low friction; and to restore dimensionality on worn, undersized, or ground parts where the chrome is overdeposited and machined back to the correct dimension. Vickers hardness values are generally in the range of 8.5 to 10.5 GPa.

The Problem: Hard chrome plating uses chromium in the hexavalent state (hex-Cr), which is highly toxic and a known carcinogen. Therefore, the Environmental Protection Agency has issued stringent air and water emissions standards, and the Occupational Safety and Health Administration (OSHA) has issued permissible worker exposure limits for chrome plating operations. It is anticipated that OSHA will soon issue new, significantly lower exposure limits that will greatly increase the cost of chrome plating to military and private activities.

Particularly in the military and civilian aerospace sector, there are concerns related not only to the increased cost and liability associated with more stringent OSHA and EPA regulations, but also to the in-service performance of chrome plating. Because of increased demands on aircraft and decreasing funding for aircraft maintenance within the DoD, increased materials performance that would lead to reduced life-cycle costs is becoming more essential. The technology area that is most promising in terms of achieving these goals (i.e., improved performance with no environmental concerns), and that is also sufficiently developed for demonstration/validation and technology insertion, is thermal spraying.

The Solution: In 1996, NRL partnered with several DoD aircraft maintenance activities and private companies to submit a proposal to the DoD Environmental Security Technology Certification Program (ESTCP) to demonstrate and validate high-velocity oxygen-fuel (HVOF) thermal spray coatings as a replacement for hard chrome plating. The proposal was approved, and the Hard Chrome Alternatives Team (HCAT) was formed under NRL management. Execution of the program involves all aspects of the qualification process. These include extensive materials testing (e.g., fatigue, corrosion, wear), full-scale component testing, acquisition and installation of HVOF equipment at aircraft depots, personnel training, cost analyses, and development of standards.[1]

HVOF Thermal Spraying: An HVOF thermal spray gun uses an internal combustion jet to generate supersonic gas velocities of approximately 1800 meters/second. Combustion fuels that are mixed with oxygen in the gun include propylene, propane, hydrogen, or kerosene. The types of materials that can be deposited include metal alloys, ceramic/metal composites, and polymers; powders of the coating materials are injected directly into the combustion region of the gun under automatic control. The semi-molten powder particles are accelerated in the gas stream exiting the nozzle of the gun to velocities of about 400 meters/second and impact on the surface of the part being coated. For most HVOF coatings, the porosity is less than 1%, the oxide content is less than 1%, and the bond strength exceeds 80 MPa. These properties make HVOF the most attractive of the thermal spray technologies for chrome replacement.

Materials and Operational Testing: It is well known that application of hard chrome causes a fatigue debit in most materials, especially high-strength steels, but this is something that structural engineers have been willing to live with to obtain the benefits of chrome. Since the HVOF coatings would have to be applied to many fatigue-sensitive, flight-critical parts, this type of testing was essential for qualification. Extensive low-cycle and high-cycle axial fatigue testing was conducted on 4340 high-strength steel, 7075 aluminum alloy, and PH13-8Mo stainless steel onto which hard chrome and HVOF WC/Co (83%/17%) and Tribaloy 400 coatings had been applied. The results for the 4340 steel (Fig. 1) indicate virtually no loss of fatigue strength for the HVOF-coated samples.[2]

Three types of corrosion testing (ASTM B117 salt fog, GM9540P/B cyclic, and atmospheric) were conducted on the same materials at the NRL Marine Corrosion Test Facility in Key West, Florida. Results showed either superior or equivalent performance for the HVOF coatings compared to chrome.[2] Wear testing that simulated either fretting or the action of a hydraulic cylinder on a bushing all indicated superior performance of the HVOF coatings.

HVOF WC/Co coatings have been applied to several components from Navy aircraft and are in operational testing. Figure 2 shows the deposition of the coating onto a P-3 main landing gear cylinder, and Fig. 3 shows the coated component installed on an aircraft that operates out of the Naval Air Station in Jacksonville, Florida. The HVOF coatings are being inspected at six-month intervals, and performance to date has been excellent.

Ongoing activities: At present, the HCAT is partnering with two tri-service organizations, the Joint Group on Pollution Prevention and the Propulsion Environmental Working Group, to conduct full-scale demonstration/validation projects to qualify HVOF coatings on landing gear, hydraulic actuators, helicopter dynamic components, and gas turbine engine components. Funding support comes from these two organizations, ESTCP, the Air Force, and the Navy. In addition, NRL negotiated a Project Arrangement with the Canadian Government to jointly execute the project on landing gear. Altogether, the level of effort for the entire program will be close to $20 million over a seven-year period, with NRL having a major role in management and materials testing.

Ultimate Payoff: Initial economic analyses have indicated that the total cost related to application of HVOF coatings is less than that for hard chrome plating. This, together with their anticipated increased performance, holds the promise that the transition to HVOF will improve sustainability while lowering the total cost-of-ownership to the DoD for its aircraft.
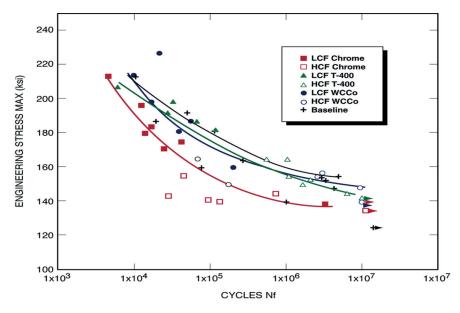
FIGURE 1
Fatigue data showing number of cycles to failure for different stress levels for noncoated 4340 steel (baseline), hard-chrome-plated 4340 steel, and HVOF WC/Co and Tribaloy 400 coated 4340 steel. (LCF - low-cycle fatigue; HCF - high-cycle fatigue).

FIGURE 2
Application of HVOF WC/Co coating to
Navy P-3 main landing gear cylinder.

FIGURE 3
HVOF-coated main landing gear cylinder after
installation on aircraft.

At the completion of the program, it is expected that
HVOF will be in production in many manufacturing
and maintenance activities in both the U.S. and
Canada, resulting in both a cleaner environment and
the savings of millions of dollars in maintenance costs.

[Sponsored by DOD ESTCP]

References
[1] B.D. Sartwell and P.E. Bretz, "HVOF Thermal Spray Coatings
Replace Hard Chrome," *Adv. Mat. Proc.* **156**, 25-28 (1999).
[2] B.D. Sartwell, K. Legg, and B. Bodger, "HVOF Thermal Spray
Coatings as an Alternative to Hard Chrome Plating on Military
and Commercial Aircraft," *Proceedings of the AESF/EPA
Conference for Environmental Excellence*, Orlando, FL,
American Electroplating and Surface Finishing Society, January
1999, pp. 231-237.   ✦

Volume Reduction Strategy for Solid Radioactive Waste Resulting from the Decommissioning of Russian Nuclear Submarines

B.J. Spargo
Chemistry Division

Introduction: Solid radioactive waste from
nuclear submarine decommissioning is a significant
problem in the Russian Federation. A trilateral pro-
gram called the Arctic Military Environmental Coop-
eration (AMEC) between the United States, the King-
dom of Norway, and the Russian Federation has been
established to address environmental issues resulting
from the submarine decommissioning activities in the
Kola region of northwest Russia.

Many Russian Navy nuclear submarines have
reached their expected useful lives or are being taken
out of service to meet arms reduction goals and await
defueling and decommissioning (Fig. 4). Currently,
more than 150 nuclear-powered submarines have
been taken from service[1] and remain in temporary
storage. Two-thirds of them are from the Russian
Northern Fleet at Arctic naval bases at Severodvinsk
and on the Kola Peninsula. Many of the older sub-
marines are in very poor condition and pose a sig-
nificant threat to the fragile Arctic environment.

The primary wastes generated from the decom-
missioning activities include the spent nuclear fuel
(SNF), the liquid radioactive wastes (LRW), and the
solid radioactive wastes (SRW). Approximately 8,500
cubic meters of SRW are at Andreeva Bay on the
Kola Peninsula and at shipyards,[2] with an estimated
activity of 37 TBq (1000 Ci). SRW includes combus-
tible materials (paper, wood, fabric), pressable mate-
rials (plastics, rubber), sorbents, metal (equipment,
fittings, pipes), and nonprocessable materials (high-
level waste and reactor protective systems) (Fig. 5).
The generation rate of SRW is about 1000 cubic
meters per year, and it is expected to increase as the
rate of submarine decommissioning increases.

Mobile SRW Pretreatment Facility: To ad-
dress the SRW storage and disposal needs in the re-
gion, we have developed a novel mobile SRW Pre-
treatment Facility (MPF).[3] A key feature of the concept
is the mobility aspect, which will allow this system to
be transported between shipyards such as Nerpa, and
other intermediate storage sites such as Gremikha
and Andreeva Bay.

FIGURE 4
An Echo-II class nuclear submarine moored at the naval shipyard Sevmorput.

FIGURE 5
Solid radioactive waste compartment in Paldiski, Russia.

The mobility concept will be achieved by the use of International Standards Organization-type or equivalent containers as modular units to house the various unit operations (Fig. 6). Workers in the first module, the Waste Receipt Module, will assess radiation levels of materials and perform size reduction via cutting and shearing. Workers in this area would be outfitted in full personnel protective equipment (PPE). The largest unknown is the actual state and variability of the waste to be processed, therefore this module must exhibit flexibility in configuration and functionality. Waste in this module is moved via overhead crane with a grapple or electromagnetic attachment and assayed for radiation activity. Workers in the second module, the Compaction Module, address radiation measurement and recording, shredding, and in-drum compaction of wastes. Workers in this area do not require full PPE, since all operations are carried out in a glove box or without the need for direct contact with the waste. Wastes placed on the evaluation and sorting table from the Waste Receipt Module will be hand-sorted and classified using the glove box. Compactible waste is placed on a conveyor belt and fed to a shredder. Fluff from the shredder falls into a hold bin from which it is augered to an in-drum compactor. The low-force compactor will volume reduce the waste, resulting in reduction ratios of 5 to 7 or more. Filled drums will be removed and temporarily stored for eventual transportation to a central processing facility for super compaction. The third module, the Worker Service Module, provides the required worker dress-out and control area to limit contamination spread. Also provided are toilet and shower facilities and storage for PPE and personal radiation dose monitoring and measuring devices.

Summary: This project and its related projects in the AMEC program will have a significant impact on the environmental condition and security of the region. The cooperation between each of the countries in developing and implementing technology dealing with radioactive materials resulting from the Cold War nuclear submarine activities will help to

FIGURE 6
Mobile SRW pretreatment facility.

restore the region and protect the fragile Arctic environment.

References
[1] A. Griffith, T. Engøy, A. Diashev, P.R. Schwab, A. Nazarian, A. Ustyuzhanin, P. Moskowitz, and M. Cowgill, "Radioactive Waste Storage Technologies in the Arctic for the Russian Navy," *Proceedings of "Waste Management 99,"* Tucson, Arizona, 1-4 March 1999 (WM Symposia, Tucson, AZ, 1999).
[2] ICC Nuklide, "Designing and Creation of Systems of Processing of Solid Radioactive Waste (SRW), Obtained and Accumulated as a Result of Utilization of Russian Nuclear Submarines," AMEC Project 1.3 Internal Report, 1998 <www.denix,osd.mil>.
[3] B.J. Spargo, "Design and Construction of Treatment Systems for Solid Radioactive Wastes Generated and Accumulated during the Decommissioning of Russian Nuclear Submarines," NRL ltr report, SER6110/368 (1998). ✦

Ammonothermal Crystal Growth of Cubic GaN

A.P. Purdy
Chemistry Division

Gallium nitride (GaN) is a wide-bandgap semiconductor that is currently the focus of much research because of its application in blue and green LED (light-emitting diode) and laser devices. Two crystal forms of GaN are stable at ordinary pressures, namely a hexagonal phase of the wurtzite structure (h-GaN) and a cubic phase of the zinc-blende structure (c-GaN). The cubic phase is predicted to have some advantages: a higher carrier mobility, easier p-type doping, and a slightly narrower energy gap.[1] Both crystal forms can be grown heteroepitaxially on several substrates, but native substrates eliminate any lattice and thermal expansion mismatch and therefore are normally the most desirable substrate for any growth process. Several methods of growing bulk h-GaN crystals are known.[2] However until this work, phase-pure c-GaN had been synthesized only by chemical vapor deposition (CVD) processes. Recently, I discovered a method, using supercritical ammonia solutions, for the growth of single-phase c-GaN crystals.[3] This methodology has the potential for producing large c-GaN single crystals for use as native substrates.

Experimental Description: Crystal growth is done in a sealed quartz tube that contains a feedstock or starting reagents, a solvent, and a solubilizing agent called a mineralizer. The pressure in the tube is determined by the temperature and the amount of solvent present (fill factor), and the tube is counterpressurized with water to prevent bursting.

Synthesis: When elemental gallium or a number of its compounds are heated in supercritical anhydrous ammonia with acidic mineralizers (ammonium halides), both the hexagonal and cubic phases of GaN are formed. Most of the experiments to date have used gallium metal, gallium triiodide, or gallium imides as the Ga feedstock.

Gallium metal reacts with ammonia when only a catalytic amount of ammonium chloride, bromide, or iodide is present at temperatures above 250 °C.

This provides a fine yellow precipitate of submicron GaN crystallites at the bottom of the tube (Eq. (1)). Powder x-ray diffraction shows that these precipitates contain both the cubic and hexagonal GaN phases, and the relative amounts of each are highly dependent on temperature, halide ion, mineralizer concentration, and other conditions. Ammonolysis of GaI$_3$ (Eq. (2)) takes place above 400 °C and also produces a mixture of c-GaN and h-GaN.

$$Ga + NH_3 \xrightarrow{NH_4X} GaN + 3/2H_2, \qquad (1)$$

$$GaI_3 + 4NH_3 \longrightarrow GaN + 3NH_4I. \qquad (2)$$
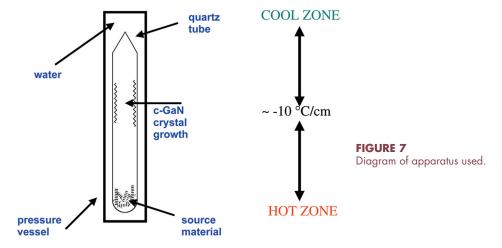
Phase-pure c-GaN powders are obtained by heating a gallium imide-iodide above 275 °C with NH$_4$I in supercritical NH$_3$. The imide-iodide is prepared from the reaction of GaI$_3$ with KNH$_2$ in liquid NH$_3$. These imide-iodides are of poorly defined composition and only serve as precursors to c-GaN when a trace amount of silicone grease (polydimethylsiloxane) is present in the imide synthesis reaction. The role of the silicone in catalyzing the formation of c-GaN is not understood.

Crystal Growth: At a sufficiently high temperature, the precipitate or the feedstock in the bottom of the tube (hot zone) dissolves, and crystals of GaN grow in a cooler portion of the tube (Fig. 7). The crystals nucleate on the quartz surface and are usually at least 10 micrometers long (Fig. 8). The largest c-GaN needles obtained to date are about 0.1 mm long. The temperature and fill factor ranges required for c-GaN crystal growth are primarily a function of the halide ion used (Table 1), but are not very sensitive to the identity of the feedstock.

Many variables, including choice of feedstock, temperature program, heating time, reactant concentration, and additives, affect the quantity and phase purity of the crystal deposits. When crystals of both phases grow, the cubic phase has a tendency to predominate at the cooler end of the growth zone; Fig. 9 provides a striking example. The halide ion largely determines the color of the c-GaN crystals: I$^-$, orange to yellow; Br$^-$, yellow; Cl$^-$, greenish yellow. The colors are presumably caused by traces of halide impurity in the lattice. The h-GaN crystals are typically gray to white.

Large Crystals: The development of this ammonothermal process into a practical means of growing native c-GaN substrates will involve overcoming many obstacles. The factors that control product phase need to be more fully understood. Preliminary indications are that both the nature of the intermediates in solution and crystal nucleation may play a role in determining product phase. Any large-scale application of this process will require the use of c-GaN feedstock and seeds to grow c-GaN crystals. The latter is necessary to avoid the consumption of ammonia or the build-up of byproducts (H$_2$ or NH$_4$X) that change conditions during the growth process and to avoid inadvertent nucleation of the hexagonal phase. It is expected that controlled seeded growth will greatly improve crystal quality.

FIGURE 7
Diagram of apparatus used.
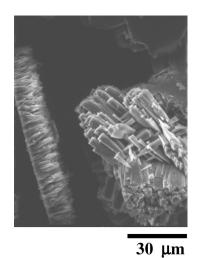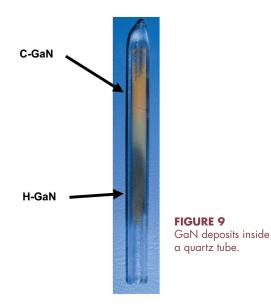
FIGURE 8
Scanning electron micrograph of a typical c-GaN deposit.

FIGURE 9
GaN deposits inside a quartz tube.

Table 1— Effect of Halide Ion on Conditions for Cubic GaN Growth

Halide Ion	Hot Zone Temperature (°C)	Growth Zone Temperature (°C)	Fill Factor Range
I⁻ Br⁻ Cl⁻		350-400 320-350 250-330	~25-70% <40-70% >40%

References
[1] H. Yang, L.X. Zheng, J.B. Li, X.J. Wang, D.P. Xu, Y.T. Wang, X.W. Hu, and P.D Han, "Cubic-phase GaN Light Emitting Diodes," *Appl. Phys. Lett.* **74**, 2498 (1999).
[2] R. Niewa and F.J. DiSalvo "Recent Developments in Nitride Chemistry," *Chem. Mater.* **10**, 2733 (1998).
[3] A.P. Purdy "Ammonothermal Synthesis of Cubic Gallium Nitride," *Chem. Mater.* **11**, 1648 (1999). ✦

Electronics and Electromagnetics

At-Sea Test of a Multifunction Transmitter on R/V *Lauren*

D.C. Wu, I.P. deGrandi, and J. Heyer
Tactical Electronic Warfare Division

Background: The concept for a new transmitter array for the Multifunction Transmitter System has been chosen to bring 1990s technology to the Fleet. This includes the development of a broadband array element, solid-state wideband microwave monolithic integrated circuit (MMIC) transmit modules, and photonics beamforming and transmission networks. The development used a joint industry/government team to design, fabricate, and demonstrate the deployable transmitter. The successful development of this electronic attack (EA) transmitter provides the surface Navy with a system capable of stand-alone jamming that will be required for next-generation surface combatants.
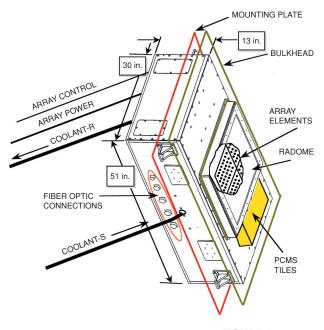
EA Transmitter Description: The EA transmitter is partitioned into outboard and inboard subsystems to provide the signal formation and control portion at a convenient location within the ship, while the antenna portion is installed at an appropriate location on the ship structure for proper angular coverage. The outboard portion consists of a planar array of radiating elements and a power amplification network (Fig. 1). The inboard portion consists of a fiber optic beamforming, switching, and distribution network and includes waveform/technique generators for RF signal operation. A single EA transmitter, envisioned to service one quadrant of a designated ship, forms and radiates the required number of beams at the selected power levels, frequencies, and pointing angles in either simultaneous or time-shared modes.

At-Sea Test: As part of the Advanced Multifunction Transmit System (AMRFS) program, the research vessel R/V *Lauren* (Fig. 2) and the NRL NP-3D aircraft were used for the at-sea test. The test was conducted in July 1999 at the Eglin Air Force Base, Florida, operational area in the Gulf of Mexico to demonstrate multifunction capability.

The EA transmitter array was flush-mounted on the broadside of the ship (Fig. 3). The DC power supply was safely secured below deck. Coolant and dry nitrogen were fed to the array from below deck. The system controller and beamforming computer were located in the operation room along with the photonics source and the techniques generator. All control and RF signals were transmitted via fiber optic cables. To perform EA tests against advanced antiship missile (ASM) simulators, a simplified receive antenna connected to a digital RF memory unit was installed near the transmitter array. The techniques generator used this antenna to capture threat missile RF information necessary to generate various EA waveforms.

Since no receiver was available to provide direction-of-arrival information from the missile simulator
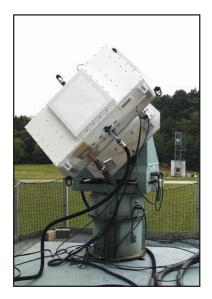
FIGURE 1
EA transmitter array.

FIGURE 2
Research vessel R/V *Lauren*.
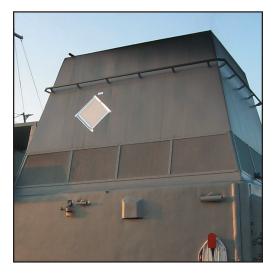
FIGURE 3
Flush-mounted EA transmitter array.

on the NP-3D aircraft, a means was required to point the pencil beam of the phased array antenna on the ship toward the ASM simulators on the aircraft. This was accomplished by the use of the Global Positioning System (GPS). The position of the aircraft as measured by GPS onboard the aircraft was transmitted to the ship by a data link. A clinometer and another GPS unit were installed onboard the ship to provide ship heading, yaw, pitch, and roll, through which the steering commands for the antenna beam toward the simulator on the NP-3D were obtained using coordinates transformation.

NP-3D Aircraft: Because only one transmitter was available for installation on the R/V *Lauren*, and the phased array angular coverage is restricted to ±45° from boresight, the NP-3D aircraft flew inbound on the same radial on every run. The aircraft flew toward the ship on a radial trajectory at an altitude of approximately 500 feet. Each run commenced with the initial starting range of the aircraft located 7 to

10 nautical miles from the ship. The ASM simulators were installed on the NRL NP-3D aircraft for the EA test. To demonstrate an AMRFS function, a communication receiver was interfaced with the APS-80 antenna system on the aircraft to receive voice transmissions from the array.

Summary: During the two-day test, a total of 40 runs were performed. Both the electronic warfare and communication functions were successfully demonstrated. With the added capability of the EA transmitter array, new counter-terminal techniques were developed and evaluated in an at-sea environment. To demonstrate its multifunction capability, the transmitter array was used to communicate a voice message from the ship to the aircraft. The at-sea exercise showed that the EA transmitter array was well-suited, both electrically and mechanically, for shipboard applications. The design parameters of the array and associated electronics proved capable of withstanding the rigors of real-life conditions and ambient temperature as well as vibration in different sea states.

Infrared Missile Simulator and Ship Signature Measurements of the USS *Mahan* (DDG-72)

E.F. Williams and J.W. Dries
Tactical Electronic Warfare Division

Introduction: The Tactical Electronic Warfare Division (TEWD) is intimately involved in the development, test, and evaluation of infrared (IR) countermeasure devices and in analyzing the tactical implementation of these assets by conducting electronic warfare (EW) exercises with U.S. naval surface combatants. The recent EW exercise conducted in February 1999 off the coast of Tampa, Florida, with the newly commissioned USS *Mahan* (DDG-72), which incorporates technologies to reduce its radar cross section (RCS) and IR signature, is an example of such

activities. These comprehensive tests were designed to evaluate the operational Navy's ship self-defense capabilities against IR antiship cruise missiles (ASCM) for the year 2000 and beyond.

Background: The introduction of the MK245 Giant IR decoy to the Fleet required significant software modifications to the AN/SLQ-32A (V3) EW system's software load. These software modifications were essential for the ship to effectively utilize this new decoy system. These tests were coordinated with the Naval Surface Warfare Center (NSWC) Dahlgren, Virginia, and NSWC, Crane, Indiana, to assure proper configuration of the decoy launching system and software modifications. Several naval system commands, with contributions from the Fleet activities, developed the major test objectives. The primary objectives for this test series were to:

- evaluate the effectiveness of the MK245 Giant IR decoy against current and advanced imaging ASCM threats to U.S. Navy ships;

- utilize the Enhanced Nuclear Biological Contamination (ENBC) system to vary the IR signature of the ship and evaluate this signature change with advanced IR seeker simulators;

- characterize the IR signature of the stack and nonstack components for a variety of environmental and operational conditions; and

- measure the tactical effectiveness of the MK245 Giant decoy when using tactics generated by

R17.03 operational software controlling the AN/SLQ-32A (V3) EW system and the MK36 decoy launching system (DLS) with the DECM/Decoy Integration (DDI) program.

Test Assets and Procedures: To accomplish the test objectives, TEWD used the Effectiveness of Naval Electronic Warfare (ENEWS) flyable simulators (Fig. 4) installed on the NRL NP-3D aircraft based at the Naval Air Test Center, Patuxent River, Maryland. These flyable simulators represent current and advanced ASCM threats that include imaging and nonimaging optical designs.

The IR radiometric measurements were performed from a UH-1 helicopter utilizing advanced imaging radiometers. These imagers are used to generate contrast radiant intensity (DWatts/steradian) in the missile spectral response regions as a function of azimuth angle.

The USS *Mahan* (Fig. 5) was responsible for firing the decoys and executing all procedures associated with cycling the ENBC system (Fig. 6). Alternative approaches to implementing tactical procedures were analyzed, but the standard R17.03 operational software was given priority during this test.

The general procedure was for the NP-3D aircraft to approach the ship at multiple aspects, whereas the test ship would execute the appropriate tactical countermeasure solution to detract the missile simulators. At various points in the test series, radiometric signature measurements were performed to correlate missile detection range studies.

FIGURE 4
NRL Effectiveness of Navy Electronic Warfare Systems (ENEWS) IR flyable simulators.

FIGURE 5
MK245 Giant decoy deployed from USS *Mahan* being evaluated by the NRL NP-3D flying over the ship.

FIGURE 6
Water washdown viewed from NP-3D aircraft and helicopter.

Test Results and Conclusion: The test series was very successful in assessing the overall effectiveness of the MK245 Giant decoy when utilizing the R17.03 software load for the AN/SLQ-32A EW system. The results showed the AN/SLQ-32A software control of Giant decoy launches was superior in terms of ease of use and timing accuracy and was preferred by the EW operators with respect to the purely manual control currently used by the Fleet. An alternative laptop-prompted manual control was slightly more accurate and consistent than the purely manual control, although in neither case were the deviations sufficient to affect Giant effectiveness against the missile simulators.

Detailed IR signature measurements of a modern naval combatant were collected. These data sets will be used in the current live fire test and evaluation (LFT&E) studies for soft-kill and hit-point analysis. An additional benefit of this activity is the enhanced

data sets that will be incorporated into IR ship signature prediction and tactical EW models.

Near-Real-Time Imaging of Ocean Fronts with an Airborne, Real Aperture Radar
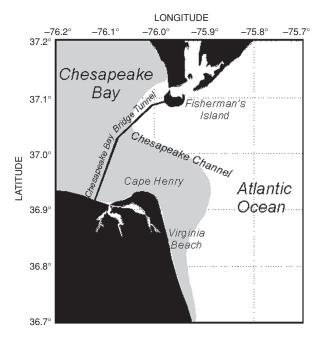
M. Sletten
Remote Sensing Division

D.J. McLaughlin*
University of Massachusetts-Amherst

Background: The flow of estuarine water into the coastal ocean impacts many aspects of the coastal environment. The tidally forced flow of water into and out of an estuary plays a significant role in the life cycle of many pelagic species, in the dispersal of coastal and estuarine pollutants, and in the distribution of sediments. To gain a better understanding of these processes, NRL conducted phases 2 and 5 of the Chesapeake Bay Outflow Plume Experiment (COPE2 and COPE5) in May 1997 and May 1999. The objective of these experiments was to understand the dynamics of the freshwater plume that forms outside the mouth of the Chesapeake Bay through data fusion, using a variety of sensors.[1, 2] This article presents radar imagery from these experiments, collected with the NRL Real Aperture Radar (NRL RAR).

Figure 7 is a conceptual sketch of the plume. The front forms along the boundary between the lighter, fresher water from the Chesapeake Bay and the heavier, saltier waters of the continental shelf. Tidal forcing causes pulses of freshwater to exit the bay mouth during the ebb portion of the cycle and partially retract during flood, thereby modulating both the position and strength of the front. Winds and seasonal variations in the bay discharge rate also

*Formerly with Northeastern University

FIGURE 7
Chesapeake Bay outflow plume and its associated front. The front forms along the boundary between the lighter, fresher water from the bay (shaded region) and the heavier water of the continental shelf.

affect the front location and visibility. However, a comparison of imagery from COPE2 and COPE5 indicates that the spatial evolution of the front is primarily controlled by factors such as bathymetry (bottom topography) that do not vary appreciably with time. Even though these two experiments were conducted two years apart, the observed spatial evolution was remarkably similar. Sample RAR imagery that illustrates this similarity is described below.

Near-Real-Time Imaging with the NRL RAR: The NRL RAR is an X-band (9.375 GHz), dual-polarized system designed for ocean remote sensing research. During COPE2 and COPE5, the system was deployed onboard one of NRL's P-3 Orion research aircraft to provide large-scale "maps" of the oceanic features in the bay mouth and to track the spatial evolution of the outflow plume front. The range resolution of the system is 10 m, and the azimuthal resolution is approximately 25 m at a range of 2 km. Pulse-to-pulse switching and a dual-polarized fan beam antenna allow simultaneous collection of vertically and horizontally polarized imagery.

In cooperation with Northeastern University, imaging software and a wireless local area network (WLAN) have also been developed to allow near-real-time generation and dissemination of the RAR imagery. The software is written for use with IDL/ENVI, a standard software package in the remote sensing community. The WLAN itself is constructed from off-the-shelf components developed for cellular telephone applications. Throughout COPE5, the WLAN was used to supply a research vessel with near-real-time

RAR imagery that provided information on the location and translation rate of fronts in the operations area. Figures 8(b) and 9(b) show COPE5 imagery that were available to researchers on the ship. Personnel on the vessel used this information on many occasions to guide the deployment of their in situ sensors.

Evolution of the Plume Front: Figures 8 and 9 are images of the plume front during the late flood and peak ebb portions of the tidal cycle, respectively. Figures 8(a) and 9(a) are COPE2 images, collected on May 22 and 21, 1997; Figs. 8(b) and 9(b) are COPE5 images, collected on May 20, 1999. (The COPE2 data were collected on separate flights, flown 18 hours apart; the COPE5 data were collected during one continuous flight.) During flood tide (Fig. 8), the front was positioned over the Chesapeake shipping channel and was observed to migrate slowly to the northeast. This was observed in both COPE2 and COPE5. Of particular interest is the small cusp in both images near 35°57′ N, 75°56′ W. In COPE2, the growth and southeastward translation of this feature was observed over the course of a short flight lasting approximately 1.5 hours. In COPE5, a much longer flight was possible, and this feature was observed continuously for nearly 9 hours. As in COPE2, it was initially observed to translate southeast. But later in the flight, it evolved into the large pair of cusps observed in Fig. 9(b) between 36°57′ N and 36°54′ N. A comparison with Fig. 9(a) shows that a similar pair of cusps with a similar location was observed in COPE2 during ebb tide. In view of these

(a) COPE2, May 22, 1997

(b) COPE5, May 20, 1999
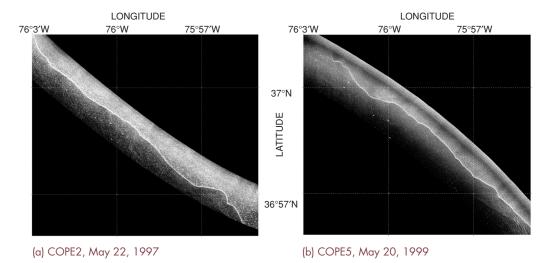
FIGURE 8
NRL RAR images of the plume front collected during the late flood portion of the tidal cycle.

(a) COPE2, May 22, 1997

(b) COPE5, May 20, 1999

FIGURE 9
NRL RAR images of the plume front collected during the peak ebb portion of the tidal cycle.

similarities, it is most likely that the cusps in Fig. 9(a) evolved from a small cusp such as those seen in Fig. 8, and that the small cusp seen in Fig. 8(a) evolved into a pair of cusps such as those in Fig. 9. It thus appears that the cusp evolution observed in COPE5 is repeatable with little variation, even over a period of two years.

Such reproducibility suggests that the frontal evolution is governed by factors that do not vary appreciably from year to year. Bathymetry is such a factor. Additional evidence of an important bathymetric influence comes from the fact that the cusps seen in the COPE2 and COPE5 imagery appear to be

spawned over a region of the bay mouth that contains a steep bathymetric feature.[2] Theoretical modeling is underway to investigate this hypothesis.

References
[1] J. Miller, M. Goodberlet, and J. Zaitzeff, "Airborne Salinity Mapper Makes Debut in Coastal Zone," *EOS Trans. AGU* **79**(173),176-177 (1998).
[2] M. Sletten, G. Marmorino, T. Donato, D. McLaughlin, and E. Twarog, "An Airborne, Real Aperture Radar Study of the Chesapeake Bay Outflow Plume," *J. Geophys. Res.* **104**(C1) 1211-1222 (1999).

Energetic Particles,
Plasmas, and Beams

Arabian Gulf Clutter Measurements with the AN/SPS-49A(V)1 Radar

R.M. Crisler, J.L. Walters, and D.L. Wilson
Radar Division

Background: The AN/SPS-49A(V)1 is the latest version of the Navy's principal two-dimensional (2D) long-range search radar. NRL played a major role in the development and fielding of the A(V)1, as well as in earlier versions of the radar. More than 200 of the various versions have been delivered to the Fleet.

The changing threat environment faced by today's Navy requires modern radars to detect fast, low cross section targets. The AN/SPS-49A(V)1 radar incorporates new signal processing developed at NRL. It allows the radar to operate at full receiver sensitivity over all ranges and significantly improves the ability of the radar to see these kinds of targets.

To provide full receiver sensitivity, the sensitivity time control (STC) was removed. This permits the radar to see low cross section targets but also opens the radar to many unwanted detections (clutter). The new signal processing makes radial velocity and radar cross section estimates on each contact. These characteristics are used to discriminate threat targets from birds and other clutter and to provide improved maneuver detection and faster promotion to firm track by an associated tracker.

To make velocity measurements on every contact, the radar was changed from a low PRF (pulse repetition frequency) radar, highly ambiguous in velocity but unambiguous in range, to a medium PRF radar. Changes in PRF and operating frequency can resolve range and velocity ambiguities in a medium PRF radar. Thus, the radar can still accurately measure range to 250 miles and the velocity of each contact to ±3600 knots.

Medium PRF radars are subject to long-range ducted clutter because of the ambiguous waveform. To measure the impact of ducted clutter on the A(V)1, the authors rode USS *Carr* (FFG 52) in the Arabian (Persian) Gulf. Special instrumentation recorded data not normally available from the radar signal processor, including I&Q (in-phase and quadrature) data and contact event data used to calculate a detection centroid. Balloonborne radiosondes collected atmospheric data to calculate the ducting conditions. Examples of some of these data follow. They include contact data, I&Q data, and ducting conditions.

Radar Contact Data: Figure 1 shows a plot of contacts reported by the A(V)1 from 553 scans. Maximum range is 250 miles. The contact history shows aircraft over mountain ranges, even over the high (red-colored) mountains in the upper right-hand corner, indicating that the radar detects aircraft over strong, mountainous terrain. Notice the patches of returns in the sector from ~290 to ~310 degrees, where there is only open water to the northern end of the Gulf, 420 miles away. In certain propagation conditions, clutter from this coastline is brought back as multiple time around returns. This "folded" return can be countered by the use of "fill" pulses described in the next section.

I&Q Data: Normally the A(V)1 radar transmits eight pulses using the same PRF and frequency in a coherent processing interval (CPI). The first pulse return contains echoes from the first ~80 miles, determined by the pulse repetition frequency. The second received pulse has echoes from 0 to ~80 miles from its own transmitted pulse but also has echoes from ~80 to 160 miles from the first pulse. The third return pulse contains echoes from its own pulse from 0 to 80 miles, from the second pulse from 80 to 160 miles, and from the first pulse from 160 to 240 miles. The Doppler processor of the radar uses a bank of six finite-impulse response filters as part of the process to resolve target velocities. Six pulses are required to fill the filters. The detection path of the processor uses the last six pulses in a CPI to form the filter outputs so that the Doppler filters will process "matched" pulse returns giving optimum filter performance. The first two pulses of the CPI are termed "fill pulses" and are not processed. An additional fill pulse may be added to the CPI by an operator to combat the effects of strong, ducted clutter from long range.

Figure 2 shows a stack of individual pulse returns obtained from one I&Q recording. They have been plotted with a vertical displacement between pulses for legibility. For this recording, the additional fill pulse was selected by the operator. The I&Q recording equipment recorded the last eight pulses of the nine-pulse CPI. The lowest trace in the plot is the second pulse return of the CPI, and the top return is the last return. In this instance, saturating clutter first appears from ranges beyond 240 miles so that the third trace and succeeding pulse returns look similar, and good Doppler processing results.

Normally, for a shipboard radar, clutter at long range is hidden over the horizon. In the Arabian Gulf,

FIGURE 1
Contact history from 553 scans, 250-mile maximum range.
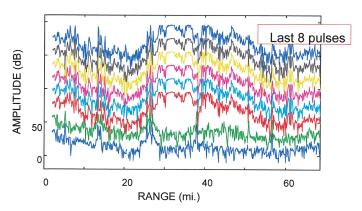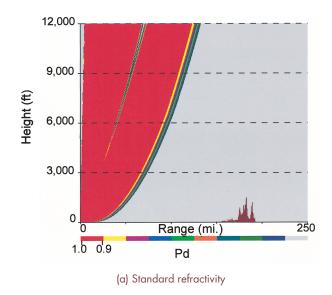
FIGURE 2
Successive pulses in a coherent processing interval, 285° bearing.

(a) Standard refractivity

(b) Measured atmospheric conditions
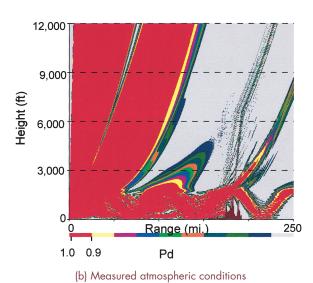
FIGURE 3
Predicted vertical plane coverage.

however, and in similar regions around the world, the proximity of precipitous shores can combine with atmospheric ducting to return very strong clutter from long range. While ducting can be, and has been on some occasions, used to detect low targets at great distances over the horizon, the concern here was to avoid the corruption of Doppler filter performance that could hide air targets.

Atmospheric Data: Figure 3 shows predicted vertical plane coverages for the SPS-49A(V)1 radar located in the region of the Gulf shown in the circular inset map in Fig. 1. The dark red areas of range and altitude values show regions with a high probability of detection. The plot made for standard refractivity shown in Fig. 3(a) would give visibility to a target above 6,000 feet height and inside 100 miles range, for example. Atmospheric conditions measured on 10 September 1998 resulted in the coverage prediction shown in Fig. 3(b). This indicates that targets and clutter would be detected below 1,500 feet out to ranges greater than 170 miles and would include clutter from any land mass. Note the diffraction seen from the sharp mountain peaks. These plots were produced by the AREPS software.[1]

Summary: This shipboard test of the new AN/SPS-49A(V)1 radar was performed on an operating U.S. Navy ship in the Arabian Gulf. It gave the first measured performance of the radar in a heavy ducting environment. Results of the measurements have been reported. The measurements indicated that an additional fill pulse (already designed into the radar in anticipation of this need) should be used to combat long-range, ducted clutter.

[Sponsored by NAVSEA]

References

[1] W.L.Patterson, "Advanced Refractive Effects Prediction System (AREPS) Version 1.0 Users Manual," Technical Document 3028, Space and Naval Warfare Systems Center, San Diego, CA 92152-5001, April 1998. ✦

Clutter Cancellation for the AN/SPN-43C Radar

H. Faust, B. Connolly, F. Caherty, and B. Cantrell
Radar Division
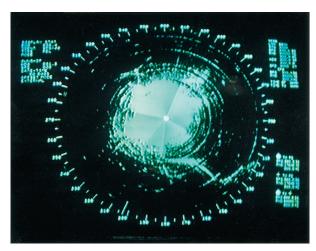
The AN/SPN-43C radar, installed on all aircraft carriers (CV, CVN class) and landing assault craft (LHA, LHD class), provides air traffic control out to 80 nautical miles in range. This pulsed, S-band, magnetron radar, initially deployed in the early 1960s,
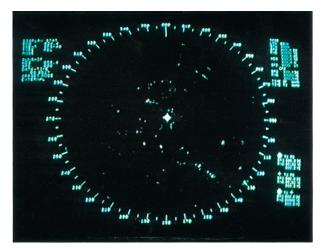
has three variants: A, B, and C (the latest). The main problem with all three versions is the absence of any clutter cancellation ability; consequently, the AN/SPN-43C radar detects rainstorms quite well. Whenever the ship's aircraft enter rain, they are lost in the clutter patch displayed on the planning position indicator (PPI). Operational procedures require the air traffic controller to declare a lost track if there are more than three consecutive scans without video "paint." To maintain radar contact, the operator must switch to video from another radar such as the AN/SPS-49. Furthermore, the recent emphasis on littoral warfare compounds the problem by introducing land clutter into the environment. The Fleet must be able to perform air marshalling over land and water, in theater, which opens up the possibility of ducted multiple interval clutter. To keep pace with its changing mission, the AN/SPN-43C radar needs the capability to function effectively in common adverse conditions—rain and land clutter.

The Moving Target Indicator (MTI) System: NRL proposed a digital MTI system based on commercial off-the-shelf components to give the AN/SPN-43C radar the ability to attenuate strong clutters and perform its mission in contemporary battle scenarios. NRL also designed, built, and tested an advanced development model (ADM) MTI system that provided 50 dB of measured clutter cancellation. All of this was achieved at very low development cost.

The ADM system functions concurrently with the AN/SPN-43C radar while maintaining all of the original radar functions. It consists of a dual-channel receiver, a 21-slot commercial VME card cage (MTI processor), a timing interface card, and an interface chassis. All of the components were integrated into a 19-inch standard rack that is four feet in height. The system includes the rack, monitor, keyboard, and an uninterruptible power supply. The ADM system provides timing and transmit waveform parameters to the radar through the interface card and accepts RF and microwave signals from the radar, via the receiver, for MTI processing. The system generates both unprocessed and MTI-processed video signals for the PPI display so that both can be displayed simultaneously. The receiver downconverts an attenuated version of the transmit waveform as well as the target echoes for sampling by an analog-to-digital converter (ADC) residing within the MTI processor. The processor card complement includes six commercially available processor cards to perform such tasks as downconversion of the ADC data to baseband, MTI cancellation, and multiple-interval clutter rejection. Instead of a single AN/SPN-43C transmitted waveform, the MTI algorithm requires six new

(a) Without MTI or STC

(b) With MTI and mild STC

FIGURE 4
AN/SPN-43C PPI photo; range scale 26 nmi.
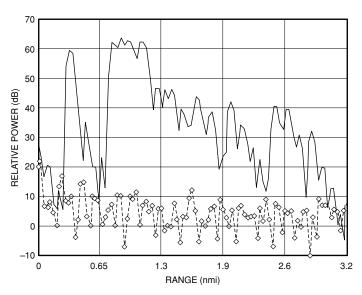
FIGURE 5
Actual clutter levels at the video output.

transmit waveforms, each with a distinct pulse repetition interval (PRI). NRL personnel developed all of the required software for the MTI processing, video generation, and timing. The interface chassis provides buffered output signals to the display and tracking systems connected to the AN/SPN-43C.

MTI System Testing: Throughout the year, the ADM system underwent landbased testing at the Naval Air Warfare Center Aircraft Division (NAWC-AD), Webster Field, Maryland, and at-sea testing aboard the USS *Kearsarge* (LHD-3) and the USS *Harry S. Truman* (CVN-75). Figure 4 shows two photos of the PPI display aboard the *Truman* while in port.

Figure 4(a) is the displayed video output of the SPN-43C PPI without MTI processing or sensitivity time constant (STC). The clutter is dense and blooms the PPI display out to 14 nmi. Most of the clutter is from stationary objects such as ships, buildings, and towers. Rings are visible from strong point clutters received through the antenna sidelobes. The curved artifact from 135° to 170° is a bridge across the inlet to the Chesapeake Bay. Figure 4(b) shows the MTI video output with the STC adjusted to its lowest setting. The STC, which is part of the AN/SPN-43C radar, removes clutter (and moving targets) at the close-in ranges. Even though Fig. 4(b) shows changes in two variables over Fig. 4(a), it illustrates actual Fleet

use of the MTI system. Moreover, there was no other way to remove the extremely close clutter, most of which was 80 dB above the video noise level. With all of the heavy clutter gone, all that remains is the moving traffic on the bridge. Figure 5 shows quantitatively the degree of clutter cancellation achieved by the ADM system during landbased testing. The horizontal axis is the range bin, the vertical axis is the relative signal strength in dB. The 0 dB reference is the thermal noise level at the video output. The upper curve, with the MTI disengaged, shows clutter levels close in range exceeding 60 dB. On the other hand, the lower curve, with the MTI engaged, shows clutter cancellation approaching the thermal noise level. Together, the two curves show 50 dB of cancellation with the MTI modification!

Infrared Fibers for Missile Jamming

J.S. Sanghera, L.E. Busse, and I.D. Aggarwal
Optical Sciences Division

Infrared Countermeasures for Missile Defense: When an infrared (IR) guided missile is launched at an aircraft, response to the threat must occur automatically within a few seconds and a sequence of events must be triggered quickly. IR detectors (operating in the 2 to 5 μm atmospheric window and mounted on the aircraft surface) locate the missile. Then, a specific, modulated laser signal must be directed from the aircraft by a beam pointing device (jam head) to the missile, sending it off course away from the aircraft. These events summarize the action of an infrared countermeasures system (IRCM), which significantly enhances aircraft survivability against attack from missiles.

Shortcomings of Current Missile Defense Systems: A missile defense system includes a high-power IR laser operating in the 2 to 5 μm region. Laser output is guided to two jam heads, located remotely on the surface of the aircraft. Each head is capable of multi-axis rotation to direct the laser energy to the missile. Currently, an articulated arm is used as an optical link from laser to jam head, in lengths ranging from 0.5 to 3 meters. This arm is a 1.5-inch diameter tube with 90° bends containing mirrors. This arm is heavy, bulky, and difficult to maintain; it is also expensive (a 3-meter arm costs more than $50,000). Furthermore, in many of the new Navy/DoD aircraft (such as jet fighters) absolutely no space is available for an articulated arm. Thus there is need for a flexible, lightweight, low-cost conduit to guide the laser beam to the jam heads. A similar conduit could replace the costly and high-maintenance actuated mirrors and bulk optics inside the jam head. The question arises as to what can be used for the conduit?

The NRL Solution: IR-transmitting optical fibers are a natural choice for a compact, low-cost optical link from the laser to jam head. Chalcogenide glasses such as arsenic sulphide transmit in the 2 to 5 μm wavelength region. Unfortunately, fibers made in the past by other research groups possessed high optical losses, were extremely fragile to handle, and could not tolerate high laser power. Consequently, there was a ubiquitous myth that these poor qualities were intrinsic, which made the fibers impractical for applications. At NRL, we believed that if we could determine why the previous fibers were of such poor quality, we could then develop new techniques to improve the fibers and make them useful for missile defense systems.

NRL Fiber Development: We have identified impurities responsible for the high losses and have subsequently developed dynamic distillation processes for the precursors and glass fabrication processes to significantly reduce both particulate and gaseous impurities. Appropriate core and clad glass compositions have been developed. These have similar thermal properties for ease of fiber fabrication, with the core glass having slightly higher refractive index than the clad glass ($\Delta n \sim 1\%$), to create a fiber optic waveguide. We have also developed[1] new fiberization techniques (Fig. 6) that have resulted in optical fibers with record low optical loss of ~0.1 dB/m (~98% T in 1 meter) in continuous 500-meter fiber lengths.[1] Typically, the fiber is jacketed on-line in the draw tower with an ultraviolet (UV)-curable acrylate coating for mechanical abrasion resistance. Figure 7 shows the optical loss of the fiber made using techniques developed at NRL compared with fibers made using old technology. Subsequently, the fibers were used to transmit high power (30 kW peak power; peak input power density = 1.4 GW/cm^2) from an IR laser with output in the 2 to 5 μm region with absolutely no resultant damage. We also fabricated preliminary protective plastic cables, which were strong and capable of more than 20,000 cycles of flexure without breakage. Since the fibers now

FIGURE 6
Double crucible technique for making chalcogenide glass fibers.
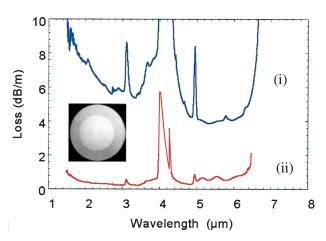
FIGURE 7
Optical loss of fibers made using (i) old technology and (ii) new technology developed at NRL. Insert shows a fiber cross-section.

possessed low optical loss and were strong and capable of high power transmission, they were ready for use in a missile defense demonstration.

Missile Defense Demonstration Using IR Fiber: The first system field demonstration using NRL fiber cables with the IRCM laser and jam head took place in August 1999. Figure 8 shows the system hardware, along with the old articulated arm. The output from the laser was transmitted via fiber to the jam head and through fiber "wired" inside the jam head. This eliminated several actuated mirrors and servo loops, thereby enhancing reliability. The demonstration consisted of mounting the jam head on a vibration platform, simulating a helicopter, and send-ing the IR laser beam 800 meters down range from the jam head while simultaneously tracking an IR source that represented a missile plume at that location. Results showed that the jam head containing the fibers maintained excellent beam pointing accuracy at the target, even while undergoing excessive vibrations.[2] Therefore, the NRL all-fiber-path approach significantly reduces the complexity, weight, and cost and enhances the reliability of current missile defense systems.

Summary: IR fibers developed at NRL have been successfully used in an IRCM system demonstration for missile defense. Future work will focus on application of broadband antireflection coatings to mini-
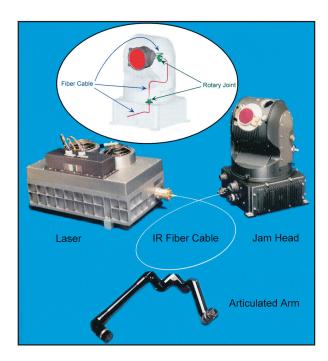
FIGURE 8
Missile defense system hardware showing IR fiber cable developed at NRL connecting laser to jam head. A 1-meter-long articulated arm is shown for comparison. The insert is a schematic showing path of the IR fiber cable inside the jam head.

mize endface reflection losses associated with the high refractive indices of the glasses as well as ruggedized protective cables for aircraft implementation. Other applications using the IR fibers are being explored. These applications include remote fiber optic spectroscopy for environmental pollution monitoring, fiber cables for laser surgery, and imaging bundles for threat warning systems.

[Sponsored by ONR, U.S. Army CECOM, AFOSR]

References
[1] J.S. Sanghera, P.C. Pureza, I.D. Aggarwal, and R. Mossadegh, "Process for Making Optical Fibers from Core and Cladding Glass Rods," U.S. Patent 5,879,426, awarded March 9, 1999.
[2] "Sanders ATIRCM Laser-based Jammer Uses Optical Fiber," *Mil. Aerosp. Electron.* **10**(12) 1 (December 1999). ◆

Midwave-Infrared Antimonide "W" Lasers

W.W. Bewley, D.W. Stokes, and J.R. Meyer
Optical Sciences Division

I. Vurgaftman and C.L. Felix
Unified Industries, Inc.

M.J. Yang
Electronics Science and Technology Division

Introduction: Since the 1960s, infrared-guided missiles have accounted for more than 70 percent of U.S. aircraft losses in combat. Jamming with a high-power midwave infrared (mid-IR) (3-5 μm) laser can confuse a heat-seeking missile and cause it to miss its target. Inadequate laser performance, however, is currently the primary bottleneck in the development of infrared countermeasure (IRCM) systems. Both DoD and industry also need convenient and inexpensive mid-IR lasers for detecting trace concentrations of chemical and biological agents. Applications include warning against chemical/biological attack, pollution monitoring, leak detection, chemical process control, and base clean-up.

Compact semiconductor diodes operating at ambient temperature now fully dominate the $3 billion per year world market for visible and near-IR lasers out to $\lambda \approx 1.6\,\mu$m. Unfortunately, performance at mid-IR wavelengths beyond 3 μm has been poor, and following a first demonstration of lasing at liquid nitrogen temperature (77 K) in 1963, incremental improvements have come at an excruciatingly slow rate. In particular, a large and expensive refrigeration system has been needed to cool the tiny diode, making widespread commercialization unattractive.

NRL has recently developed a new class of "W" lasers based on antimonide quantum wells. These lasers have appreciably advanced the standards of performance for the mid-IR spectral range. As a result, practical noncryogenic mid-IR diode lasers for IRCM, chemical sensing, and other applications are finally on the horizon.

W Quantum Well Active Region: Figure 9 illustrates three periods of the active region for a W quantum well laser, which takes its name from the shape of the conduction-band profile.[1] Each period of the structure contains four layers: InAs/GaInSb/InAs/AlAsSb, which all have similar lattice constants that are suitable for growth by molecular beam epitaxy (MBE) on GaSb or InAs substrates. The GaInSb

129
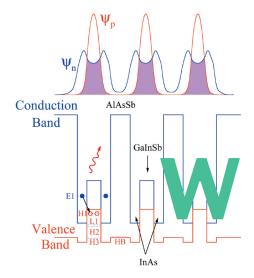
FIGURE 9
Conduction and valence band profiles, energy levels, and wavefunctions for the three periods of an InAs/GaInSb/InAs/AlAsSb "W" laser.

layer, which acts as a quantum well for the holes, is surrounded by two InAs electron wells that are in turn surrounded by AlAsSb barriers. In spite of the electron and hole quantum wells being in different materials, the layers are so thin that their wavefunctions have a strong overlap (upper portion of the figure) that is enhanced by the second electron well in each period. This leads to gain when the electrons and holes recombine to emit mid-IR photons. The W structure has several key advantages over earlier mid-IR lasers, including excellent carrier confinement by the high AlAsSb barriers and a considerable suppression of Auger (3-carrier) recombination, which robs electrons and holes at high temperatures without producing any mid-IR photons.

Optically Pumped W Lasers: The simplest way to inject electrons and holes into the quantum wells is optically, by pumping with a shorter-wavelength laser. Devices designed and tested at NRL were grown by MBE at the NRL Electronics Science and Technology Division Epi-Center, Sarnoff Corporation, and the University of Houston. For pulsed operation, optically pumped W devices were the first interband mid-IR lasers to operate above ambient (room temperature is about 300 K). They have emitted to $\lambda = 7.3$ μm, which is more than 2 μm longer than any earlier *interband* III-V device (although low-power IV-VI lasers and *intersubband* quantum cascade lasers have emitted longer wavelengths).

Most applications will require that the laser produce either a continuous wave (CW) or long pulses at high duty cycle. To optimize the thermal manage-

ment that becomes critical under those conditions, we have developed a novel heat-sinking approach called diamond pressure bonding (DPB).[2] As shown schematically in Fig. 10, the semiconductor wafer is mechanically pressed against a polished man-made diamond crystal (which has one of the highest known thermal conductivities). Besides requiring almost no processing, DPB produces an excellent thermal bond to the epitaxial side of the laser bar where the heat is being generated. Furthermore, since there is no metallization as in conventional mounting, it also allows top optical access through the diamond at wavelengths that would be strongly absorbed by the substrate were pumping attempted from the back. A DPB-mounted W laser emitting at $\lambda = 3.0$ μm recently achieved CW operation nearly to room temperature (290 K).[2] The plot in Fig. 11 of maximum CW operating temperatures vs wavelength for many semiconductor mid-IR lasers from the literature shows that this exceeds all other T_{max} by >100 degrees. Furthermore, the decrease of T_{max} with increasing wavelength is quite gradual, so that another W device at $\lambda = 5.9$ μm lased CW to 210 K. A CW output power of >0.5 W was obtained at 78 K ($\lambda = 3.2$ μm), which is higher than any previous mid-IR result.

W-Diode Lasers: Because of their potential for extreme compactness, low power consumption, and low cost, electrically pumped lasers are the ultimate answer to the military and commercial mid-IR needs. Recently, NRL in collaboration with Sarnoff Corporation achieved the first room-temperature (310 K) pulsed operation of a III-V interband laser emitting beyond 3 μm, a goal pursued by the mid-IR diode
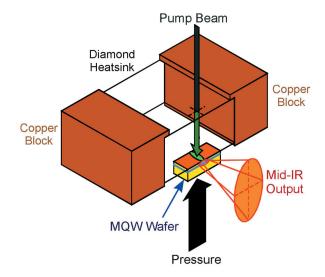
FIGURE 10
NRL diamond pressure bonding (DPB) heat sink.
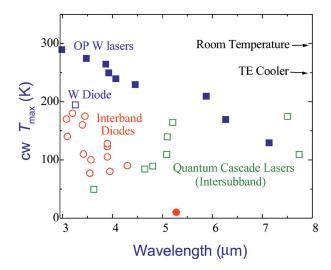
FIGURE 11
Maximum CW operating temperatures vs wavelength for NRL W (blue), other interband III-V (red), and intersubband quantum cascade (green) lasers.

community for more than three decades. The active region of the device was a W structure with specially designed AlGaAsSb barriers that permit holes to tunnel from one period to the next via light-hole states and the electrons to tunnel efficiently. The structure also contains a Sarnoff-developed "broadened waveguide," which reduces the internal losses for reduced threshold and enhanced efficiency.

A CW W-diode with five active quantum well periods generated 140 mW at 78 K, and lased up to 195 K at $\lambda = 3.25$ μm. Despite being the highest CW T_{max} for any electrically pumped III-V laser emitting beyond 3 μm (open square in Fig. 11), the structure is far from optimized, and substantial further improvements are expected. It is projected that CW mid-IR diodes operating at ambient temperatures or with compact thermoelectric coolers (T 230 K) will become practical in the foreseeable future.

[Sponsored by ONR]

References
[1] J.R. Meyer, C.A. Hoffman, F.J. Bartoli, and L.R. Ram-Mohan, "Type-II Quantum-Well Lasers for the Mid-wavelength Infrared," *Appl. Phys. Lett.* **67**, 757-759 (1995).
[2] W.W. Bewley, C.L. Felix, I. Vurgaftman, D.W. Stokes, E.H. Aifer, L.J. Olafsen, J.R. Meyer, M.J. Yang, B.V. Shanabrook, H. Lee, R.U. Martinelli, and A.R. Sugg, "High-Temperature Continuous-Wave 3-6.1 mm "W" Lasers with Diamond-Pressure-Bond Heat Sinking," *Appl. Phys. Lett.* **74**, 1075-1077 (1999). ✦

Information Technology and Communication

Immersive Scientific Visualization

R. Rosenberg, M. Lanzagorta, E. Kuo, R. King,
and L. Rosenblum
Information Technology Division

Introduction: In the next-generation Navy, weapons systems—from material composition to functional requirement—will be designed and tested through large-scale computational simulation and modeling, saving the DoD billions of dollars in live testing and laboratory processing. Such calculations are spanning length and time scales from the microscopic to the macroscopic. Continuum and first-principle approaches must be co-calculated, resulting in massive, intricate, scientific data sets that capture physical phenomena on both large and small scales. Little is known about the effective display of really complex scientific data sets. However, scientific visualization of very large and highly complex data sets has emerged as a critical part of the scientific process by exploiting the human brain's natural pattern-recognition ability. Immersive virtual environments (VE) have been found to be valuable for visualizing these data sets, since such environments provide a natural human-computer interaction for data interrogation and analysis of three-dimensional (3D) data sets.

Immersive Virtual Environments: The NRL's Virtual Reality (VR) Laboratory conducts basic and applied research in VR, augmented reality, and 3D graphics, and houses the 3D immersive room known as the GROTTO. The GROTTO consists of three rear-projected screens (front and lateral walls) and one front projected screen (floor) occupying a 10 × 10 × 10-foot area. An SGI Onyx workstation with IR graphics that can render millions of polygons per second drives the projectors. Liquid-crystal shutter glasses provide stereoscopic vision. The Onyx generates left and right eye images. IR sensors, synchronized to the computer, operate in conjunction with the glasses to ensure that the left eye images reach only the left eye and right eye images reach only the right eye. GROTTO is referred to as being an *immersive display* because its graphical display area covers the walls and floor of a room. Thus, instead of looking *at* the display, the user is immersed *within* the display. Six researchers can comfortably enter the GROTTO and jointly examine a scientific data set. Interaction with the GROTTO display occurs through a 3D joystick that is used primarily for navigation and object manipulation within the VE. Electromagnetic trackers coordinate the scene view with the location of the viewer's head.

The NRL's Scientific Visualization Laboratory and the NRL's VR Laboratory are developing in-house VR software for rapid prototyping of VR applications for scientific visualization. Using this software, scientists develop visualization applications at their desktop and then port their application into the GROTTO without a large investment in time and knowledge of computer graphics.

With this rapid prototyping environment, we were able to port 20 scientific applications to the GROTTO in a short period of time. Applications were from ongoing NRL research projects, spanning diverse scientific areas: chemistry, material science, computational fluid dynamics, solar physics, and optics. In what follows we briefly discuss some of these applications.

Applications: Dr. George Spanos (Materials Science and Technology Division) is interested in the 3D morphology of the internal microscopic structures of materials. Using a 3D-reconstruction technique, a microstructure was visualized in the GROTTO (Fig. 1). The stereoscopic viewing and the size of the images displayed were enough to give the user a real sense of the morphology of the microstructures and their spatial distribution that cannot be matched by the normal computer monitor screen. During one of the VR visualization sessions, Dr. Spanos made an important discovery: a new kind of structure was observed that had not been seen before. Although such structure can be observed on the computer monitor screen, it had not been noticed until the examination in the immersive room. This shows that the capabilities of VR may actually ease the labor of the scientist, at least in the analysis of 3D information.

In Fig. 2, Dr. Spiro Antiochos (Space Science Division) examines the structure of solar magnetic field lines. The visualization shows the essential physics for the support process of a solar prominence. The VR visualization allowed Dr. Antiochos to examine all the features of this complex, fully 3D system and compare the model with solar observations. Inside the GROTTO, Dr. Antiochos is able to look at the solar magnetic field structures as if he were standing on the surface of the Sun. Real-time interaction with his data permits him to sample the magnetic field lines in various regions, and in doing so, he is able to more clearly understand the mechanisms that support the prominence mass against gravity.

A variety of computational fluid dynamics applications have been ported to the GROTTO: combustion dynamics, missile blasts, torpedo launch dynamics, and many others. Some of these applications are interactive simulations running in the NRL's Origin 2000 supercomputer. Figure 3 shows Dr. Will-

FIGURE 1
Immersive visualization of
a microstructure.

FIGURE 2
Immersive visualization of
solar magnetic field lines.
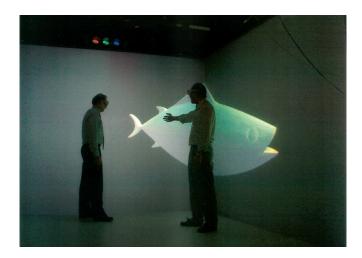
FIGURE 3
Immersive visualization of
the dynamics of a swimming
tuna.

iam Sandberg and Dr. Ravi Ramamurti (Laboratory for Computational Physics and Fluid Dynamics) studying the dynamics of a swimming tuna inside the GROTTO.

Conclusions: Virtual reality offers many advantages for scientific visualization: stereoscopic rendering, large images, wide angle of view, and a natural human-computer interaction interface. VR seems to be an excellent technology for the visualization of complex 3D data sets and shows great potential as a device for the communication and dissemination of visual information.

[Sponsored by NRL and ONR] ✦

Virtual Ship Combat Information Center Training System

H. Ng, S. Guleyupoglu, and P. Melody
Information Technology Division

As the U.S. defense budget decreases, the Navy training community is more cost-conscious than ever. In current U.S. shore-based surface combatant training facilities, new crews are trained using real combat consoles in a classroom environment. This has the considerable expense of supporting, maintaining, and reconfiguring the consoles used in these facilities. In addition, a limited number of training consoles are available, limiting time available to each student to use.

The Naval Sea Systems Command tasked the staff of the Advanced Information Technology branch in the Information Technology Division to investigate a cost-effective solution for training. With the advent of more powerful and cheaper graphics computers, virtual reality technology has become a cost-effective training solution. This technology allows users to be immersed into a simulated graphical environment where they see the virtual environment through a computer monitor or a head-mounted display. It also provides input through various devices such as a keyboard, mouse, or more sophisticated alternatives. We have coupled virtual reality and distributed simulation technology to develop a distributed virtual ship combat information center (CIC) for surface ship training. The goal is to create a distributed immersive learning environment to complement current training capability with reduced maintenance cost and higher availability. CIC crew members can then perform team learning and training in a virtual ship environment. The virtual environment offers a true interactive three-dimensional (3D) view of the interior of the CIC (Fig. 4). The visual simulation portion of the Virtual CIC is intended to provide the "look and feel" of the actual CIC through the use of extensive 3D models, phototextures, and sound clips. Virtual environments create a new level of training by making the training experience "realistic" instead of a classroom-like environment. It also simulates the equipment that the crew interacts with to perform detection, classification, and target engagement activities. Each student appears in the environment as a 3D human representation, an avatar. A picture of each student's face is scanned and mapped onto his
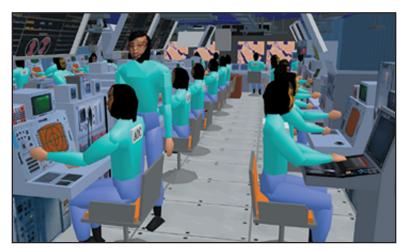
FIGURE 4
Virtual ship combat information center.

avatar with the 3D texture mapping technique so that each student can recognize others inside the Virtual CIC. The Virtual CIC's networking capability is implemented using the Department of Defense's distributed simulation standard, the High Level Architecture (HLA). This allows students at different geographical locations to train together in a unified virtual environment over a wide-area network. This networking capability not only allows the crews in the same ship CIC to be distributed at different locations for training, it also provides the capability to simulate the whole virtual battle group operations (multiple ships) (Fig. 5).

Before the project was started, we met with the instructors and students at the AEGIS Training and Readiness Center (ATRC) in Dahlgren, Virginia, to identify system requirements. One desired feature is to provide visualization aids that can help students understand how to apply different warfare doctrines and the implications of different modes in the combat system consoles. Various information visualization aids were incorporated into the virtual environment to help students learn different tactical deployments of the combat systems. For example, we have created a "holocube" that allows the student to visualize the entire battlespace (Fig. 6). This allows students to correlate sensor data with a visual 3D display of a god's-eye view, facilitating understanding of sensor capabilities and operations. This holographic-like display also allows for visualization of sensor coverage, emission restrictions, operational

boundaries, and other doctrinal concepts and entities. As the student changes watchstation console mode, the holocube view could change to reflect the performance of that mode. This visual augmentation can assist in teaching tactical deployment of offensive and defensive capabilities to incoming sailors. A multimedia hypertext tutorial is integrated into the virtual world, detailing information about console operations, responsibilities, and workflow of watchstations in the CIC. The Virtual CIC application can be run in a variety of display and input configurations. These include a simple single monitor with mouse and keyboard input for individual training, stereoscopic large multiscreen panoramic displays for group viewing or playback, and stereoscopic head-mounted displays with hand and body movement tracking devices for fully immersive team training to meet different training needs.

An initial version of the Distributed Virtual Ship CIC Training System was delivered to ATRC for testing and evaluation with good results. For maximum efficiency, virtual consoles are easily reconfigured or rearranged as needed for different ship configurations. By combining the virtual environment with a ship simulation model, operational procedures under various tactical scenarios can easily be explored and refined. System performance can be stressed in a realistic scenario without risking accidents or tying up real operational hardware. Incorporated information visualization aids allow students to learn and understand the operations much faster than in a regu-
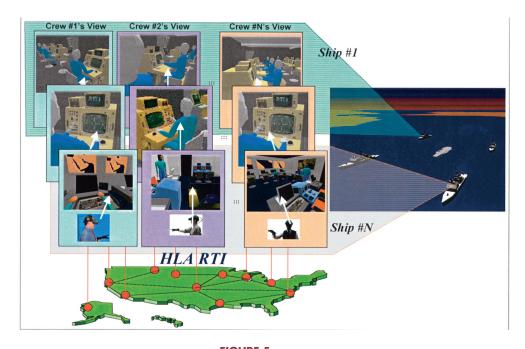
FIGURE 5
Virtual battle group.
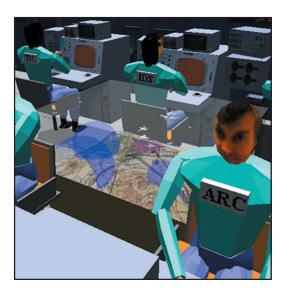
FIGURE 6
Holocube visualization aid.

lar classroom environment. Virtual-reality-based training also allows students to train with advanced systems before the hardware has been built, or try out new physical layouts that do not currently exist, as well as experiment with and develop new operational procedures. The system described can be applied to land-based or mobile command centers as well as the ship CIC. Also, it is not limited to training applications. Currently, we are extending the system to virtual prototyping (i.e., design and develop new systems in a virtual environment before building the real physical system).

[Sponsored by OPNAV]   ✦

Fleet Demonstration of a Completely Digital Reconnaissance System, TARPS-CD

J.N. Lee, M.R. Kruer, and D.C. Linne vonBerg
Optical Sciences Division

Introduction: The Navy operates the only deployed DoD manned tactical reconnaissance system, TARPS—Tactical Air Reconnaissance Pod System. The TARPS system consists of several film cameras within a pod flown off aircraft carriers by F-14 aircraft. However, film systems cannot meet current requirements for real-time targeting of relocatable targets (e.g., SCUD missiles) and timely wide-area surveillance. Air tasking that relies on TARPS film

data typically is accomplished in no less than 12 hours, and may extend to days. Digital imagery is seen as the solution. Imagery could then be directly transmitted from the aircraft, with better fidelity than analog video; digital processing could lead to faster and more accurate target location; and digital networks could allow immediate targeting decisions. However, significant technological and operational-concept hurdles still need to be overcome in several areas before the full potential can be realized. System challenges include providing sufficient airborne camera coverage and resolution and a capability for establishing and holding a high-bandwidth data link to the aircraft for rapid transmission of target data. Also needed is a capability to immediately form raw imagery, locate target coordinates, and forward target images to users.

NRL Optical Sciences Division has designed, implemented, and demonstrated an all-digital reconnaissance system, designated TARPS-CD (TARPS completely digital); the system consists of three elements:

- A very-high-resolution step-stare framing camera (25 million pixels/frame), a wideband 274-Mbps CDL (common data link), an Ampex DCRsi digital tape recorder, and a reconnaissance management system (RMS) controller installed in an empty TARPS film pod. Figure 7 shows the pod payload configuration. The step-stare camera is the CA-261, which was developed under NRL's Advanced Reconnaissance Program by Recon Optical, Inc. The RMS controller is run from the existing TARPS control panel in the F-14 cockpit. The airborne CDL hardware feeds a small omnidirectional antenna located on the underside of the pod. The data packetizer simultaneously sends the camera data to the CDL and the onboard DCRsi recorder, while forming data packets that enable very-low-error-rate performance.

- The CHBDL (common high bandwidth data link) surface terminal for tracking and receiving the CDL data link signal. The CHBDL system is being deployed on all aircraft carriers and command and control ships, and many large-deck and amphibious assault ships.

- An image-formation and screening station, designated NAVIS (Navy input station) that decompresses the downlinked data, forms and displays imagery for screening by an operator, and interfaces into intelligence and air tasking

FIGURE 7
Pod payload and locations within the pod.

processes. One high-resolution NAVIS monitor "waterfalls" a mosaic display of low-resolution "thumbnails" (Fig. 8); a second monitor displays operator-selected thumbnails at high resolution and permits roaming, zoom-in, and other image-enhancing operations on these images. The NAVIS was developed under NRL's Advanced Reconnaissance Program by Space Dynamics Laboratory, Inc., Logan, Utah.

The first test of the TARPS-CD was a demonstration of all the involved technologies on a limited flight over the Pentagon in June 1998.

System Development Phase: Pod-payload development, installation, and test, followed by carrier qualification of the full TARPS-CD pod, were accomplished in 1998. Training of F-14 squadron VF-102 reconnaissance personnel at NAS Oceana (Virginia) with the pod began in early 1999. TARPS-CD missions were then inserted into the VF-102 training at NAS Fallon (Nevada) in preparation for their USS *John F. Kennedy* deployment. For flights over full aircraft capabilities, the CA-261 camera reliability was increased with new software and shutters. To enable data downlink from the aircraft, interfacing circuits

between CHBDL data-link hardware and the NAVIS ground station were built, and shortfalls in CHBDL capabilities for tracking tactical aircraft were identified and overcome. New operational procedures for CHBDL were developed. New capabilities were incorporated into the NAVIS ground station, including image target mensuration and search via latitude/longitude. Finally, software was installed to allow the air crew to manually control CA-261 camera exposure via the cockpit control panel, especially for the background brightness change in the transition from land to maritime targets.

Fleet Evaluations: VF-102 crews and reconnaissance personnel of Air Wing One exercised at NAS Fallon in February 1999 in preparation for deployment on the USS *John F. Kennedy*. TARPS-CD first demonstrated CA-261 camera capabilities. A capability to surveil 10,000 square nautical miles per hour was demonstrated on a flight over the San Francisco Bay area. Figure 8 is a waterfall mosaic of thumbnail images over San Francisco. The left-hand side of Fig. 9 is a zoom into the thumbnail highlighted in Fig. 8. The right-hand side of Fig. 9 is the full-resolution of USS *Hornet* contained within the thumbnail. The aircraft was flying at an altitude of
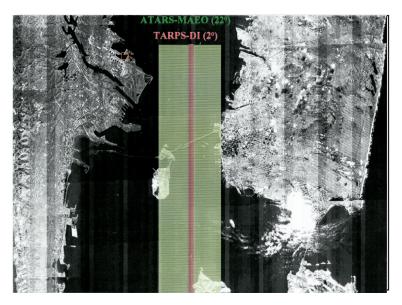
FIGURE 8
NAVIS waterfall mosaic display of thumbnail images from flight over Oakland –
San Francisco, California, area. Coverage is 121 degrees (approximately 20
nautical miles) in 11 cross-track frames, and coverage rate is 10,000 square
nautical miles per hour. Green and pink strips represent coverage of ATARS and
TARPS-DI systems developed earlier.
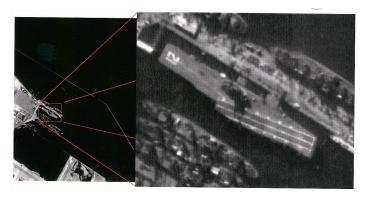
FIGURE 9
Left: Expanded view of one thumbnail (from second row of Fig. 2, on east
side of San Francisco Bay (north at bottom)). Right: Full-resolution image
of USS *Hornet* from thumbnail.

33,500 feet and a speed of 540 knots. At these pa-
rameters, the camera covered a cross-track width
of about 20 nautical miles while simultaneously dis-
tinguishing cars from vans. This corresponds to an
approximate NIIRS scale rating of about 4.5. In May
1999, Sixth Fleet was briefed on these TARPS-CD
capabilities, which would potentially enable the Fleet
to use organic assets to image all of Kosovo at least
once every hour and to provide targeting informa-
tion on relocatable targets. The flight over San Fran-
cisco did not involve any data downlink because of
the limited range of the omnidirectional antenna

(<100 nmi). Missions carried out over the NAS Fallon
ranges were able to downlink because of the proxim-
ity of the ranges to the base station. Real-world mis-
sions, such as a SCUD Hunt, were successfully ex-
ecuted with real-time downlink.

Success at NAS Fallon led to evaluation on the
USS *John F. Kennedy* in April 1999. TARPS-CD
operations were integrated with the carrier intelli-
gence center (CVIC) operations (Fig. 10). On mis-
sions off the *John F. Kennedy*, TARPS-CD success-
fully performed real-time imaging and downlinking,
including imaging and reporting to CVIC of moving

FIGURE 10
Fleet demonstration configuration for TARPS-CD system into a JSIPS-N (Joint Services Image Processing – Navy) architecture proposed for CVIC.

military targets of opportunity, and performed on short notice during an emergency requirement to image an accident scene. The capability for playback of significant, marked imagery obtained outside of the downlink range was also developed and demonstrated. The repeated carrier catapult and arrestments of the aircraft and pod did not have any measurable adverse effects on performance.

The demonstration on the USS *John F. Kennedy* showed that for digital reconnaissance systems to succeed, shipboard groups that are now operating independently must be trained to operate together. Real-time coordination of flight operations, downlink operation, and reception and utilization of imagery must be developed to provide timely products for air tasking. Because of successful demonstrations of capabilities off carrier-based aircraft, Commander, Carrier Battle Group 6 mandated that the TARPS-CD system deploy with the USS *John F. Kennedy* for evaluation in theater.

To adequately support the evaluation, OPNAV N880 deemed necessary the construction of a second TARPS-CD pod and the assembly of a comprehensive diagnostics package. Construction of the second pod and the design and implementation of test equipment for TARPS-CD for deployment was completed in about three months, in time for deployment. Present planned activities include partici-

pating in the Navy's Fleet Battle Experiment-Foxtrot to test concepts for real-time precision targeting.

Future: TARPS-CD is now serving its intended purpose of reducing risk for the Navy's next-generation Shared Airborne Reconnaissance Pod (SHARP) program, having already solved some of the technological and concept-of-operations issues. The need for early risk reduction on SHARP is very high because SHARP must begin replacing the TARPS film systems that are scheduled to retire, starting as soon as mid-2003.

[Sponsored by ONR and OPNAV N88] ◆

Geospatial Information Database in Support of Urban Warrior Exercise

M.J. Chung, R.A. Wilson, R. Ladner, and K.B. Shaw
Marine Geosciences Division

Introduction: The Mapping, Charting, and Geodesy Branch participated in the Urban Warrior Advanced Warfighting Experiment in March 1999. The Marine Corps Warfighting Laboratory (MCWL)

funded NRL to support an Integrated Marine Corps Multi-Agent Command and Control System (IMMACCS) by using the Geospatial Information Database (GIDB) as one of its components. GIDB demonstrated an ability to actively manage National Imagery and Mapping Agency (NIMA) mapping data in an object-oriented manner that could be interfaced with components developed by Stanford Research Institute (InCon), California Polytechnic Institute (Intelligent Agents), and NASA's Jet Propulsion Laboratory (SharedNet). The GIDB demonstrated that this integrated database could be viewed and engaged by area-of-interest via a simple Internet browser. The GIDB served primarily as the focal handling point for geospatial information. Additionally, privileged users, known as data co-producers, were given the ability to perform remote updates on the geospatial data in the GIDB.

GIDB Architecture: The Geospatial Information Database (GIDB) uses a client and server architecture. It is composed of a server, interface, and client module. The server uses an object-oriented database management system (ODBMS). All the geospatial data, including NIMA digital maps, as well as both DoD and commercial imagery, are resident in the server.

The interface between the clients and the server is an object-request broker (ORB) that complies with the Common Object Request Broker Architecture (CORBA). This broker serves as a middleware between the server and the client in facilitating request and response. Through the ORB, clients can remotely execute commands on the objects that reside on the server, independent of the programming language on the server and client, as well as the platforms of server and client. Figure 11 is an overview of the GIDB system. A Web browser, InCon, and SharedNet are IMMACCS clients to GIDB via ORB interfaces; the Internet three-dimensional display and front-end graphic user interface (GUI) for a non-Internet application are non-IMMACCS clients that are a part of the overall geospatial information system developed by the Mapping, Charting, and Geodesy Branch. The Web browser is a typical Web client for the GIDB.

Dynamic Updating Capability: A peer-to-peer system configuration has been implemented for information distribution. GIDB design is based on "smart client pull." The following assumptions are made in using this "smart client pull"

1. A server is up and running constantly. Clients are on-line as needed.
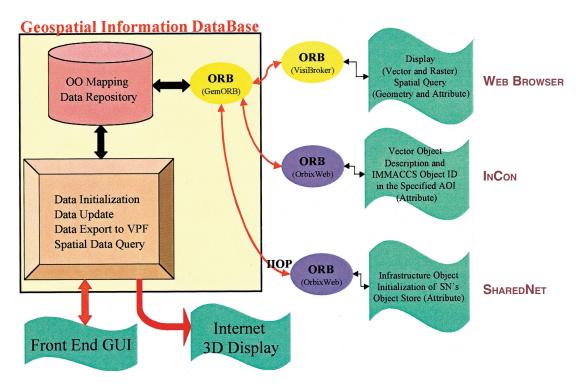
FIGURE 11
System overview.

FIGURE 12
Network updating design.

2. Both server and client maintain a log. A server maintains an *update* history log. The client maintains a client *history* log.
3. A client initiates an update check. When a user logs onto the server, a request is sent to the server via ORB-to-ORB communication to check for any updates. A check on whether a client needs an update from a server's change log is based on a timestamp and the state of the feature in terms of its location and attributes.

This "smart client pull" allows background processing to automatically update the changes from the selected server. The system alerts the client with a list of available updates. A client then selects those updates that are of interest. Figure 12 shows a protocol to facilitate the updating capability.

The GIDB Network Update capability was recently tested during the Marine Corps Warfighting Laboratory's Urban Warrior Advanced Warfighting Experiment in March 1999. On March 8, updates were made on the NIMA server at Bethesda, Maryland, for features in the Digital Nautical Chart (DNC01) database, harbor library. In the Navigational coverage, several buoys were deleted, and one had its attribute values changed. In the Hydrography coverage, attribute changes were made on bottom characteristic points. On March 10, the client on the USS *Coronado*, at sea in the Pacific Ocean, received the updates from the NIMA server, and the updates were verified on the client. The CORBA communication occurred over a network, via satellite transmissions from ship to shore.

Quantitative measures of the update times were not taken during this initial testing of the GIDB network update capability. On average, retrieval of the list of updates from the server over a network took about 5 seconds. Retrieval and update of features took on average less than 30 seconds per feature, and this average decreased as the number of updated features increased. Also, performance of the network updating is extremely hard to measure because of the variety of parameters involved: the number of features being updated, the types of updates to be performed, the traffic on the network, the load of the client/server, etc. However, benchmarking studies will be performed in the near future.

The GIDB and the Urban Warrior Experiment clearly demonstrated in an exercise setting that the future of geospatial data handling and updating for the Marine Corps will be object-oriented.

[Sponsored by Marine Corps Warfighting Laboratory]   ✦

The BMDO Virtual Data Center

S.E. McDonald, B.N. Dorland, and
H.M. Heckathorn
Space Science Division

Introduction: The Ballistic Missile Defense Organization (BMDO) has sponsored numerous ground and space-based experiment programs over the last decade. To date, these programs have collected more than 18 terabytes of engineering data. These data are stored at the three BMDO Data Centers (the Advanced Missile Signature Center in Tullahoma, Tennessee, the Missile Defense Data Center in Huntsville, Alabama, and the Ballistic Missile Defense Simulation Support Center in Colorado Springs, Colorado) and at other resource sites distributed across

the United States. Because these sites came into existence independently, they currently maintain separate data dictionaries, tools, and services and in most cases serve a separate set of users.[1] A user interested in using these data and services must travel to the sites where the data are located and must often manage a variety of data formats, hardware and software configurations, and operating procedures.

To provide analysts with easier access to data and services, NRL proposed, then built, the Virtual Data Center (VDC), an innovative system that integrates these resources via a classified intranet.[1,2] The VDC provides desktop computer access to BMDO experimental data, physics-based models, analysis tools, and, ultimately, system-level simulations. The VDC takes advantage of World-Wide-Web (WWW) technology to provide interoperability among resources on the network. With this system, a user is able to locate and retrieve data and information from multiple sites, pass information from one site to another to run models and/or simulations, then retrieve results for comparison, fusion, display, and further analysis. These capabilities are available to anyone on the network with a proper security clearance, a need-to-know, a personal computer, and a WWW browser.

VDC Development: As the software development team, NRL faced the difficult task of building a complex distributed system. We also had to contend with a distributed development effort that involved several organizations. We used a rigorous software engineering process to coordinate efforts between software development teams and to ensure a properly documented system. We controlled configuration management of the software and led an independent testing effort.

We adopted an object-oriented (OO) approach to designing the architecture and constructing the software. We captured the functional requirements by developing a set of "use cases" that describe the behavior of the system from a user's perspective. These use cases were then used to define the architecture, which is documented in the Unified Modeling Language (UML). Java was chosen as the primary development language since it is capable of running on a variety of computer platforms. Because the VDC software must be distributed over many different platforms to connect to the resource sites, CORBA (Common Object Request Broker Architecture) was chosen as the means for distributing objects over the network.

VDC Architecture: Figure 13 is a conceptual model for the VDC and illustrates a three-tier client/server architecture. The first tier consists of the client or user's Web browser. The client connects to the VDC system, represented by the middle tier, and the VDC software communicates with the heterogeneous distributed resources in the third tier. This architecture can support continuous evolution and scaling of the system without disrupting service to the user because the third tier can continue to expand without affecting the user interface. The middle tier

User Nodes	VDC Infrastructure	Resource Sites

Tier 1	Tier 2	Tier 3

FIGURE 13
Conceptual model of the VDC.
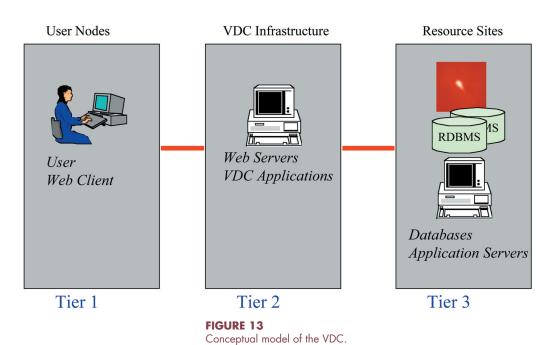
FIGURE 14
VDC high-level architecture.

provides data location transparency since it is responsible for providing the communications infrastructure linking users to the VDC resources. High-level metadata describing the various resources, along with a powerful search engine and other utilities, are all part of this middle tier. This architecture is currently running on the Defense Research and Engineering Network (DREN) and is configured to process information at the Secret level in the System High mode.

VDC Capabilities: The development of the VDC led to several innovations in the development of large-scale distributed systems. NRL has developed a very flexible architecture for querying geographically separate, heterogeneous databases. We have also designed a simple security solution that ensures users of the VDC gain access only to information for which they have a need to know, and that the resource sites maintain access control of that information.

Figure 14 shows the high-level architecture of the VDC, with an emphasis on the query distribution mechanism. The Global Catalog is a relational database that holds high-level metadata describing the various available resources. Users query the Global Catalog to find information located at any of the resource sites. Queries that cannot be satisfied at the Global Catalog level are distributed to the resource site databases via the CORBA servers. Results are returned to the user's Web browser.

The security architecture (not shown) is structured around a suite of Netscape products and uses public key cryptography for user authentication. Each user is issued a digital certificate, a copy of which is stored on a directory server, to provide the user with single sign-on access to the resources for which the user is authorized. This certificate solution also uses the Secure Socket Layer (SSL) protocol, which provides a layer of software encryption on the VDC network.

Summary: The VDC is capable of providing timely access to the most current data, models, simulations, analysis tools, and expertise. Connectivity to relevant BMD mission-oriented data and information via the VDC will increase the productivity of data analysis; reduce data analysis cost, time, and level of effort; and avoid potential duplication of data management.

The concept of the VDC has broad application to distributed information systems in both Government and industry and can be expanded for use with a wide variety of data and tools to provide an innovative collaborative environment for the scientific community.

[Sponsored by BMDO]

References
[1] B.N. Dorland, W.A. Snyder, D. Bradley, C. Arias, B. Rogers, and E. Andrew, "The BMDO Distributed Data Management System," *Proceedings of the 1997 Meeting of the IRIS Specialty Group on Targets, Backgrounds and Discrimination, Vol. I*, November 1997.
[2] S.E. McDonald, C. Poole, and J. Gara, "The BMDO 'Virtual' Data Center: High Level Architecture," *Proceedings of the 1999 Meeting of the IRIS Specialty Group on Missile Defense Sensors, Environments and Algorithms, Vol I,* May 1999. ◆

Materials Science and Technology

X-ray Computed Microtomography for Material Mesoscale Analysis

R.K. Everett and K.E. Simmonds
Materials Science and Technology

B.A. Dowd
National Synchrotron Light Source

Introduction: Synchrotron X-ray computed microtomography (XCMT) is a new tool for studying the internal structure of organic, metallic, and ceramic materials. Just as CAT (computerized axial tomography) scanning has revolutionized medical imaging, XCMT is providing a unique and exciting look into the microstructures of advanced engineering materials for the Navy. Three-dimensional, high-resolution micro- and mesostructural images can be determined with greater detail than previously possible. This information provides insight and better understanding of the mechanisms involved in materials damage and failure. Furthermore, they provide an unprecedented level of detail for advanced image-based finite-element modeling, which is used to accurately predict materials properties and mechanical behavior under complex loads.

Performing XCMT: NRL is a member of a participatory research team (PRT) devoted to XCMT at the National Synchrotron Light Source (NSLS). Much of the specialized hardware and software required for XCMT have been developed by NSLS staff over the past few years. This third-generation instrument, located on beamline X27a, is capable of producing tomographic volumes of 1 to 2 micron resolution over a 2 to 3-mm field of view. Figure 1 shows a schematic representation of the data collection apparatus. A sample is placed on a rotary stage where it can be exposed to the intense, collimated X-ray beam produced by the synchrotron. Illumination can be either by "white" beam or monochromatic (selectable from approximately 6 to 36 keV) radiation. The X rays pass through the sample and strike a scintillator crystal (YAG or CsI), which converts the energy to visible light. A folding mirror and microscope objective lens direct the visible light to a two-dimensional (2D) array, CCD (charge-coupled device) camera. To create a tomogram, a series of radiographs with the sample at various angular orientations is captured by the CCD array under computer control. These data are converted to 3D images using specialized reconstruction programs incorporating a Fast Filtered (Fourier) Back Transformation algorithm. Essentially, the images are 3D maps of the X-ray at-
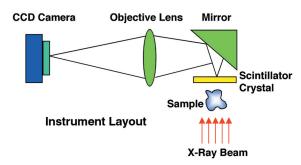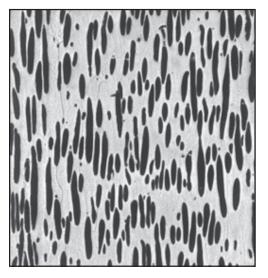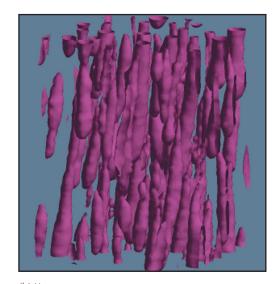
FIGURE 1
Schematic of the data collection geometry and instrument layout used for XCMT.

tenuation exhibited by the sample. Data can be captured and images computed in a matter of a few minutes to a few hours (depending on the sample volume and the desired resolution), promising near-real-time response. Commercial visualization software is then used to highlight features of interest in the data. Samples as diverse as ABS plastic solid freeform parts, HY100 steel, porous polymers, and zirconium titinate/Nicalon continuous fiber ceramic matrix composites have been studied by NRL with XCMT. Other PRT members have investigated assorted materials such as wood, rock, and bone.

Microstructural Imaging Using XCMT: Figure 2 illustrates the power of XCMT to improve our visualization of microstructures. The figure shows the elongated pore structure of GASAR copper materials. Figure 2(a) is a standard optical micrograph of the material while Fig. 2(b) is a tomogram. These materials are formed by directional solidification of a hydrogen-saturated melt. The average pore diameter is approximately 18 microns. The mechanical properties depend on the size, shape, and spatial distribution of the pores. No information is available about the neighboring pores just above or just below the plane of polishing in the optical micrograph. The tomogram clearly displays the spatial relationships better than the micrograph. Animations and steroscopic projections of the tomographic images are also possible.

(a) Optical micrograph

(b) X-ray tomogram

FIGURE 2
Elongated pore structure of GASAR copper.

XCMT also provides new opportunities for understanding mechanisms operating at the mesoscale, as shown in Fig. 3. Two samples of copper sheet that had been impacted at two different velocities were provided by Los Alamos National Laboratory (LANL). Voids are formed inside the sample as the result of interactions between tension and compression waves caused by the impact. The three-dimensional nature of the micron-sized voids is clearly visible, and marked differences (in the density, size, and connectivity of voids) between the lower and higher velocities can be seen.

Image-Based Modeling Using XCMT: The mesostructural information provided by XCMT, such as the spatial arrangements of second phases or voids, is of interest for improved understanding of the physical properties and mechanical performance of advanced materials. The size, shape, and positions of these features can be measured and used as input for image-based finite-element simulations. The strong, local interactions of these features can dominate the bulk behavior of materials. It has been difficult to adequately capture the behavior of these nonlinear interactions using either standard models,

(a) 250 m/s impact

(b) 350 m/s impact

FIGURE 3
Voids in LANL copper impact samples at two different velocities. Copper matrix is shown semitransparent.

which generally assume idealized arrangements of isolated features, or serial sectioning techniques, which can be time-consuming and destructive. The large, rich data sets provide by XCMT herald a change toward more realistic models and simulations.

Summary and Outlook: Current XCMT imaging is changing the way we envision materials microstructures. Increases in computing power and speed are impacting XCMT data collection and analysis. As the trend toward near-real-time imaging accelerates, larger volumes at higher resolutions are increasingly possible. The PRT is working to incorporate in situ loading such that deformation localization between mesoscale features can be tracked. These new tools will enhance future research and lead us toward more realistic, image-based models.

[Supported by ONR, NRL, and DOE] ✦

FIGURE 4
The relative energy alignments (eV) of the conduction band (CB) and valence band (VB) edges of InAs, GaSb, and AlSb at 0 K. The forbidden energy gaps are given by the colored rectangles.

6.1 Å III-V Semiconductors for Electronic and Optoelectronic Applications

B.V. Shanabrook
Electronics Science and Technology Division

Heterostructures formed from the nearly lattice-matched 6.1 Å III-V semiconductor material system (InAs/GaSb/AlSb) provide enormous flexibility in designing electronic and optical devices. Long-wave infrared (IR) detectors, midwave IR lasers, high-frequency field-effect transistors (FETs), and resonant tunneling diodes (RTDs) formed from heterostructures of 6.1Å materials are under development at NRL.[1] The need for adequate control and understanding of the structural and electronic properties of heterostructures formed from individual layers with thicknesses of several nanometers is required. This presents significant challenges to molecular beam epitaxy (MBE) growth technology, conventional materials characterization techniques, heterostructure physics simulations, and device modeling.

The diversity of applications offered by the 6.1 Å III-V material system arises from the relative band alignments of the constituent layers and the resulting flexibility in band structure engineering. Figure 4 shows the bandgaps and band alignments between InAs, GaSb, and AlSb. Because the conduction band of InAs is lower than the valence band of GaSb, one has the ability to tune the band gap of heterostructures from ~0-1 eV. This flexibility allows optoelectronic devices to be engineered to operate in the atmo-

spheric transmission windows important for DoD applications. The small band gap of InAs results in carriers with very high electron mobility and allows ultra-low-power, ultra-high-frequency electronic devices to be created for applications in digital radar systems and unmanned air vehicles.

Material Characterization: Imperfections in interfaces result in lower carrier mobilities, cause deleterious effects in tunneling-based devices, and broaden optical linewidths. We have used cross-sectional scanning tunneling microscopy (STM), high-resolution transmission electron microscopy (HRTEM), X-ray diffraction, and Raman scattering to determine the magnitude of interfacial intermixing as a function of changes in the MBE growth procedure.[1] Figure 5 illustrates the information that can
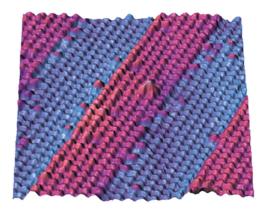
FIGURE 5
A color-enhanced 3D cross-sectional STM image of a GaSb/InAs superlattice performed on a cleaved (110) surface. The Sb (red) and As (blue) atoms can be seen.

be obtained from cross-sectional STM. This color-enhanced three-dimensional (3D) rendered STM image shows the atomic-scale structure of the interfaces in a GaSb/InAs superlattice in cross-section. A piece of the wafer was cleaved in vacuum to expose the (110) surface, and then the tip was positioned over the superlattice. Because of the structure of the crystal, only every-other lattice plane is exposed on the (110) surface. In this image that probes the filled surface states, we observe every other plane of Sb (red) and As (blue) atoms. The atoms are 0.43 nm apart along the rows, with a corrugation of <0.05 nm. This image clearly shows the excellent control achieved in the growth process, as well as the power of the STM technique. Specifically, a careful examination of the InAs layers (blue layers) reveals that a small number of Sb atoms (red peaks) have segregated into the InAs layers.

Because of the close interaction between the material scientists, physicists, chemists, and electrical engineers, we are able to design iteratively, optimize sample structures, and determine the relationship between changes in material properties and device characteristics.

Electronic Devices: The material properties that have the greatest impact on the high-speed performance of high electron mobility transistors (HEMTs) are the sheet-charge density in the 2D electron gas and the effective electron velocity. InAs/AlSb quantum wells are expected to make excellent HEMTs because of the high electron mobility (30,000 cm^2/V-s) and velocity (4×10^7 cm/s) of InAs and high electron sheet charge densities (3.4×10^{12} cm^{-2}). The current NRL design for AlSb/InAs HEMTs has resulted in a transconductance of 850 mS/mm and a unity-current-gain cutoff frequency (f_T) of 180 GHz at a drain/source voltage of 0.6 V. After subtracting the gate bonding pad capacitance, an intrinsic f_T of 250 GHz was estimated. This is a world record for this materials system and is approaching the current f_T performance record held by InP-based HEMTs. We anticipate that optimization of the device design will allow us to reduce impact ionization and achieve the highest f_T of any FET technology. The excellent performance exhibited at low drain voltages (200 mV) is better than any other HEMT technology and indicates the significant advantages that InAs/AlSb HEMTs exhibit in the low-power, high frequency application arena.

Because resonant tunneling diodes (RTDs) have been shown to operate at nearly terahertz frequen-

cies, these devices could be components in digital circuits operating at frequencies orders of magnitude faster than those available today. To obtain devices operating at these high frequencies, it is necessary to produce RTDs with peak currents $>10^4$ A/cm^2 and high peak-to-valley ratios. The peak current requirement means that the tunnel barriers must be 1 to 2 nm thick. In the design currently under study, electrons from an InAs layer tunnel through an AlSb barrier into the valence band of a GaSb quantum well, through a second AlSb barrier, and finally into the InAs collector. Figure 6 shows the current density obtained from this design with 1.5-nm AlSb barriers and 8.2-nm GaSb wells. This device exhibits a peak current density of 2.6×10^4 A/cm^2 and a peak to valley ratio of ~15. These devices can operate at low power because the peak current occurs at voltages of only ~100 mV.

Logic circuits composed of antimonide-based RTDs and HEMTs have the potential to set new standards for high speed and low-power consumption. NRL is developing the building blocks needed to build digital circuits in the antimonide-based system. We are monolithically integrating AlSb/InAs/GaSb RTDs and AlSb/InAs HEMTs to form logic circuits. Integration of the RTD and the HEMT is a critical advancement that will provide the enabling technology needed for a new class of very dense, ultra-high-speed logic circuits with high functionality and very low power dissipation. These advances in technology could play an important role in the future development of digital radar systems.
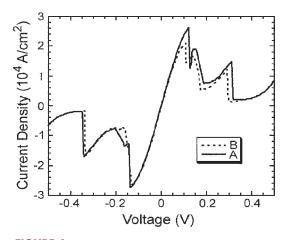
FIGURE 6
Current density vs voltage for a InAs/AlSb/GaSb/AlSb/InAs RTD. Curves A and B result from growth-induced changes in interface structure.

Optoelectronic Devices: The theoretically predicted intrinsic material properties of superlattices constructed from InGaSb/InAs suggest that it is possible to construct multicolor long-wavelength infrared focal plane arrays an order of magnitude more sensitive than those based on HgCdTe. The flexibility in wavelength control comes from the band alignment between InAs and GaSb denoted in Fig. 4. By changing the layer thicknesses of InGaSb and InAs, it is possible to tune the energy gap from nearly zero to 0.5 eV. NRL is involved in the MBE growth of detector structures, the fabrication of detector elements, and the measurement of detector efficiency. Figure 7 shows the sensitivity of a p-n diode as a function of reciprocal temperature. $R_o A$ is the product of the dynamic resistance at zero bias with the area of the detector and is related to the sensitivity of the detector. There is a increase in sensitivity as the temperature is decreased, with an activation energy of 0.16 eV that is determined by the engineered cutoff wavelength of 8 µm. Near 120 K, the dynamic resistance is determined by a defect-related tunneling mechanism that limits the increase in sensitivity. We are examining how changes in the growth and processing procedures impact the defect-related tunneling currents. In particular, we are investigating the role of interface formation, growth temperature, strain, and anion species. Reflection high energy electron diffraction, X-ray diffraction, STM, photoluminescence, and HRTEM are used to evaluate growth procedures. Improved growth procedures are incorporated into long-wave infrared device structures to determine the impact on detector performance. The current focus of our research is to minimize the defect-related tunneling mechanism and obtain an $R_o A$ of 7000 at 80 K. This would allow detectors made from this material system to be used in missile seekers, infrared search and track, missile threat warning, and reconnaissance Navy missions.

Semiconductor lasers constructed from 6.1 Å materials show potential to operate at room temperature and be used in infrared countermeasure applications. Highlights of the excellent progress in development of lasers operating between 3 to 8 µm are described in another paper in this *NRL Review*, "Midwave-Infrared Antimonide "W" Lasers," by W.W. Bewley, Jr. et al. (Energetic Particles, Plasma, and Beams section).

Conclusion: Heterostructures formed from III-V semiconductors with the 6.1 Å lattice spacing (InAs, GaSb, AlSb, and related alloys) are attracting significant interest because of their potential to revolution-
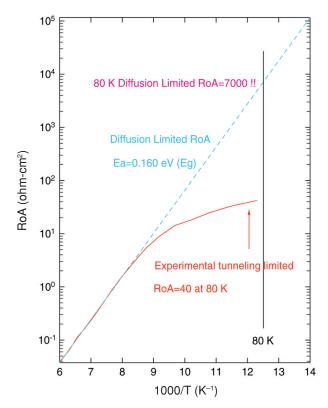
FIGURE 7
Plot of the product of the area scaled dynamic resistance of a GaSb/InAs superlattice p-n junction as a function of reciprocal temperature. The dynamic resistance is related to the sensitivity of the detector.

ize high-speed logic circuits, terahertz transistors, sensitive infrared detectors, and mid-infrared semiconductor lasers. This revolution could significantly increase the capabilities used in Navy missions, such as infrared countermeasures, digital radar, infrared search and track, and unmanned air vehicles.

References
[1] B.V. Shanabrook, W. Barvosa-Carter, R. Bass, B.R. Bennett, J.B. Boos, W.W. Bewley, A.S. Bracker, J.C. Culbertson, E.R. Glaser, W. Kruppa, R. Magno, W.J. Moore, J.R. Meyer, B.Z. Nosho, D. Park, P.M. Thibado, M.E. Twigg, R.J. Wagner, J.R. Waterman, L.J. Whitman, and M.J. Yang, "Engineered Heterostructures of 6.1 Å III-V Semiconductors for Advanced Electronic and Optoelectronic Applications," *Engineered Nanostructural Films and Materials*, SPIE **3790**, 13 (1999). ◆

GaN Electronic Materials and Devices for High-Power Microwave Applications

S.C. Binari, J.A. Roussos, K. Ikossi-Anastasiou,
D. Park, R.L. Henry, D.D. Koleske, and
A.E. Wickenden
Electronics Science and Technology Division

There is an extensive effort throughout the world to develop GaN and related compounds for electronic device applications. This work is driven by the ever-increasing system demands for high-power, solid-state microwave devices. The GaN materials system is especially attractive for these applications because it is possible to make high electron mobility transistors (HEMTs) with nearly lattice-matched AlGaN/GaN epitaxial structures. These HEMTs have demonstrated record output power densities and increased the state-of-the-art tenfold. NRL has been a leader in the development of this technology. This article discusses the properties of GaN that make it useful for microwave power applications and the current status of the materials growth and device technology at NRL.

Introduction: The GaN-based material system consists of GaN, AlN, InN, and their alloys. This material system has become the basis of an advanced, microwave-power-device technology for a number of reasons. GaN has a high breakdown field, estimated to be 3 MV/cm, which is ten times that of Si or GaAs. These high breakdown fields have made GaN an attractive material for the design of high-power devices. For microwave device operation, a high electron velocity is required, and GaN fulfills this requirement with its high peak velocity of 3×10^7 cm/s. An additional characteristic that distinguishes GaN from other wide bandgap semiconductors is the ability to make heterostructure devices that support a high carrier density with high mobility. Because of these properties, excellent high-frequency, high-power device performance has been achieved with GaN-based HEMTs.

Materials and Device Results: NRL has the capability to grow GaN materials by both molecular beam epitaxy (MBE) and metalorganic vapor phase epitaxy (MOVPE). NRL has an MBE system instrumented with an RF plasma nitrogen source, a custom-built MOVPE system, and a commercial MOVPE system. These reactors have been used to produce metal-semiconductor field-effect transistor (MESFET) and HEMT structures. Excellent material properties

have been demonstrated (e.g., a 300 K Hall mobility of 1500 cm^2/V-s, with a sheet carrier concentration of 1.2×10^{13} cm^{-2}). As a result of these material properties, HEMTs have been fabricated with a transconductance of more than 200 mS/mm, a maximum drain current I_D of greater than 1A/mm, and a cut-off frequency f_T of more than 50 GHz. This material base has been used to support the development of high-power density GaN HEMTs. Continuous bias (CW) power densities of 3.1 W/mm, with a power-added efficiency of 42% and an associated gain of 9.7 dB, were attained at an operating frequency of 3.8 GHz.

In general, two mechanisms typically degrade the power performance of these devices: self-heating with the associated degradation in power output resulting from the increase in operating temperature, and trapping effects that restrict the ability to modulate the drain current. Pulsed microwave measurements, which use a pulsed drain bias, can be used to distinguish between these two effects in that they eliminate a large component of the self-heating. This technique has been used to evaluate the NRL GaN HEMTs.

Pulsed microwave measurements at the same drain-source voltage V_{DS} setting of 20 V used for the CW measurement listed above resulted in an increase in power density to 4.3 W/mm. These CW and pulsed power measurements are shown in Fig. 8. The increase in performance under pulsed operation is attributed to a higher drain current level due to a lower
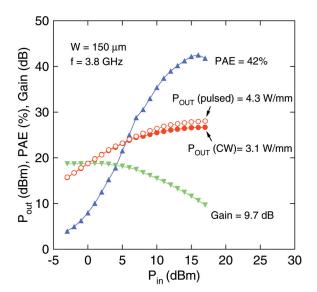
FIGURE 8
Power output, power added efficiency, and gain at 3.8 GHz for an AlGaN/GaN HEMT under continuous bias (solid symbols) and pulsed bias (open symbols).

operating temperature in the device active region. Under pulsed conditions, it was also possible to bias the devices at higher drain voltages and thus increase the output power in this manner. At a V_{DS} of 35 V, 5.9 W/mm with 37% power-added efficiency (PAE) and 12 dB gain were measured for this device. These results are among the highest achieved for GaN HEMTs on sapphire substrates and are significantly higher than what can be achieved with commercially available technologies.

Figure 9 shows an example of how pulsed microwave power measurements can be used to distinguish the reduction in power input due to self-heating from other mechanisms present in GaN HEMTs that may be limiting device performance. In Fig. 9, the measured power output as a function of drain voltage is plotted for several devices fabricated on different MOVPE wafers. A rough approximation for the maximum microwave power output is given by $I_D V_{DS}/2$. The power output should be directly proportional to the drain voltage (as it does for devices from HEMT wafer #1 in Fig. 9). However, this behavior is not generally observed for all GaN HEMTs. For devices that do not scale properly with drain voltage, even in the pulsed mode of operation (such as HEMT wafers #2 and #3 in Fig. 9), other factors are limiting the device performance. The observed saturation of power output with drain voltage is consistent with trapping at surface states or defects in the buffer layer. Research efforts directed toward understanding and eliminating these trapping effects are currently underway at NRL. Both materials growth
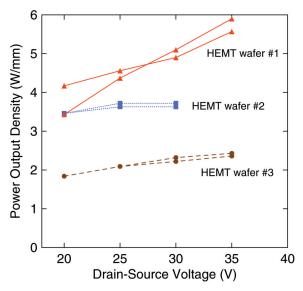
and device design studies are being conducted to eliminate trapping effects and further improve device performance.

New Materials for Uncooled IR Sensors

D.K. Shenoy,[1] K. Crandall,[2] S. Gray,[3] J. Naciri,[1] and R. Shashidhar[1]

[1]Center for Biomolecular Science and Engineering
[2]George Mason University
[3]Geo-Centers, Inc.

Introduction: Cooled infrared (IR) detectors are very useful for several military applications. However, they are expensive and require elaborate instrumentation for cooling to improve sensitivity. Uncooled detectors, on the other hand, are low-cost, consume less power, and, unlike semiconductor detectors, work over a wide range of wavelengths. They would provide significantly more flexibility in actual use. Currently available uncooled IR sensors do not have high sensitivity.

To achieve high sensitivity, the material should exhibit a large value of the pyroelectric coefficient p, as well as low dielectric constant and loss. In addition, materials currently used in uncooled detectors require processing at temperatures exceeding 600 °C. This is because, in a device, the sensing material is supported on polyimide mesas that reduce heat flow from the element to the supporting substrate. Reducing heat flow is a disadvantage during device fabrication because polyimides do not withstand such high temperatures. To overcome this problem, industry uses hybrid technology in which the detector pixels and substrate pixels are processed separately and then bump bonded. Liquid crystal materials, on the other hand, allow integrated technology to be used since room temperature processing is possible. Hence they are promising candidates for future uncooled IR sensors for both military and commercial applications.

Materials: Liquid crystals exhibit several phases.[1] In the SmC* phase, the molecules are arranged in

FIGURE 9
Measured pulse power output as a function of drain-source bias for several different HEMTs fabricated from three different wafers.

layers such that within a layer the average molecular direction (director) is tilted with respect to the layer normal. In addition to the tilt, the director twists from layer to layer. The symmetry of the phase leads to a spontaneous polarization in the material whose temperature derivative is referred to as the p coefficient. To obtain large p coefficients, we require large changes in polarization for small changes in temperature. The pyroelectric response is enhanced close to the SmC* to SmA phase transition temperature when the material is transformed into the paraelectric phase where the inherent twist and tilt disappear. In addition to a large pyroelectric coefficient, the dielectric constant and loss tangent should be as low as possible to achieve a high signal-to-noise ratio.

Materials Characterization: Material properties are measured for approximately 3-micron-thick liquid crystal cells. The liquid crystal is sandwiched between two plates, one of which has a patterned gold electrode and the other an obliquely deposited SiO alignment layer on transparent indium tin oxide-coated glass. Before measurement, the liquid crystal is aligned by heating into the isotropic phase and then cooling at a slow rate in the presence of an applied electric field. This process yields large regions with uniform alignment.

The pyroelectric coefficient is determined directly by using the Byer Roundy method; Fig. 10 shows the equipment setup. In this experiment, the temperature of the sample is ramped linearly while pyroelectric current, temperature, and time are simultaneously recorded. The pyroelectric coefficient is calculated from the measured current, the area of the device, and the ramp rate. Figure 11 shows the temperature dependence of the pyroelectric coefficient. A large increase in the p coefficient (on the order of $100 \text{ nC/cm}^2 \text{K}$) is observed close to the Curie temperature. These p values are the largest known for liquid crystal materials and exceed the values reported in the literature for some of the ceramic materials. As stated earlier, dielectric properties are also important in determining the sensitivity of the material. Hence, the dielectric constant and loss tangent are measured on the same cell whose p value is measured. Since these properties depend on frequency, temperature, and applied bias voltage, the variables are chosen to suit device conditions. For device operation, a temperature is chosen in the SmC* phase close to the Curie temperature. To reduce the dielectric constant, an external bias voltage is applied. Figure 12 shows the effect of bias. Dielectric constants (ε') as low as 10 and loss tangents ($\tan \delta$) the order of 0.07 have been demonstrated. Figure-of-merit evaluations from the measured values of p and dielectric properties indicate that devices based on our materials are likely to have IR sensitivity far exceeding those that are currently available.

FIGURE 10
Measurement setup for p using Byer Roundy method. Sample chamber design minimizes electrical noise and provides controlled temperature ramp.
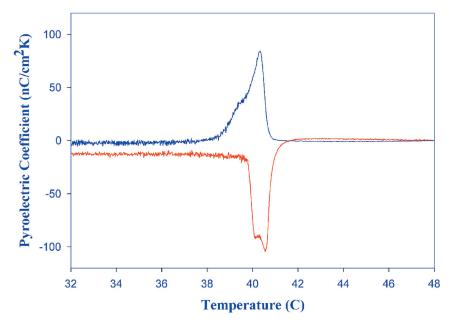
FIGURE 11
Temperature-dependence of the pyroelectric coefficient showing peak close to Curie temperature.
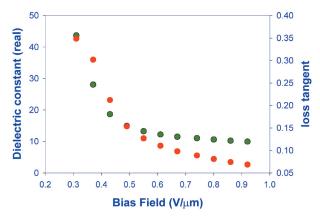
FIGURE 12
Plot of dielectric constant (ε′) (green) and loss tangent (tan δ) (red) as a function of DC bias field.

Summary: New materials for pyroelectric applications are characterized. The large values of the pyroelectric coefficients coupled with the low values of the dielectric constant and loss tangent lead to high sensitivity. A significant advantage of these materials is that room temperature processing is possible. Uncooled IR sensors using these novel liquid crystal materials are envisioned.

[Sponsored by ONR]

Reference
[1] P.G. de Gennes and J. Prost, *The Physics of Liquid Crystals* (Oxford University Press, Oxford, 1993). ✦

90 Ah Dependent Pressure Vessel (DPV) Nickel Hydrogen Battery Qualification Test Results

J.C. Garner and W.E. Baker, Jr.
Space Systems Development Department

W.R. Braun
Spacecraft Engineering Department

Introduction: When aerospace nickel hydrogen (NiH_2) battery cells are charged, they generate hydrogen gas in proportion to the ampere-hours (Ah) received. When fully charged, a cells pressure is typically $5.52 \times 10^6 \, N/m^2$. To contain the pressure safely, NiH_2 cells use independent pressure vessels (IPV), which are cylindrically shaped with hemispherical ends. The vessels are constructed from high-strength Inconel 718 stainless steel. For typical NiH_2 batteries of 22 series-connected cells, the packaged volume of the battery is large and the resulting energy density (Wh/l) is low.

What if you could reduce the volume by changing the pressure vessel shape from cylindrical to a flat circular vessel with rounded ends? Then the cells could be stacked closely together, the volume of the battery reduced, and the energy density increased.

In 1995, the Space Systems Development Department was asked to qualify a new NiH_2 battery

157

cell concept that tried to incorporate this idea. Called the NiH$_2$ dependent pressure vessel (DPV) cell, the new design used a flat, canteen-shaped pressure vessel with rounded ends and reduced wall thickness. With the flat shape and the thinner vessel wall, the DPV cell is dependent on an adjacent DPV cell or battery structure for support and to maintain pressure vessel integrity. Seventeen 90 Ah NiH$_2$ DPV cells were delivered to NRL in 1998 for qualification tests. An 11-cell half battery pack was manufactured and tested to validate the advantages of the DPV design.

Background: Per a 1995 agreement between Eagle Picher, Inc. (EP) of Joplin, Missouri, and NRL, EP would develop three NiH$_2$ DPV battery cell designs. The development of the 40 and 60 Ah cells was funded internally by EP, and NRL and its sponsors funded the development of a 90 Ah cell. Figure 13 shows the configuration of the 90 Ah NiH$_2$ DPV battery cell design.
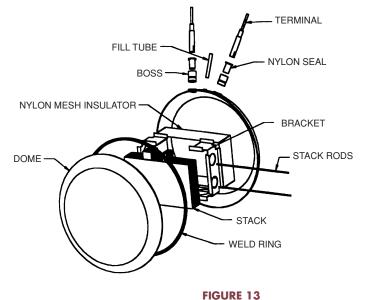
90 Ah NiH$_2$ DPV Cell Mechanical Design: Fill Tube—The electrolyte fill tube of the 60 Ah DPV cell was initially located between the battery cell terminals (Fig. 13). During the vibration test of the 60 Ah DPV cell design, a fill tube failed, and the cell vented. Post test analysis determined that the fill tube had been weakened at the weld joint from the stress of supporting a pressure gauge. To remove this weak point in the design, EP incorporated the fill tube into the negative terminal of the battery cell.

Electrode Stack Bracket—To minimize the weight of the cell, the electrode stack bracket was fabricated from a nickel 200 material. Nickel 200 is a lightweight metal with high thermal conductivity but low compressive strength. Post radiographic examination of a 60 Ah cell that failed the vibration test revealed that the cell stack compression bracket deformed after the fill tube opened, and the loss of internal pressure left the cell subject to the force of the adjacent cells. Because the venting of one or more cells in a battery is a possible failure mode, a redesign of the bracket was required. The new bracket has a crenellated design and is machined from Inconel 718. Because the bracket and pressure vessel are made from the same material, this facilitates the welding of the bracket to one half of the pressure vessel.

Electrical Performance Tests: To demonstrate that DPV cells function similar to other NiH$_2$ cell designs, two prototype cells were subjected to a series of electrical tests at the EP facility. The tests results showed stable capacity over a wide temperature range, excellent charge retention, and peak load performance.

Eleven-Cell Battery Design: To fully demonstrate that the DPV battery concept would be lighter and occupy less volume, a battery design of 11 series-connected DPV cells was initiated. The design, shown in Fig. 14, consists of 11 NiH$_2$ DPV cells, two 6061-T6 aluminum endplates, and alternating heat

Rated capacity	90 Ah
Predicted capacity	97.4 Ah
No. of (+) electrodes	18
(+) Electrode thickness	0.035 in.
Separator	Dual Zircar
Weight	2200 g
Specific energy	55.29 Wh/kg
Diameter	9.6 in.
Height	1.50 in.
Vessel wall thickness	0.015 in.
Maximum expected operating pressure	700 psig

FIGURE 13
90 Ah DPV NiH$_2$ battery cell design.
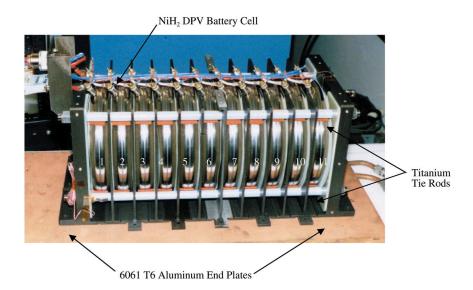
FIGURE 14
Eleven-cell NiH$_2$ DPV battery pack.

sink fins held together with four titanium tie rods. Design requirements included ease of assembly, survival of launch loads, restraint of the cells during charge/discharge cycles, and passive thermal control.

Qualification Test Results: Electrically, the NiH$_2$ DPV battery cells performed satisfactorily in the 11-cell stack. The cells experienced no electrolyte leaks as a result of the battery assembly or the random vibration tests.

Weight/Volume Comparison with IPV: Comparing the properties of a 90 Ah IPV NiH$_2$ battery cell with a 90 Ah DPV NiH$_2$ battery cell, the IPV battery cell weighs approximately 0.140 kg less. When the cells are packaged into a typical 22-cell battery, the results are even less favorable. The DPV battery weighs 102 kg compared to the IPV battery weight of 58 kg and occupies 7.1×10^{-3} m^3 of additional volume.

Significance: The goal of the NRL program was to investigate the NiH$_2$ DPV battery as a lower volume replacement for the NiH$_2$ IPV battery. However, a review of the qualification data from the 11-cell battery pack indicates that an optimized DPV battery design will require as much volume as an IPV battery design and have equal or greater mass. As the power requirements of communication satellites grow into the 1.5×10^{-3} to 2.0×10^{-3} J/s range, the volume and mass of the NiH$_2$ batteries to support them will be tremendous. Until other high specific energy electrochemistries such as lithium-ion are flight-qualified, the volume and mass of large capacity NiH$_2$ batteries will continue to limit the capabilities of the higher power spacecraft.

Ocean Science and Technology

Adaptive ASW Search Tactics in Littoral Areas

D.R. DelBalzo
Acoustics Division
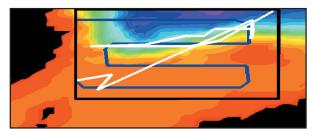
Introduction: The Naval Research Laboratory, in association with Wagner Associates, has developed a set of algorithms and software tools to aid undersea warfare search planning that have direct application to antisubmarine warfare (ASW). At the core of this new technique is the use of genetic algorithms (GA) to determine the optimal search tactic (e.g., tracks, depths, modes) for the sensor to maximize a user-selected measure-of-effectiveness (MOE) in a complicated environment against an hypothesized threat distribution. The solution is based on many environmental factors, including daily nowcasts of water sound speed structure. The structure of the decision aid permits spatial and directional variation in transmission loss, ambient noise, target strength, reverberation, etc.

Background on Genetic Algorithms: Genetic algorithms have been used to solve many search and optimization problems, including resource allocation, machine learning, and game theory. The distinguishing characteristic of GA is that it is based on the process of natural selection. In nature, biological entities are often found that have physical structures optimized for their local environment. Natural selection is the engine that drives this process. Biological structure is genetically encoded, and natural selection favors more "fit" entities. These basic ideas from biology have now been applied to the Navy's ASW search planning mission. The GA is used here to produce generations of search paths that become successively better than previous generations, as defined by a scenario-dependent fitness function. A Monte Carlo simulation using the lambda-sigma fluctuation model for detection with several possible MOEs (e.g., cumulative detection probability (CDP)) is used to evaluate the fitness function.
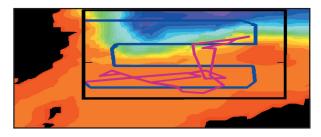
Search Tactics: Environmentally sensitive search tactics can be explained as follows. In a simple, homogeneous environment (e.g., deep water) with a uniform threat distribution, the most effective search tactic is a simple ladder pattern.[1] However, in nonhomogeneous environments (shallow water regions) against smart targets that maneuver in nonuniform ways, the ladder search is not optimal, and a different approach, such as the GA, is needed to produce the optimal search track. The GA track is a compromise solution that emphasizes good performance areas and high probability target positions in a joint fashion.

Simulations in the Strait of Korea: Computer simulations using the GA approach for search planning were performed in the Strait of Korea (a complex, highly range-dependent area, typical of many littoral regions). Figure 1 shows standard ladder (blue) and optimum search tracks (white) for an SQS-53 active sonar searching for a submarine. The search ship is constrained to begin near the southwest corner and to travel at an average speed of 12 knots for 20 hours. The underlying contours represent bathymetry: shallow water in the south (typically about 100-m depth) and deeper water in the north (typically about 2000-m depth), with a continental slope in between.

Figure 1(a) shows the result against a uniformly distributed target. The CDPs for the ladder and GA tracks are 0.25 and 0.41, respectively. The 64% performance gain attributed to the environmentally sensitive GA tactic is significant. The GA track allocates much search time over the slope, where downslope reverberation is low, and no search time in the southeast quadrant, where shallow-water reverberation is

(a) Target with uniform distribution.

(b) Target with nonuniform distribution.

FIGURE 1
GA and standard ladder search tactics for simulated SQS-53 sonar operations in the Strait of Korea.

high. One implication of the GA simulation is that an active SQS-53 sonar is not a good sensor in certain shallow-waters areas during summer, and therefore, other sensors (e.g., passive acoustic and nonacoustic) should be considered.

In Fig. 1(b), a smarter, environmentally aware target is simulated to spend only 20 percent of its patrol in the northern two-thirds of the box (deeper water) and 80 percent in the southern one-third of the box (shallow water). The ladder pattern (blue) is the same as in Fig. 1(a), and the GA track (purple) shows a concentrated effort in the southern area. This smarter threat tactic reduces the ladder CDP by almost 40 percent, from 0.25 to 0.16. By contrast, the GA solution maintains a CDP only slightly reduced from 0.41 to 0.37.

Experimental Results in Sea of Japan: The SHAREM 126 Fleet ASW exercise was conducted in September 1998 off the coast of South Korea, in the Sea of Japan. The GA was embedded in a series of environmental and performance-prediction computer programs and was used for the first time at sea during this exercise. The complete package was called GRASP (Genetic Range-dependent Algorithm for Search Planning). Optimization was based on ocean sound speed profiles obtained from the Navy's nowcast system, called MODAS.

Figure 2 shows GRASP-optimized search tracks for two ships equipped with the SQS-53 sonar, the USS *Curtis D. Wilbur* (left) and the USS *Cushing*

(right), searching for a uniformly distributed submarine. The USS *Wilbur* spends considerable time searching downslope, thereby reducing upslope reverberation. In deep-water, the USS *Cushing* avoids searching upslope over the seamount to reduce reverberation and concentrates search efforts to the south and east of the bathymetric feature.

Discussion: No sophisticated tools are currently available to the Fleet for ASW search planning in complicated environments. The GA approach is unique and will provide a powerful means to maximize effectiveness with available resources and minimize the time necessary to complete a mission. The new ideas presented here provide a solution that may be considered as components of a future tactical decision aid.

Reference
[1] B.O. Koopman, *Search and Screening* (Pergamon Press, New York, 1980). ◆
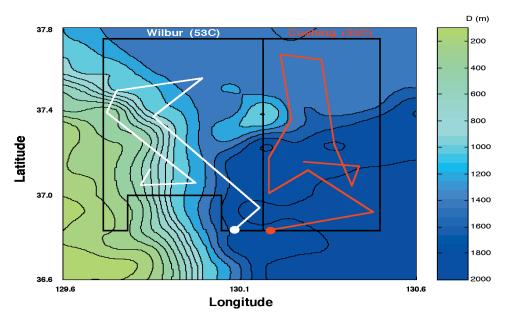
FIGURE 2
Optimized GRASP search tracks for SHAREM 126 in Sea of Japan.

Directional Wavenumber Spectra and Nonlinear Interaction of Ocean Surface Waves

P.A. Hwang and D.W. Wang
Oceanography Division

E.J. Walsh, W.B. Krabill, and W. Wright
NASA

R.N. Swift
EG&G

Introduction: It is currently believed that weakly nonlinear processes largely control wind wave evolution. The nonlinear theory has been remarkably successful in predicting many aspects of wind wave behavior. Numerical computations show that application of the nonlinear theory results in a bimodal directional spreading.[1] Measurements from directional wave buoys or wave gauge arrays, however, generally indicate that the wave field is unimodal. As a result, unimodal directional distribution has been assumed in all wave models for scientific and engineering applications. The directional resolution of the conventional wave measurements, however, is also known to be poor, and significant variations are found in the analysis results when using different processing methods. Nonlinear wave-wave interaction theory was introduced in the early 1960s, but the contradiction between predicted bimodal and measured unimodal directional distributions has still not been resolved. The directional characteristics of random ocean waves have remained an unsettled issue over the past four decades.

Airborne Scanning Lidar Wave Mapping: An airborne topographic mapper (ATM, an airborne scanning lidar system) acquires three-dimensional (3D) topography of the ocean surface. The ATM optics scans a laser beam along an elliptical locus on the ocean surface. The laser return is sampled at 5 kHz, which translates to 1.5-meter intervals between consecutive data points on the ocean surface. The vertical resolution of the system is 0.08 meters (rms). The 2D wave spectrum derived from the 3D topography yields exceptional directional resolution,[2] and represents an ideal measurement to resolve wave directionality unambiguously.

Directional Spectral Analysis: Figure 3(a) shows an example of the ocean surface topography
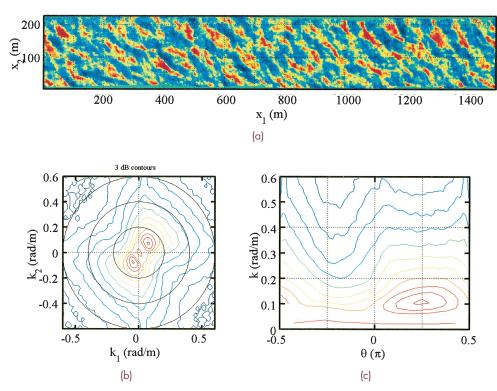
FIGURE 3
A segment of the 3D surface topography of ocean waves (a), and their 2D wavenumber spectrum, presented in (k_1, k_2) coordinates (b), and (k, θ) coordinates (c).
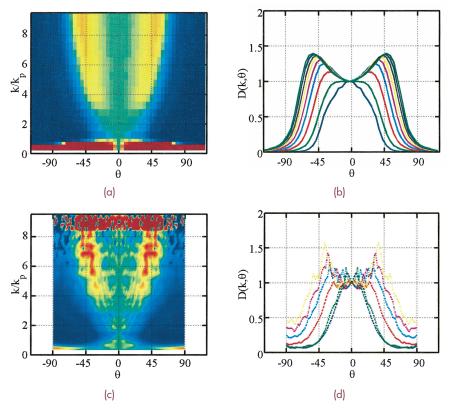
FIGURE 4
Directional distributions of ocean wave spectra based on numerical computation of nonlinear wave-wave interaction theory (a, b), and based on analysis of 3D surface topography obtained by an airborne scanning lidar system (c, d). Bimodality is clearly indicated. [Data for (a) and (b) are provided by I. Young.]

obtained by the scanning lidar system. The dominant direction of wave propagation is estimated to be approximately 45 degrees (referenced to the flight track). This is very close to the average wind direction, 42 degrees relative to the flight direction. There are considerable 3D structures showing the short-crested nature of the wave field. Two-dimensional wavenumber spectra are calculated using a standard 2D fast Fourier transform procedure. The 2D wavenumber spectrum can be mapped into either (k_1, k_2) or (k, θ) coordinates (Figs. 3(b) and 3(c), respectively), where k is wavenumber, θ is wave direction, and subscripts 1 and 2 refer to along-track and cross-track directions. The 2D spectra displayed in Fig. 3 show that the directional spreading becomes broader as wavenumber increases. Bimodal distribution starts to develop at wavenumber slightly greater than $\sim 2k_p$, where k_p is the wavenumber at the spectral peak. The angular separation of the distribution lobes increases toward higher wavenumber. Quantitative analyses of the directional wave spectra confirm the robust feature of bimodal directional spreading of ocean waves throughout the entire wave evolution

process. As discussed earlier, bimodality is a distinctive signature of nonlinear wave-wave interaction as revealed by elaborate numerical calculations of the nonlinear theory (Figs. 4(a), (b)). The quantitative analysis establishes that directional bimodality is a robust feature of a random ocean wave field (Figs. 4(c), (d)). These results revolutionize our current concept (unimodal directionality) of the ocean wave field and provide strong evidence supporting nonlinear wave-wave interaction theory.[2]

Summary: Clarification of various physical mechanisms is a key step to improve numerical models to provide forecast, nowcast, and hindcast. The confirmation of directional bimodality of ocean waves is significant in clarifying the role of nonlinear wave-wave interaction mechanism governing the evolution of ocean waves and in enhancing our wave modeling capabilities. Accurate prescription of the directional properties is also crucial to realistic representation of the ocean surface, which is required input for many electro-optical and electromagnetic remote sensing applications. In many civilian applications

such as coastal and harbor engineering, beach protection, and offshore engineering projects, wave amplitude and wave direction are key parameters defining the wave force on the beach and coastal or offshore structures. These ocean engineering projects are costly. Accurate formulation of the wave directional properties is critical to design optimization.

[Sponsored by ONR]

References

[1] M.L. Banner and I. R. Young, "Modeling Spectral Dissipation in the Evolution of Wind Waves. Part I: Assessment of Existing Model Performance," *J. Phys. Oceanogr*. **24**, 1550-1571 (1994).

[2] P.A. Hwang, D.W. Wang, E.J. Walsh, W.B. Krabill, W. Wright, and R.N. Swift, "Airborne Measurements of the Directional Wavenumber Spectra of Ocean Surface Waves. Part 2: Directional Distribution," accepted for publication, *J. Phys. Oceanogr.* (2000).   ◆

Quantitative Modeling of Bioirrigation in Benthic Mesocosms

Y. Furukawa and D. Lavoie
Marine Geosciences Division

S. Bentley
Louisiana State University

Introduction: The benthic boundary layer in marine and estuarine environments is inhabited by abundant populations of bottom-dwelling macroinvertebrates. Many of these animals inhabit burrows that they irrigate to keep the oxygen levels high and toxic metabolites low. This bioirrigation dictates the courses of early diagenesis through rapid solute transport, thus affecting sediment properties of Naval interest such as gas bubble concentrations and organic matter fabric. Today, we use numerical prediction tools to solve these problems. Consequently, a quantitative and mechanistic understanding of the bioirrigation processes is crucial, yet today's prediction tools treat bioirrigation by using highly parameterized mathematical expressions that are not based on mechanistic understanding of the processes. This is because few quantitative studies link bioirrigation mechanisms to the spatial and temporal distribution of chemical constituents.

One of the first models to treat bioirrigation mechanistically was established by Aller.[1] In his tube model, the sediment subject to bioirrigation is idealized as a collection of equally sized and spaced cylinders, each with a cylindrical void space (i.e., burrow) of an identical geometry in the center. This configuration is based on the assumption that all burrows have the same vertical extent. The water in the void space is continuously maintained at the composition of the overlying water. In this model, Aller mathematically reduces bioirrigation to the diffusive exchange of solutes along the burrow wall.

NRL has developed a model that extends the capabilities of Aller's tube model. Our model treats bioirrigation as the diffusive exchange of solute along burrow walls while allowing the number of infauna to decrease with depth, reflecting actual observations that burrows have varied depths. Comprehensive data from benthic mesocosm experiments, which include burrow geometry, depth-dependent distribution of burrows, and spatial distribution of chemical constituents, are used to evaluate the model. All the necessary parameters for the model were determined independently from experimentation in the laboratory mesocosms. None of these parameters was treated as adjustable during the model runs. Consequently, any mismatch between the measured and modeled solute profiles can be used to evaluate the state of our mechanistic understanding of the early diagenetic processes.

Laboratory Mesocosm Experiments: Two laboratory aquaria were loaded with saline water and fine-grained sediments from the Bay of St. Louis, Mississippi. These starting sediments were sieved prior to loading to eliminate any macrofauna. The sediment was allowed to settle for 41 days (Fig. 5(a)). A species of tube-dwelling macroinvertebrate, *Schizocardium* sp., was introduced, with a population density of 800 animals m^{-2} for one tank and 96 animals m^{-2} for the other. Within 57 days, the worms altered the seabed structure through the construction of fecal mounds (Fig. 5(b)). An equally rigorous bioirrigation was observed using deliberate aqueous tracers. The spatial distribution of burrows after 57 days of worm introduction was observed using x-radiography (Fig. 5(c)), indicating the depth-dependent decrease of burrows. The sediment structure is altered also at the microscale: transmission electron micrographs of sediments show the porosity difference between sediments unaffected by bioturbation (Fig. 5(d)) and sediments within the fecal mounds (Fig. 5(e)).

Model: The bioirrigation model is based on the conical geometry shown in Fig. 6. The original geometry of Aller's tube model is also shown for comparison. The radius of the sediment for each radial environment increases with depth because the number of burrows decreases with depth. With increasing depth, fewer burrows accommodate larger radial

167

(a)

(b)

(c)

(d)

(e)

FIGURE 5

(a) Laboratory mesocosm before animal introduction. (b) Within 57 days of animal introduction. The worms build fecal mounds through their ingestion/egestion of sediment particles. (c) X-radio-graph of a slab core, 17-cm wide, showing burrow network. (d) Transmission electron micrograph (7.0 μm × 9.3 μm) of the experimental sediments unaffected by bioturbation. (e) Transmission electron micrograph (7.0 μm × 9.3 μm) of sediments within a fecal mound. Rigorous reworking is evident in the alteration of pore structure.

(a)

(b)

FIGURE 6

(a) Model geometry used for the depth-dependent tube model. (b) Model geometry of the original Aller's tube model in which burrows are assumed to have identical vertical extent.
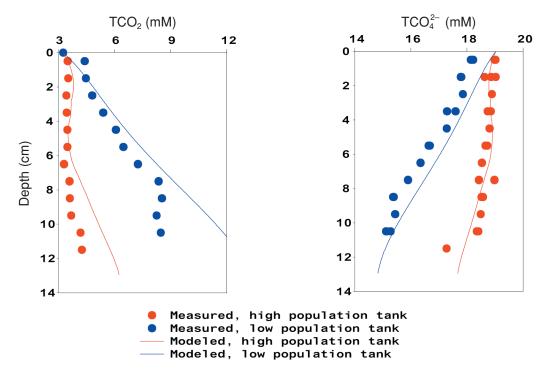
FIGURE 7
Measured and modeled depth profiles of total dissolved inorganic carbon (TCO_2) and sulfate (SO_4^{2-}) in pore water.

diffusion space. The concentration of a given solute at a given position in space can be determined by the following equation that combines vertical diffusion perpendicular to the water-sediment interface, radial diffusion perpendicular to the burrow wall, and production or consumption of the solute due to biogeochemical reactions:

$$\frac{\partial C}{\partial t} = D' \frac{\partial^2 C}{\partial x^2} + \frac{D'}{r}\frac{\partial}{\partial r}\left(r\frac{\partial C}{\partial \frac{D'}{r}}\right) + R.$$

Here, C is the solute concentration, t is the time, x and r are the vertical and radial coordinates, respectively, D' is the tortuosity-corrected diffusion coefficient, and R is the rate of production or consumption. This equation is solved numerically using the explicit scheme with boundary conditions derived from the geometry shown in Fig. 6(a).

Results: Figure 7 shows the depth profiles of sulfate (SO_4^{2-}) and total dissolved carbonate carbon (TCO_2). In the high population tank (800 animals

m^{-2}), bioirrigation maintains the pore water chemistry to be very close to that of overlying water. Less bioirrigation in the low population tank meant an increase in metabolites such as CO_2 and H_2S, and a resulting decrease in SO_4^{2-}. Measured and modeled profiles show reasonable agreement.

Summary: This study shows that the three-dimensional irrigation model, in which spatial distribution of burrows is explicitly considered, is an appropriate tool for studying the solute transport by *Schizocardium* sp. and other benthic infauna that create and flush deep burrows.

Reference
[1] R.A. Aller, "Quantifying Solute Distributions in the Bioturbated Zone of Marine Sediments by Defining an Average Microenvironment," *Geochim. Cosmochim. Acta* **44**, 1955-1965 (1980).

An Aerogeophysical Study of the Eurasia Basin

J.M. Brozena
Marine Geosciences Division

The Eurasia Basin is the segment of the Arctic Ocean that extends from Greenland to the Laptev Sea and from Lomonosov Ridge to the Barents/Kara Sea margin. The basin includes the North Pole and Fram Strait, the only deep-water connection of the Arctic to the world's ocean system. Much of the detail of the structure and evolution of this ocean and its margins has been enigmatic because of the permanent ice cover of most of the region. A new airborne field program completed this year provides a detailed geophysical framework for the basin and its margins. The study covers a 1,200,000 km^2 region between the Eurasia margin and the Canada Basin/ Fletcher Abyssal Plain, and provides a first regional image of the structural elements of the basin. These include the midocean spreading ridge, Lomonsov Ridge, Yermak Plateau, Morris-Jessup Rise, and the Eurasian margin between Svalbard and Franz Josef Land.

Background: In contrast to the temperate ocean areas of the world, the structure and tectonic evolution of the Arctic Ocean basins has been difficult to determine because of the logistic difficulties of conventional shipboard operations in this permanently ice-covered region. Additionally, the polar gap in coverage from altimetric satellites such as SEASAT, GEOSAT, and ERS1/2 precludes visualization of the submarine crustal structure by satellite altimetry-derived gravity maps. Consequently, much of what is known in the scientific literature about the geologic history of the region has been obtained from aeromagnetic investigations carried on by the U.S. and Russian navies during the 1970s.[1] Since those earlier investigations, airborne gravity measurement has become an accepted tool for remote sensing,[2] greatly enhancing the geophysical information available for analysis of such remote environments. NRL's Marine Geosciences Division has been conducting airborne geophysical studies of the high-Arctic Ocean basins and margins since 1992. An integrated set of geophysical sensors has been used that simultaneously measures the gravity, magnetic, and sea-surface topography signatures of the geologic features underlying the pack-ice and ocean cover. The first five field seasons of the program covered most of the Cretaceous aged Amerasia Basin located between Canada,

Alaska, and western Siberia. For the last two field seasons (1998 and 1999), the program shifted focus to the Eurasia Basin of the Arctic Ocean, extending the multiyear basic research effort into the eastern seas adjacent to North Greenland, Svalbard, and western Siberia (Fig. 8).

The first-order spreading history of the Eurasia Basin is fairly well understood, due largely to the early 1970s aeromagnetic investigations. The deep-water basin opened by very slow spreading on the Nansen Ridge that propagated north and eastward from the opening Atlantic, rifting the Lomonosov Ridge continental sliver away from the Svalbard/Siberian margin in the mid to late Paleocene in a manner analogous to the present day rifting of the Baja Peninsula from the California margin. The Nansen (also called Gakkel) Ridge terminates eastward at the Laptev Sea margin of Siberia in a region of continental extension near the Lena River. The eastern portion of the ridge axis is abnormally deep, with few if any fracture zones to disturb the linear continuity of the Arctic mid-ocean ridge, and is buried by sediments as it approaches the Siberian margin.

In spite of the well established first-order view of the Eurasia Basin, much of the detail of the structure and evolution of this ocean and its margins has been elusive as the result of the permanent ice cover of most of the region. With the exception of a few ice-breaker-based seismic cruises and the new submarine bathymetric and gravity traverses of the basin provided by the SCICEX program, little additional geophysical data have been obtained over the region in the last two decades. However, because of the importance of this area for research in paleoclimate, environmental pollution issues, Arctic margin evolution, and the potential economic geologic resources of the Barents Sea, Kara Sea, and Siberian margins, several new programs of study have been proposed or have begun. While each of these efforts will provide valuable knowledge, a comprehensive regional aerogeophysical study provides the structural and evolutionary framework of the basin and its margins as a framework for interpretation of the more detailed in situ measurement programs proposed for the region.

NRL Aerogeophysical Study: The study covered the southwestern block of the Eurasia Basin from margin to margin with a bidirectional grid (18×100 km) of low-altitude tracks (Fig. 8). The great range capability of the NRL P-3 Orion research aircraft and logistic support from Svalbard allowed more than 1,200,000 km^2 of this remote ocean basin to be
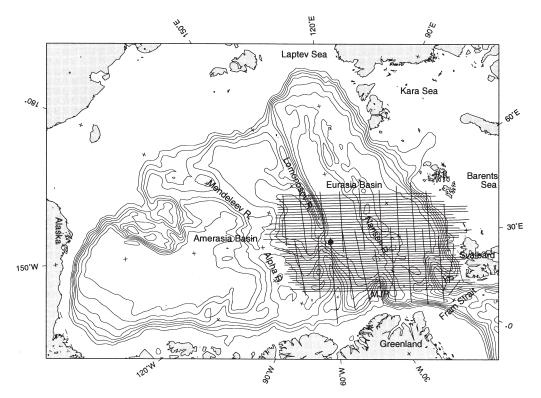
FIGURE 8
Basemap of the Arctic Ocean showing the generalized bathymetry (500-m contour interval), major features, and aircraft tracks over the eastern Eurasia Basin (MJR - Morris Jessup Rise, YP - Yermak Plateau, R. - Ridge, FJL - Franz Josef Land.) Black dot indicates the North Pole.
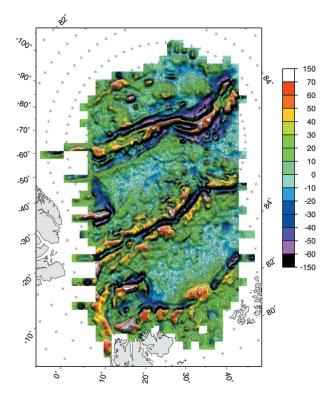
examined in two one-month deployments of the aircraft. This scientific operation of a military aircraft from Svalbard was a first, with permission granted by the Norwegian government only after several years of negotiations headed by Admiral Gaffney, the Chief of Naval Research.

The airborne gravity data (Fig. 9) provide a regional view of the structural elements of the basin including Nansen Ridge, Lomonsov Ridge, Yermak Plateau, Morris-Jessup Rise, and the Eurasian margin between Svalbard and Franz Josef Land. The new aeromagnetics, which include numerous tie-lines and crossings of the older Navy aeromagnetic data, also allow the production of a much improved magnetic anomaly map for the basin (Fig. 10). When analyzed in conjunction with the gravity map, the paired, conjugate magnetic isochrons in Fig. 10 and the time sequence of reversals of Earth's magnetic field permit the development of a model for the evolution of the basin since the initial opening about 65 million years ago.

Nansen Ridge, one of the slowest spreading ridges on Earth (< 10 mm/yr), is characterized by enor-

mous gravity gradients between the flanking rift mountains and the central rift valley. Unlike the intermediate spreading rate Mid-Atlantic Ridge to the south, it is segmented along its length by changes in strike/obliqueness rather than by fracture-zone offsets. The aerogeophysical data reveal a complex rifted continental structure for Lomonosov Ridge and the conjugate Eurasia margin. On reconstruction of the basin to closure, a space problem in the southern part of the basin is only partially resolved by the known continental extension within the southern Yermak Plateau. The reconstruction requires the early opening connection of the basin to the North Atlantic to have been through the Labrador Sea west of Greenland rather than into the Norwegian-Greenland Sea, as has been assumed, and the independent motion of Lomonsov Ridge as a microplate. The new interpretation may have important implications for the timing and geometry of the opening of Fram Strait, the controlling factor for establishing deep-water circulation between the North Atlantic and the Arctic Ocean.

In addition to the basic geologic and geophysical knowledge to be gained from the structure and evo-

FIGURE 9
Gravity map obtained from the NRL aerogeophysical study. The contour interval is 2.5 mGals (10^{-5} m/s^2) in the interval between –35 and +35 mGals, and 10 mGals outside this range. The gravity variations, which total approximately 200 parts/million across the map, primarily reflect the density interface between the water and the ocean bottom, with secondary variation due to crustal thickness and density variations.

FIGURE 10
Aeromagnetic map produced by leveling and combining the historical aeromagnetic data in the region with more accurate, new aeromagnetic data obtained in this experiment. The yellow lineations mark seafloor spreading anomalies produced during the opening of the Eurasia Basin along Nansen Ridge. The heavy black lines indicate the Eurasia continental margin and the rifted continental fragment of Lomonosov Ridge. The high amplitude features at the top of the map are related to anomalous ocean crust in the Amerasia Basin influenced by volcanism from giant submarine basalt plateaus, the Alpha and Mendeleev Ridges.

lution of this ocean basin, the data are being used: to improve Earth gravitation models; by Norway to help establish the extent of their Economic Zone under the U.N. Law of the Sea treaty; and for economic geology applications along the Eurasian margin. The aircrew was also successful in launching a few test airborne expendable conductivity-temperature-depth (AXCTD) sonobuoys into leads in the ice. This demonstrated the feasibility of supplementing or replacing submarine CTD casts for future oceanographic observations in the Arctic. The opening up of Svalbard as a logistics base for long-range airborne scientific operations makes it possible to operate effectively in this remote area.

[Sponsored by ONR and NIMA]

References
[1] P.R. Vogt, P.T. Taylor, L/C. Kovacs, and G.L. Johnson, "Detailed Aeromagnetic Investigation of the Arctic Basin," J. Geophys. Res. **84**, 1071 (1979).
[2] J.M. Brozena, "Airborne Gravimetry," in *CRC Handbook of Geophysical Exploration at Sea*, second edition: Hard Minerals, ed. by R.A. Geyer (CRC Press, Boca Raton, FL, 1992). ◆

Optical Science

Photonic Analog-Digital Converter

T.R. Clark, M. Currie, and P.J. Matthews
Optical Sciences Division

Introduction: Analog-digital converters (ADCs) form the link between analog sensor systems (including radar, communications, and electronic support measures) and digital signal processing systems. To extract information from the microwave and radio frequency (RF) carriers used in current Navy sensor systems (carrier frequencies of 1 to 18 GHz), several stages of mixing and filtering are required to reduce the signal frequency for digitization by currently available low-speed electronic ADCs. This process can be expensive, limit reliability and instantaneous bandwidth, and increase system size and weight. In addition, each stage introduces signal distortion and increases electromagnetic interference susceptibility. A high-speed, high dynamic range ADC permitting the direct digitization of high-frequency signals would enable significant advances in jamming suppression through digital beamforming, target detection within clutter from increased dynamic range, and target identification with a larger instantaneous bandwidth.

Current photonic technology offers many advantages. These advantages include high-speed optical clocks (operating at tens to hundreds of gigahertz) and high bandwidth electro-optic modulators (up to 80 GHz instantaneous bandwidths demonstrated). They also include nearly lossless fiber-optic signal remoting, practically implemented parallel process-ing, and immunity to electromagnetic interference. Fiber-optic signal remoting offers the potential for reducing outboard components to the antenna and an electro-optic modulator. The weight, size, and outboard power requirements for each transmit/receive (TR) module would be reduced significantly by eliminating the need for bulky microwave and RF components and cables. The remaining processing and control would be performed at an inboard central location away from the TR modules.

Photonic ADC Architecture: The photonic ADC architecture under investigation is based on discrete wavelength domain to time domain mapping. Figure 1 illustrates the principle of the system. Spectrally broad optical pulses from a mode-locked fiber laser pass through a polarizing beam splitter (PBS) and are sliced by a wavelength division multiplexer (WDM) into N-wavelength distinct channels (four channels are pictured in Fig. 1). Each channel's pulse is retroreflected and multiplexed by the WDM on the second pass and directed to a single optical fiber. The length of each channel's path is chosen to create a pulse train N times the original repetition rate. The resultant pulse train contains only those wavelengths to be used in sampling and digitizing the input signal. The system sample-and-hold process is performed by an electro-optic Mach-Zehnder modulator (MZM), which encodes the RF signal onto the optical pulse train. The energy from each optical pulse now represents the amplitude of the RF signal at discrete points in time. A second WDM is used to
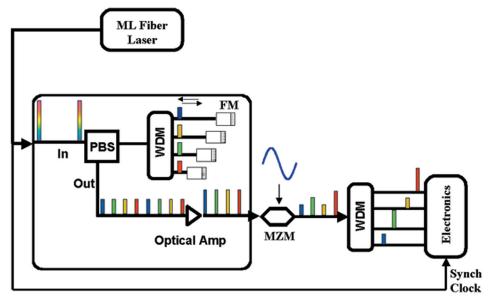
FIGURE 1
Photonic analog-digital converter architecture.

demultiplex the time- and wavelength-interleaved pulse train. This creates parallel channels of optical pulses that are then converted to electrical pulses by conventional photodetectors and digitized using electronic ADCs. The digitization of each channel occurs N times slower than the photonic ADC sampling rate, thus significantly reducing requirements on the electronic components. The electronic ADCs are synchronously clocked by the pulse train from the optical clock to preserve the precision of the sampled values. Subsequent processing of the digitized values and knowledge of the wavelength-time mapping allows reconstruction of the RF signal. Figure 2 shows this reconstruction as the output of a two-channel real-time system.
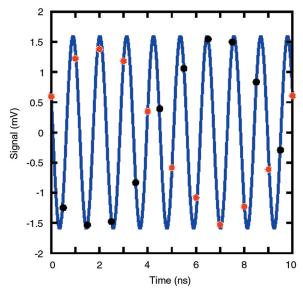
FIGURE 2
Real-time two-channel photonic analog-digital converter output. Note that neither channel 1 (red dots) nor channel 2 (black dots) alone would be sufficient to interpret the signal correctly.

Demonstration and Results: The constructed system uses a highly stable mode-locked fiber laser[1] operating at 1 GHz as the system clock. The 2-nm optical bandwidth output pulses are nonlinearly broadened in a dispersion decreasing fiber[2] to ~100 nm (~12 THz) of usable bandwidth, sliced by an 8-channel WDM of 1 nm (~125 GHz) channel passbands and interleaved into an 8 GHz pulse train. Only 25 nm of the available 100-nm bandwidth is used, indicating the potential for highly parallel, wide bandwidth operation using commercially available 1 GHz electronic components. Two channels of this 8-channel system were used to demonstrate a fully func-

tional, 8-bit, 2 gigasample-per-second (GSPS) system. Figure 2 shows the 2 GSPS digitized data reconstruction of a 900 MHz input sine wave. Note that reading only one channel (red or black dots alone) would result in an erroneous determination of the input signal, due to the insufficient sampling rate of a single channel.

Summary: NRL has successfully demonstrated a real-time photonic wavelength-time mapped analog-digital converter. The high speed and large bandwidth potential of photonics, along with the inherent advantages of fiber-optic remoting, make this system an attractive alternative to conventional all-electronic methods of digitization.

[Sponsored by DARPA]

References
[1] T.R. Clark, T.F. Carruthers, P.J. Matthews, and I.N. Duling III, "Phase Noise Measurements of Ultrastable 10 GHz Harmonically Modelocked Fibre Laser," *Electron. Lett.* **35**, 720 (1999).
[2] G.P. Agrawal, *Nonlinear Fiber Optics*, 2nd ed. (Academic Press, San Diego, CA, 1995). ✦

Artificial Insect Vision for Robotic Aircraft

G.L. Barrows
Tactical Electronic Warfare Division

Problem: NRL is developing micro air vehicles (MAV), which are small (less than 15 cm) robotic aircraft capable of transporting a several-gram payload to a desired location. A typical envisioned use of an MAV is to transport a sensor to or to image a dangerous or unreachable location. To be useful to the military, MAVs must fly autonomously. Furthermore, due to bandwidth and security limitations, all of the processing for sensing and flight control must be performed onboard.

One of the tasks to be performed is in-flight, small-scale navigation. This primarily includes controlling the MAV's flight path to avoid collisions with obstacles and with the ground. To perform small-scale navigation, an MAV must include sensors to perceive the locations of obstacles in the environment and processing to select an appropriate flight path.

Insect Vision: Research into insect vision and behavior provides ideas on how we might be able to provide small-scale navigation capability to an MAV.

The eyes of an insect are too close together to be able to perceive depth by stereo vision. However, they are able to perceive depth from visual motion, or "optic flow." Optic flow is defined as the apparent angular motion of the environment, as seen from the insect, resulting from relative motion between the insect and the environment. Optic flow is typically formulated as a vector field, with the vectors representing the apparent motion of different texture features in the visual field.

Much information about the environment can be obtained from the optic flow. For example, if an insect is flying a straight path, it can estimate the distance to a wall on its left or right side by observing the rate at which the wall appears to be moving. The closer the insect is to the wall, the faster the optic flow. An insect can fly down the middle of a tunnel simply by choosing a flight path such that the optic flow on the left and right sides is equal. This applies even as the tunnel bends with changes in width. Finally, an insect can detect a collision with a wall or an obstacle by detecting a rapid expansion in texture in the forward direction. The more rapid the expansion, the more imminent the time until collision.

Optic Flow Sensor: These findings suggest that appropriately mounted optic flow sensors can allow an MAV to perform small-scale navigation. For example (Fig. 3), a sensor aimed downward can be used to estimate the MAV's altitude by measuring the optic flow moving backward. Similar sensors aimed sideways can be used to measure the distance to obstacles on the left and right sides. A sensor aimed forward can be used to detect obstacles by observing expansion in the optic flow.

The challenge is to design an optic flow sensor that meets the weight and size requirements to fit on an MAV. The measurement of optic flow is known to be computationally intensive when using conventional CCD (charge-coupled device) imagers. This is because the measurement of optic flow requires the processing of multiple image frames, using equations that span the two-dimensional spatial dimensions and the one-dimensional time dimension. We are choosing the alternate "sensor approach" (Fig. 4). A front-end analog integrated circuit contains specially shaped photoreceptors and analog circuits to perform low-level processing. These circuits are hardwired and optimized for performance, size, and power consumption. Furthermore, the circuit structures mimic the neurological structures found in an insect's vision system. A back-end single-chip microcontroller completes the sensor using digital processing. Figure 5 shows a prototype optic flow sensor.

In-flight Demonstration: To obtain a proof-of-concept, the sensor shown in Fig. 5 was mounted on a handheld glider and used to control the glider in flight. In the first experiment, the sensor was aimed downward to measure the glider's altitude. The sensor was programmed to raise a tail elevator when the optic flow surpassed a threshold. When the glider was released, it flew gently toward the ground until just before landing. At this point, the sensor detected
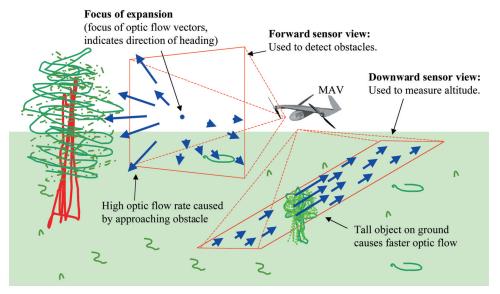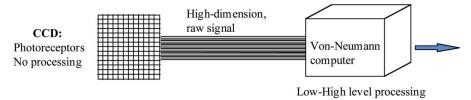
FIGURE 3
Use of optic flow for small-scale navigation.

Conventional Machine Vision

CCD:
Photoreceptors
No processing

High-dimension, raw signal

Von-Neumann computer

Low-High level processing

Sensor Approach

Sensor Head:
Photoreceptors,
Low and mid-level processing

Low-dimension, High-level signal

Only essential information is computed

microcontroller

High-level processing
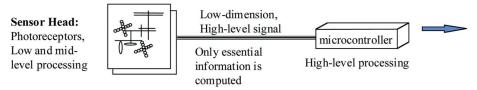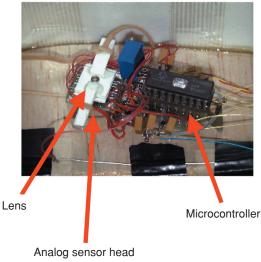
FIGURE 4
Conventional vs sensor approach to machine vision.

Lens

Microcontroller

Analog sensor head

Mass: 25 grams
Power: <10 mW

FIGURE 5
Prototype sensor.

the increased optic flow rate and caused the elevator to be raised. This caused the glider to "porpoise" upward just before landing. In the second experiment, the sensor was aimed sideways and programmed to turn a rudder when the measured optic flow surpassed a threshold. When the glider was tossed toward a wall at a shallow angle, the sensor detected when the glider was too close to the wall, and turned the rudder to cause the glider to avoid the wall. A second prototype sensor that looks both left and right was fabricated and was used to allow the glider to avoid both walls.

[Sponsored by ONR] ✦

High-Resolution Multilayer-Coated Ion-Etched Gratings for Soft X-ray Spectroscopy

M.P. Kowalski and R.G. Cruddace
Space Science Division

W.R. Hunter
SFA, Inc.

Introduction: It has been "known" since Roentgen's time that X rays do not reflect from mirrors. More correctly, their reflectance at normal incidence is essentially zero, but they do reflect from surfaces at grazing incidence. In fact, grazing incidence optics are the basis for an enormous variety of diagnostics and facility instruments, including the Chandra X-ray Observatory launched by NASA this past summer. The use of multilayer coatings has made it possible to achieve high X-ray reflectance at normal incidence. A number of space experiments have already used multilayer-coated mirrors to image the Sun, including NRL's Extreme Ultraviolet Imaging Telescope (EIT) on the Solar and Heliospheric Observatory (SOHO). We have now put such coatings on high-quality diffraction gratings and are using them in a sounding rocket instrument, the Joint Astrophysical Plasmadynamic Experiment (J-PEX), which will produce the highest spectral resolution yet achieved for a cosmic X-ray source.

Basic Research: A multilayer is composed of alternating layers of two materials that have large differences in absorption. It is analogous to an atomic

crystalline lattice and so obeys Bragg's modified law of refraction. The quality of the multilayer depends primarily on reducing roughness at the interfaces and preventing interdiffusion of the two materials. The control of thin film deposition now has reached the level of "atomic engineering" so that the high normal-incidence reflectance predicted theoretically is approached in practice. Only a few laboratories in the world can produce high-quality multilayers, and we have relied on Dr. Troy W. Barbee, Jr., of the Lawrence Livermore National Laboratory (LLNL), for magnetron sputtered multilayers and Dr. Ulrich Heinzmann of the University of Bielefeld, Germany, for thermally evaporated multilayers. At wavelengths greater than 125 Å, molybdenum and silicon are among the best materials, and typically up to 40 layer-pairs are applied.

For more than a century, reflection gratings have been ruled using a stylus. However, a new process has been developed at a few firms in which the groove pattern is exposed holographically in a photoresist layer deposited on a superpolished substrate. An ion beam is used to etch the grooves directly into the substrate. This process greatly improves the control of the groove profile and yields a surface roughness close to that of the original substrate (~4 Å rms). This improves grating efficiency and reduces the total scattered flux.

We have obtained test gratings of high groove density from the leading ion-etched grating firms, Carl Zeiss in Germany and Spectrogon (formerly Tayside Optical) in the United Kingdom. Multilayers were applied, and we measured the wavelength response and efficiency at near-normal incidence using the NRL beamline X24C at the National Synchrotron Light Source. Table 1 summarizes the major results chronologically. The grating efficiency figure of merit, the derived groove efficiency, is defined as the ratio of the measured grating efficiency to the measured reflectance of the coating. The advantage in measured efficiency of replacing a single layer of gold with a multilayer is evident. The results also demonstrate the superiority of ion-etched gratings in comparison with replicated ruled gratings. The atomic force microscope images in Fig. 6 make this result understandable as the multilayer faithfully transmits the profile of the underlying grating substrate, which is smoother in the ion-etched sample.[1]

The table shows a steady improvement in the groove efficiency of multilayer-coated ion-etched gratings. In a recent investigation, we achieved a value of 34% in the first inside order for a laminar (rectangular groove profile) multilayer grating, which approaches the theoretical maximum of 40.5%.[2] The groove efficiencies for blazed gratings are significantly less than the theoretical maximum of 100%. This is a shortcoming of all current techniques, which at high groove density tend to round off the sawtooth profile. Studies of the spectroscopic performance of multilayer test gratings, using an NRL 2.2-meter McPherson spectrograph, have demonstrated resolving powers up to 14000.[3]

J-PEX Astrophysics Application: The four flight gratings for J-PEX were made by Zeiss and are the largest multilayer-coated ion-etched gratings yet produced, each having an area of 16 × 8 cm with 3600 grooves/mm. The multilayer consists of eight pairs of magnetron sputtered molybdenum-silicon, each of thickness 125.8 Å. To determine uniformity, we mapped the efficiency at many locations over each grating. Figure 7 shows the calibration results at 29 locations on one grating over the J-PEX bandpass of 225 to 245 Å.[4] The average measured near-normal

Table 1 — Efficiency Measurements at Near-Normal Incidence of a Series of Coated Gratings

Year	Grating	Groove Density (mm⁻¹)	Multilayer or Coating	λ (Å)	Order	Measured Coating Reflectance	Measured Grating Efficiency	Derived Groove Efficiency
1990	Laminar ion-etched	2000	Mo-Si	175	±1	0.30	0.060	0.20
1993	Blazed ruled replica	2000	Single Au Mo-Si Mo-Si	136 136 151	−2 −2 −1	0.00165 0.54 0.34	0.00012 0.015 0.016	0.07 0.03 0.05
1995	Blazed ion-etched	3600	Mo-Si	130	−2	0.55	0.130	0.24
1995	Blazed ion-etched	2400	Mo-Si	147	−2	0.28	0.075	0.27
1997	Laminar ion-etched	2400	Mo-Si	151 149	+1 −1	0.478 0.464	0.163 0.150	0.34 0.32

FIGURE 6
Atomic force microscope images of the top layer on a multilayer-coated ruled replica grating (left) and a multilayer-coated holographic ion-etched grating (right). The vertical scale has been exaggerated to show the groove profile and texture. For both gratings, the groove period is 2778 Å and the average groove height is 150 Å.
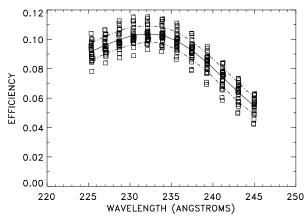
FIGURE 7
Measured efficiency of a J-PEX multilayer-coated ion-etched flight grating in the first inside order and at an angle of incidence of 5°. The solid curve is the average of all 29 locations and the dot-dashed curves show the standard deviation.

of the white dwarf G191-B2B. This is a crucial step in understanding the evolutionary paths of white dwarf stars. In the short observing time available with a sounding rocket (~300 seconds), the mission is possible only because of the use of efficient multilayer-coated ion-etched gratings.

incidence peak efficiency at the target peak wavelength of 234 Å is 10.3 ± 0.6%, where the spread in values is less than a tenth of the average. The derived groove efficiency is 34.4 ± 1.9%. These values exceed previously published values for a high-density grating

J-PEX is a high-resolution spectrometer to be launched in 2000 by the NASA sounding rocket 36.162 DG to study absorption features of singly ionized helium and heavier elements in the spectrum

References
[1] J.F. Seely, M.P. Kowalski, W.R. Hunter, T.W. Barbee, Jr., R.G. Cruddace, and J.C. Rife, "Normal-incidence Efficiencies in the 115-340-Å Wavelength Region of Replicas of the Skylab 3600 l/mm Grating with Multilayer and Gold Coatings," *Appl. Opt.* **34**, 6453 (1995).
[2] M.P. Kowalski, R.G. Cruddace, J.F. Seely, J.C. Rife, K.F. Heidemann, U. Heinzmann, U. Kleineberg, K. Osterried, D. Menke, and W.R. Hunter, "Efficiency of a Multilayer-coated, Ion-etched Laminar Holographic Grating in the 14.5-16.0-nm Wavelength Region," *Opt. Let.* **22**, 834 (1997).
[3] M.P. Kowalski, J.F. Seely, W.R. Hunter, J.C. Rife, T.W. Barbee, Jr., G.E. Holland, C.N. Boyer, C.M. Brown, and R.G. Cruddace, "Dual Waveband Operation of a Multilayer-coated Diffraction Grating in the Soft X-ray Range at Near-normal Incidence," *Appl. Opt.* **32**, 2422 (1993).
[4] M.P. Kowalski, T.W. Barbee, Jr., K.F. Heidemann, H. Gursky, J.C. Rife, W.R. Hunter, G.G. Fritz, and R.G. Cruddace, "Efficiency Calibration of the First Multilayer-coated Holographic Ion-etched Flight Grating for a Sounding Rocket High-resolution Spectrometer," *Appl. Opt.* **38**, 6487 (1999). ◆

Remote Sensing

Unraveling the Dynamics of a Coastal Buoyancy Jet

D.R. Johnson,[1] M. Kappus,[2] R. Arnone,[1]
C.O. Davis,[2] A. Weidemann,[2] and M. Routhier[3]
[1]*Oceanography Division*
[2]*Remote Sensing Division*
[3]*University of Southern Mississippi*

Background: The littoral zone has become a strong focal point for naval operations. Within this zone, estuarine outflows produce highly variable environmental conditions that significantly affect optical and acoustic sensors. Under the influence of the Earth's rotation, estuarine discharges of fresh, buoyant water containing excess loads of particulate and dissolved materials spread along the coastline in narrow, strong, and variable flows known as coastal buoyancy jets. We know that estuarine discharges are primarily driven by seasonal runoff and are highly modulated by oceanic tides and by local winds. However, the fate of this water within the buoyancy jet as it spreads along the coast and the influence of its optical character on the littoral zone has been unclear. In this study, we have attempted to understand the dynamics of the coastal buoyancy jet and the causes for variations in its inherent (independent of sunlight) optical character. We are motivated to provide a basis for prediction of the optical character of the littoral zone as well as for interpretation of its optical and dynamic character from remotely sensed images.

Chesapeake Bay Coastal Buoyancy Jet: Figure 1 shows the location of the field study along the coasts of Virginia and North Carolina, south of Chesapeake Bay. This image from the SeaWIFS ocean color satellite clearly shows the high chlorophyll content of the fresh water discharge, first in an inertial bulge just south of the bay entrance and then extending in a narrow band for about 100 km along the coast south of the bay. An aircraft carrying the Hyperspectral Digital Imagery Collection Experiment (HYDICE) flew along several lines perpendicular to the coast during the field program while an array of moorings and two ships measured in situ conditions.

Results from this study[1,2] clearly demonstrate the highly variable nature of this buoyancy jet and its strong relationship to wind forcing. When the wind blows in an upwelling favorable direction (toward the north), the coastal trapped buoyant water is quickly dispersed offshore in a thin near-surface flow and
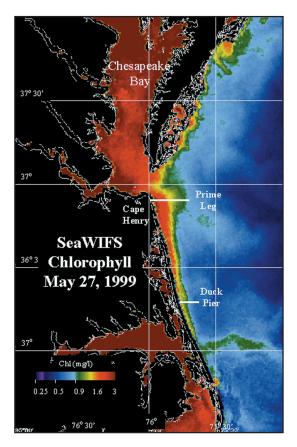
SeaWIFS image (chlorophyll) of Chesapeake Bay discharge spreading along the south coast in a coastal buoyancy jet. Heavy white horizontal lines show two overflight paths by the HYDICE aircraft spectral imager and denote the extent of coastline that was sampled by ship surveys and mooring arrays.

mixed into midshelf waters. When the wind relaxes or blows in a downwelling favorable direction (toward the south), the buoyant water begins to propagate southward at overground speeds of 0.4 to 0.75 m/s, taking about a day and a half to reach the Army Corps of Engineer's Field Research Facility (FRF) pier at Duck, North Carolina. Propagation speeds slow and the jet becomes more stable as it progresses southward, commensurate with the loss of water and momentum to ambient shelf waters. Wind-forced pulses of outflowing water can be observed in alongshore variations in the buoyancy jet, mimicking instability processes.

Figure 2 shows the temporal relationships among winds, currents, and water properties at a mooring site about 17 km north of the FRF pier in 10 m of water. The vertical dotted lines in this figure locate the arrival time of these coastal jet fronts (defined at
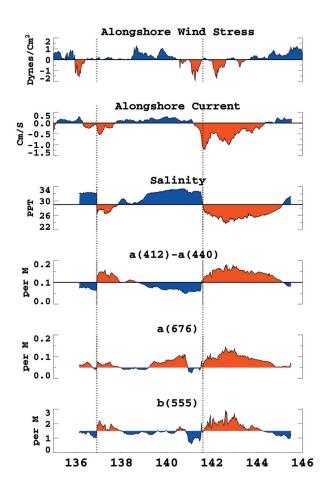
FIGURE 2
Alongshore component of wind stress at (FRF)-Duck, North Carolina, with current, salinity and optical components at a mooring 17 km north of Duck in 10 m of water. The two vertical dotted lines mark arrival of low salinity water in the coastal buoyancy jet, spawned by reversal of wind stress to downwelling favorable about 36 hours prior. The high currents and strong changes in optical character denote the arrival of estuarine water. Increases of chlorophyll (a676) during upwelling of favorable winds mimic estuarine water and provide a challenge for separating the effects of advection vs local bloom caused by upwelling in satellite imagery.

a salinity of 29 ppt). The arrival of the fronts many hours after the turn of wind stress into a downwelling favorable state is clearly seen in the sharp drops in salinity, in excess of 6 ppt. When the winds switch to upwelling favorable, salinity increases to midshelf values. Currents exceeding 1 m/s and radical changes in inherent optical properties are associated with the arrival of the jet.

Optical absorption (a) and scattering (b) spectra are used to infer the nature of the optical contributors to the water mass. The spectral difference between a(412) (absorption at 412 nanometers) and a(440) is dominated by colored dissolved organic matter (CDOM) while a(676) is dominated by chlorophyll-a and b(555) is dominated by particle scattering. Figure 2 shows that the inverse relationship between salinity—an excellent tag of discharged water —and CDOM is remarkably good (correlation: $r = -0.97$), making CDOM a valuable surrogate for salinity in optical satellite imagery. However, relationships between salinity/chlorophyll-a ($r = -0.52$) and salinity/particle scattering ($r = -0.78$) are compromised by upwelling events that induce local blooming and resuspend settled materials. A future chal-

lenge for optical satellite interpretation of in situ events in the coastal buoyancy layer involves improved separation of CDOM and chlorophyll-a in the image spectra, thereby separating advective from local water mass forcing. This is where we expect future contributions from hyperspectral imaging to be most valuable.

Aircraft Remote Imaging: Figure 3 is a mosaic of three passes with the aircraft HYDICE imaging system centered on the FRF pier at Duck, North Carolina. The pier is visible in the upper center; an offshore foam line associated with the edge of the coastal buoyancy jet is visible in the lower part of the image, separating brighter fresh water nearshore from the darker offshore ambient shelf water into which the jet is intruding. New algorithms allow the retrieval of inherent optical properties from mixing of pixel intensities across several channels. In addition, repeated passes enable dynamics to be monitored. For example, each imaging pass in this mosaic was made at about 15-minute intervals, accounting for the displacement of the foam line. Using this displacement and assuming a parabolic curvature at this location
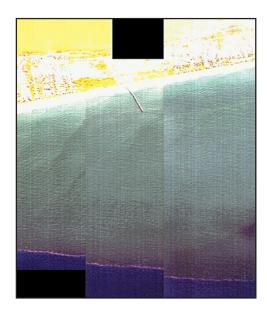
FIGURE 3
Mosaic of three aircraft HYDICE images at about 10-minute intervals. Note FRF pier at Duck, North Carolina, in upper center and foam line (displaced between passes) in the lower image, which delineates the edge of the coastal buoyancy jet.

near the head of the jet, simple geometry can be used to estimate the over-ground speed of the jet. The resulting speed, 0.35 ± 0.07 m/s, is a reasonable value considering the slowing of the front at this distant location from its source. It should be noted that the currents within the jet are higher than the front propagation speed and cannot be estimated with this technique. A second future challenge is to remotely infer the currents associated with this buoyancy jet.

References
[1] D.R. Johnson, A. Weidemann, R. Arnone, and C.O. Davis, "The Chesapeake Bay Outflow Plume and Coastal Upwelling Events: Physical and Optical Properties," submitted to *J. Geophys. Research*, 1999.
[2] S.E. Rennie, J.L. Largier, and S.J. Lentz, "Observations of a Pulsed Buoyancy Current Downstream of Chesapeake Bay," *J. Geophys. Res.* **104**(C8), 18227-18240 (1999). ◆

WindSat Antenna Development

W.L. Lippincott
Space Systems Development Department

P. Gaiser
Remote Sensing Division

Introduction: WindSat is a spaceborne imaging polarimetric microwave radiometer (Fig. 4) currently in development at NRL. The system is designed to demonstrate the capability of polarimetric radiometry to measure ocean surface wind speed and direction. It also detects sea surface temperature, water vapor, cloud liquid water, and precipitation. Polarimetric radiometry measures the radiometric Stokes vector, which fully characterizes the polarization of radiated emissions off the ocean. The Stokes parameters vary with ocean surface roughness, which in turn varies with wind speed and direction.

Reflector Antenna System: The wind-driven ripples on the ocean surface induce low-level cross-polarization (cross-pol) components in the emitted radiation. To successfully measure the Stokes vector, a system with low inherent cross-pol must be used. To meet this requirement, along with high beam efficiency and calibration and mechanical design factors, a scanning offset parabolic reflector is being used. The inherent cross-pol levels of –25 dB for this antenna are then calibrated on a range, and the effects are removed in postprocessing.
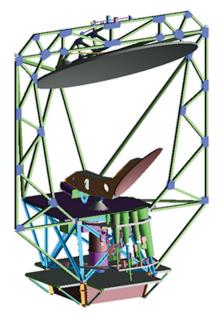
FIGURE 4
WindSat antenna.

The reflector is fed by 11 conical corrugated feed horns (Fig. 5) in a cluster at 6.8, 10.7, 18.7, 23.8, and 37 GHz. Three of the frequencies are polarimetric (having vertical/horizontal, ±45 deg, and circular polarizations). Output from the various horns are combined in a postprocessing algorithm to optimize predictions of the wind vector. A cold sky reflector and warm load are alternately passed over the feeds to calibrate the receiver electronics.

FIGURE 5
Conical corrugated feed horn.

System Calibration: An outdoor range located in Melbourne, Florida, is being used to calibrate the WindSat antenna (Fig. 6). Modeling shows that range multipath has the most significant effect on Stokes accuracy, so a high elevation tower with horizontally and vertically polarized sources is being used to reduce the multipath component to −70 dB. A reference antenna located to the side of the WindSat reflector also receives the polarized signals from the tower. This signal is subtracted from the WindSat received signal in the network analyzer so that the drift in the tower electronics is removed and replaced by drift in the reference antenna, which is located in an environmentally controlled area.

The third Stokes component (±45 deg polarization) is very sensitive to rotation of the fields. Alignment of the tower polarizations must be known relative to the alignment of the WindSat platform to within ±0.018 deg. This difficult requirement is met through the use of a source reflector antenna with a very high polarization purity grid and very accurate inclinometers.

A pathfinder test in the summer of 1999 demonstrated that the Melbourne range could adequately characterize the WindSat antenna performance. Through careful design of the range and rigorous calibration, the postcalibration antenna cross-pol is now −30 dB, which enables WindSat to meet its wind vector requirements.

Computer Modeling: The GRASP8W reflector code (from Ticra Engineering Consultants) is being used to model the system using both predicted and measured feed horn patterns. The GRASP8W is an industry standard used for modeling reflector antennas and is used to perform various analyses for the project. These include near- to far-field performance predictions (for 37 GHz); modeling the im-
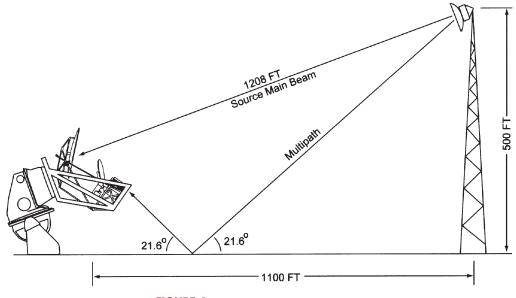
FIGURE 6
Range geometry used to calibrate the system.
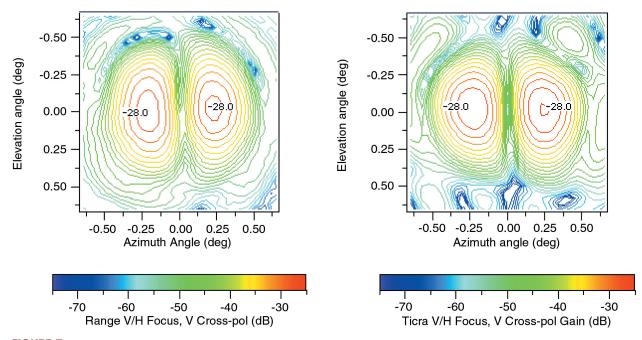
FIGURE 7
Comparison of the range and modeling results for the vertical cross-polarization at 37 GHz.

pact of the struts and the reflector support structure on the reflector performance, and the impact of cold sky reflector blockage; studies to access the impact of reflector distortion data from a finite-element thermal and stress analysis program; and a study of the effects of feed rotation and cross-pol imbalance on performance. Figure 7 shows a comparison of the modeling and some preliminary range results for the vertical cross-polarization at 37 GHz.

Conclusions: The WindSat system is on schedule to meet the Navy/National Polar-orbiting Operational Environmental Satellite System (NPOESS) requirement for ocean wind speed and direction measurements of ±2 m/s and ±20° for wind speeds of 3 to 25 m/s with a horizontal spatial resolution of 20 km. The launch date is December 2001.

Optical Geolocation and Tracking System: RIT Airship Demonstration

A.S. Hope, J.W. Middour, and H.M. Pickard
Space Systems Development Department

Introduction: The Space Systems Development Department (SSDD) of the Naval Center for Space Technology (NCST) participated in a flight test for the Revolutionary Imaging Technology (RIT) program. The test was conducted at the Naval Air Station, Lakehurst, New Jersey, in August and September 1999. This test combined the joint efforts of the Optical Sciences and Remote Sensing Divisions, as well as SSDD and the Spacecrafting Engineering Department from the NCST. SSDD engineers designed and integrated an open-loop, precision pointing and tracking system as part of this technology demonstration. The system is designed to point and stabilize a sparse aperture imaging camera while independently pointing and stabilizing a laser communication transmitter. Both of these instruments are key elements of the RIT program.

The system points the payload camera at an area on the ground to maintain an apparent still image and, simultaneously, directs a 2 milliradian laser communication beam at a ground station to downlink the collected images in real time. All this is accomplished

by compensating in real time for the motion of the airship and the rotation of the Earth. The testing was performed using a SKYSHIP600 airship as the airborne platform. The airship provided an overhead perspective for imaging while maintaining a relatively low dynamic environment for the imaging and pointing system.

System Description: Precise knowledge of position and attitude are required to point and control the camera and laser transmitter. The pointing and control system uses all off-the-shelf components: a real-time differential kinematic Global Positioning System (GPS) receiver provides position, and a ring laser gyro (RLG) tracks the attitude motion of the pointing and control bench assembly. A pair of two-axis gimbals performs camera and laser pointing and control. The four devices (GPS, RLG, and two gimbals) are rigidly mounted to an optical bench assembly that can be lowered through a hole in the belly of the airship gondola. Figure 8 shows the optical bench assembly. The individual components of the pointing and control assembly are simultaneously controlled by one personal computer where information from the GPS and RLG is combined to produce gimbal control commands 30 times per second.

The RLG is initialized using an Earth-centered Earth-fixed alignment range near the airship take-off area. Differential GPS surveying techniques fix the relative positions of targets on the alignment range to better than 1 centimeter over a 300-meter baseline (33 microradians.) The initial gyro orientation is found using a 1-meter focal length telescope with a magnification factor of ~225×. Once the gyro is initialized, it is transferred to the optical bench and fastened using mechanical stops and a large flat surface area to assure repeatability of attachment between the alignment bench and the flight bench. Timing for the system is also determined by GPS.

To compensate for Earth rotation, the algorithms for pointing and control use precise models for Earth orientation. While in flight, the operator of this system is able to view the area where the laser is pointing by using an electronic video camera and monitor. Biases in the system are removed through interactive commanding by the operator to reorient the camera onto the laser receiver optics on the ground. During the flight test, the camera was pointed at various presurveyed targets by computer control. The camera can also be pointed manually at any target of interest. After acquisition, the control algorithms keep the camera locked on target and report the target latitude and longitude.

Summary: The pointing and control system developed for the RIT airship demonstration test was successful in pointing, stabilizing, and controlling two independent devices through an unpredictable, dynamic flight on an airship. Thousands of images were collected onboard the airship, and several of those images were linked in real time to the portable ground station. Figures 9 and 10 show an example of a raw sparse aperture image and the algorithmically corrected image.

This pointing and stabilization apparatus is a promising technology for many tracking and communications applications that require precision, autonomous pointing and control. A second flight is planned for December 1999 to collect more images using additional aperture masks.
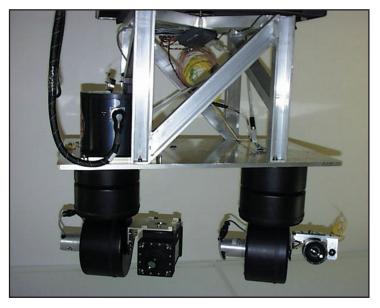
FIGURE 8
Optical bench assembly. RLG is at top left. Imaging camera is on left gimbal; laser communication aperture is on right gimbal. Large lens on right gimbal is coboresighted camera for fine laser steering.

FIGURE 9
Raw camera image.

FIGURE 10
Processed image.

Simulation, Computing, and Modeling

Electronic Warfare Simulation and Analysis

L.C. Schuette and B.T. Solan
Tactical Electronic Warfare Division

The Interactive Scenario Builder (Builder) is an electronic warfare (EW) simulation that allows the interactive manipulation and viewing of scenarios in two-dimensional (2D) ("God's eye" view) and three-dimensional (3D) (out-the-window) perspectives. Features such as platform motion, emitter characteristics and scan patterns, electromagnetic propagation, terrain masking, jamming, and target characteristics are modeled. Builder has extensive interfaces to emitter and platform characteristic databases as well as National Imagery and Mapping Agency (NIMA) terrain elevation and chart products. Builder is particularly well suited for determining radar coverage in littoral regions where terrain masking can occur. This article discusses the rationale for developing the Builder system, the design philosophy used by the developers, examples of the modeling and simulations (M&S) performed, and example uses of Builder by Fleet assets.

Introduction: Builder is a software simulation that provides a "point and click," mouse-driven graphic user interface that allows the user to create and visualize military combat scenarios. Figure 1 is a screen capture of Builder at start up. Across the upper portion of the display are the drop-down menus, graphic short cuts, and controls for scenario time and animation. The window also shows the default spherical Earth model[2] on which scenarios can be developed. (The spherical Earth is created using the World Geodetic System – 1984 (WGS-84) model. This mathematical reference ellipsoid corrects for the nonspheroidal shape of the planet Earth.) The program specializes in scenarios related to electronic warfare. As such, Builder provides extensive capabilities in electromagnetic simulation and visualization. The Builder simulation incorporates models of the crucial elements of the radar range equation, including transmitter characteristics, the propagation and jamming environments, and the radar cross section (RCS) of the target. For one-way propagation modeling such as that required for a radio frequency (RF) emission detectability or communication link analysis, Builder also models the characteristics of the receiver. These models provide the ability to compute coverage areas that take into account the effects of electromagnetic propagation, terrain masking, jamming, and target characteristics—all of which can vary with time.

The extensive visualization capability allows the user to observe 2D or 3D viewing perspectives, with the orientation and manipulation of both point-of-view and motion about a platform selectable among any of several options (Figs. 2 and 3). For example,
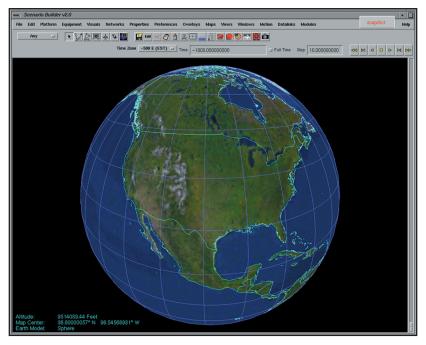
FIGURE 1
Start-up window of Builder software.
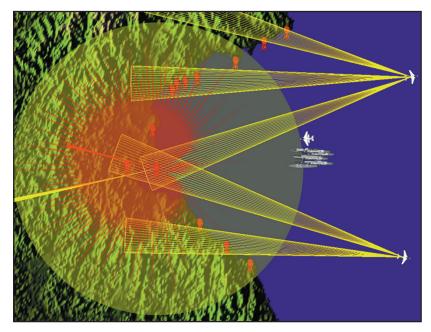
FIGURE 2
A top-down graphical assessment of jammer effectiveness.
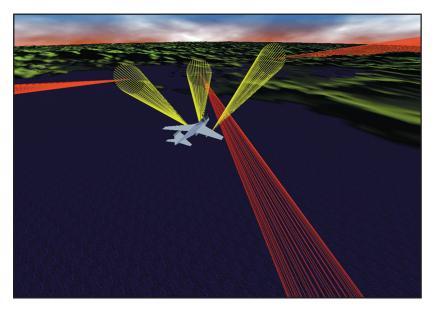
FIGURE 3
3D view of an airborne jammer in action against ground-based radars.

Builder allows the user to pan, zoom, and rotate about a platform in an easy and intuitive fashion. The user can build simple scenarios such as a single ship or aircraft traversing a path in a specific geographic location, with specified emitters present; or, complex scenarios that include multiple moving and/or stationary platforms, each with multiple emitters with varying scan patterns and on/off times. Moreover, Builder also allows the user to visualize time sequences of events, in order to watch, for example, an aircraft or ship traverse the path that has been programmed, while various emitters turn on and off. It is this flexibility, combined with accurate models of the EW environment, that make Builder attractive to both the electronic warfare system designer and the Fleet operator.

Scenario Development: The user typically begins with a fairly clear idea of the friendly platforms (ships, land sites, aircraft, and missiles) intended to participate in a given engagement. The standard equipment on those platforms such as radars and EW equipment is defined in the databases. For R&D purposes, where the user wants to explore "what if…" situations, Builder allows the user to add new equipment or to modify the standard equipment fits on any platform. Depending on the user's need, opposing forces can be defined according to databases on known deployments in the selected geographical area, constructed by the user, or by a combination of the two. Normally, definition is done by querying the database and then modifying the type or placement of hostile equipment to suit the need. Once again, the user can use the standard parameters built into the databases or modify any of them to suit the needs of the scenario. The user defines the temporal and spatial relationships of friendly and hostile platforms. In general, the user would approach scenario development with a plan for maneuvers and platform motions, and then perhaps refine these interactively as the scenario building process proceeds. The end result is a time sequence of events and interactions of the platforms, their radars, EW equipment, communication systems, and the environment.

Application of the Software: Builder has revolutionized the way the ENEWS Program Office creates and uses large-scale EW scenarios. ENEWS has used Builder to support the design, specification, and evaluation of EA-6B and AN/SLY-2 (AIEWS) EW systems from the conceptual through the design stages. Recently, the operational community has found interest in the interactive capabilities of Builder. The Fleet Information Warfare Center (FIWC) has deployed Builder on several Carrier Battle Group

deployments, and it was used during Operation Desert Fox and the Kosovo campaign. During the deployments, Builder was used to assist in EW asset scheduling and allocation. Builder is also used by the U.S. Army's 160th Special Operations Aviation Regiment (Airborne) for mission planning and mission rehearsal. Future enhancements include porting Builder to a Windows NT environment using a cross-platform graphic user interface that is compliant with the Defense Information Infrastructure Common Operating Environment (DII-COE). When completed, Builder will provide an EW planning system on a low-cost, easy-to-use platform that is readily available in the Fleet community.

Computational Design of Molecular Magnets

M.R. Pederson
Center for Computational Materials Science

Background: The defense and civilian industries continue to be interested in the design and optimization of miniaturized electronic and magnetic devices. However, as system size approaches the molecular scale, device design will involve consideration of fundamental limitations imposed by quantum mechanics. For example, a key challenge related to the miniaturization of magnetic storage devices is the ability to develop single-domain nanoscale particles or molecules that retain their magnetic orientation at relatively high temperatures. A second challenge is to determine a low-energy mechanism for switching the orientation of the magnetic particle. Of fundamental importance to this endeavor have been a series of recent experiments on an assembled array of bistable molecular magnets such as the one shown in Fig. 4. In contrast to classical magnets, molecular moment reorientation is achieved without dramatic movements of the atomic positions. Experimentalists have demonstrated that these molecules hold their moment orientation well above liquid-helium temperatures and have demonstrated the quantum-mechanical phenomenon of resonant tunneling
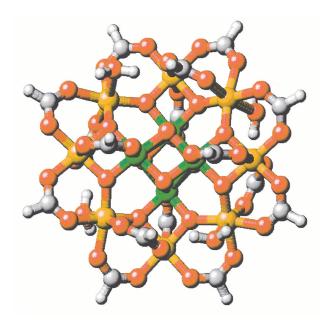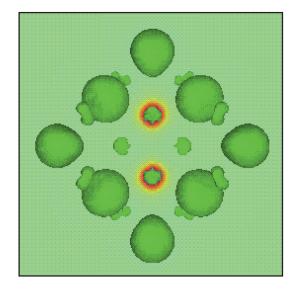
FIGURE 4
$Mn_{12}O_{12}(COOR)_{16}(H_2O)_4$ molecular magnet. The inner minority spin Mn atoms appear in gold, and the outer majority spin Mn atoms appear in green.

of magnetic moment orientation.[1,2] When well-defined magnetic fields are applied, discontinuities in the hysteresis loops appear, indicating facile switching of moment orientation. In 1937, Van Vleck first explained that the moment-reorientation temperature, also referred to as the magnetic anisotropy energy, is due to relativistic interactions such as spin-orbit coupling. A key challenge to computational materials science then is to determine the magnetic anisotropy energy of these molecules and to predict the magnetic field strengths at which resonant tunneling of spins occurs.

Mn-Acetate Molecular Magnet: The molecular assembled Mn-acetate crystal is composed of $Mn_{12}O_{12}(COOR)_{16}(H_2O)_4$. We have used the all-electron density-functional-based Naval Research Laboratory Molecular Orbital Library (NRLMOL)[3] code to investigate the chemical, physical, and magnetic properties. Our studies[4] show that the nonmagnetic organic ligands play a key role in stabilizing the magnetically interesting Mn-based part of the molecule. In the absence of the ligands, the molecule relaxes strongly and a nonmagnetic, topologically different structure is significantly more stable. In addition to stabilizing the $Mn_{12}O_{12}$ framework, the ligands effectively isolate neighboring $Mn_{12}O_{12}$ cores and quench the dipolar interactions. The resulting structure exhibits ferrimagnetic ordering with a minority-spin Mn_4O_4 cube surrounded by a majority-spin Mn_8O_8 framework. Figure 5 shows the majority-spin density. The calculated electronic structure approaches

FIGURE 5
Three-dimensional plot of the total majority-spin density illustrates the ferrimagnetic ordering found in this molecule.

half-metallic behavior with a large minority-spin gap (2.08 eV) and a small majority-spin gap (0.44 eV). In accord with experiment, we predict that this molecule has a large net spin of 20 μ_B. Figure 6 shows the density due to the 20 excess majority spin electrons that, as discussed below, account for most of the anisotropy energy. Heuristically, these electrons are important in forming the anisotropy energy because they visit all parts of the molecule, thereby observing the nonspherical environment.
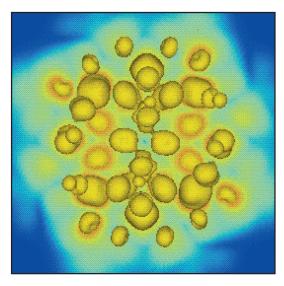
FIGURE 6
Three-dimensional contour plot of the 20 excess majority spin electrons that are energetically closest to the Fermi level. These electrons are primarily responsible for the formation of the large magnetomolecular anisotropy energy observed in this system.

New Technique: Results discussed above describe how relatively large nonrelativistic interactions stabilize a molecule with a high net spin. However, high spin does not necessarily imply high magnetomolecular anisotropy energies and many well-known high-spin clusters and molecules exhibit super paramagnetic behavior at rather low temperatures. We have developed a new mathematical method for exactly computing the explicit coupling between spin and spatial degrees of freedom and have used this method to calculate the anisotropy barrier for the Mn-acetate molecule.[5] This method includes all effects due to spin-orbit coupling as well as qualitatively similar effects occurring in the nonspherical interstitial region of the molecule. Our calculated second-order contribution to the anisotropy energy is

determined to be 56.7 K, in very good agreement with the experimentally determined value of 56.6 K. An additional advantage of this new method is that the electrons responsible for forming the barrier can be determined. It is the electrons within a few eV of the Fermi level that account for 98 percent of the anisotropy barrier. Furthermore, it is coupling between pairs of occupied and unoccupied electrons with antiparallel spins that account for 86 percent of the interaction. It is also possible to definitively determine that the core electrons do not contribute to the anisotropy energy, even though the single-electron relativistic effects on these faster moving electrons are larger. Interactions between majority spin occupied and unoccupied states (which are the closest in energy) are also of negligible importance because they reside in spatially disparate parts of the molecule.

Conclusion: The ability to quantitatively determine which electrons are important for forming the anisotropy energy allows computational materials scientists to more easily investigate how chemical and physical modification of assembled arrays of molecular magnets will affect thermal reorientation barriers and spin-tunneling fields. Several similar arrays of molecules in this size regime are currently being studied and provide a template for identifying technical uses and fundamental limitations of molecular-scale magnets. In addition to possible uses in molecular-scale magnetic storage devices, knowledge gleaned from such investigations may also be useful to the quantum computing community.

References
[1] J.R. Friedman, M.P. Sarachik, J. Tejada, and R. Ziolo, "Macroscopic Measurement of Resonant Magnetization Tunneling in High-Spin Molecules," *Phys. Rev. Lett.* **76**, 3830 (1996).
[2] A. Fort, A. Rettori, J. Villain, D. Gatteschi, and R. Sessoli, "Mixed Quantum-Thermal Relaxation in Mn_{12} Acetate Molecules," *Phys. Rev. Lett.* **80**, 612 (1998).
[3] M.R. Pederson and K.A. Jackson, "Variational Mesh for Quantum-mechanical Simulations," *Phys. Rev. B* **41**, 7453 (1990).
[4] M.R. Pederson and S.N. Khanna, "Electronic and Geometrical Structure and Magnetic Ordering in Passivated $Mn_{12}O_{12}$-acetate Nanomagnets," *Chem. Phys. Ltr.* **307**, 253-258 (1999).
[5] M.R. Pederson and S.N. Khanna, "Magnetic Anisotropy Barrier for Spin Tunneling in $Mn_{12}O_{12}$ Molecules," *Phys. Rev. B* **60**, 9566 (1999).

Automatic Scatterer Identification from Measured Ship RCS Data Using Underlying Physical Models

S. Wolk
Tactical Electronic Warfare Division

Introduction: Radar cross section (RCS) is a primary determinant of ship susceptibility to attack by antiship cruise missiles. RCS management benefits from the clear association of individual scatterers on a ship with measured ship RCS data, which is the scatterer identification problem. It is an inverse scattering problem in which the scattering object is extremely complex, and the measurement channel is corrupted by environmental effects such as multipath and ducting. NRL has developed a new method of solving this important problem. The novel approach uses high-fidelity models of ship RCS, of the radar signal processing, and of the environment in a constrained optimization framework. In so doing, major advances are made in the areas of scatterer identification and predictive RCS model validation. Promising experimental results are presented that directly relate scatterers in a predictive RCS model of a ship to measurements of the ship taken in a maritime environment.

Approach: Our approach to scatterer identification (Fig. 7) uses physical models whose parameters may be perturbed to account for uncertainties that were present during the measurement process. Differences between measurements and the model's output are used to perturb the model to bring its output into agreement with the measured data. In this article we focus on perturbations to scattering parameters. The family of perturbations that brings the model into agreement with measured data is the set of solutions to the scatterer identification problem. If the solution is unique, then all uncertainties will have been resolved, and the scatterer identification problem will have been uniquely solved for all scatterers simultaneously.

This approach uses all available measured data and a priori information, and can enforce a consistent application of all of the geometric, electromagnetic, and signal processing relationships in the underlying models. This is a significant improvement over the projection methods that in the past have been applied to ship scatterer identification. Phenomena that stymie projection methods (especially phenomena that cause scatterers to image in ways that do not permit direct geometric inferences about their positions to be made) can be correctly accounted for in our approach. Moreover, using our approach, the prediction error is quantified, resulting in an estimate of each scatterer's actual RCS.

Measurements: Figure 8(c) illustrates coherent stepped frequency RCS measurements of a ship at
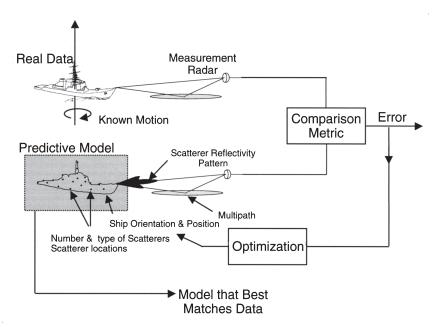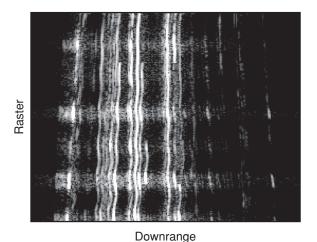
FIGURE 7
Framework for constrained optimization approach.
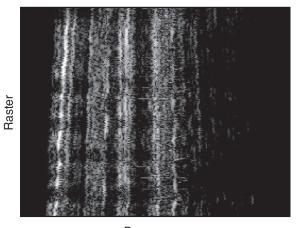
(a) Simulated data (before optimization)

(b) Simulated data (after optimization)

(c) Measured data

FIGURE 8
Ship RCS.

sea as it turns in front of a measurement radar. Successive rasters correspond to successive pulse bursts, and therefore successively illuminated aspect angles. The abscissa is the sample number of an inverse discrete Fourier transform, and so, can be thought of as a downrange distance. The bright white vertical traces in Fig. 8(c) correspond to scatterers of significant RCS that persist over an interval of aspect angles.

Physical Models: NRL Radar Division's Radar Target Signature (RTS) prediction model is the basis of our ship representation. Computer-aided design (CAD) drawings define the ship geometry, and modules within RTS organize the elemental objects on the ship and compute the target's RCS using high-frequency calculations to approximate Maxwell's

equations. RTS incorporates scatterer blockage, multiple-bounce interactions, ship motion, and sea multipath. To reduce computation time, a reduced order model was developed and incorporated into NRL Tactical Electronic Warfare Division's *CRUISE_Missiles* model.[1] Its scatterers are a subset of those in RTS, and were chosen to maintain extremely tight tolerances to RTS predictions over the angles of interest.

Figure 8(a) illustrates the RCS that results from simulation, in which coherent radar processing and ship movements replicate those of the real-world RCS measurements of Fig. 8(c). The similarities between these two figures are readily apparent. Major scatterers that manifest themselves in the measured data have counterparts in the simulation, although in the

199

FIGURE 9
Normalized mean-squared error.

example given, the simulation overpredicts the RCS of many scatterers. These differences in RCS shown in Figs. 8(a) and 8(c) are attributable in large part to the idealization of scattering geometry inherent in CAD descriptions that are fed into the RTS ship model. Actual scatterer geometry may deviate from ideal drawings for practical manufacturing reasons. Examples include nonorthogonal corners and concavities in ostensibly flat plates.

Optimization: In cases where the RCS of the ship is driven by the mainbeam patterns of its scatterers, as in Fig. 8, we approximate the effects of nonideal scattering surfaces by the application of scalar gains to scatterer reflectivity patterns computed by RTS. We seek to minimize the mean-squared error between the measured data and the predicted ship RCS by scalar perturbations to the underlying scatterers' reflectivity patterns. Figure 8(b) illustrates the result of using a gradient projection method to solve this optimization problem. Figure 8(b) is in substantial agreement with the measured data illustrated in Fig. 8(c). In particular, the bright vertical traces in Fig. 8(a) have, as a result of the optimization process, been brought in Fig. 8(b) into conformity with those of the measurements in Fig. 8(c). Figure 9 illustrates the rate of convergence of normalized mean-squared error with respect to visible scatterers. The optimization has effectively modified the underlying ship model's scatterer reflectivities to bring the simulation into close agreement with the measurements.

Summary: NRL has developed a new formulation and method of solution to the ship scatterer identification problem, which is based on underlying physical models. Formulated as a constrained optimization problem, the solution associates specific scattering surfaces in a high-fidelity ship model with each pixel of measured RCS data. The differences between the predictive RCS model output and measured data are quantified, providing an estimate of each scatterer's true RCS. Research efforts are now focused on improvements to the method by using higher resolution and applying constraints that relate scatterer perturbations more directly to the geometry of likely scatterer deformations.

[Sponsored by ONR]

References
[1] A. Goldberg and R. Futato, "*CRUISE_Missiles* Electronic Warfare Simulation," 1993 *NRL Review*. ◆

Contaminant Transport Modeling for Consequence Management

B.Z. Cybyk, J.P. Boris, T.R. Young, and C.A. Lind
Laboratory for Computational Physics and Fluids Dynamics

Introduction: To help counter the threat posed by the worldwide proliferation of chemical and biological weapons, civilian and military organizations

are increasingly relying on modeling and simulation to support force protection and counter-terrorist planning, as well as military training, campaign planning, and operations. Contaminant transport models enable first responders to make timely, educated decisions regarding rescue and evacuation procedures. They can also be used as planning tools for the optimal use of resources to mitigate natural disasters involving the release of deadly contaminants. Current hazard prediction tools used by the Department of Defense (DoD) are generally limited to outdoor scenarios using limited terrain data. A clear need exists for models that can compute the flow and deposition of contaminant particles and gases within and around buildings of varying complexity under a variety of meteorological conditions. In response to this need, NRL has recently extended its scalable FAST3D computational fluid dynamics (CFD) model to contaminant transport problems in urban environments and/or complex terrain.

The application of CFD models to chemical/biological (C/B) transport problems is relatively new and requires considerably more computer resources than traditional models. However, the gains are proportionally dramatic. Advantages include the ability to model complex geometry, to dynamically resolve flow field details, and to handle applications where neither zonal (indoor) nor Lagrangian "puff" (outdoor) models are valid. Assumptions in CFD models are, in general, fewer and less restrictive than in zonal and Gaussian models.

Approach: A technology program is now underway to further develop and mature this complex geometry CFD capability aimed at supporting C/B consequence management operations. The program contains a number of components; these include urban (i.e., external) and building (i.e., internal) geometry specification, model enhancement, model calibration and validation, coupling to other relevant models, and unclassified and classified applications. The primary objective of the effort is to develop, calibrate, validate, and document FAST3D-CT, the contaminant transport version of FAST3D, as a hazard assessment model for operational C/B use. A secondary objective is to perform a documented set of simulations and sensitivity studies to: provide a reliable, high-resolution database for calibrating other models; analyze a few important scenarios whose characteristics are of immediate national and military concern; and extract "rules of thumb" from the simulations that are suitable for training Incidence Response Teams tasked with consequence management.

Model: The CFD code FAST3D-CT solves the dynamic transport equations for air and airborne contaminants. It is an extension of the complex-geometry FAST3D model to the particle and flow physics of contaminant transport problems. The model was designed from the beginning to be compatible with new, cost-effective, parallel computer architectures. Its three-dimensional flow solver is based on the flux-corrected transport algorithm, while complex geometry capabilities are provided by the virtual cell embedding algorithms. Multispecies particle and gas phase contaminants can be initialized, sprayed, or injected from localized sources, transported, and diagnosed without restarting the model at any time during the simulation. A sophisticated (tensor) turbulence model ensures that the flow correctly adapts to complex terrain with vertical and re-entrant surfaces. To account for meteorological effects, FAST3D-CT is loosely coupled to NRL's COAMPS mesoscale atmospheric model.

Field Trials: The viability of using a detailed CFD model such as FAST3D-CT to support C/B consequence management was recently demonstrated during the 911-Bio Advanced Concept Technology Demonstration (ACTD). The ACTD leveraged existing technology by applying select CFD and zonal airflow models to consequence management problems. The ACTD release scenarios, involving two different facilities, were successfully simulated by the FAST3D-CT model, and the resulting "blind" predictions compared favorably with experimental measurements.[1-2]

Large-Scale Demonstrations: Large-scale exterior computations of urban environments are being used to demonstrate newly developed technologies and model enhancements.[3] The most recent demonstration showcases a new tile-based method of database generation and integration of the grid generator with the flow solver, both driven by the need for rapid and inexpensive digital specification of complex urban geometry and subsequent grid generation. In this particular FAST3D-CT computation, an external release scenario in a 1.5×2.1-kilometer region of a generic city (Fig. 10) is computed to 4-meter resolution via 6.1 million grid points using High Performance Computing Challenge Project resources. The scenario involves the instantaneous release of contaminant from three stationary point-sources under steady 2.5 m/s winds from the southwest. Figure 11 presents the distribution of contaminant predicted by FAST3D-CT at a constant elevation of 2 meters above ground level 7.5 minutes after release.
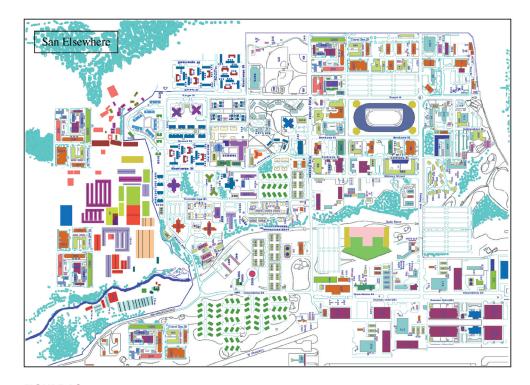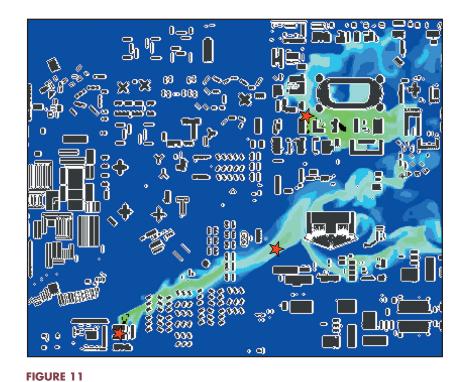
FIGURE 10
Tile database of a 1.5×2.1-kilometer section of a generic city.

FIGURE 11
Snapshot of contaminant distributions predicted by FAST3D-CT, 2 meters above ground level after being driven by 2.5 m/s winds from the southwest for 7.5 minutes. The three release points are denoted in red.

Significance: The Navy, Marine Corps, DoD (and U.S.) require a modeling capability to counter the threat to high-profile targets from the proliferation of C/B weapons. Potential targets include strategic U.S. and coalition military sites, urban locations, and highly populated civilian areas. Such a modeling system must account for complex physical processes and varying meteorological conditions in geometrically complex environments to effectively support consequence management doctrine, training, and operations. Our in-house effort contributes to the framework required for a comprehensive, high-resolution, contaminant transport capability.

[Sponsored by OSD and ONR]

References

[1] B.Z. Cybyk, T.R. Young, J.P. Boris, and C.A. Lind, "Coupled Interior-Exterior Computations of Contaminant Transport in a Multi-Compartment Structure," submitted to the *J. Fluids Eng.*, September 1999.

[2] B.Z. Cybyk, J.P. Boris, and T.R. Young, "Influence of Facility Characterization and External Winds on Contaminant Release Modeling," NRL/MR/6410-99-8362, Naval Research Laboratory, Washington, DC, 1999.

[3] B.Z. Cybyk, J.P. Boris, T.R. Young, A.M. Landsberg, and C.A. Lind, "A Detailed Contaminant Transport Model for Urban and Environmental Hazard Assessment," AIAA-99-3441, 30th Plasmadynamics and Lasers Conference, Norfolk, VA, June 1999.

Atmospheric Transport Modeling

D.L. Westphal and T.R. Holt
Marine Meteorology Division
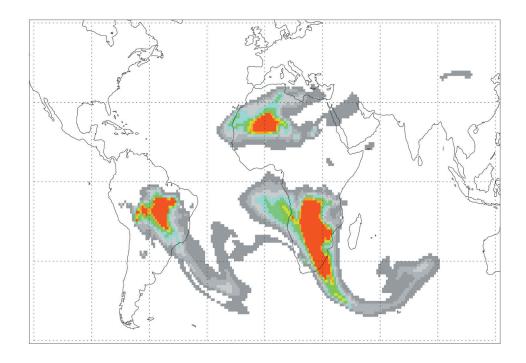
M. Liu
SAIC

A number of naturally occurring and anthropogenic atmospheric particulates affect U.S. Navy operations in nearly all parts of the world. These range in extent from continental-scale dust storms to regional-scale contaminant plumes. These atmospheric aerosols can have a tremendous impact on the performance of naval weapon sensors and systems and on human health. No operational capability presently exists for predicting the transport of these aerosols on regional or global scales. In response to Navy needs, NRL has developed an atmospheric transport modeling capability for scales ranging from global to regional.

Global Modeling: Our global modeling is done with the NRL Analysis and Prediction System (NAAPS, <www.nrlmry.navy.mil/aerosol>), which uses satellite data, emissions inventories, surface weather reports, and global weather data to drive a multicomponent global aerosol model. NAAPS has been run daily since 1996 to produce realistic simulations of the global distribution of sulfate, dust, and smoke aerosols. It is the only model in the world with this capability and coverage that runs with this frequency. The daily NAAPS simulations have revealed a higher-than-expected frequency of cases of intercontinental aerosol transport. These include the transport of Asian dust and pollution to North America, biomass smoke from South America to Africa, and from Africa to Australia. An example of this intercontinental transport is evident in NASA's Total Ozone Mapping Spectrometer (TOMS) aerosol index (AI) for September 10, 1999 (Fig. 12). High amounts of aerosol are detected over the Sahara, South America, and southern Africa, in addition to isolated aerosol plumes over the oceans. However, the intercontinental transport is not clear because water clouds inhibit the AI retrieval. The NAAPS optical depth (a vertical integral of the visible-wavelength opacity due to aerosols) for the same day shows similar features. It clearly shows that the area of high AI west of Australia is from African biomass burning. Also clarified are transport of South American smoke toward Africa and the beginnings of a Saharan dust outbreak (green shades) that will eventually reach the Caribbean.

The anthropogenic sulfate aerosol plumes seen in NAAPS as red shades in Fig. 12 are not detected in the TOMS absorbing AI. They do, however, appear in other satellite imagery such as that shown in Fig. 13 for the eastern seaboard for July 16, 1999, the day J.F. Kennedy, Jr. perished in a plane crash. The satellite imagery shows an area of haze leaving the continent with an axis along Long Island Sound and Nova Scotia, but it gives no indication of the vertical distribution of the haze. NAAPS produces a similar horizontal distribution (Fig. 13) but, more importantly, it provides the vertical distribution (not shown) of anthropogenic aerosol. When combined with meteorological data, we found that the area was dominated by a dry, polluted, continental air mass with low visibility—in contrast to early speculation of a deep, moist, marine layer with low visibility. At their request, the NAAPS simulation and analyses were provided to the National Transportation Safety Board (NTSB) and will be used verbatim in their report on the environmental conditions surrounding the plane crash.
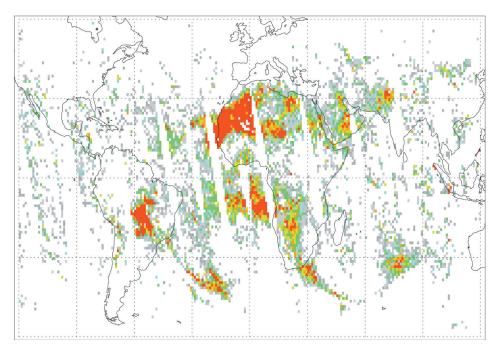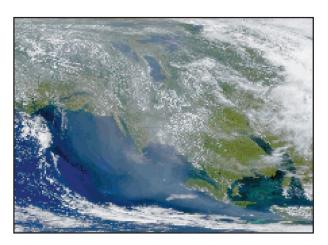
FIGURE 12
Top panel: NAAPS simulation for September 10, 1999 showing the distribution of absorbing aerosol optical depths, contoured at 0.1, 0.2, 0.4 etc. Bottom panel: TOMS AI (arbitrary units) for September 10, 1999 showing the global distribution of absorbing aerosols.
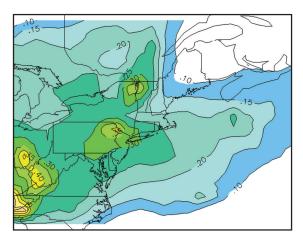
FIGURE 13

Left panel: Sea-viewing wide field-of-view sensor (SEAWIFS) visible imagery for 1630Z, June 16, 1999. Right panel: NAAPS simulation of sulfate aerosol optical depth for 0000Z, June 17, 1999.
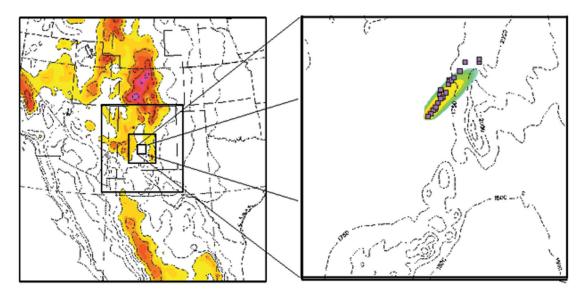
FIGURE 14

Left panel: Triply nested COAMPS domains used in simulations of the DTRA-sponsored weapons test and transport experiment October 29, 1998 at White Sands, NM. Topography is contoured and shaded. Right panel: colored contours are the 36-h COAMPS/Aerosol model forecast (1-km resolution) accumulated dosage. Magenta boxes show the observed location of the surrogate chemical agent plume at 5-min intervals.

Regional Modeling: The mesoscale transport model couples the Navy's operational mesoscale model COAMPS (Coupled Ocean/Atmosphere Mesoscale Prediction System) with a regional aerosol/gas transport model that solves the generalized continuity equation for each aerosol size or gas specie. Real-time forecasts and research simulations of transport have been performed for a wide range of applications including: the investigation of Gulf War illnesses (GWI);[1] weapons tests at White Sands Missile Range (WSMR), New Mexico; and the Tokaimura, Japan, nuclear accident.

In the WSMR experiment, surrogate tracers were released by a weapons test on a concrete building and then tracked with remote sensing as it was transported downwind. The Defense Threat Reduction Agency (DTRA) used the experiment to evaluate several transport and dispersion models, in addition to the weapons test. NRL used COAMPS to predict the weather and subsequent transport and provided a 36-hour forecast of dosage and concentration in real-time. The model results showed good agreement with the observations. Subsequent studies with higher resolution have generated even better results (Fig. 14).

Building on expertise within NRL, we have developed a multiscale modeling system for atmospheric transport. Our early results demonstrate the skill and practicality of the models and the promise of a future capability in real-time predictive modeling. When combined with the urban-scale modeling of the Laboratory for Computational Physics and Fluid Dynamics and the marine boundary layer aerosol modeling in the Remote Sensing Division, NRL is one of the most capable U.S. laboratories for multiscale aerosol modeling.

[Sponsored by ONR]

Reference
[1] D.L. Westphal, T.R. Holt, S.W. Chang, N.L. Baker, T.F. Hogan, L.R. Brody, R.A. Godfrey, J.S. Goerss, J.A. Cummings, D.J. Laws, and C.W. Hines, "Meteorological Reanalysis for the Study of Gulf War Illnesses: Khamisiyah Case Study," *Wea. Forecast.* **14**, 215-241 (1999). ◆

Space Research and Satellite Technology

Physics of Coronal Mass Ejections

J. Chen and J. Krall
Plasma Physics Division

R.A. Howard and J.D. Moses
Space Science Division

For several decades, a number of important energetic phenomena on the Sun have received intense attention in theoretical solar physics. However, the mechanisms responsible for violent eruptions, such as solar flares, coronal mass ejections (CMEs), and closely associated prominence eruptions, have defied clear understanding. CMEs, in particular, are not only of scientific interest but are also of practical importance: Earth-directed CMEs can produce solar wind (SW) structures propagating to the Earth and causing severe geomagnetic disturbances. Figure 1 shows an image of a CME that erupted on 9 September 1997. This figure is a composite of two images: the outer image (red scale) was captured by NRL's Large Angle and Spectrometric Coronagraph (LASCO) onboard the Solar and Heliospheric Observatory (SOHO) satellite, located approximately one million miles toward the Sun, and the inner image (blue scale) was taken by the Mauna Loa Solar Observatory Mark III coronameter (MK3), operated by the High Altitude Observatory, Boulder, Colorado.
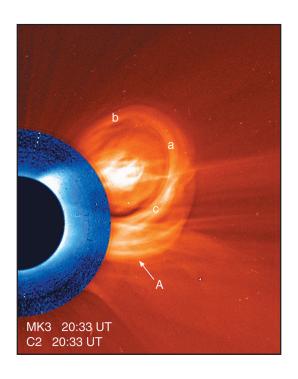
CMEs were first observed in the early 1970s, but theoretical models have not been successful in elucidating the basic physics of CMEs. Recently, a new

theory has been proposed to explain the phenomenon.[1] The basic hypothesis of the theory is that the magnetic field underlying CMEs is that of a magnetic "flux rope." While the previous models are based on the paradigm that the magnetic energy powering solar eruptions is entirely stored in the corona above the photosphere, the new model allows the energy below the photosphere to emerge into the corona and play a major role in causing CME eruptions. The theory yields a quantitative and physics-based explanation of the CME dynamics near the Sun and in the heliosphere. Initial examination of the new LASCO/SOHO data shows good agreement between theory and observation.[2,3] We have initiated a systematic effort to test the theoretical model using LASCO data.

LASCO Observations: In the event shown in Fig. 1, the motions of the leading edge (*a*) and the upper (*b*) and lower (*c*) edges have been measured in the fields of view of LASCO C2 and C3 telescopes, covering a region from 2 to approximately 32 solar radii. Figure 2(a) shows measured positions of the leading edge (squares) and the centroid (circles), which is defined as the midpoint of the line segment connecting *b* and *c*. Here, the solid symbols are the LASCO data points. Similar measurements were made with the MK3 data. The MK3 instrument observes the region inside the LASCO field of view (blue scale), and the data provide information during the early phases of the eruption. The curves are the theoretical results for this event.

FIGURE 1
A fast CME observed on 9 September 1997. The black semicircle on the left corresponds to the west half of the Sun. The bright Sun itself is blocked so that faint features in the corona can be observed. In this figure, the leading edge (*a*) and the upper (*b*) and lower (*c*) edges of the frontal loop of the CME are marked. This CME is best described as a projection of a three-dimensional flux rope viewed obliquely. Arrow *A* points to the southern extension of the flux rope curving away from the plane of this figure. The CME is expanding away from the Sun at approximately 800 km/s (500 miles per second). The diameter of the Sun is 1.4 million kilometers (roughly one million miles).
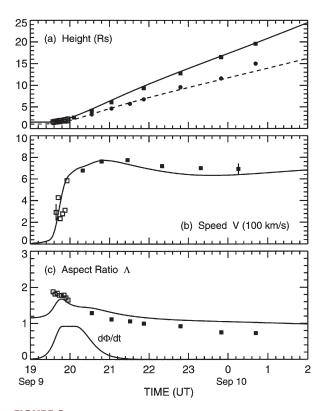
FIGURE 2

MK3/LASCO data and calculated flux rope dynamics. In each panel, the solid symbols represent LASCO data and the open symbols are the MK3 data points. The curves are the theoretical results. (a) Measured positions of the leading edge a (squares) and the centroid (circles). (b) The projected speed V of (a) (squares). (c) Observed and theoretical aspect ratio Λ. Theoretical flux injection profile $d\Phi_P/dt$ is shown in units of 6×10^{18} Mx/s.

The speed of the CME is obtained from the measured positions and is shown in Fig. 2(b) for the leading edge a (squares). The figure shows that the CME motion exhibits a complex profile, accelerating rapidly to approximately 800 km/s and then continuing expansion away from the Sun at nearly a constant speed. We see from Figs. 2(a) and 2(b) that the theoretical predictions are in excellent agreement with the observed CME motion.

Figure 2(c) shows the aspect ratio Λ of this CME, defined to be ratio of the height of the CME from the surface to the width (line segment bc). Theory has previously predicted that this quantity is nearly constant away from the Sun but that it should be greater near the Sun if the CME is rapidly accelerated. Indeed, the measured aspect ratio is in agreement with the prediction of the model flux rope (except for the first few data points, where other complications may arise). This is significant because the aspect ratio embodies a relationship between two perpendicular dimensions of one expanding structure, providing a strong observational constraint on any proposed model.

New Theory: A novel concept of the theoretical model is that the eruption is caused by the emergence of an azimuthal magnetic field from below the photosphere into the corona. This component is parallel to the solar surface as the flux emerges. This hypothesis is in contrast to the long-held paradigm that the magnetic energy responsible for eruptions must be stored in the corona. Subtle magnetic signatures in the photosphere are predicted,[1] but at the present time, magnetic field vectors in the solar environment cannot be measured with accuracy and sufficient time resolution to directly observe the predicted signatures. However, the theoretically predicted increased value of the aspect ratio Λ near the Sun shown in Fig. 2(c) arises from the emergence of an azimuthal magnetic field in the model. Thus, the good agreement shown in this figure is evidence supporting the new hypothesis.

In addition to the example shown here, several other CMEs have been successfully described by the model, suggesting that a class of CMEs exists that can be understood as erupting flux ropes. The degree and extent of quantitative agreement obtained by the theoretical model throughout the LASCO field of view, the largest distance over which CMEs have been observed to date, is unprecedented.

An international satellite program is under development that will have the capability to measure magnetic field vectors at the solar surface with sufficient accuracy to directly test the predictions of the model. If the new hypothesis of emerging magnetic flux as the initiation mechanism is proven correct, it will represent a fundamental change in understanding solar and similar stellar eruptions.

References

[1] J. Chen, "Theory of Prominence and Propagation: Interplanetary Consequences," *J. Geophys. Res.* **101**, 27499 (1996).

[2] J. Chen, R.A. Howard, G.E. Brueckner, R. Santoro, J. Krall, S.E. Paswaters, O.C. St. Cyr, R. Schwenn, P. Lamy, and G.M. Simnett, "Evidence of an Erupting Magnetic Flux Rope: LASCO Coronal Mass Ejection of 1997 April 13," *Astrophys. J. Lett.* **490**, L191 (1997).

[3] J. Chen, R.A. Santoro, J. Krall, R.A. Howard, R. Duffin, J.D. Moses, G.E. Brueckner, J.A. Darnell, and J.T. Burkepile, "Magnetic Geometry and Dynamics of the Fast CME of 1997 September 9," *Astrophys. J.*, in press (2000).

High Dynamic Range, Long-Wavelength Imaging of a Nearby Active Galactic Nucleus

N.E. Kassim,[1] F.N. Owen,[2] J.A. Eilek,[2,3]
and T.J.W. Lazio[1]
1Remote Sensing Division
2National Radio Astronomy Observatory
3New Mexico Institute of Mining and Technology

Introduction: High dynamic range images of farfield sources at high frequency (HF) and very high frequency (VHF) radio frequencies can address a number of astrophysical and DoD applications. On the astrophysical side, such images can be used to find and study active radio galaxies, particularly those at large distances; study the magnetohydrodynamics of a supernova, including the shock acceleration of cosmic rays; and determine the three-dimensional (3D) spatial distribution of thermal and nonthermal emitting gas in the Milky Way. Production of high dynamic range images requires compensation for ionospheric phase fluctuations. The Navy has a strong interest in the development of ionospheric compensation techniques, such as the use of the global positioning system (GPS). Future DoD applications of wide-field imaging and ionospheric compensation techniques include using HF solar radar for predicting arrival times of Earthward bound coronal mass ejections for geomagnetic storm prediction and tracking naturally and artificially generated ionospheric waves.

Active radio galaxies are a class of galaxies distinguished by luminosities in the radio spectrum in excess of 10^{39} W and by emitting structures up to 10^{23} m (approximately 10 million light years) in length. Observations at HF and VHF frequencies can be used to study two complementary aspects of their evolution: First, because of the cosmological expansion, higher frequency emission in the rest frame of distant radio galaxies is redshifted to the HF and VHF in our frame. Second, the emission mechanism of these galaxies is synchrotron radiation from relativistic electrons, and at these frequencies the synchrotron lifetime of the electrons is longer than the age of the Universe. Thus, the evolutionary history of nearby active galaxies can be explored. This report focuses on this second aspect.

Methodology: The complexity of high dynamic range imaging of farfield sources at HF and VHF radio frequencies has prevented routine imaging at the limiting sensitivity and angular resolution inher-ent in the data. These limits arise because most radio interferometers are noncoplanar, and a 2D Fourier inversion, commonly used to derive an image from the measured interferometric data, is inadequate. Furthermore, ionospheric structure introduces phase errors that had been thought to irreversibly vitiate the interferometric data. At frequencies above 1000 MHz, the various phase errors are small, and high-resolution images are routinely produced with sensitivities at the thermal noise limit. At lower frequencies, the combination of noncoplanar arrays, ionospheric structure, an intrinsically larger field of view, and the increased space density of radio sources introduces errors that have precluded achieving the desired thermal-noise-limited sensitivities. Algorithms to implement the required 3D treatment are available, but the computational expense of applying them to real data has been prohibitive, and only low-resolution images have been produced until recently.

We have recently demonstrated how existing "self-calibration" algorithms can be used to remove ionospheric effects.[1] Ionospheric phase errors are introduced along the line of sight between each antenna in the interferometer and the source of emission. However, the interferometer measures the phase between pairs of antennas. Thus, the *N(N-1)/2* antenna pairs can be used to self-calibrate and remove the *N* ionospherically introduced antenna phase errors.

We have equipped the 27-antenna Very Large Array (VLA) radio interferometer (maximum baseline 35 km) at the National Radio Astronomy Observatory (NRAO) near Socorro, New Mexico, with 74 MHz receivers designed and built in the Remote Sensing Division. The NRL-NRAO 74 MHz system joins an existing 330 MHz system and has made the VLA the world's highest angular resolution, highest dynamic range interferometer operating below 1000 MHz. We process the data acquired from these systems using a serial version of a combined self-calibration and 3D, wide-field imaging algorithm on SGI Origin 2000s computers at the Army Research Laboratory in Aberdeen, Maryland, a Major Shared Resource Center of the DoD High Performance Computing Modernization Program.

Results: Figure 3 shows a 330 MHz image of the nearby active galaxy Virgo A (also known as Messier 87). It is located at the center of the nearby Virgo supercluster and has a radial extent of about 10^{21} m. The galaxies in the Virgo supercluster are immersed in a 10^7-10^8 K gas, observed to be cooling through X-ray emission. The radio halo had been known from previous work, but it was assumed to be
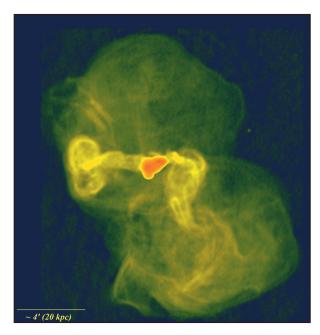
FIGURE 3
Virgo A at 330 MHz. This image was made from data acquired at the Very Large Array. The galaxy Virgo A is the bright feature in the center of the image. The radio halo is the large-scale feature in the image, and the jets are the linear features in the center, particularly left-center of the image. The bar at the bottom left indicates an angular distance of 4 ft (approx. 20 kpc = 3×10^{19} m at the distance of Vir A). The 74 MHz image is essentially identical.

part of the larger "cooling flow." However, estimates of the power delivered by Vir A's jets indicate that the halo could expand in a time much shorter than it could cool through X-ray emission. Furthermore, the images at 74 and 330 MHz are nearly indistinguishable. If the halo were a remnant of past activity, we would expect relativistic electrons emitting at 330 MHz to lose energy more quickly than those emitting at 74 MHz, resulting in a smaller halo at 330 MHz. We conclude that the halo is "alive" and is, or until recently was, being fueled by the "central engine" of Vir A.

There is considerable evidence that the central engine of Vir A is a supermassive black hole (10^8-10^9 times as massive as the Sun). The short time (10^8 years) required to inflate the radio halo to its present size indicates that it is probably the result of transient activity from the central engine. We suggest that the inner regions of superclusters are dynamic—in perhaps a cyclical competition between outflow, driven by the central supermassive black hole, and cooling inflow, driven by the gravity of the supercluster.[2]

[Sponsored by ONR]

References
[1] N.E. Kassim, R.A. Perley, W.C. Erickson, and K.S. Dwarakanath, "Subarcminute Resolution Imaging of Radio Sources at 74 MHz with the Very Large Array," *Astron. J.* **106**, 2218-2228 (1993).
[2] F.N. Owen, J.A. Eilek, and N.E. Kassim, "The Virgo Cluster and the M 87 Radio Halo: Outflow, Not Cooling Flow," *Astrophys. J.*, in preparation (2000).

The Starshine Satellite—Built for the Students of the World

W.R. Braun, C.J. Butkiewicz, I.L. Sokolsky, and J.A. Vasquez
Spacecraft Engineering Department
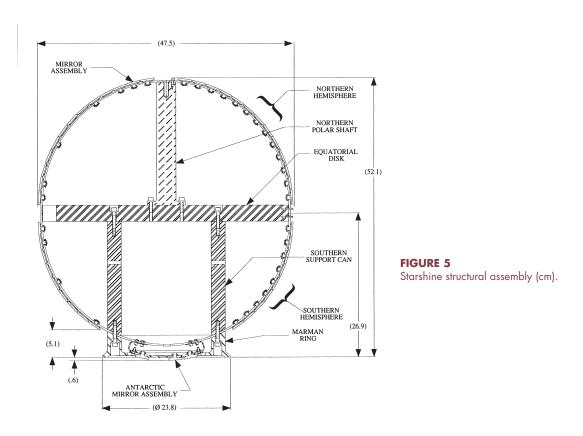
Introduction: On June 5, 1999, Orbiter Discovery deployed Starshine into low Earth orbit. Starshine, a small spherical satellite, was built by the Naval Research Laboratory's Naval Center for Space Technology (NCST) for the students of the world (Fig. 4). Project Starshine, coordinated by the Rocky Mountain NASA Space Grant Consortium, provides a hands-on opportunity for students from around the world to participate in the construction and tracking of a satellite. The outer surface of the satellite is covered with 878 aluminum mirrors. These mirrors were hand polished by 25,030 students in 18 countries. Sunlight is reflected to observers on the ground by the mirrors. Student observers record the position of the satellite and provide this information to the project's Website. These observations will be used to determine the satellite's orbit. Changes in Starshine's orbit are used to calculate the density of Earth's upper atmosphere and examine how the density of the upper atmosphere varies with solar activity.

Project Starshine promotes the study of mathematics and science by combining classroom study with a real application. Students learn about orbits, astronomy, the Earth's atmosphere, the effects of solar activity on the Earth, and the construction and testing of satellite hardware. As Starshine circles the Earth, about every 90 minutes, students from around the world can look up and see a satellite that was built for students by students.

Starshine Satellite: Engineers at NCST designed, built, and tested the Starshine satellite to meet Space Shuttle Hitchhiker Payload specifications in a period of only four months. Starshine is a passive satellite with no moving parts or electrical components. The spherical satellite, shown in Fig. 5, is con-

FIGURE 4
Starshine satellite.

FIGURE 5
Starshine structural assembly (cm).

structed primarily of aluminum with A-286 steel fasteners. Starshine has an outer diameter of 47.5 cm, a height of 52.1 cm, and a weight of 39.2 kg. Stock materials and fasteners as well as established operating procedures were used as much as possible to reduce development and fabrication lead times. The hemispherical domes were sized to an existing mandrel to save fabrication time. Mirrors are attached to the hemispherical domes and the Antarctic Bracket by using a method designed to minimize mirror warping due to temperature changes seen on orbit as well as stresses induced from mirror installation and launch loads. The innovative mounting technique developed by the engineers at the NCST eliminated the mirror warping issue and allowed the installation of 878 mirrors in a timely manner.
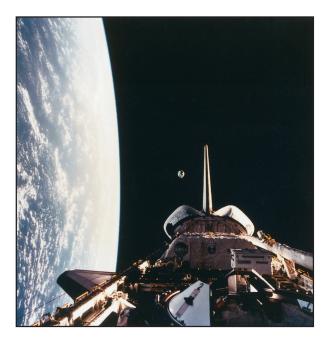
FIGURE 6
Starshine deployed by Orbiter Discover.

Testing of the Starshine satellite was conducted in the NCST's Payload Processing Facility. Testing included sine sweep (structure frequency determination), random vibration (workmanship and flight qualification to Orbiter vibration levels), and sine burst (material strength) testing. These tests were conducted in three orthogonal axes and witnessed by more than 70 students from local schools.

Starshine Deployment: Once all the testing was completed, Starshine was shipped to the NASA Goddard Space Flight Center for integration onto the Hitchhiker Ejection System and in the Hitchhiker Canister. The canister was installed in the cargo bay of Orbiter Discovery. On June 5, 1999, Starshine was deployed into a nearly circular orbit, with an initial altitude of 380 km and an inclination of 51.6 degrees (Fig. 6). It is expected to remain in orbit for approximately eight months, depending on solar activity and related fluctuations in upper atmospheric density. An international network of student observers has been established to measure and report Starshine's angular position at precise times, so that its orbit can be computed as it descends into the atmosphere. A display of its daily altitude is being presented on the Starshine Website, <http://www.azinet.com/starshine>. Together with images of the Sun, students can make a correlation between sunspot activity and the rate of decay of the satellite's orbit. This provides insight into the relationship between sunspot activity and the fluctuation of the Earth's atmospheric density.
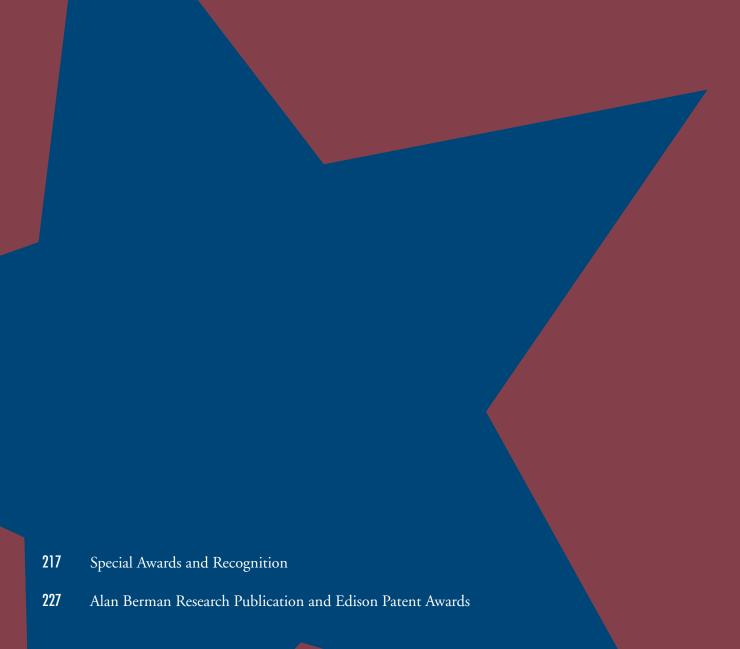
Summary: Using technical expertise in the area of satellite hardware design, fabrication, test, and integration, the NCST produced a satellite for the students of the world in four months. An international network of student observers has been established to measure and report Starshine's angular position at precise times, so that its orbit can be computed as it descends into the atmosphere. NRL's successful effort to meet the hardware delivery deadline for a flight on the Space Shuttle has led to the participation of thousands of students from around the world in a space experiment.

NRL's technical contributions to the first Starshine satellite will allow student groups the chance to build additional satellites that can be flown on shuttle missions annually to measure the response of the Earth's atmosphere to changes in solar activity. The NCST participation in the Starshine project provides the opportunity to install optical corner reflectors on future versions of Starshine. This will allow NRL to measure solar and atmospheric interaction with satellites in low orbits with greater precision than currently possible.

[Sponsored by ONR]   ✦

Special Awards and Recognition

Special Awards and Recognition

NRL is proud of its many distinguished scientists, engineers, and support staff. Here we feature some who have received awards from prestigious institutions, the Department of the Navy, and NRL.

1999 PRESIDENTIAL RANK OF DISTINGUISHED EXECUTIVE IN THE SENIOR EXECUTIVE SERVICE (SES)

Mr. Peter G. Wilhelm — *Naval Center for Space Technology*

The Presidential Rank Awards were established to recognize a select group of career Senior Executives who have demonstrated exceptional performance over an extended period of time. Nominees are outstanding leaders and must consistently demonstrate strength, integrity, industry, and a relentless commitment to public service. Through their personal conduct and their results-oriented program management, they will have established and maintained a high degree of public confidence and trust. Mr. Wilhelm was recognized for his "extraordinary leadership, superb engineering accomplishments, and inspiring vision that have contributed substantially to the nation's space program. He contributed to and led the design, development, and deployment of 84 scientific and defense satellites. Through projects like *Clementine*, he has pioneered the development of low cost, high quality spacecraft."

AMERICAN INSTITUTE OF AERONAUTICS AND ASTRONAUTICS (A1AA) 1999 GODDARD ASTRONAUTICS AWARD

Mr. Peter G. Wilhelm — *Naval Center for Space Technology*

This award is the oldest AIAA tribute for notable achievement in the field of astronautics and is named in the honor of Mr. Robert H. Goddard, "a rocket pioneer whose early liquid rocket engine launches opened up the world of astronautics." Mr. Wilhelm was cited for "extraordinary engineering, astute leadership, and zealous dedication to excellence in responding to the needs and advancing the technology of the United States Space Program." Under Mr. Wilhelm's direction, the Naval Center for Space Technology and the Navy have achieved numerous successes and "firsts" in space, including the first Global Positioning System (GPS) satellite and the highly successful *Clementine* Deep Space Mission, which demonstrated the capability of, and has become the model for, low-cost, high-value space exploration. Mr. Wilhelm's achievements include contributions to the design, development, and operation of 87 scientific and Fleet-support satellites.

DOD DISTINGUISHED CIVILIAN SERVICE AWARD

Mr. Peter G. Wilhelm — *Naval Center for Space Technology*

Mr. Wilhelm was recognized for "his technical expertise, outstanding management, and dedication to excellence in support of Navy and national space programs. He provided technical and managerial leadership for each of the scientific and fleet support satellites launched by the Navy. His technical achievements have been critical to maintaining the United States' superiority in space. Also, his innovative concepts in the areas of satellite orbit insertion, transfer, and maneuvering systems made major national space systems affordable and permitted their ultimate development and operational deployment in service of the warfighter. Mr. Wilhelm's superb accomplishments reflect great credit upon himself and the Department of Defense."

1999 PRESIDENTIAL RANK OF MERITORIOUS EXECUTIVE IN THE SENIOR EXECUTIVE SERVICE (SES)

Dr. John A. Montgomery — *Tactical Electronic Warfare Division*

A Presidential Rank Award is among the highest honors a public employee may receive. It is recognition of sustained outstanding achievements, which have brought great credit not only upon the recipient, but the entire Department of the Navy. The accomplishments have contributed in large measure to the ability to provide for the national security in the most efficient and effective manner. Dr. Montgomery was recognized for fostering an innovative climate within NRL's Tactical Electronic Warfare Division. Under his leadership, the TEWD is recognized as the U.S. Navy's foremost authority on electronic warfare technology throughout the Department of Defense and in the international electronic warfare community.

NAVY DISTINGUISHED CIVILIAN SERVICE AWARD

Dr. John A. Montgomery — *Tactical Electronic Warfare Division*

Dr. Montgomery was cited for "his exceptional technical expertise, outstanding management skill, and zealous dedication to excellence in support of Navy, national, and international electronic warfare (EW) programs such as Specific Emitter Identification, NULKA, and TTCP. He has provided technical and managerial leadership for significant portions of the EW systems nomenclatured and fielded by the Fleet. His achievements in high-performance, broad coverage, multiple threat-addressing systems, passive and active decoy systems, low-power/low-weight electronics, ECM positioning vehicles, and advanced technology ECM systems have been critical to maintaining U.S. superiority in EW. His innovative concepts in the areas of defensive ECM electronic payloads and their placement systems have made ECM systems affordable and have permitted their development and deployment in service of the warfighter. Uncompromising in his pursuit of quality, he insists on the application of continuous improvement in every major EW development effort for which he is responsible, all with ultimate needs of the warfighter in mind. Dr. Montgomery's extraordinary leadership, superb scientific and technological accomplishments, and inspiring vision have contributed substantially to Navy leadership in electromagnetic warfare."

1999 PRESIDENTIAL RANK OF MERITORIOUS EXECUTIVE IN THE SENIOR EXECUTIVE SERVICE (SES)

Dr. Bhatka Rath — *Materials Science and Component Technology Directorate*

A Presidential Rank Award is among the highest honors a public employee may receive. It is recognition of sustained outstanding achievements, which have brought great credit not only upon the recipient, but the entire Department of the Navy. The accomplishments have contributed in large measure to the ability to provide for the national security in the most efficient and effective manner. Dr. Rath was recognized for exploiting new opportunities, reorganizing the Directorate to respond to emerging scientific and technological needs and breakthroughs, and renovating NRL's core materials and chemistry focus area work. He has sought not only to anticipate change, but also to promote and foster it in a number of ways. His workshop program for the Directorate explores two or three new topics each year, and has effectively kept the Directorate's researchers on the cutting edge of new developments in materials science.

WASHINGTON ACADEMY OF SCIENCES' 1999 AWARD FOR SCIENTIFIC ACHIEVEMENT IN ENGINEERING SCIENCES

Mr. Francis J. Campbell — *Condensed Matter and Radiation Sciences Division (retired)*

Mr. Campbell was selected for his ingenious and intensive studies focused on increasing the reliability of many Navy systems. The award nomination cited "His most important contribution was the unraveling of the mystery of the unexpectedly high number of electrical system failures and electrical wiring fires occurring in Naval aircraft during their operation. …As a result of his investigations, critical redesign of electrical systems has been implemented by the Navy, resulting in the reduction of these incidents and increasing the operational safety and reliability of the Fleet."

SIGMA XI 1999 PURE SCIENCE AWARD

Dr. John P. Apruzese— *Plasma Physics Division*

The nomination for this award stated that Dr. Apruzese has "made fundamental advances in both the science and modeling of radiation transport, and also has made important contributions to the theory of x-ray lasers. His theoretical work has played a seminal role in advancing basic understanding and experimental milestones in both fields." During his tenure at NRL, Dr. Apruzese has made extensive contributions in plasma kinetics, radiation trasnport, and high power x-ray sources. His research also encompassed the radiation physics of the terrestrial atmosphere, and its effect on the temperature balance from the stratosphere to the lower thermosphere.

SIGMA XI 1998 PURE SCIENCE AWARD

Mr. Richard J. Colton — *Chemistry Division*

The nomination for this award recognized Dr. Colton "for his work on nanotechnology and in particular his leadership role in the development of revolutionary biosensors based on their new force discrimination assay." Dr. Colton's current research interests include the measurement of the nanochemical properties of materials using atomic force microscopy and the development of new sensors using electron tunneling and force transducers.

INSTITUTE OF ELECTRICAL AND ELECTRONICS ENGINEERS (IEEE) 1999 PETER HAAS PULSED POWER AWARD

Dr. Gerald Cooperstein — *Plasma Physics Division*

The Haas award, established in 1987, bears the name of the late Peter Haas, a former director of the Defense Nuclear Agency, who is recognized for his many contributions to a strong and vigorous pulsed-power program through sound management, steadfast conviction, and farsighted technical acumen. The award is presented to those individuals who share Mr. Haas' dedication, leadership, and administrative vision for pulsed power. Dr. Cooperstein received the award in recognition for his leadership and technical contributions in the pulsed-power field. The citation cited Dr. Cooperstein for his leadership and technical contributions over the past three decades, which have greatly benefited the pulsed-power field and resulted in important advances in pulsed power, the growth of important new areas of research, and the promotion of information exchange.

INSTITUTE OF ELECTRICAL AND ELECTRONICS ENGINEERS (IEEE) 1999 MICROWAVE APPLICATION AWARD

Dr. Christian Rauscher — *Electronics Science and Technology Division*

This award is given periodically to individuals for an outstanding application of microwave theory and techniques. Dr. Rauscher was cited for "proposing and demonstrating innovative approaches to the design of microwave filters and frequently channelizers." Dr. Rauscher is a Fellow of the IEEE. He has received several notable awards, including the 1987 IEEE Microwave Prize for his work on microwave distributed active filters, as well as the 1991 NRL Sigma Xi Applied Science Award. He holds ten patents on his inventions in the area of microwave and millimeter-wave circuits. He is currently serving a three-year term as IEEE Distinguished Microwave Lecturer.

SOCIETY OF FIRE PROTECTION ENGINEERS' 1999 FIRE PROTECTION PERSON OF THE YEAR AWARD

Dr. Frederick W. Williams — *Chemistry Division*

This award was created in 1973 by the Society of Fire Protection Engineers to recognize "significant achievement in the protection of man and his environment from the ravages of unwanted fire and an outstanding contribution to fire protection from outside the membership of the Society of Fire Protection Engineers." According to the citation, "the contributions of Fred Williams, both in terms of advancing the science of fire protection engineering as a sponsor and program manager, and individually conducting significant research, are broad and far reaching. His efforts have had a direct impact on Navy fire protection as well as the Fire Protection Engineers community as a whole."

1999 FEDERAL LABORATORY CONSORTIUM AWARD FOR EXCELLENCE IN TECHNOLOGY TRANSFER

Dr. Ranganathan Shashidhar — *Center for Bio/Molecular Science and Engineering*

The Federal Laboratory Consortium for Technology Transfer promotes technology transfer nationwide and facilitates the rapid movement of federal laboratory research results and technologies into the mainstream of U.S. economy. Dr. Shashidhar was recognized for "his significant contributions to the development of advanced liquid crystal displays (LCDs), and has been instrumental in transferring these technologies to industry through cooperative research and development agreements (CRADAs) and licensing agreements. With his colleagues, Dr. Shashidhar has developed several new classes of materials that have revolutionized liquid crystal technology.

NATIONAL DEFENSE INDUSTRIAL ASSOCIATION (NDIA) UNDERSEA WARFARE DIVISION BRONZE AWARD

Dr. Michael Czarnecki — *Marine Geosciences Division*

The National Defense Industrial Association Undersea Warfare Division recognized the contributions of Dr. Czarnecki by presenting the award of the Bronze Medal. Dr. Czarnecki leads the team that operates the SPAWAR Planning Facility (SPF). The SPF is a rapid-response decision aid for developing and exploiting new and innovative environmental techniques for using existing data sets in the Integrated Undersea Surveillance Systems (IUSS) Program. Dr. Czarnecki and his team provide an analysis of available survey data, make recommendations as to what additional surveys and data are required, and ensure that the planned data collection effort meets the specifications and resolution requirements. The newly collected data are integrated to provide a comprehensive high-resolution database that supports a wide range of system installation, performance, and survival decisions.

NAVY SUPERIOR CIVILIAN SERVICE AWARD

Mr. John Gossner— *Acoustics Division*

Mr. Gossner was cited "for sustained superior civilian service as operations analyst on the staff of the Commander, Surface Warfare Development Group from February 1987 to January 1998. Mr. Gossner consistently performed his demanding duties in an exemplary and highly professional manner. Through demonstrated technical expertise, unparalleled tactical ability, and unmatched initiative, he provided numerous tactical and technical products to the fleet to enhance Anti-Submarine Warfare capabilities and procedures. He was instrumental in the production of a widely acclaimed and unique series of Anti-Submarine Warfare tactical memoranda, providing site and threat specific guidance to fleet operators. He developed and executed an innovative methodology for the evaluation and revision of this guidance, a system in which he personally played a key role. An avid advocate for the deckplate sailor, his unrelenting commitment, superb professional ability, and unmatched knowledge of every facet of Anti-Submarine Warfare have resulted in the production of sustained, superior tactical guidance to the Fleet. His reputation for excellence and direct personal involvement with other agencies significantly improved the command's ability to accomplish its mission."

NAVY SUPERIOR CIVILIAN SERVICE AWARD

Dr. William B. Mosely — *Oceanography Division*

Dr. Moseley was cited for "his superior innovative leadership in serving the Navy, Department of Defense, and the Nation as Superintendent of the Oceanography Division, Naval Research Laboratory, and as Technical Director of its predecessor organization, from 0December 1987 to December 1998. He led the Oceanography Division since inception, through major changes in technical direction where it is currently recognized as the premier research and development organization in the Department of Defense. Under his astute leadership, the division has earned both national and international recognition for innovative and leading edge technical accomplishments in ocean and littoral modeling. This capability to undertake research, develop the technology, and transition the open ocean and littoral models has given the Navy an operational ocean characterization and forecast capability that is second to none, and is a key factor in the Naval Research Laboratory's reputation as a national and international leader in oceanography. Dr. Moseley's leadership, professionalism, and total dedication to duty, reflect great credit upon himself, the Office of Naval Research, and the Naval Research Laboratory and are in keeping with the highest traditions of the United States Naval Service."

AMERICAN PHYSICAL SOCIETY (APS) 1999 AWARD FOR OUTSTANDING DOCTORAL DISSERTATION IN PLASMA PHYSICS

Dr. Thomas R. Clark, Jr. — *Optical Sciences Division*

This award was established to recognize exceptional young scientists who have performed original doctoral thesis work of outstanding scientific quality and achievement in the area of plasma physics. The award citation stated that Dr. Clark is recognized "for his comprehensive elucidation of the hydrodynamics and the optical mode structure of the plasma waveguide." Dr. Clark's work at NRL has led to the lowest measured timing jitter of an actively mode-locked fiber laser and the demonstration of a multi-gigahertz photonic analog-digital conversion architecture based on wavelength-time mapping. His current interests are in the development of low-noise ultrafast fiber laser systems, photonic analog-digital conversion, ultrafast materials and high-speed photonic devices, and phase noise characterization of photonic systems.
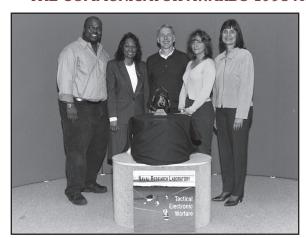
1998 E.O. HULBURT SCIENCE AWARD

Dr. Thomas L. Reinecke — *Electronics Science and Technology Division*

The E.O. Hulburt Science Award is the highest civilian honor awarded for scientific achievement by the Naval Research Laboratory. Dr. Reinecke was commended for being "a leading contributor in establishing a broad fundamental understanding of the optical, transport, and electromagnetic behavior of semiconductor quantum well, quantum wire, quantum dot, and microcavity systems, and in exploring their opportunities in technology…made important theoretical contributions and introduced innovative concepts in understanding a broad range of issues from the optical properties of quantum dots to thermoelectric transport in superlattices and to the photonic properties of microcavities…a leader in stimulating high quality theoretical research in this area and in drawing new researchers into this work…played a key role in bringing together experimental and theoretical work in advancing the understanding of these systems…an internationally recognized authority on the physics of low-dimensional systems."

THE COMMUNICATOR AWARDS 1998 AWARD OF DISTINCTION

Mr. Jim A. Marshall, Jr., Ms. Leona M. Jackson, Mr. Ray E. Reynolds, Ms. Carol Hambric, and Mrs. Linda F. Greenway — *Technical Information Division*

For the second year in a row, the Technical Information Division's multimedia group is a winner in The Communicator Awards 1998 Television Commercials/Programs/News and Video/Film competition. NRL's CD-ROM "Tactical Electronic Warfare" has won the 1998 Award for Distinction, which is awarded for projects that exceed industry standards in production or communication skills. The video production "POAM" won an honorable mention. Winners of The Communicator Awards come from video production companies, independent producers, directors, writers, videographers, editors, and other production professionals, corporate communications departments, government entities, broadcast and cable television operations, advertising and public relations agencies, and other businesses and individuals throughout the country.

ROGER L. EASTON AWARD FOR EXCELLENCE IN ENGINEERING ACHIEVEMENT

Dr. Thomas G. Giallorenzi— *Optical Sciences Division*

This annual award, established in 1996, is NRL's highest civilian award for engineering achievement. Dr. Giallorenzi was cited "for his leading role in developing the most effective multidisciplinary electro-optics research and development organization in the Department of Defense (DoD) over the past 20 years. His leadership has encouraged his team to identify important new technologies, remove practical obstacles to their implementation, and demonstrate their potential to resolve critical Navy and DoD problems. His dynamic participatory management style has resulted in resolution of many scientific, technical, and management issues and in obtaining the necessary resources." The citation also states, "Dr. Giallorenzi has been the principal leader for the development and use of fiber-optics in DoD. He is recognized as the father of the fiber-optics sensor field in which very high performance fiber-optic acoustic sensors, gyroscopes, and magnetic sensors have been realized."

NAVY MERITORIOUS CIVILIAN SERVICE AWARD

Dr. Donald W. Forester— *Systems Directorate*

Dr. Forester was acknowledged for "sustained superior performance in research contributions and technical leadership from August 1969 to March 1998, resulting in major advances in magnetic device materials and breakthrough developments in low-observables technologies for Navy and DoD, air, ground, and sea platforms; for extraordinary efforts to assure technology transitions to national-level manufacturing and military platform installation; and for continual insistence on insertion of innovative discoveries from within NRL."

NAVY MERITORIOUS CIVILIAN SERVICE AWARD

Mr. Jeffrey D. Hawkins— *Marine Meteorology Division*

This award cited Mr. Hawkins for "his meritorious achievement and dedication to the United States Navy, the Naval Meteorology and Oceanography Command, and the Naval Research Laboratory, while serving as a satellite meteorologist from November 1996 to August 1998." He was instrumental in obtaining European Remote Sensing (ERS-1) satellite scatterometer surface winds and geostationary cloud and water vapor-tracked winds for operational use by the U.S. Navy. Both data sets filled large data voids, providing crucial information for the numerical weather prediction models and for stand-alone satellite data products that aided the operational Navy's need for real-time forecasts over large oceanic domains. According to the citation, the information derived from these important data sources was incorporated into independent solutions at the Naval Atlantic Meteorology and Oceanography Center, Norfolk, Virginia, and formed the basis for modifying a track forecast of an approaching hurricane. The decision not to sortie the fleet, which was based on this corrected forecast, translated into enormous saving for Navy operations.

NAVY MERITORIOUS CIVILIAN SERVICE AWARD

Dr. David J. Nagel— *Condensed Matter and Radiation Sciences Division*

Dr. Nagel was commended for his accomplishments during his tenure at NRL as the foremost expert in the Navy in the development and the use of x-rays for plasma diagnostics. As a key member of a team, he pioneered the use of x-ray spectroscopy to characterize nuclear weapon performance. He became an internationally recognized expert on x-ray spectroscopy and diagnostics through his numerous publications. Dr. Nagel spearheaded the development of the NRL beam lines at the National Synchrotron Light Source at Brookhaven National Laboratory, and had the vision to form the Complex Systems Theory Brancy for materials properties computation.

NAVY MERITORIOUS CIVILIAN SERVICE AWARD

Dr. Robert K. Parker— *Electronics Science and Technology Division*

Dr. Parker was acknowledged for "his outstanding contributions to the Navy and to the national defense effort during his tenure as head of the Vacuum Electronics Branch in the Electronics Science and Technology Division. His service at NRL is distinguished by his strong technical and managerial accomplishments in RF vacuum electronics and his effective leadership in this critical area of defense electronics. Of particular significance to the Navy are his key contributions to three major projects: the microwave power module that has proven pivotal to the development of advanced radar, electronic countermeasure, and communication capabilities; the gyroklystron, a break-through technology for the production of high power at millimeter wavelengths that opens this frequency range for the development of significant new defense capabilities; and modeling simulation of RF vacuum amplifiers resulting in a suite of modern design codes that have greatly accelerated the pace of device development while improving overall device performance."

NAVY MERITORIOUS CIVILIAN SERVICE AWARD

Dr. Chester F. Poranski, Jr.— *Chemistry Division*

This award cited Dr. Poranski for his "performance in leading the NRL Sonar Dome Reliability Task. This task has provided the Navy with tools to monitor the condition of its surface ship sonar domes, especially the x-ray backscatter nondestructive inspection system; information about mechanisms of failure that led to improvements in manufacturing; test procedures for evaluating new materials for domes; information about dome behavior at sea; and support with the introduction of advanced materials for dome costruction." Dr. Poranski has been the program manager for the NRL Sonar Dome Reliability Task since 1986, shortly after joining the task team in 1985. He has led and coordinated the efforts of a team that, over the years, has included NRL scientists, NRL research and development contractors, university researchers, industrial partners, and various components of Naval Warfare Centers.

THE 1999 NRL REVIEW ARTICLE AWARDS

Mr. Allyn B. Jacoby, Dr. Chris A. Rowe, Mr. Joel P. Golden, Dr. Frances Ligler, Dr. James N. Templeman, Mr. David J. Singh, Dr. Altan Turgut, Dr. Stephen N. Wolf, and Dr. Marshall H. Orr

Awards for NRL Review articles recognize authors who submit outstanding research articles for this scientific publication. The articles are judged on the relevance of the work to the Navy and DoD, readability to the college-graduate level, clearness and conciseness of writing, and the effective use of graphics that are interesting and informative. The following awards were presented for articles that appeared in the 1999 NRL Review.

FEATURED RESEARCH ARTICLE
"Array-based Biosensor for Multianalyte Sensing," *Mr. Joel P. Golden, Dr. Chris A. Rowe, and Dr. Frances Ligler (Center for Bio/Molecular Science and Engineering)*

DIRECTORATE AWARDS FOR SCIENTIFIC ARTICLES
Systems Directorate: "Gaiter: A Locomotion Control for Distributed Simulation," *Dr. James N. Templeman and Ms. Linda J. Sibert (Information Technology Division)*

Materials Science and Component Technology Directorate: "Computational Screening of Candidate Thermoelectric Materials," *Mr. David J. Singh (Materials Science and Technology Division)*

Ocean and Atmospheric Science and Technology Directorate: "Estimation of Seabed Properties from Chirp Sonar Data," *Dr. Altan Turgut, Dr. Stephen N. Wolf, and Dr. Marshall H. Orr (Acoustics Division)*

Naval Center for Space Technology: "Interim Control Module (ICM)," *Dr. Allyn B. Jacoby (Spacecraft Engineering Department)*

NRL AWARD FOR EXCELLENCE IN MISSION SUPPORT

Dr. Jean E. Osburn — *Information Technology Division*

This award is the highest NRL award for staff contributions to the accomplishment of NRL's mission. Dr. Osburn and Ms. Frommeyer were cited for "exceptional service as the Naval Research Laboratory (NRL) High Performance Computing (HPC) Service/Agency Approval Authorities (S/AAA) to the Department of Defense during the period FY95 – FY98. During this 4-year period, Dr. Osburn and Ms. Frommeyer successfully formulated, monitored, managed, and competed for NRL's share of the Department of Defense's HPC resources." According to the citation, "They have been champions for all NRL HPC users in obtaining new hours (during the year where and whenever possible) and redistributing existing allotted hours to meet the evolving needs of those users. Dr. Osburn and Ms. Frommeyer have been especially effective in securing, monitoring, and managing the HPC resources that DoD allocates to NRL. The availability of machine time of the magnitudes that these representatives bring to NRL represents a significant financial commitment by DoD and an enviable computational resource that has allowed principal investigators to make significant advances in numerous areas of scientific research."

Ms. Marguerite Frommeyer — *Ocean and Atmospheric Science and Techology Division*

COMMANDING OFFICER'S AWARD FOR EXCELLENCE IN SECRETARIAL SUPPORT

Ms. Barbara J. Walter — *Patuxent River Flight Support Detachment*

Ms. Walter was cited for "her dedicated service, loyal assistance, and superior performance of her duties as the Executive Secretary for the Officer in Charge, supporting the men and women of the Flight Support Detachment…Since joining the command in 1984, she has established herself as an extremely capable and meticulous administrator." Ms. Walter was recognized for the administrative support she provided during the 1998 fiscal year for 12 highly visible research projects, 1503 mishap-free flight hours, and a budget of over $7 million. As the sole secretary for the detachment, she handles the daily administrative requirements for 9 officers, 80 enlisted, and 4 civilian personnel. The citation notes that Ms. Walter is "widely regarded as the de facto authority for her unprecedented knowledge of and unfailing attendance to administrative matters, especially noted during the periods of tenuous availability of primary administrative personnel due to worldwide detachment."

Alan Berman Research Publication
and Edison Patent Awards

The Annual Research Publication Awards Program was established in 1968 to recognize the authors of the best NRL publications each year. These awards not only honor individuals for superior scientific accomplishments in the field of naval research but also seek to promote continued excellence in research and in its documentation. In 1982, the name of this award was changed to the Alan Berman Research Publication Award in honor of its founder.

There were 269 separate publications submitted by the divisions in 1999 to be considered for recognition. Of those considered, 34 were selected. These selected publications represent 143 authors, each of whom received a publication awards certificate, a bronze paperweight, and a booklet listing the publications that were chosen for special recognition. In addition, NRL authors share in their respective division's monetary award.

The winning papers and their respective authors are listed below by their research units. Non-Laboratory coauthors are indicated by an asterisk.

NRL also recognizes patents as part of its annual publication awards program. The NRL Edison Patent Award was established in January 1991 to recognize NRL employees for outstanding patents issued to NRL by the U.S. Patent and Trademark Office during the preceding calendar year. The award recognizes significant NRL contributions to science and engineering as demonstrated by the patent process that are perceived to have the greatest potential benefit to the country. Of the 18 patents considered for 1999, 3 were selected, representing 5 inventors. They are listed under the NRL Edison Patent Awards.

Radar Division

Dual Polarized, UWB Radar Measurements of the Sea at 9 GHz
James P. Hansen, Kim M. Scheff, and Eric L. Mokole

Time-Frequency Analysis of Radar Cross-Section Signatures
Ronald D. Lipps, Victor C. Chen, and A. Maitland Bottoms

Information Technology Division

Transcoding Between Two DoD Narrowband Voice Encoding Algorithms (LPC-10 and MELP)
George S. Kang and David A. Heide

Anycast Routing for Mobile Networking
Vincent D. Park and Joseph R. Macker

Optical Sciences Division

Double-Pulse Heterodyne Rayleigh Backscattering in an Acoustically Driven Single-Mode Fiber
Marc D. Mermelstein, Alan B. Tveten, Clay Kirkendall, and Anthony Dandridge

Phase Noise Measurements of Ultrastable 10 GHz Harmonically Modelocked Fibre Laser
Thomas R. Clark, Thomas F. Carruthers, Paul J. Matthews, and Irl N. Duling

Tactical Electronic Warfare Division

A Method for Determining the Angle of Impinging Radio Waves in the Presence of Multipath
Joseph H. Frankovich and Anthony Y. Tse

Enhanced Emitter Identification Using Scaled Conventional Pulse and Intrapulse Parameters
Shah-An Yang, Vijayanand C. Kowtha, Geoffrey L. Barrows, John C. Sciortino, and David A. Stenger

Chemistry Division

$NCOCH_2(CF_2)_6CH_2OCN$ Cyanate Ester Resin. A Detailed Study
Arthur W. Snow, Leonard J. Buckley, and J. Paul Armistead

Pull-Off Behavior of Epoxy Bonded to Silicone Duplex Coatings
Irwin L. Singer and James G. Kohl

Materials Science and Technology Division

Three-Dimensional Analysis of Proeutectoid Cementite Precipitates
George Spanos and Milo V. Kral

Growth of Organic Thin Films by the Matrix Assisted Pulsed Laser Frequency (MAPLE) Technique
Alberto Piqué, R.A. McGill, Douglas B. Chrisey, Darrin Leonhardt, Barry J. Spargo,
John H. Callahan, and Michael A. Bucaro

Laboratory for Computational Physics and Fluid Dynamics

New Target Designs for Direct-Drive ICF
Lee S. Phillips, John H. Gardner, Stephen E. Bodner, Denis G. Colombant, Stephen P. Obenschain,
Andrew J. Schmitt, Jill P. Dahlburg, Thomas Lehecka, Avraham Bar-Shalom, and Marcel Klapisch

Numerical Simulation of Detonation Initiation in a Flame Brush: The Role of Hot Spots
Alexei M. Khokhlov and Elaine S. Oran

Plasma Physics Division

Direct Drive Acceleration of Planar Liquid Deuterium Targets
John D. Sethian, Stephen E. Bodner, Denis G. Colombant, Jill P. Dahlburg,
Stephen P. Obenschain, Carl J. Pawley, Victor Serlin, John H. Gardner,
Yefim Aglitskiy, Yung Chan, Alban V. Deniz, Thomas Lehecka, and Marcel Klapisch

*A Laser-Accelerator Injector Based on Laser Ionization and
Ponderomotive Acceleration of Electrons*
Christopher I. Moore, Antonio C. Ting, Harris R. Burris,
Phillip Sprangle, Stuart J. McNaught, and Joseph Qiu

Electronics Science and Technology Division

Measurements of intrinsic Short Noise in a 35 GHz Gyroklystron
Jeffrey P. Calame, Bruce G. Danly, and Morag Garven

Theory of Thermopower in Disordered Mixed Crystals: Application to Si-Ge Systems
Pay-June Lin-Chung and Attipat K. Rajagopal

Center for Bio/Molecular Science and Engineering

Array Biosensor for Simultaneous Identification of Bacterial, Viral, and Protein Analytes
Chris A. Rowe, Leonard M. Tender, Joel P. Golden, Frances S. Ligler, Mark J. Feldstein,
Stephanie B. Scruggs, Brian D. MacCraith, and John J. Cras

Mn-Doped ZnS Nanoparticles as Efficient Low-Voltage Cathodoluminescent Phosphors
Banhalli R. Ratna, David S. Hsu, Henry F. Gray, Syed B. Qadri, Y. Tian, and A.D. Dinsmore

Acoustics Division

Localization of Submarine-Radiated Noise Sources Using Scale Models
Earl G. Williams, Brian H. Houston, Joseph A. Bucaro, and Douglas M. Photiadis

Echo Components for Aspect-Independent Detection and Classification
Charles F. Gaumond

Remote Sensing Division

Influence of Seidel Distortion on Combining Beams from a Phased Telescope Array
Robert L. Lucke

Transport of a Passive Scalar at a Shear-Free Boundary
in Fully Developed Turbulent Open Channel Flow
Robert A. Handler, John R. Saylor, Richard I. Leighton, and Amy L. Rovelstad

Oceanography Division

Winds and Waves in the Yellow and East China Seas: A Comparison of
Spaceborne Altimeter Measurement and Model Results
Paul A. Hwang, William J. Teague, Gregg A. Jacobs, Steven M. Bratos,
Donald T. Resio, and David W. Wang

Spatial Relationships Between Marine Bacteria and Localized Corrosion on Polymer Coated Steel
Brenda J. Little, Richard I. Ray, Patricia A. Wagner, Joanne M. Jones-Meehan,
C.C. Lee, and F. Mansfield

Marine Geosciences Division

Autonomous Bathymetry Survey System
Brian S. Bourgeois, Andrew Martinez, Pete J. Alleman, Jami J. Cheramie, and John M. Gravley

Arctic Environmental Atlas
Jennifer L. Galasso and Kathleen Crane

Marine Meteorology Division

An Assessment of the Singular-Vector Approach to Targeted Observing
Using the FASTEX Dataset
Ronald Gelaro, Rolf H. Langland, Gregg D. Rohaley, and Thomas E. Rosmond

Mesoscale Simulation of Supercritical, Subcritical, and Transcritical Flow along Coastal Topography
Stephen D. Burk, Tracy Haack, and R.M. Samelson

Space Science Division

Global Measurements of Stratospheric Mountain Waves from Space
Stephen D. Eckermann and Peter Preusse

Efficiency Calibration of the First Multilayer-Coated Holographic Ion-Etched Flight Grating
for a Sounding Rocket High-Resolution Spectrometer
Michael P. Kowalski, Herbert Gursky, Gilbert G. Fritz, Raymond G. Cruddace, Jack C. Rife,
Troy W. Barbee, Jr., Klaus F. Heidemann, Carl Zeiss, and William R. Hunter

Space Systems Development Department

Orbit Determination and Prediction Concept for NEMO, The Naval EarthMap Observer Program
Patrick W. Binning, Alan S. Hope, and Mark T. Soyka

Onboard Navigation State Vector Propagation for the Interim Control Module
of the International Space Station
Mark T. Soyka and Robert R. Dasenbrock

Spacecraft Engineering Department

An Integrated GPS/Gyro/Smart Structures Architecture
for Attitude Determination and Baseline Metrology
N. Glenn Creamer, George C. Kirby, Ronald E. Weber, Albert B. Bosse,
Shalom Fisher, and Fred A. Tasker

NRL Edison (Patent) Awards

Apparatus and Method for Measuring Intermolecular Interactions by Atomic Force Microscopy
Gil U. Lee and John-Bruce Green

Atmospheric Ozone Concentation Detector
Charles M. Roland and Peter H. Mott

High Temperature Epoxy-Phthalonitrile Blends
Teddy M. Keller

Programs for
Professional Development

Programs for NRL Employees

During 1999, under the auspices of the Employee Development Branch, NRL employees participated in 3250 individual training events.

One common study procedure is for employees to work full time at the Laboratory while taking job-related scientific courses at universities and schools in the Washington area. The training ranges from a single course to full graduate and postgraduate programs. Tuition for training is paid by NRL. The formal programs offered by NRL are described here.

GRADUATE PROGRAMS
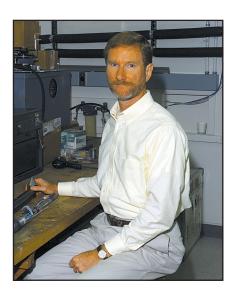
• The **Advanced Graduate Research Program** (formerly the Sabbatical Study Program, which began in 1964) enables selected professional employees to devote full time to research or pursue work in their own or a related field for 1 year at an institution or research facility of their choice without the loss of regular salary, leave, or fringe benefits. NRL pays all educational costs, travel, and moving expenses for the employee and dependents. Criteria for eligibility include professional stature consistent with the applicant's opportunities and experience, a satisfactory program of study, and acceptance by the facility selected by the applicant. The program is open to paraprofessional employees (and above) who have completed 6 years of Federal Service, 4 of which have been at NRL.

• The **Edison Memorial Graduate Training Program** enables employees to pursue advanced studies in their fields at local universities. Participants in this program work 24 hours each workweek and pursue their studies during the other 16 hours. The criteria for eligibility include a minimum of 1 year of service at NRL, a bachelor's or master's degree in an appropriate field, and professional standing in keeping with the candidate's opportunities and experience.

• To be eligible for the **Select Graduate Training Program**, employees must have a college degree in an appropriate field and must have demonstrated ability and aptitude for advanced training. Students accepted into this program devote a full academic year to graduate study. While attending school, they receive one-half of their salary, and NRL pays for tuition and laboratory expenses.

• The **Naval Postgraduate School** (NPS), located in Monterey, California, provides graduate programs to enhance the technical preparation of Naval officers and civilian employees who serve the Navy in the fields of science, engineering, operations analysis, and management. It awards a master of arts degree in national security affairs and a master of science degree in many technical disciplines.

NRL employees desiring to pursue graduate studies at NPS may apply for a maximum of six quarters away from NRL, with thesis work accomplished at NRL. Specific programs are described in the NPS catalog. Participants will continue to receive full pay and benefits during the period of study.

• In addition to NRL and university offerings, application may be made to a number of noteworthy programs and fellowships. Examples of such opportunities are the **Capitol Hill Workshops**, the **Legislative Fellowship (LEGIS) program**, the **Federal Executive Institute (FEI)**, the **Fellowship in**

Dr. William Elam, of the Chemistry Division, participated in the Advanced Graduate Research Program at the National Institute of Standards and Technology (NIST) in Gaithersburg, Maryland.

Congressional Operations, and the **Women's Executive Leadership Program**. These and other programs are announced from time to time, as schedules are published.

• Research conducted at NRL may be used as **thesis material for an advanced degree**. This original research is supervised by a qualified employee of NRL who is approved by the graduate school. The candidate should have completed the required course work and should have satisfied the language, residence, and other requirements of the graduate school from which the degree is sought. NRL provides space, research facilities, and supervision but leaves decisions on academic policy to the cooperating schools.

CONTINUING EDUCATION

• Local colleges and universities offer **undergraduate and graduate courses** at NRL for employees interested in improving their skills and keeping abreast of current developments in their fields. These courses are also available at many other DoD installations in the Washington, D.C. area.

• The Employee Development Branch at NRL offers **short courses** to all employees in a number of fields of interest including technical subjects, computer operation, supervisory and management techniques, and clerical/secretarial skills. Laboratory employees may attend these courses at nongovernment facilities as well. Interagency courses in management, personnel, finance, supervisory development, and clerical skills are also available.

For further information on any of the above programs, contact the Staffing, Classification, and Training Branch (Code 1810) at (202) 767-8313.

TECHNOLOGY TRANSFER

• The **Office of Research and Technology Applications Program** (ORTA) ensures the full use of the results of the Nation's federal investment in research and development by transferring federally owned or originated technology to state and local governments and the private sector. (Contact Code 1004, Dr. Catherine Cotell at (202) 404-8411.)

TECHNOLOGY BASE

• The **Navy Science Assistance Program** (NSAP) establishes an information loop between the Fleet and the R&D shore establishments to expedite technology transfer to the user. The program ad-

Mr. Joseph Peak, of the Signature Technology Office, Systems Directorate, participated as an Edison scholar in the program at the University of Maryland, University College, College Park, Maryland.

dresses operational problems, focuses resources to solve specific technical problems, and develops a nucleus of senior scientific personnel familiar with the impact of current research and system performance on military operations. The program also provides 2-year science advisor positions in the Fleet. NRL is a participant of this ONR program.

• The **Scientist-to-Sea Program** (STSP) provides increased opportunities for Navy R&D laboratory/center personnel to go to sea to gain firsthand insight into operational factors affecting system design, performance, and operations on a variety of ships. NRL is a participant of this NSAP-ONR program.

For further information on these and other Technology Base Programs, including BMD, SBIR, and critical technology, contact Dr. Stephen Sacks, Code 5006, at (202) 767-3666.

PROFESSIONAL DEVELOPMENT

NRL has several programs, professional society chapters, and informal clubs that enhance the professional growth of employees. Some of these are listed below.

• **The Counseling Referral Service** (C/RS) helps employees to achieve optimal job performance through counseling and resolution of problems such as family, stress and anxiety, behavioral, emotional, and alcohol- or drug-related problems that may adversely impact job performance.

C/RS provides confidential assessments and short-term counseling, training workshops, and referrals to additional resources in the community. (Contact Dr. Ralph Surette at (202) 767-6857.)

• A chartered chapter of **Women in Science and Engineering** (WISE) was established at NRL in 1983. In 1997, the NRL WISE Chapter and the NRL Women in Science and Technology Network merged to form the NRL WISE Network. The goals of the organization are to encourage and promote the professional growth of women in science and engineering. Informal luncheons and seminars are scheduled to discuss scientific research areas, career opportunities, and career-building strategies, and to brainstorm solutions to problems encountered by women in science and engineering. WISE also sponsors a colloquium series that features outstanding women scientists. (Contact Dr. Elizabeth A. Dobisz at (202) 767-5159, Margaret Powell at (202) 404-4065, or Dr. Penny Warren at (202) 767-5381.)

• **Sigma Xi**, the scientific research society, encourages and acknowledges original investigation in pure and applied science. As an honor society for research scientists, individuals who have demonstrated the ability to perform original research are elected to membership in local chapters. The NRL Edison Chapter, comprising approximately 600 members, recognizes original research by presenting awards annually in pure and applied science to outstanding NRL staff members. The chapter also sponsors lectures at NRL on a wide range of scientific topics for the entire NRL community. These lectures are delivered by scientists from all over the nation and the world. The highlight of the Sigma Xi lecture series is the Edison Memorial Lecture, traditionally featuring a distinguished scientist. (Contact Dr. B. Ratna at (202) 404-6061 or Dr. Vijay Kowtha at (202) 404-6037.)

• The **NRL Mentor Program** was established to provide an innovative approach to professional and career training and an environment for personal and professional growth. It is open to permanent NRL employees in all job series and at all sites. Mentorees are matched with successful, experienced colleagues with more technical and/or managerial experience who can provide them with the knowledge and skills needed to maximize their contribution to the success of their immediate organization, to NRL, to the Navy, and to their chosen career fields. The ultimate goal of the program is to increase job productivity, creativity, and satisfaction through better communication, understanding, and training. NRL Instruction 12400.1 established the NRL Mentor Program, and it provides the policy and procedures for the program. (Contact Ms. Dawn Brown at (202) 767-2957.)

• The Charlotte Moore-Sitterly Chapter of **Federally Employed Women, Inc.** (FEW) was char-

tered at NRL in 1993. FEW is an international organization of federally employed women and men whose purpose is to eliminate sex discrimination and sexual harassment and enhance career opportunities for women in government. FEW works closely with other Federal agencies and organizations, including the Office of Personnel Management, Equal Employment Opportunity Commission, and Federal Women's Program subcommittees. (Contact Dr. Virginia Degiorgi at (202) 767-9027.)

• Employees interested in developing effective self-expression, listening, thinking, and leadership potential are invited to join either of two NRL chapters of **Toastmasters International**. Members of these clubs, who possess diverse career backgrounds and talents, meet two to four times a month in an effort to learn to communicate not by rules but by practice in an atmosphere of understanding and helpful fellowship. NRL's Commanding Officer and Director of Research endorse Toastmasters as an official training medium at NRL. (Contact Kathleen Parrish at (202) 767-2782 for more information.)

EQUAL EMPLOYMENT OPPORTUNITY (EEO) PROGRAMS

Equal employment opportunity is a fundamental NRL policy for all employees regardless of race, color, national origin, sex, religion, age, or physical/mental handicap. The NRL EEO Office is a service organization whose major functions include counseling employees in an effort to resolve employee/management conflicts, processing formal discrimination complaints, providing EEO training, and recruiting for affirmative employment candidates. The NRL EEO Office is also responsible for sponsoring special-emphasis programs to promote awareness and increase sensitivity and appreciation of the issues or the history relating to: females; individuals with disabilities; Hispanic Americans; African Americans; and individuals of American Indian/Alaskan-Native and Asian-American/Pacific Islander descent. (Contact the NRL Deputy EEO Officer at (202) 767-5264 for additional information on any of our programs or services.)

OTHER ACTIVITIES

• The **Community Outreach Program** traditionally has used its extensive resources to foster programs that provide benefits to students and other community citizens. Volunteer employees assist with and judge science fairs, give lectures, tutor, mentor, coach, and serve as classroom resource teachers. The program also sponsors African American History Month

On December 15, 1998, seven students from the Patterson Communications Youth Club completed an experimental, four-week advanced communications course. Thomas Edison Toastmaster's Leslie Chaplin of the Acoustics Division, and Kathy Parrish, of the Technical Information Division coordinated the fall course with the help of Patterson's guidance counselor, Ms. Vivian Gibson.

art and essay contests for local schools, student tours of NRL, a student Toastmasters Youth Leadership Program, an annual holiday party for neighborhood children, and other programs that support the local community. Also through this program, NRL has active partnerships with four District of Columbia, three Aberdeen, Maryland, and three Calvert County, Maryland, public schools. (Contact Mr. Dom Panciarelli at (202) 767-2541.)

• Other programs that enhance the development of NRL employees include four computer user groups (**IBM PC**, **Mac**, **NeXT**, and **Sun**) and the **Amateur Radio Club**. The **Recreation Club** encourages wide interest in sports for employees with its many facilities and programs, such as a heated indoor pool;

basketball and volleyball court; weight room; table tennis; hot tub and sauna; five martial arts disciplines; aerobics classes; swimming lessons; water walking and exercise; swing dance sessions; and softball and basketball leagues. Sportswear, NRL paraphernalia, discount tickets to amusement parks, and film-developing services are available at the Rec Club office. The **Showboaters** (25 years, 1999) is a nonprofit drama group that presents live theater for the enjoyment of NRL and the community. Traditionally, NRL Showboaters perform two major productions each year in addition to occasional performances at Laboratory functions and benefits for local charities. Although based at NRL, membership is not limited to NRL employees. (Contact Ms. Barbarajo Cox at (202) 404-4998.)

Programs for Non-NRL Employees

Several programs have been established for non-NRL professionals. These programs encourage and support the participation of visiting scientists and engineers in research of interest to the Laboratory. Some of the programs may serve as stepping-stones to federal careers in science and technology. Their objective is to enhance the quality of the Laboratory's research activities through working associations and interchanges with highly capable scientists and engineers and to provide opportunities for outside scientists and engineers to work in the Navy laboratory environment. Along with enhancing the Laboratory's research, these programs acquaint participants with Navy capabilities and concerns.

RECENT PH.D., FACULTY MEMBER, AND COLLEGE GRADUATE PROGRAMS

• The **National Research Council (NRC) Cooperative Research Associateship Program** selects associates who conduct research at NRL in their chosen fields in collaboration with NRL scientists and engineers. The tenure period is 2 years (renewable for a possible third year).

• The **Office of Naval Research (ONR) Postdoctoral Fellowship Program**, administered by the American Society for Engineering Education (ASEE), aims to increase the involvement of highly trained scientists and engineers in disciplines necessary to meet the evolving needs of naval technology. Appointments are for 1 year (renewable for a second and possible third year).

• The **Consortium for Oceanographic Research Education (CORE) Postdoctoral Fellowship Program** is administered in much the same manner as the above two programs. However, this program is focused on selecting associates with advanced degrees in the oceanic and atmospheric environmental sciences. The purpose of this program is to recruit scientists and engineers in these specialized areas.

• The American Society for Engineering Education also administers the **Navy/ASEE Summer Faculty Research and Sabbatical Leave Program** for university faculty members to work for 10 weeks (or longer, for those eligible for sabbatical leave) with professional peers in participating Navy laboratories on research of mutual interest.

• The **NRL/United States Naval Academy (USNA) Cooperative Program for Scientific Interchange** allows faculty members of the U.S. Naval Academy to participate in NRL research. This collaboration benefits the Academy by providing the opportunity for USNA faculty members to work on research of a more practical or applied nature. In turn, NRL's research program is strengthened by the available scientific and engineering expertise of the USNA faculty.

• The **National Defense Science and Engineering Graduate Fellowship Program** helps U.S. citizens obtain advanced training in disciplines of science and engineering critical to the U.S. Navy. The 3-year program awards fellowships to recent outstanding graduates to support their study and research leading to doctoral degrees in specified disciplines such as electrical engineering, computer sciences, material sciences, applied physics, and ocean engineering. Award recipients are encouraged to continue their study and research in a Navy laboratory during the summer.

For further information about the above six programs, contact Ms. Lesley Renfro at (202) 404-7450.

PROFESSIONAL APPOINTMENTS
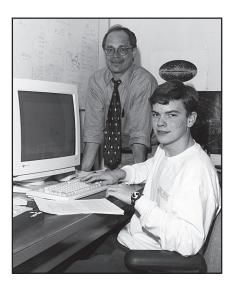
• **Faculty Member Appointments** use the special skills and abilities of faculty members for short periods to fill positions of a scientific, engineering, professional, or analytical nature.

• **Consultants and experts** are employed because they are outstanding in their fields of specialization or because they possess ability of a rare nature and could not normally be employed as regular civil servants.

• **Intergovernmental Personnel Act Appointments** temporarily assign personnel from state or local governments or educational institutions to

the Federal Government (or vice versa) to improve public services rendered by all levels of government.

STUDENT PROGRAMS

The student programs are tailored to the undergraduate and graduate students to provide employment opportunities and work experience in naval research. These programs are designed to attract applicants for student and full professional employment in fields such as engineering, physics, mathematics, and computer sciences. The student employment programs are designed to help students and educational institutions gain a better understanding of NRL's research, its challenges, and its opportunities. Employment programs for college students include the following:

• An agreement between NRL-SSC and **Mississippi's Alliance for Minority Participation** places students whose background and interests match the Laboratory's field of research with NRL mentors in a 10-week research environment. Together with accomplished senior researchers and faculty advisors, students plan, develop, and conduct a summer research project to include challenging, hands-on experiences with research equipment and principles of modern research. (Contact Ms. Linda Ladner at (601) 688-4754.)

• The **Student Career Experience Program** (formerly known as Cooperative Education Program) employs students in study-related occupations. The program is conducted in accordance with a planned schedule and a working agreement among NRL, the educational institution, and the student. Primary focus is on the pursuit of bachelors degrees in engineering, computer science, or the physical sciences.

• The **Student Temporary Employment Program (STEP)** enables students to earn a salary while continuing their studies and offers them valuable work experience.

• The **Summer Employment Program** employs students for the summer in paraprofessional and technician positions in engineering, physical sciences, computer sciences, and mathematics.

• The **Student Volunteer Program** helps students gain valuable experience by allowing them to voluntarily perform educationally related work at NRL.

Kurt Elliott Mitman, a senior at Thomas Jefferson High School for Science and Technology (TJHSST) who has been working in NRL's Space Science Division, was selected as one of 40 finalists in the prestigious Intel Science Talent Search. He was recognized for astrophysics research performed at NRL as a participant in DoD's Science and Engineering Apprentice Program (SEAP) and TJHSST Mentorship program.

For additional information on these undergraduate and graduate college student programs, contact Code 1810 at (202) 767-8313.

HIGH SCHOOL PROGRAMS

• **The DoD Science & Engineering Apprentice Program (SEAP)** employs high school juniors, seniors, and college students to serve for 8 weeks as junior research associates. The college students must have participated in SEAP during high school. Under the direction of a mentor, students gain a better understanding of research, its challenges, and its opportunities through participation in scientific programs. Criteria for eligibility are based on science and mathematics courses completed and grades achieved; scientific motivation, curiosity, and capacity for sustained hard work; a desire for a technical career; teacher recommendations; and achievement test scores. The NRL Program is the lead program and the largest in DoD.

For additional information, contact Dawn Brown (Code 1850) at (202) 767-2957.

General Information

Technical Output

The Navy continues to be a pioneer in initiating new developments and a leader in applying these advancements to military requirements. The primary method of informing the scientific and engineering community of the advances made at NRL is through the Laboratory's technical output—reports, articles in scientific journals, contributions to books, papers presented to scientific societies and topical conferences, patents, and inventions.

The figures for calendar year 1999 presented below represent the output of NRL facilities in Washington, D.C.; Bay St. Louis, Mississippi; and Monterey, California.

In addition to the output listed, NRL scientists made more than 1822 oral presentations during 1999.

Type of Contribution	Unclassified	Classified	Total
Articles in periodicals, chapters in books, and papers in published proceedings	1117	0	1117
NRL Formal Reports	18	12	30
NRL Memorandum Reports	87	10	97
Books	2	0	2
Patents granted			88
Statutory Invention Registrations (SIRs)			4

*This is a provisional total based on information available to the Ruth H. Hooker Research Library and Technical Information Center on January 6, 2000. Additional publications carrying a 1999 publication date are anticipated.

Technology Transfer at NRL

Many of NRL's technologies have commercial applications in addition to the defense-oriented objectives for which they were originally developed. NRL developments in areas such as radar, radio, satellite navigation, fiber optics, chemical and biological sensors, and a wide variety of materials and coatings have made significant contributions to the safety and welfare of the civilian community.

The transitioning of NRL's dual-use technologies to the private sector is facilitated by NRL's Technology Transfer Office. This office implements the Technology Transfer Act by which Congress authorized Federal Laboratories such as NRL to participate in Cooperative Research and Development Agreements (CRADAs) and patent licensing agreements. During the last ten years, NRL has entered into more than 200 CRADAs with industry, universities, nonprofit organizations, and other government organizations. In addition, NRL has executed more than 40 licenses to its inventions.

Among DoD laboratories, NRL is a recognized leader in the area of Technology Transfer. Numerous NRL staff members have been awarded the Federal Laboratory Consortium's Award for Excellence in Technology Transfer. In 1999, this award was presented to Dr. Ranganathan Shashidhar of NRL's Center for Bio/Molecular Science and Engineering to recognize his success at transitioning liquid crystal display technology by means of CRADAs and licenses.

Entering into a CRADA is an excellent way for U.S. companies to gain access to commercially important NRL research and development. As the Navy's corporate laboratory, NRL draws on the powerful resources of an interdisciplinary combination of scientific expertise and modern facilities. NRL's technical staff is recruited from all disciplines of engineering and the physical sciences and is available to work with private companies to solve technical problems in any area of research that is consistent with NRL's mission.

During 1999, NRL signed CRADAs with small and large companies, universities, and other nonprofit organizations. In some cases, NRL is assisting a company in commercializing NRL technology that has, or will be, licensed. In other cases, NRL is contribut-

Lake Shore Cryotronics markets this Hall Effect Measurement System for research and development applications where highly accurate materials characterization is required. The system consists of Lake Shore's hardware integrated with NRL's patented Quantitative Mobility Spectrum Analysis (QMSA) software and is sold under license from the Navy. The inventors on the patent are Drs. Jerry Meyer, Filbert Bartoli, and Craig Hoffman of NRL's Optical Sciences Division, and collaborators from the University of Western Australia. The Lake Shore system is fully computer-automated and measures Hall voltage, resistance, magnetoresistance, and current-voltage characteristics. In addition, it calculates carrier concentrations and mobilities. The NRL scientists have been working with Lake Shore to integrate improvements to the system under the scope of a Cooperative Research and Development Agreement (CRADA).

ing expertise in the development of new technology for commercial use or to benefit the civilian community.

For example, the Surface Modification Branch in the Materials Science and Technology Division is collaborating under the scope of a CRADA with Cyrano Sciences, Inc., to develop new materials and new approaches to the fabrication of electronic "noses." NRL first became involved with research in this field to develop detectors for chemical weapons. These devices, which consist of an array of sensors specific to particular chemicals, can also be used in the food industry, animal husbandry, and contraband law enforcement.

Under the scope of another CRADA signed in 1999, NRL and the University of Texas at Houston Health Science Center are adapting Navy-developed satellite telecommunication technology to allow two-way audio, video, and data communication of emergency medical information between an ambulance in the field and a hospital trauma center.

NRL supports an active licensing program and has more than 500 patents available for licensing in fields as diverse as advanced materials, chemistry, biotechnology, optics, ocean and atmospheric sciences, electronics, radar, and satellite technology. A license to a Navy invention authorizes the licensee to manufacture and sell a product based on NRL's technology in exchange for royalty payments that are shared by the Laboratory and the inventors.

Lockheed Martin signed a license with the Navy in 1999 for NRL's LaserNet Fines Oil Debris Monitor, which was originally developed for Navy condition-based maintenance programs. The LaserNet Fines system uses laser imaging technology and wear particle analysis software to perform online measurements of wear debris in engine lubricants. The small size of the system makes it ideal for deployment onboard ships, at field sites, and on factory floors to identify potential breakdown of machinery.

For additional information, contact NRL's Technology Transfer Office, Code 1004, 4555 Overlook Avenue, S.W., Washington, D.C. 20375-5320, or call (202)767-7230; e-mail: techtransfer@nrl. navy.mil; URL: http://labwide14/techtransfer.

Key Personnel

Code	Office		Phone Number
	EXECUTIVE DIRECTORATE		
1000	Commanding Officer	CAPT D.H. Rau, USN	767-3403
1000.1	Inspector General	CAPT J.P. Horsman, Jr., USN	767-3621
1001	Director of Research	Dr. T. Coffey	767-3301
1001.1	Executive Assistant	Mr. D. DeYoung	767-2445
1002	Chief Staff Officer	CAPT J.P. Horsman, Jr., USN	767-3621
1004	Head, Technology Transfer	Dr. C. Cotell	404-8411
1006	Head, Office of Program Administration and Policy Development	Ms. L. McDonald	767-3091
1008	Office of Counsel	Mr. J. McCutcheon	767-2244
1030	Public Affairs Officer	Mr. R. Thompson (Acting)	767-2541
1200	Head, Command Support Division	Mr. J.C. Payne	767-3048
1220	Head, Security	Dr. J.T. Miller	767-0793
1240	Head, Safety Branch	Mr. J.S. Burns	767-2232
1400	Head, Military Support Division	CDR A. Leigh, USN	767-2273
1600	Officer-in-Charge, Flight Support Detachment	CDR T.A. McMurry, USN	301-342-3751
1800	Director, Human Resources Office	Ms. B.A. Duffield	767-3421
1803	Deputy EEO Officer	Ms. D. Erwin	767-5264
3204	Deputy for Small Business	Ms. L. Byrne	767-6263
	BUSINESS OPERATIONS DIRECTORATE		
3000	Associate Director of Research	Mr. D. Therning	767-2371
3200	Head, Contracting Division	Mr. J.C. Ely	767-5227
3300	Comptroller, Financial Management Division	Mr. D. Therning	767-3405
3400	Supply Officer	Ms. C. Hartman	767-3446
3500	Director, Research and Development Services Division	Mr. S. Harrison	767-3697
	SYSTEMS DIRECTORATE		
5000	Associate Director of Research	Dr. R.A. LeFande	767-3324
5200	Head, Technical Information Division	Mr. J. Lucas (Acting)	767-2187
5300	Superintendent, Radar Division	Dr. G.V. Trunk	767-2573
5500	Superintendent, Information Technology Division	Dr. R.P. Shumaker	767-2903
5600	Superintendent, Optical Sciences Division	Dr. T.G. Giallorenzi	767-3171
5700	Superintendent, Tactical Electronic Warfare Division	Dr. J.A. Montgomery	767-6278
	MATERIALS SCIENCE AND COMPONENT TECHNOLOGY DIRECTORATE		
6000	Associate Director of Research	Dr. B.B. Rath	767-3566
6030	Head, Laboratory for Structure of Matter	Dr. J. Karle	767-2665
6100	Superintendent, Chemistry Division	Dr. J.S. Murday	767-3026
6300	Superintendent, Materials Science & Technology Division	Dr. D.U. Gubser	767-2926
6400	Director, Lab. for Computational Physics and Fluid Dynamics	Dr. J.P. Boris	767-3055
6600	Superintendent, Condensed Matter & Radiation Sciences Division	Dr. D.J. Nagel	767-2931
6700	Superintendent, Plasma Physics Division	Dr. S. Ossakow	767-2723
6800	Superintendent, Electronics Science & Technology Division	Dr. G.M. Borsuk	767-3525
6900	Director, Center for Bio/Molecular Science and Engineering	Dr. J.M. Schnur	404-6000
	OCEAN AND ATMOSPHERIC SCIENCE AND TECHNOLOGY DIRECTORATE		
7000	Associate Director of Research	Dr. E.O. Hartwig	404-8690
7100	Superintendent, Acoustics Division	Dr. E.R. Franchi	767-3482
7200	Superintendent, Remote Sensing Division	Dr. P. Schwartz	767-3391
7300	Superintendent, Oceanography Division	Dr. E.M. Stanley (Acting)	228-688-4670
7400	Superintendent, Marine Geosciences Division	Dr. H.C. Eppert, Jr.	228-688-4650
7500	Superintendent, Marine Meteorology Division	Dr. P.E. Merilees	831-656-4721
7600	Superintendent, Space Science Division	Dr. H. Gursky	767-6343
	NAVAL CENTER FOR SPACE TECHNOLOGY		
8000	Director	Mr. P.G. Wilhelm	767-6547
8100	Superintendent, Space Systems Development Department	Mr. R.E. Eisenhauer	767-0410
8200	Superintendent, Spacecraft Engineering Department	Mr. H.E. Senasack, Jr.	767-6411

Employment Opportunities for Entry-Level and Experienced Personnel

The *NRL Review* illustrates some of the exciting science and engineering carried out at the Naval Research Laboratory, as well as the potential for new personnel. In this regard, NRL offers a wide variety of challenging positions that involve the full range of work, from basic and applied research to equipment development. The nature of the research and development conducted at NRL requires professionals with experience. Typically there is a continuing need for electronics, mechanical, aerospace, ceramic and materials engineers, metallurgists, computer scientists, and oceanographers with bachelor's and/or advanced degrees and physical and computer scientists with Ph.D. degrees. Opportunities exist in the areas described below:

Ceramic Engineers and Materials Scientists/ Engineers. These employees are recruited to work on materials, microstructure characterization, electronic ceramics, solid-state physics, fiber optics, electro-optics, microelectronics, fracture mechanics, vacuum science, laser physics technology, and radio frequency/microwave/millimeter wave/infrared technology.

Electronics Engineers and Computer Scientists. These employees may work in the areas of communications systems, electromagnetic scattering, electronics instrumentation, electronic warfare systems, radio frequency/microwave/millimeter wave/ infrared technology, radar systems, laser physics technology, radio-wave propagation, electron device technology, spacecraft design, artificial intelligence, information processing, signal processing, plasma physics, vacuum science, microelectronics, electro-optics, fiber optics, solid state, software engineering, computer design/architecture, ocean acoustics, stress analysis, and expert systems.

Mechanical Engineers. These employees may be assigned to spacecraft design, remote sensing, propulsion, experimental fluid mechanics, experimental structural mechanics, solid mechanics, elastic/plastic fracture mechanics, materials, finite-element methods, nondestructive evaluation, characterization of fracture resistance of structural alloys, combustion, and CAD/CAM.

Chemists. Chemists are recruited to work in the areas of combustion, polymer science, bioengineering and molecular engineering, surface science, materials, fiber optics, electro-optics, microelectronics, electron-device technology, and laser physics.

Physicists. Physics graduates may concentrate on such fields as materials, solid-state physics, fiber optics, electro-optics, microelectronics, vacuum science, plasma physics, fluid mechanics, signal processing, ocean acoustics, information processing, artificial intelligence, electron-device technology, radio-wave propagation, laser physics, ultraviolet/X-ray/gamma-ray technology, electronic warfare, electromagnetic interaction, communications systems, radio frequency/microwave/millimeter wave/infrared technology, and computa-tional physics.

Oceanographers, Meteorologists, and Marine Geophysicists. These employees work in the areas of ocean dynamics, air-sea interaction, upper-ocean dynamics, oceanographic bio-optical modeling, oceanic and atmospheric numerical modeling and prediction, artificial intelligence applications for satellite analyses, benthic processes, aerogeophysics, marine sedimentary processes, and advanced mapping techniques. Oceanographers and marine geophysicists are located in Washington, D.C., and the Stennis Space Center, Bay St. Louis, Mississippi. Meteorologists are located in Washington, D.C., and Monterey, California.

APPLICATION AND INFORMATION

Interested applicants should submit an Application for Federal Employment (SF-171), an Optional Application for Federal Employment (OF-612), or a resume. The OF-612 and SF-171 can be obtained from local Office of Personnel Management and Human Resource Offices of federal agencies.

Direct inquiries to:

Naval Research Laboratory
Human Resources Office, Code 1810 RV
Washington, DC 20375-5324
(202) 767-3030

Location of NRL in the Capital Area

Naval Research Laboratory
4555 Overlook Avenue, SW
Washington, DC 20375-5320
(202) 767-3200 (Personnel Locator)

Contributions by Divisions, Laboratories, and Departments

Subject Index

Author Index

Technical Output

The Navy continues to be a pioneer in initiating new developments and a leader in applying these advancements to military requirements. The primary method of informing the scientific and engineering community of the advances made at NRL is through the Laboratory's technical output—reports, articles in scientific journals, contributions to books, papers presented to scientific societies and topical conferences, patents, and inventions.

The figures for calendar year 1999 presented below represent the output of NRL facilities in Washington, D.C.; Bay St. Louis, Mississippi; and Monterey, California.

In addition to the output listed, NRL scientists made more than 1822 oral presentations during 1999.

Type of Contribution	Unclassified	Classified	Total
Articles in periodicals, chapters in books, and papers in published proceedings	1117	0	1117
NRL Formal Reports	18	12	30
NRL Memorandum Reports	87	10	97
Books	2	0	2
Patents granted			88
Statutory Invention Registrations (SIRs)			4

*This is a provisional total based on information available to the Ruth H. Hooker Research Library and Technical Information Center on January 6, 2000. Additional publications carrying a 1999 publication date are anticipated.

Technology Transfer at NRL

Many of NRL's technologies have commercial applications in addition to the defense-oriented objectives for which they were originally developed. NRL developments in areas such as radar, radio, satellite navigation, fiber optics, chemical and biological sensors, and a wide variety of materials and coatings have made significant contributions to the safety and welfare of the civilian community.

The transitioning of NRL's dual-use technologies to the private sector is facilitated by NRL's Technology Transfer Office. This office implements the Technology Transfer Act by which Congress authorized Federal Laboratories such as NRL to participate in Cooperative Research and Development Agreements (CRADAs) and patent licensing agreements. During the last ten years, NRL has entered into more than 200 CRADAs with industry, universities, nonprofit organizations, and other government organizations. In addition, NRL has executed more than 40 licenses to its inventions.

Among DoD laboratories, NRL is a recognized leader in the area of Technology Transfer. Numerous NRL staff members have been awarded the Federal Laboratory Consortium's Award for Excellence in Technology Transfer. In 1999, this award was presented to Dr. Ranganathan Shashidhar of NRL's Center for Bio/Molecular Science and Engineering to recognize his success at transitioning liquid crystal display technology by means of CRADAs and licenses.

Entering into a CRADA is an excellent way for U.S. companies to gain access to commercially important NRL research and development. As the Navy's corporate laboratory, NRL draws on the powerful resources of an interdisciplinary combination of scientific expertise and modern facilities. NRL's technical staff is recruited from all disciplines of engineering and the physical sciences and is available to work with private companies to solve technical problems in any area of research that is consistent with NRL's mission.

During 1999, NRL signed CRADAs with small and large companies, universities, and other nonprofit organizations. In some cases, NRL is assisting a company in commercializing NRL technology that has, or will be, licensed. In other cases, NRL is contribut-

Lake Shore Cryotronics markets this Hall Effect Measurement System for research and development applications where highly accurate materials characterization is required. The system consists of Lake Shore's hardware integrated with NRL's patented Quantitative Mobility Spectrum Analysis (QMSA) software and is sold under license from the Navy. The inventors on the patent are Drs. Jerry Meyer, Filbert Bartoli, and Craig Hoffman of NRL's Optical Sciences Division, and collaborators from the University of Western Australia. The Lake Shore system is fully computer-automated and measures Hall voltage, resistance, magnetoresistance, and current-voltage characteristics. In addition, it calculates carrier concentrations and mobilities. The NRL scientists have been working with Lake Shore to integrate improvements to the system under the scope of a Cooperative Research and Development Agreement (CRADA).

ing expertise in the development of new technology for commercial use or to benefit the civilian community.

For example, the Surface Modification Branch in the Materials Science and Technology Division is collaborating under the scope of a CRADA with Cyrano Sciences, Inc., to develop new materials and new approaches to the fabrication of electronic "noses." NRL first became involved with research in this field to develop detectors for chemical weapons. These devices, which consist of an array of sensors specific to particular chemicals, can also be used in the food industry, animal husbandry, and contraband law enforcement.

Under the scope of another CRADA signed in 1999, NRL and the University of Texas at Houston Health Science Center are adapting Navy-developed satellite telecommunication technology to allow two-way audio, video, and data communication of emergency medical information between an ambulance in the field and a hospital trauma center.

NRL supports an active licensing program and has more than 500 patents available for licensing in fields as diverse as advanced materials, chemistry, biotechnology, optics, ocean and atmospheric sciences, electronics, radar, and satellite technology. A license to a Navy invention authorizes the licensee to manufacture and sell a product based on NRL's technology in exchange for royalty payments that are shared by the Laboratory and the inventors.

Lockheed Martin signed a license with the Navy in 1999 for NRL's LaserNet Fines Oil Debris Monitor, which was originally developed for Navy condition-based maintenance programs. The LaserNet Fines system uses laser imaging technology and wear particle analysis software to perform online measurements of wear debris in engine lubricants. The small size of the system makes it ideal for deployment onboard ships, at field sites, and on factory floors to identify potential breakdown of machinery.

For additional information, contact NRL's Technology Transfer Office, Code 1004, 4555 Overlook Avenue, S.W., Washington, D.C. 20375-5320, or call (202)767-7230; e-mail: techtransfer@nrl. navy.mil; URL: http://labwide14/techtransfer.

Key Personnel

Code	Office		Phone Number
EXECUTIVE DIRECTORATE			
1000	Commanding Officer	CAPT D.H. Rau, USN	767-3403
1000.1	Inspector General	CAPT J.P. Horsman, Jr., USN	767-3621
1001	Director of Research	Dr. T. Coffey	767-3301
1001.1	Executive Assistant	Mr. D. DeYoung	767-2445
1002	Chief Staff Officer	CAPT J.P. Horsman, Jr., USN	767-3621
1004	Head, Technology Transfer	Dr. C. Cotell	404-8411
1006	Head, Office of Program Administration and Policy Development	Ms. L. McDonald	767-3091
1008	Office of Counsel	Mr. J. McCutcheon	767-2244
1030	Public Affairs Officer	Mr. R. Thompson (Acting)	767-2541
1200	Head, Command Support Division	Mr. J.C. Payne	767-3048
1220	Head, Security	Dr. J.T. Miller	767-0793
1240	Head, Safety Branch	Mr. J.S. Burns	767-2232
1400	Head, Military Support Division	CDR A. Leigh, USN	767-2273
1600	Officer-in-Charge, Flight Support Detachment	CDR T.A. McMurry, USN	301-342-3751
1800	Director, Human Resources Office	Ms. B.A. Duffield	767-3421
1803	Deputy EEO Officer	Ms. D. Erwin	767-5264
3204	Deputy for Small Business	Ms. L. Byrne	767-6263
BUSINESS OPERATIONS DIRECTORATE			
3000	Associate Director of Research	Mr. D. Therning	767-2371
3200	Head, Contracting Division	Mr. J.C. Ely	767-5227
3300	Comptroller, Financial Management Division	Mr. D. Therning	767-3405
3400	Supply Officer	Ms. C. Hartman	767-3446
3500	Director, Research and Development Services Division	Mr. S. Harrison	767-3697
SYSTEMS DIRECTORATE			
5000	Associate Director of Research	Dr. R.A. LeFande	767-3324
5200	Head, Technical Information Division	Mr. J. Lucas (Acting)	767-2187
5300	Superintendent, Radar Division	Dr. G.V. Trunk	767-2573
5500	Superintendent, Information Technology Division	Dr. R.P. Shumaker	767-2903
5600	Superintendent, Optical Sciences Division	Dr. T.G. Giallorenzi	767-3171
5700	Superintendent, Tactical Electronic Warfare Division	Dr. J.A. Montgomery	767-6278
MATERIALS SCIENCE AND COMPONENT TECHNOLOGY DIRECTORATE			
6000	Associate Director of Research	Dr. B.B. Rath	767-3566
6030	Head, Laboratory for Structure of Matter	Dr. J. Karle	767-2665
6100	Superintendent, Chemistry Division	Dr. J.S. Murday	767-3026
6300	Superintendent, Materials Science & Technology Division	Dr. D.U. Gubser	767-2926
6400	Director, Lab. for Computational Physics and Fluid Dynamics	Dr. J.P. Boris	767-3055
6600	Superintendent, Condensed Matter & Radiation Sciences Division	Dr. D.J. Nagel	767-2931
6700	Superintendent, Plasma Physics Division	Dr. S. Ossakow	767-2723
6800	Superintendent, Electronics Science & Technology Division	Dr. G.M. Borsuk	767-3525
6900	Director, Center for Bio/Molecular Science and Engineering	Dr. J.M. Schnur	404-6000
OCEAN AND ATMOSPHERIC SCIENCE AND TECHNOLOGY DIRECTORATE			
7000	Associate Director of Research	Dr. E.O. Hartwig	404-8690
7100	Superintendent, Acoustics Division	Dr. E.R. Franchi	767-3482
7200	Superintendent, Remote Sensing Division	Dr. P. Schwartz	767-3391
7300	Superintendent, Oceanography Division	Dr. E.M. Stanley (Acting)	228-688-4670
7400	Superintendent, Marine Geosciences Division	Dr. H.C. Eppert, Jr.	228-688-4650
7500	Superintendent, Marine Meteorology Division	Dr. P.E. Merilees	831-656-4721
7600	Superintendent, Space Science Division	Dr. H. Gursky	767-6343
NAVAL CENTER FOR SPACE TECHNOLOGY			
8000	Director	Mr. P.G. Wilhelm	767-6547
8100	Superintendent, Space Systems Development Department	Mr. R.E. Eisenhauer	767-0410
8200	Superintendent, Spacecraft Engineering Department	Mr. H.E. Senasack, Jr.	767-6411

Employment Opportunities for
Entry-Level and Experienced Personnel

The *NRL Review* illustrates some of the exciting science and engineering carried out at the Naval Research Laboratory, as well as the potential for new personnel. In this regard, NRL offers a wide variety of challenging positions that involve the full range of work, from basic and applied research to equipment development. The nature of the research and development conducted at NRL requires professionals with experience. Typically there is a continuing need for electronics, mechanical, aerospace, ceramic and materials engineers, metallurgists, computer scientists, and oceanographers with bachelor's and/or advanced degrees and physical and computer scientists with Ph.D. degrees. Opportunities exist in the areas described below:

Ceramic Engineers and Materials Scientists/ Engineers. These employees are recruited to work on materials, microstructure characterization, electronic ceramics, solid-state physics, fiber optics, electro-optics, microelectronics, fracture mechanics, vacuum science, laser physics technology, and radio frequency/microwave/millimeter wave/infrared technology.

Electronics Engineers and Computer Scientists. These employees may work in the areas of communications systems, electromagnetic scattering, electronics instrumentation, electronic warfare systems, radio frequency/microwave/millimeter wave/ infrared technology, radar systems, laser physics technology, radio-wave propagation, electron device technology, spacecraft design, artificial intelligence, information processing, signal processing, plasma physics, vacuum science, microelectronics, electro-optics, fiber optics, solid state, software engineering, computer design/architecture, ocean acoustics, stress analysis, and expert systems.

Mechanical Engineers. These employees may be assigned to spacecraft design, remote sensing, propulsion, experimental fluid mechanics, experimental structural mechanics, solid mechanics, elastic/plastic fracture mechanics, materials, finite-element methods, nondestructive evaluation, characterization of fracture resistance of structural alloys, combustion, and CAD/CAM.

Chemists. Chemists are recruited to work in the areas of combustion, polymer science, bioengineering and molecular engineering, surface science, materials, fiber optics, electro-optics, microelectronics, electron-device technology, and laser physics.

Physicists. Physics graduates may concentrate on such fields as materials, solid-state physics, fiber optics, electro-optics, microelectronics, vacuum science, plasma physics, fluid mechanics, signal processing, ocean acoustics, information processing, artificial intelligence, electron-device technology, radio-wave propagation, laser physics, ultraviolet/X-ray/gamma-ray technology, electronic warfare, electromagnetic interaction, communications systems, radio frequency/microwave/millimeter wave/infrared technology, and computa-tional physics.

Oceanographers, Meteorologists, and Marine Geophysicists. These employees work in the areas of ocean dynamics, air-sea interaction, upper-ocean dynamics, oceanographic bio-optical modeling, oceanic and atmospheric numerical modeling and prediction, artificial intelligence applications for satellite analyses, benthic processes, aerogeophysics, marine sedimentary processes, and advanced mapping techniques. Oceanographers and marine geophysicists are located in Washington, D.C., and the Stennis Space Center, Bay St. Louis, Mississippi. Meteorologists are located in Washington, D.C., and Monterey, California.

APPLICATION AND INFORMATION

Interested applicants should submit an Application for Federal Employment (SF-171), an Optional Application for Federal Employment (OF-612), or a resume. The OF-612 and SF-171 can be obtained from local Office of Personnel Management and Human Resource Offices of federal agencies.

Direct inquiries to:

Naval Research Laboratory
Human Resources Office, Code 1810 RV
Washington, DC 20375-5324
(202) 767-3030

Location of NRL in the Capital Area

Naval Research Laboratory
4555 Overlook Avenue, SW
Washington, DC 20375-5320
(202) 767-3200 (Personnel Locator)

Contributions by Divisions, Laboratories, and Departments

Subject Index

Author Index

Quick Reference Telephone Numbers

	NRL Washington	NRL-SSC	NRL-Monterey	NRL CBD
Hotline	(202) 767-6543	(228) 688-5001	(831) 656-4721	(202) 767-6543
Personnel Locator	(202) 767-3200	(228) 688-3390	(831) 656-4731	(410) 257-4000
DSN	297- or 754-	485	878	—
Direct-in-Dialing	767- or 404-	688	656	257
Public Affairs	(202) 767-2541	(228) 688-5328	(831) 656-4708	—

Additional telephone numbers are listed on page 244.

General information on the research described in this *NRL Review* can be obtained from the Public Affairs Office, Code 1030, (202) 767-2541. Information concerning Technology Transfer is available from Dr. Catherine Cotell, head of the Technology Transfer Office, Code 1004, (202) 767-7230. Sources of information on the various educational programs at NRL are listed in the chapter entitled "Programs for Professional Development."

For additional information about NRL, the *Fact Book* lists the organization, key personnel, and major facilities for each division. It contains information about Laboratory funding, programs, and field sites. The *Fact Book* can be obtained from the Technical Information Division, Publications Services Section, Code 5211, (202) 767-2782.